The Marine Geochemistry of Iron and Iron Isotopes

by

Bridget A. Bergquist

B.S. Geology
B.S. Chemistry
University of Wisconsin-Madison, 1996

Submitted in partial fulfillment of the requirements for the degree of
Doctor of Philosophy

at the

MASSACHUSETTS INSTITUTE OF TECHNOLOGY

and the

WOODS HOLE OCEANOGRAPHIC INSTITUTION

September 2004

Author: _____

Bridget A. Bergquist
Joint Program in Oceanography
Massachusetts Institute of Technology and Woods Hole Oceanographic Institution

Certified by: _____

Edward A. Boyle
Professor of Marine Geochemistry in Earth, Atmospheric, and Planetary Sciences
Thesis Supervisor

Accepted by: _____

Philip M. Gschwend
Professor in Civil and Environmental Engineering
Chair, Joint Committee for Chemical Oceanography

The Marine Geochemistry of Iron and Iron Isotopes

by

Bridget A. Bergquist

Submitted to the WHOI/MIT Joint Program in Oceanography in July, 2004, in partial fulfillment of the requirements for the degree of Doctor of Philosophy

Thesis Advisor: Edward A. Boyle, Professor of Marine Geochemistry, MIT

ABSTRACT

This thesis addressed questions about the Fe cycle by measuring detailed profiles and transects of Fe species in the ocean and also by exploring the use of a new tracer of Fe, Fe isotopic fractionation. In the subtropical and tropical Atlantic Ocean, transects and profiles are presented for dissolved Fe (<0.4 μm), soluble Fe (<0.02 μm), and colloidal Fe (0.02 to 0.4 μm). Surface dissolved Fe distributions reflect atmospheric deposition trends with colloidal Fe following dust deposition more strongly than the soluble fraction of Fe. Observed surface maxima and shallow minima in dissolved Fe were always due to variations in the colloidal Fe fraction. Deep-water dissolved and colloidal Fe concentrations vary with water mass source, age, and transport path. Elevated dissolved Fe concentrations (>1 nmol/kg) were associated with an oxygen minimum zone in the tropical Atlantic at 10°N, 45°W.

Fractionation of iron isotopes could be an effective tool to investigate the geochemistry of iron. Trace metal clean plankton tows, river samples, aerosol leachates, and porewater samples were measured for their iron isotopic composition using a GV Instruments IsoProbe Multi-collector ICPMS. The Fe isotopic composition of plankton tow samples varied by over 4‰ (in $^{56}Fe/^{54}Fe$). North Pacific plankton tow samples had isotopically lighter Fe isotopic compositions than samples from the Atlantic. The overall isotopic range observed in the Amazon River system was 1.5‰, with variability observed for different types of tributaries. The main channel river dissolved Fe samples and suspended loads were isotopically similar (≈ -0.2 to -0.45‰ relative to igneous rocks). The isotopically heaviest sample collected was dissolved Fe from an organic rich tributary, the Negro River (+0.16‰). In contrast, the suspended load from the Negro River was isotopically light (-1‰). The isotopically lightest sample from the Amazon region was shelf porewater (-1.4‰). In river water-seawater mixing experiments, the Fe isotopic signal of dissolved Fe of river water was modified by flocculation of isotopically heavy Fe. The observed range in the Fe isotopic composition of the natural samples including biological and aqueous samples demonstrates that significant and useful fractionation is associated with Fe biogeochemistry in the environment.

THESIS SUMMARY

This study addressed questions about the Fe cycle by measuring detailed profiles and transects of Fe in the ocean and also by exploring the use of a new tracer of Fe, stable Fe isotopic fractionation. Iron distribution, speciation, and dissolution were investigated on three cruises in the sub-tropical and tropical Atlantic Ocean in regions where dust deposition varies by three orders of magnitude. Detailed profiles and transects were collected and analyzed for "dissolved" Fe (DFe, 0.4 μm filtered) and "soluble" Fe (SFe, 0.02 μm filtered). The difference between DFe and SFe is inferred to be the "colloidal" fraction of Fe (CFe). Iron concentrations were measured by a new isotope dilution multi-collector inductively coupled plasma mass spectrometry (MC-ICPMS) method, which allows manganese and chromium concentrations to be measured simultaneously. Iron and manganese comparisons are useful because the source for manganese is aeolian deposition and it is removed by scavenging like iron, but the DMn profile (0.4 μm filtered) is not indicative of a nutrient-type element. In the subtropical and tropical Atlantic Ocean, surface DFe and DMn concentrations reflect dust deposition trends. CFe followed dust deposition trends more strongly than the SFe, and observed maxima in DFe profiles were always due to maxima in the CFe fraction. Where dust deposition was low (e.g., the South Atlantic), CFe concentrations were also low and sometimes negligible in surface waters.

SFe and CFe profiles had distinct profiles both in the upper water column and in deeper waters. SFe profiles were always depleted in surface waters (and in the deep pycnocline of the gyre sites) and gradually increased to relatively uniform concentrations in the deep-water (≈ 0.3 to 0.4 nmol/kg). CFe profiles showed significantly more variability. At sites with surface maxima, CFe always decreased to negligible levels at 30 to 80 m, remained low or negligible throughout the pycnocline, and increased with depth below the pycnocline. The low DFe and CFe in the deep pycnocline of the gyre sites may be due to ventilation with water from higher latitudes with lower dust input (and thus low CFe). We have not established the mechanisms that cause the shallow minima in CFe, but they may be due to (1) atmospheric deposition and downward mixing with low-CFe water and/or (2) a Fe sink within the euphotic zone such as scavenging or biological utilization (indirect or direct). At a site located on the edge of the equatorial system (10°N) with a very shallow pycnocline, DFe increased rapidly within the shallow pycnocline to concentrations >1 nmol/kg associated with an oxygen minimum zone (OMZ) at depths of 130 to 1100 m. The increased DFe in the OMZ is likely due to re-mineralization of organic matter under the high-productivity eastern equatorial upwelling region and then lateral westward spreading. Using estimates of the atmospheric flux of DFe (Vink and Measures, 2001; Chen and Siefert, 2004), surface residence times for DFe on the order of 1 to 5 months were calculated in the Atlantic.

Deep-water DFe and CFe concentrations show variability with water mass and with the source, age, and path of the water masses. DFe concentrations in North Atlantic Deep Water (NADW) are higher than DFe in Antarctic derived water masses. NADW also has a higher fraction of CFe (decreasing from 40% at 10°N to 30% at 24.5°S) from north to south). DFe concentrations in the Antarctic water masses are low ($\approx$ 0.4 nmol/kg) with lower fractions of CFe (20%), which may reflect their low-dust and low DFe source region. SFe in the deep-water of the Atlantic is relatively uniform, therefore most of the variability observed is due to CFe. A deep-water scavenging residence time for DFe of 270 ± 140 years was estimated from the DFe decrease in NADW from the North Atlantic to South Atlantic assuming a transit time of 56 years. If one assumes there is no exchange from the SFe pool to the CFe pool, then a scavenging residence time for CFe can also be estimated (140 ± 100 years).

Estimates of aerosol solubility have important consequences for models of the Fe cycle because dust solubility determines the estimated flux of DFe to the surface ocean. Currently it is being treated as a constant (usually 1 or 10%) because of the limited and variable estimates available. Aerosol dissolution experiments were performed with freshly collected remote Pacific aerosols and natural seawater. The seawater was changed every 24 hours to avoid saturation of the seawater and to minimize Fe loss to the bottle walls. Iron was continually released from the aerosols for up to four days. Based on estimates of TFe, the total amount of DFe released was 37% for the low-TFe experiment and 6.6% for the high-TFe experiment. These estimates are likely minimum estimates because Fe was still being released at the end of both experiments.

Fractionation of iron isotopes could be an effective tool to investigate and quantify the marine geochemistry of iron. Initial studies of stable iron isotopes show measurable fractionation in both field samples and laboratory studies spanning 4‰ (δ^{56}Fe, see Section 1.2 for definition). Trace metal clean plankton tows, river samples, aerosol leachates, and porewater samples were measured for their iron isotopic composition using a GV Instruments IsoProbe Multi-collector ICPMS. This system uses a hexapole collision cell to reduce molecular interferences and improve transmission. Measurements using standard-sample bracketing give an external precision of ± 0.24‰ (2σ standard deviation). The uncertainty in the average of δ^{56}Fe for samples measured more than once was typically less than ± 0.20‰ (2σ standard error).

The δ^{56}Fe of plankton tow samples varied by over 4‰ (-3.87‰ to +0.36‰) and an aerosol leachate from the North Atlantic is indistinguishable from igneous rocks. The range in the δ^{56}Fe of the plankton tow samples demonstrates that significant and potentially useful fractionation is associated with cycling of Fe in the upper ocean. The Fe in the plankton tow samples in this study is a mixture of intracellular and extracellular Fe adsorbed to the plankton. For plankton samples with Fe:C ratios greater than

70 μmol/mol, the δ^{56}Fe values were more variable and were isotopically heavier with increasing Fe:C ratios suggesting that extracellular Fe is isotopically heavier than the intracellular Fe. Plankton samples from the Atlantic scatter around a hypothetical mixing line between a planktonic intracellular δ^{56}Fe of ≈ -1.5‰ and an extracellular component of Fe that is isotopically similar to igneous rocks (0‰). The North Pacific plankton tow samples were isotopically lighter in δ^{56}Fe than the Atlantic plankton samples.

A plankton tow collected in a low salinity Amazon River plume in the open ocean had a δ^{56}Fe value of -0.34‰ and a Fe:C ratio of ≈ 600 μmol/mol. It was inferred from the high Fe:C ratio that most of the Fe collected in the plankton tow was extracellular Fe and that the δ^{56}Fe might reflect the composition of particles and Fe attached to the surface of the plankton. In order to investigate the source of Fe to the Amazon plume water, samples were collected from the Amazon River and region including filtered river water, suspended sediment, and a shelf porewater. River water-seawater mixing experiments were also performed to assess whether Fe flocculation in estuaries affects isotopic composition of the dissolved flux to the ocean. The overall isotopic variation observed in the Amazon River system was 1.5‰. The main channel river samples and suspended loads were isotopically similar (≈ -0.2 to -0.45‰). The most depleted sample was the Amazon shelf porewater (-1.4‰). The isotopically heaviest sample collected was dissolved Fe from an organic rich tributary, the Negro River, in the Amazon River system (+0.16‰). Although the Negro River dissolved phase was isotopically heavy relative to igneous rock, its suspended sediment Fe was very isotopically light (-1‰). The signature of the Negro dissolved load was not observed downstream near the mouth (≈ -0.3‰). The variability in Fe isotopic composition from different types of river tributaries draining distinct weathering terrains suggests that Fe isotopes may reflect the degree or type of weathering and overall balance of Fe in a drainage basin.

Based on river water-seawater mixing experiments, the δ^{56}Fe signal of the Amazon River may be modified in the estuary when >90 % of the Fe flocculates upon mixing with ocean water. The flocculent was isotopically heavy compared with the riverine dissolved Fe, which would lead to the dissolved Fe that is transported to the ocean being isotopically lighter than the river endmember (≈ -1‰ or lighter). However, neither the proposed isotopically light Fe from the modified riverine input nor from shelf porewater matches the Amazon plume plankton tow δ^{56}Fe. If the plankton tow δ^{56}Fe is similar to the plume water δ^{56}Fe, then processes in the euphotic zone (biological cycling/export, scavenging) may modify the proposed light δ^{56}Fe (-1‰) of the Amazon River input by preferentially removing isotopically light Fe. The above studies of Fe isotope fractionation demonstrate that aqueous and biological samples in the environment have a measurable range in δ^{56}Fe values, and that these signals might be useful in tracking Fe pathways.

ACKNOWLEDGEMENTS

This thesis was made possible by the overwhelming support, generosity, patience, and interest of many individuals at Massachusetts Institute of Technology, Woods Hole Oceanographic Institution, and elsewhere.

I am indebted to Edward A. Boyle, my thesis advisor, for his guidance and providing support and first-rate resources for this thesis project. Ed and his approach towards science provide the best possible role model for a graduate student. He has the ability to rigorously investigate the details without loosing site of the big picture. Without Ed's optimism and humor, I would have easily been overwhelmed by the complexities of my project. I am also grateful to the members of my committee. Bernhard Peucker-Ehrenbrink has provided many useful insights into my project and has always been a good friend. His expertise in isotopes and ability to understand the details was an asset to my thesis. Bettina Voelker inspired me to always think about chemistry and problems from a different perspective. She is a great teacher and role model. James Moffett's enthusiasm for my project and encouragement was always greatly appreciated, and he never let me forget about the biology. Finally, John Edmond was an anchor in my experience in the Joint Program. He constantly challenged me and taught me to critically evaluate science. His passing was a great loss.

Outside of my committee, many other faculty and scientist greatly enhanced my graduate education. Jingfeng Wu was a mentor in trace metal chemistry, and the two of us have been the trace metal crew on many cruises. In the world of high precision isotopic measurements, Ariel Anbar and Tom Bullen have always been completely open and helpful. Robert Aller has provided samples from the Amazon and shared insights into Amazon chemistry. Several other professors and scientists inspired me and encouraged me throughout my time at MIT and WHOI including Mick Follows, Sam Bowring, Edward Sholkovitz, Roger Francois, Dan McCorkle, Scott Doney, John Hayes, Tim Eglinton, Mark Kurz, and John Marshall.

So much of my research and graduate student life was experienced in E34. I owe my success to the people of E34 and their friendships and help. Rick Kayser keeps the lab running and makes all the cruises possible. Alla Skorohod has been a good friend and always made life easier. Sean Higgins and Seth John provided humor and optimism in my final years (when it was most needed). Barry Grant and Matt Reuer were essential to my learning of how the instruments and our lab works.

This work would not have been possible or as much fun without the help of numerous people in the field. I would like to thank the participants in the Biocomplexity MANTRA project for all their help at sea and useful discussions. Special thanks go to Ron Siefert and Ying Chen for providing aerosol samples and providing insight into the atmospheric cycle of Fe, Michael Newman and Matt Erickson for assisting in MITESS deployment and recovery at sea, Doug Capone and co-workers for running the large volume mesocosm experiments, Rachel Foster for helping a geochemist identify organisms, and also Ajit Subramaniam, Sarah Cooley, Adam Kustka, Dave Karl, Tony Michaels, and Nathalie Mahowald. The Amazon sampling trip was made possible by Ana Lucia Lima Braun, who guided and organized the trip.

My family and friends have always been supportive and continually inspired me to finish graduate school. They have also kept my sanity intact along with providing help and advice when needed. Special thanks go to my parents, brother, grandmother, Greg Slater, Kathee Jantzi, Amy Steffek, Diane Andreoli, Chrissy White, Mark Gray, Kate Jesdale, and Anand Reddy. Many fellow graduate students have become great friends including Linday Schoenbohm, Vanja Klepac-Ceraj, Ana Lucia Lima Braun, Payal Parekh, JP-all, PAOC-all, and G&G-all. I would like to also thank the folks from the Center for Accelerator Mass pectrometry (Lawrence Livermore National Laboratory) and especially my bosses, Jeffrey McAninch and Alfredo Marchetti.

This research was supported by NSF grants OCE-0002273 and OCE-99871442. The Amazon field trip was partially funded by the Houghton Fund at MIT. I was funded by the National Physical Science Foundation, Lawrence Livermore National Laboratory, and the Education Office of Woods Hole Oceanographic Institution.

Contents

List of Figures

List of Tables and Appendices

Chapter 1

Introduction

Iron is the fourth most abundant element in the Earth's crust and an essential nutrient for all living organisms. For example, Fe is necessary for chlorophyll production and nitrogen assimilation (RUETER and ADES, 1987). Despite its abundance in the environment, Fe is found at very low concentrations in the ocean due to the low solubility of Fe under oxidizing conditions and is a limiting nutrient for primary productivity in many of regions of the ocean (MARTIN and FITZWATER, 1988; MARTIN, 1990; MARTIN et al., 1990; MARTIN et al., 1994; COALE et al., 1996; HUTCHINS and BRULAND, 1998; BOYD et al., 2000; BOYD et al., 2004; COALE et al., 2004). This observation has lead to proposals that changes in Fe flux to the ocean may play a role in climate change by influencing primary production (and hence the carbon cycle) of the ocean (MARTIN, 1990; KUMAR et al., 1995; FALKOWSKI, 1998). In order to incorporate iron into models of climate change, it is necessary to understand and quantify the processes that control iron distributions in the ocean. There have been many attempts to model Fe in the ocean and to include Fe in models of atmospheric CO_2 and climate change (LEFEVRE and WATSON, 1999; MAHOWALD et al., 1999; ARCHER and JOHNSON, 2000; FUNG et al., 2000; SIGMAN and BOYLE, 2000; GAO et al., 2001; GREGG et al., 2003; PAREKH et al., 2004; PAREKH et al., submitted). However, it is difficult to constrain the biogeochemical models for Fe because of the paucity of data throughout the ocean. New water column profiles of Fe, especially in areas not previously sampled, and new process studies of Fe biogeochemistry are necessary to improve and challenge our current understanding of Fe in the ocean.

1.1. IRON IN THE OCEAN

Iron limitation has been demonstrated in high nutrient, low chlorophyll (HNLC) regions by iron enrichment experiments in the Southern Ocean, equatorial Pacific, sub-

artic Pacific, and seasonally in some coastal regions of the ocean (MARTIN and FITZWATER, 1988; MARTIN, 1990; MARTIN et al., 1990; MARTIN et al., 1994; COALE et al., 1996; HUTCHINS and BRULAND, 1998; BOYD et al., 2000; BOYD et al., 2004; COALE et al., 2004). It is also hypothesized that iron could indirectly affect primary productivity in the low nutrient, low chlorophyll (LNLC) regions of the subtropical gyres by limiting N_2 fixing bacteria such as Trichodesmium spp, which bring new nitrate into the system (LETELIER and KARL, 1996; MICHAELS et al., 1996; KARL et al., 1997; FALKOWSKI, 1998). Although the importance of iron in the ocean has been recognized for the past decade or two, it is difficult to study because it is especially prone to contamination and has complicated behavior in the ocean (reviews: JOHNSON et al., 1997; TURNER AND HUNTER, 2001). Iron is known for its redox chemistry, photochemistry, organic complexation, adsorption and desorption on particles, and uptake and cycling by organisms. These factors are further complicated by the low solubility and association of Fe with colloids in seawater (MILLERO, 1998; WU et al., 2001).

The main sources of Fe to the ocean are rivers, atmospheric deposition, re-suspension of sediments, and hydrothermal vents. A schematic of the Fe cycle in the open ocean is shown in Figure 1.1. Fe concentrations are highest near its sources, and concentrations decrease rapidly with distance from sources due to the reactivity and insolubility of Fe in seawater (WU and LUTHER, 1996; JOHNSON et al., 1997). High levels of Fe (~5 nmol/kg) are found in coastal areas where rivers, re-suspension of sediments, and atmospheric deposition are the main contributors. However these high levels are not observed in the open ocean (<1 nmol/kg). Fe concentrations decrease to values of less than 2% of their coastal values 100 km from the California continental margin (JOHNSON et al., 1997). Hydrothermal input of Fe is believed to be important only near its sources (mostly in the deep ocean) because most of the Fe from hydrothermal vents precipitates near the vents and ridge axis (DE BAAR and DE JONG, 2001). Because Fe from rivers and re-suspension of sediments generally does not penetrate far into the ocean interior and hydrothermal Fe input is considered localized, it is believed that the main input of Fe to the open ocean is atmospheric deposition (DUCE

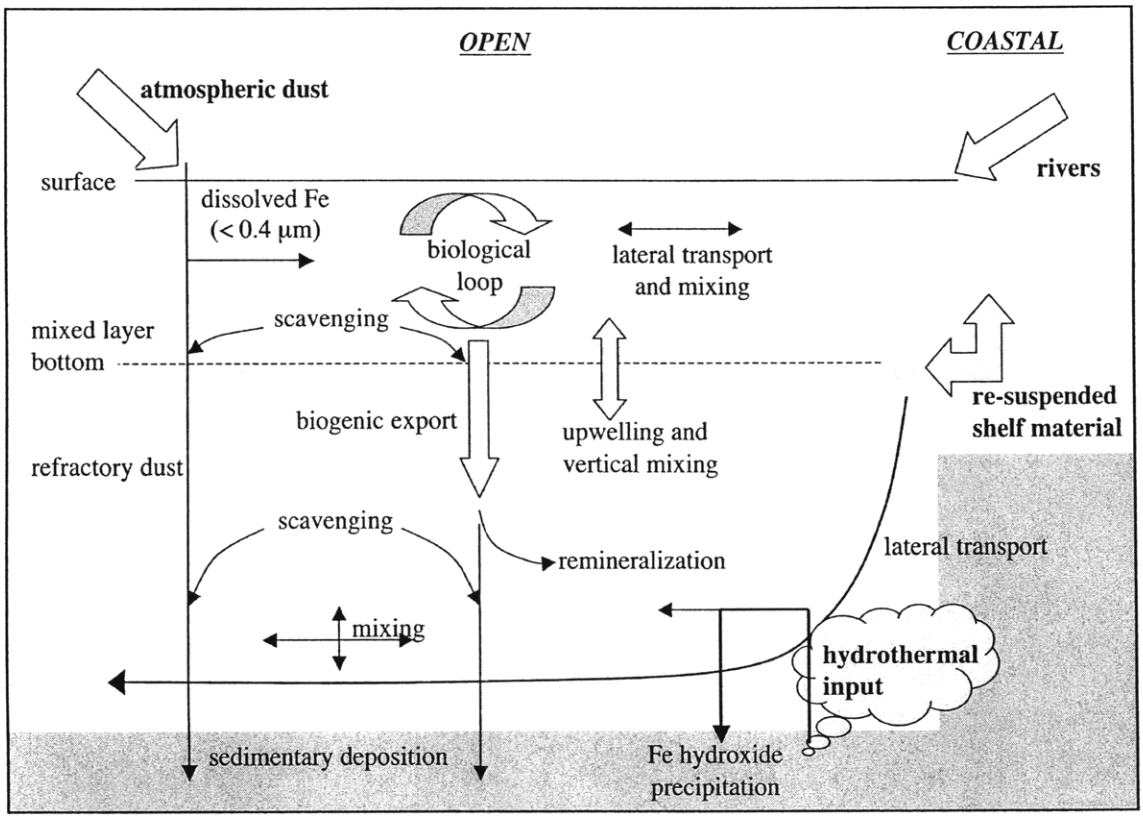

Figure 1.1: Schematic of the Fe cycle in the open ocean.

and TINDALE, 1991; WELLS et al., 1995). Scavenging onto particles and biological export followed by burial in sediments are generally thought to be the primary removal mechanisms. In the upper ocean, both aeolian deposition and upwelling/vertical mixing of deeper water are sources of Fe. Therefore, changes in atmospheric dust flux to the ocean may affect concentrations of bioavailable iron in the upper ocean by changing the amount of aerosol iron that directly dissolves in the upper ocean and by affecting Fe delivered to the deep ocean (and hence upwelled Fe).

"Dissolved" iron (DFe: <0.4 or <0.2 μm filterable Fe) profiles in the open ocean are consistent with other nutrient-type elements showing depletion in the surface waters and an increase with depth due to re-mineralization of organic matter (Figure 1.2) (MARTIN and FITZWATER, 1988; BRULAND et al., 1994; JOHNSON et al., 1997). A few published DFe profiles also show a near surface maximum followed by a minimum in the upper water column and then increasing concentrations with depth (BRULAND et al., 1994; WU et al., 2001). These near surface maxima are interpreted to be due to atmospheric aerosol deposition. In contrast to many nutrient-type elements (e.g.,P, N, Cd, Zn), DFe concentrations do not increase with increasing age of deep water as would be expected if it were accumulated from re-mineralization of sinking organic matter. This is because DFe is particle-reactive (like Al and Pb) and has a short residence time in the deep ocean, <300 years (BRULAND et al., 1994; JOHNSON et al., 1997; PAREKH et al., submitted). However, unlike concentrations of particle-reactive elements that are usually higher in the more continentally influenced Atlantic than the Pacific, deep-water DFe concentrations in both the Atlantic and Pacific are low, ≈ 0.4 to 1 nmol/kg (review: JOHNSON et al., 1997).

Another complication in interpreting DFe distributions is that DFe exceeds the inorganic solubility of Fe (III) oxides in seawater, <0.1 nmol/kg at pH 8.2, 25 °C, and 1 atm (KUMA et al., 1996; MILLERO, 1998). This observation is attributed to organic Fe complexation and colloidal Fe, small particles that pass through 0.4 and 0.2 μm filters (RUE and BRULAND, 1995; WU and LUTHER, 1995; LUTHER and WU, 1997; WU et al., 2001). Organic ligands appear to be ubiquitous in the ocean, are usually found in excess

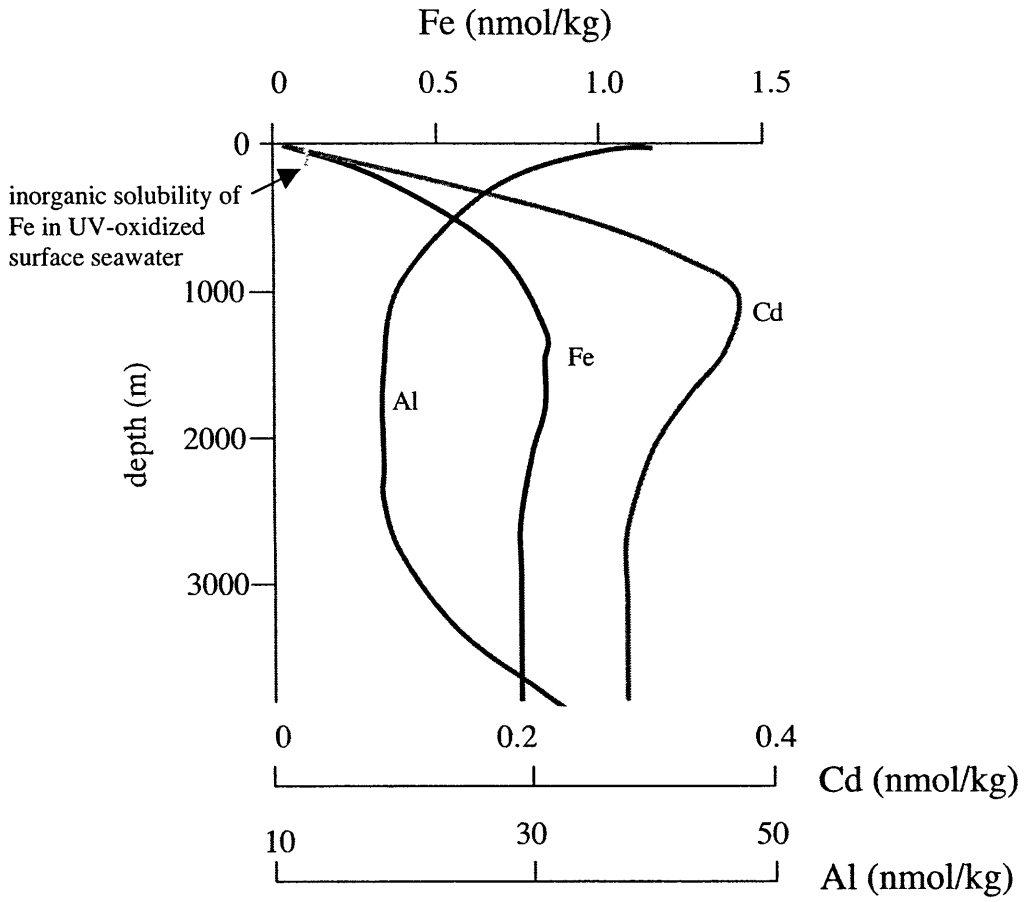

element	description	deep N. Atlantic (nmol/kg)	deep N. Pacific (nmol/kg)
Fe	N + S	0.7	0.4 to 1
Al	scavenged (S)	20-40	< 5
Cd	nutrient (N)	0.2	0.8

Figure 1.2: A schematic of a dissolved Fe water column profile in the Atlantic Ocean in the open ocean along with Al and Cd for comparison. Similar to Fe, Al is a particle-reactive element with an atmospheric lithogenenic source and shorter residence time than the mixing time of the ocean. Cd is a nutrient-type element (like Fe) that is taken up in the surface ocean and re-mineralized at depth with a longer residence time than the mixing time of the ocean. Iron is both a scavenged- and nutrient-type element and Fe concentrations exceed the inorganic solubility due to organic complexation and association with colloids.

(≈ 0.5 to 2 nmol/kg) of DFe concentrations, and are characterized by strong conditional stability constants of $10^{9.8}$ to $10^{14.3}$ M^{-1} (GLEDHILL and VAN DEN BERG, 1994; RUE and BRULAND, 1995; WU and LUTHER, 1995; WITTER and LUTHER, 1998; POWELL and DONAT, 2001). Witter and Luther (1998) also measured rates of formation (> 10^4 s^{-1}) and dissociation constants (< 10^{-5} s^{-1}) for the organic ligands in seawater. The excess of these ligands with strong binding coefficients, fast rates of formation, and slow rates of dissociation leads to >99% of the DFe being complexed by organic ligands in the ocean.

There have been several attempts to explain and model the unique distribution of DFe in the ocean (JOHNSON et al., 1997; LEFEVRE and WATSON, 1999; ARCHER and JOHNSON, 2000; PAREKH et al., 2004; PAREKH et al., submitted). The basic mechanisms of these models can be summarized as follows: 1) dissolution of atmospheric iron in surface waters, 2) biological uptake in the surface ocean, 3) transport to the deep ocean through biological export, 4) re-mineralization of organic material at depth releasing iron, 5) some solubilizing mechanism to keep iron in solution above inorganic solubility (e.g., organic complexation), and finally 6) scavenging and removal of iron. Earlier models assumed that organic ligands kept deep ocean DFe concentrations relatively constant (≈ 0.6 to 0.7 nmol/kg) and only Fe in excess of the dissolved ligands was scavenged (JOHNSON et al., 1997; LEFEVRE and WATSON, 1999; ARCHER and JOHNSON, 2000). The apparent constancy of the deep-water DFe in the ocean was over-emphasized in earlier data sets (BOYLE, 1997). There are areas of the open ocean where deep-water values deviate from the average ≈ 0.6 to 0.7 nmol/kg value. DFe concentrations at 800 m in the Southern Ocean (0.2 to 0.3 nmol/kg) are much lower (DE BAAR et al., 1999), and recent data from the ALOHA station in the Pacific observed elevated DFe and particulate Fe values at intermediate depths likely due to hydrothermal input from nearby Lohini seamount (463 km from ALOHA) (BOYLE et al., submitted). Huge parts of the deep ocean have yet to be sampled, such as the Indian Ocean, the South Atlantic, the Artic, and high dust-flux regions of the North Atlantic. It is more likely that deep-water values of iron are controlled by a balance between input of dissolved iron in the deep water, both from re-mineralization and lateral transport, and scavenging of inorganic iron when it

dissociates from organic ligands (Figure 1.1) (PAREKH et al., 2004; BOYLE et al., submitted; PAREKH et al., submitted). The organic ligand pool usually appears to be in excess of DFe concentrations (WITTER and LUTHER, 1998). Thus organic ligands likely enhance the residence time and solubility of DFe, but do not lead to uniform deep ocean values. This mechanism allows for more variable deep-water Fe concentrations.

There are many aspects of the upper ocean Fe cycle that are poorly understood such as (1) the relationship between changes in dust deposition and corresponding changes in biologically available iron, (2) the amount of atmospheric iron that becomes bioavailable (aerosol solubility), (3) the relative contributions of dry and wet deposition, (4) the residence time of Fe from a dust deposition event in the euphotic zone, (5) the changes in biological productivity and export due to increases in Fe input, (6) the Fe:C ratio of both biological uptake and re-mineralization, and (7) the variability in all of these parameters. Estimates of aerosol Fe solubility in seawater are quite variable (<0.1 to 50%) and depend greatly on the material used in experiments (e.g., atmospherically weathered aerosols versus soil or loess) and the leaching conditions chosen (pH 1 to 8) (review: JICKELLS AND SPOKES, 2001). There is also evidence that increased dust deposition to an area may not lead to a simple increase in the amount of bioavailable Fe. In laboratory experiments, the fraction of dissolvable iron from aerosols exponentially decreased with increasing particulate load (SPOKES and JICKELLS, 1996; BONNET and GUIEU, 2004). Also, the residence time and cycling of iron in the upper ocean are not well constrained. Jickells (1999) estimated a residence time of Fe in the upper ocean of 200 to 300 days for the Sargasso Sea, based on observations and laboratory estimates of aerosol solubility and estimates of atmospheric deposition. Newer estimates of residence time of Fe in the upper ocean are on the order of weeks to months (DE BAAR and DE JONG, 2001; SARTHOU et al., 2003). Wet deposition also plays an important role especially in the equatorial regions where rainfall is high. Sarthou et al. (2003) estimated that input of dissolved Fe was dominated by wet deposition in the ITCZ of the eastern equatorial Atlantic and dry deposition accounted for 73% to 97% of the deposition north and south of the Intertropical Convergence Zone (ITCZ) to 20° latitude. Globally,

Spokes and Jickells (2001) estimated that 30% of the total atmospheric Fe deposition was due to wet deposition, but that wet deposition may be more important for the dissolved Fe input due to high dissolved Fe concentrations observed in rainwater.

Another important question concerning the upper ocean Fe cycle is how do increases in Fe change Fe:C uptake and how subsequent increase in productivity from increasing Fe affect biological export and the Fe:C ratio of exported material? In a recent iron addition experiment in the Southern Ocean (COALE et al., 2004), increases in productivity from iron addition were observed for the full 28 days of the experiment along with increases in export production (BUESSELER et al., 2004). Finally, Sunda (1997) challenged the use of constant Fe:C uptake and re-mineralization ratios in models by demonstrating that this ratio may vary by a factor of two in the different ocean regimes. Models of Fe distribution are very sensitive to Fe:C ratios as they largely determine the amount of Fe that is removed from the euphotic zone into the deep ocean.

Another complication in understanding the DFe cycle is that a significant fraction of DFe is not truly dissolved, which may have consequences in the amount of DFe that is available to organisms. In addition to organically bound Fe, colloids are an important fraction of the DFe pool in the ocean. The operationally defined "dissolved" fraction of Fe (0.2 or 0.4 μm filtered) is based on the minimum size needed to remove most organisms and particles as well as the availability of clean filters with trusted pore sizes (review: (BRULAND and RUE, 2001). Wu et al. (2001) found that a substantial fraction (30 to 70% in deep-water) of DFe was colloidal (0.02 μm to 0.4 μm) in the North Atlantic and North Pacific. Also, the <0.02 μm fraction (soluble fraction) and the colloidal fraction did not have the same concentration profiles suggesting different biogeochemical behaviors for the two pools of iron. Wu et al. (2001) only observed small to negligible amounts of excess <0.02 μm filterable ligand in surface waters, therefore arguing that the large excess of ligand observed in CLE studies was in the colloidal fraction. Based on these observations, Wu et al. (2001) proposed that labile Fe introduced by dust was preferentially released into the colloidal fraction and was complexed by the excess Fe ligands inferred to be in the colloidal fraction. Deep-water

DFe from the re-mineralization of sinking organic matter was released into both the soluble and colloidal size fractions. The different behaviors of colloidal and soluble Fe have yet to be rigorously studied along with the potential biological consequences that a significant fraction of the DFe in the ocean is colloidal.

In order to understand how Fe in seawater plays a role in the biological pump, it is necessary to have an understanding of the species of Fe that are available to organisms and the mechanisms of uptake. A schematic of potential pathways of biological Fe uptake are summarized in Figure 1.3 (reviews: MOFFET, 2001; SUNDA, 2001). In general it is thought that Fe can be transported across cell membranes as labile inorganic dissolved Fe(II) or Fe(III) species (Fe(II)' and Fe(III)'). In laboratory experiments with marine diatoms, Fe uptake increased with increasing amounts of Fe(III)' and was independent of iron bound to strong organic ligands such as EDTA (HUDSON and MOREL, 1990). However, >99% of Fe in seawater is organically bound to strong organic ligands. It would be advantageous if this pool of Fe were available to organisms. Some bacteria release strong Fe ligands (siderophores) that bind and help solubilize Fe in the surrounding environment. The siderophore-Fe complexes can then transported into the cell by specific transport systems (review: SUNDA, 2001). Marine bacteria have been shown to produce siderophores in laboratory cultures (RIED et al., 1993), and recent studies suggest that a fraction of the organic ligand pool in seawater has properties consistent with siderophores (WITTER et al., 2000; MARCRELLIS et al., 2001). It has also been shown that many marine organisms can grow on siderophore bound Fe (GRANGER and PRICE, 1999; HUTCHINS et al., 1999). Despite evidence that marine organisms can use and produce siderophores, it is still unclear to what extent the siderophore transport system is used in the marine environment.

Other pathways that may enhance bioavailable Fe involve steps that produce dissolved Fe(II)' and Fe(III)' from more refractory pools of Fe (Figure 1.3). One such mechanism is the reduction of Fe (III) species to more labile Fe(II). Photochemistry has been suggested to play an important role in increasing the amount of available Fe in surface waters (reviews: MOFFET, 2001; SUNDA, 2001). Photochemical dissolution of

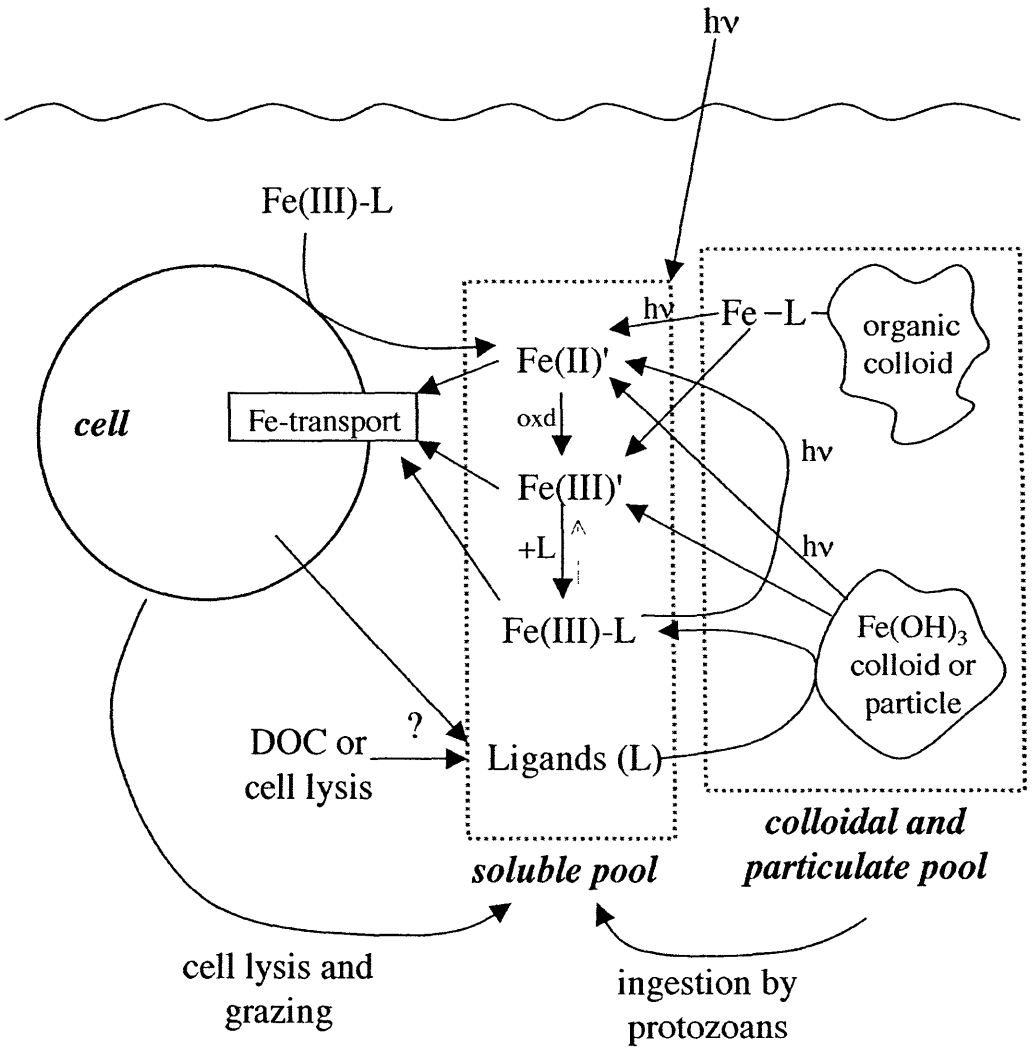

Figure 1.3: A schematic of potential pathways of biological utilization of various forms of Fe in seawater. The soluble pool of Fe includes the reactive inorganic species of Fe (Fe(II)' and Fe(III)') along with organically bound Fe (Fe(III)-L) and excess dissolved ligand (L). Fe may also be bioavailable from the colloidal and particulate pools. Colloidal Fe may exist as either as inorganic colloids such as Fe oxyhydroxides or organic colloids. Fe may also be bioavailable in particulate forms such as amorphous Fe oxide coatings. Photochemical reduction of Fe(III) is noted by the pathways with hν next to the reaction arrow. The source and identification (?) of the ligands for Fe in seawater are not known, but they may be cell degradation products (e.g., porphyrin-type ligands) or be produced by organisms to specifically bind Fe (e.g., siderophore ligands). Not shown in this figure is the role of Fe(II) ligands, the various mechanisms for Fe transport across the cell membrane, or bacteria or colonies living on particles and creating micro-environments that enhance Fe solubilization. See text for more discussion. Reviews of the potential pathways for Fe utilization can be found in Sunda (2001) and Moffet (2001).

colloidal iron oxides and enhanced biological Fe uptake have been observed in laboratory cultures (BARBEAU and MOFFETT, 2000). Also, it is hypothesized that naturally occurring Fe ligand complexes may also be photochemically labile (MOFFETT, 2001). Another mechanism by which labile Fe may be released from colloidal or particulate phases is through phagotrophy (ingestion) followed by release of Fe within the acidic, reducing microenvironments (BARBEAU et al., 1996; BARBEAU and MOFFETT, 1998; BARBEAU and MOFFETT, 2000). It has also been suggested that Fe (III) bound to a colloid or an organic ligand may be reduced to Fe(II) upon contact with the cell membrane (MALDONADO and PRICE, 2001; CHEN et al., 2003). Several pathways of Fe utilization in the marine environment are plausible and many are supported by some evidence. However, which pathways are used and the extent to which these pathways occur in natural systems need to be understood in order to fully evaluate the role of Fe in the biological cycle. Also because biological cycling is a significant player in the distribution of Fe in the ocean, there is likely a feedback between these mechanisms and Fe concentrations and speciation.

In summary, the solubility of aerosol Fe, the residence time of Fe in both the surface and deep ocean, Fe uptake and utilization mechanisms, and the distributions of Fe in the ocean all need to be better constrained in order to evaluate the role of Fe in the biological pump of the ocean. Also, a significant fraction of operationally "dissolved" Fe in the ocean is colloidal. In order to assess the role of colloidal Fe in the cycling of Fe in the ocean, we need to study the distribution, biogeochemical cycling, and biological utilization of colloidal and soluble Fe and how these two pools interact.

1.2. IRON ISOTOPES

Stable isotope variations yield invaluable insights into processes in the environment, such as the use of carbon isotopes to investigate carbon assimilation pathways (HAYES, 1993) and nitrogen isotopes to quantify nitrate utilization in the upper ocean (FRANCOIS et al., 1997; SIGMAN et al., 1999). There are four stable isotopes of Fe, ^{54}Fe, 5.84%; ^{56}Fe, 91.76%; ^{57}Fe, 2.12%; and ^{58}Fe 0.28% (TAYLOR et al., 1992), with a

relative mass difference of 7% from ^{54}Fe to ^{58}Fe. Significant fractionations (up to 10‰ in $\delta^{56}Fe$) of Fe isotopes are predicted to occur between Fe phases that are common in natural systems including fractionation between Fe(II) and Fe(III) aquo-complexes (POLYAKOV, 1997; SCHAUBLE et al., 2001; ANBAR et al., submitted). Iron isotope measurements in this thesis are reported in delta notation (‰) based on the $^{56}Fe/^{54}Fe$ ratio where the standard is the mean of igneous rock samples.

$$\delta^{56}Fe\ (‰) = \left(\frac{^{56}Fe/^{54}Fe_{sample}}{^{56}Fe/^{54}Fe_{standard}} - 1 \right) \times 1000$$

Isotopic fractionation is dependent on both equilibrium processes (e.g., temperature and phase changes) and kinetic fractionation (e.g., enzymatic pathways). The biogeochemical cycling of Fe in the environment is very complicated; Fe is subject to redox cycling, photochemical reduction, adsorption and desorption on surfaces, biological utilization, mineral formation, and chemical and biological leaching from mineral sources. With such active chemistry, interpreting $\delta^{56}Fe$ variations in nature requires a background in the mechanistic studies of Fe isotope fractionation.

Although the field of Fe isotope analysis is very young (late 1990s), there are several laboratory studies that have investigated both biological and inorganic fractionations (Table 1.1). The strongest evidence for biological fractionation comes from laboratory culture experiments of Fe reducing bacteria ($4Fe^{+3} + H_2O + \text{“}CH_2O\text{”} \rightarrow CO_2 + 4Fe^{+2} + 4H^+$). Microbially reduced Fe is depleted in $\delta^{56}Fe$ (-1.3‰) relative to the Fe(III) substrate (BEARD et al., 1999; BEARD et al., 2003a; ICOPINI et al., 2004). A variety of Fe(III) substrates have been used including ferrihydrite, hematite, and goethite. Icopini et al. (2004) also added an electron shuttle to cultures and observed the same isotopic depletion in the Fe(II) product suggesting that the Fe fractionation is not related to the kinetics of electron transfer. Anaerobic photosynthetic oxidation of Fe(II) also generates products that are isotopically depleted (-1.5‰) (CROAL et al., in press). In contrast, magnetotactic bacteria produce magnetite that is isotopically the same as the

Table 1.1: Summary of Laboratory Process Studies of Iron Isotope Fractionation			
Study	**description**	**direction of fractionation**	$\Delta\delta^{56}Fe$ (‰)
Biotic:			
Bullen and McMahon, 1998	laboratory bacterial mediated Fe reduction in Fe(III) gel suspension	produced Fe(II) was 2 ‰ lighter than Fe(III) substrate	-2
Beard et al., 1999, 2003a; Icopini et al., 2004	laboratory bacterial mediated Fe reduction, bacteria growing on ferrihydrite	produced Fe(II) was 1.2 to 1.3 ‰ lighter than Fe(III) substrate	-1.3
Anbar et al., 1999, AGU	siderite formed by Fe-reducing bacteria in lab culture	siderite 0.4 ‰ lighter than starting material	-0.4
Bullen et al., 1999, AGU	magnetite formed by magnetotactic bacteria	indistinguishable from starting material	0
Mandernack et al., 1999	magnetite formed by magnetotactic bacteria	indistinguishable from starting material	0
Brantley et al., 2001	biotically enhanced leaching of hornblende	Fe released lighter than abiotically dissolved hornblende in same medium	-0.8
Croal et al., 2004	anaerobic photosynthetic Fe(II) oxidation	hydrous Fe(III)-oxide products lighter than $Fe(II)_{aq}$ starting material	-1.5
Abiotic			
Anbar et al., 2000	FeCl4- ion exchange column (Fe chloride species)	heavy Fe eluted from column faster than lighter Fe	
Bullen et al., 2001	$Fe(II)_{aq}$-ferrihydrite	dependent on solution chemistry (amount of aq. CO_2 present), precipitate heavy by 0.8 to 1.8 ‰	-0.8 to –1.8
Brantley et al., 2001	$Fe(II)_{aq}$-hornblende	organic leaching of hornblende; Fe released lighter	-0.6
Matthews et al., 2001	Fe(II)-bipyridine and FeCl4-fractionation	kinetic fractionation	
Johnson et al., 2002; Welch et al. (2003)	$Fe(II)_{aq}$- $Fe(III)_{aq}$ equilibrium fractionation	Fe(II) light, Fe(III) heavy	-2.9
Skulen et al., 2002	$Fe(III)_{aq}$-hematite kinetic precipitation of hematite over 12 hours	aqueous heavy, hematite light	+1.3
Skulen et al., 2002	$Fe(III)_{aq}$-hematite equilibration	aqueous light, hematite heavy	-0.1
Wiesli et al. , 2003	$Fe(II)_{aq}$-siderite	siderite light by 0.6 ‰	+0.6
Wiesli et al. 2003	$Fe(II)_{aq}$-green rust	green rust was heavy by 0.16 ‰	-0.16
Johnson et al. 2002; Welch et al. 2003	$Fe(II)_{aq}$-hematite	aqueous light, hematite heavy	-3
Bulter et al. 2003	$Fe(II)_{aq}$-FeS	aqueous heavy, FeS light	+0.3
Icopini et al., 2004	$Fe(II)_{adsorbed}$-goethite	In experiments where 1/3 of Fe(II) in solution with goethite adsorbed to goethite, remaining aqueous Fe(II) was depleted 0.8 ‰	-0.8

source Fe (MANDERNACK et al., 1999). Based on predicted fractionations between aqueous Fe and magnetitite, it has been suggested that the null fractionation observed in the magnetotactic bacterial cultures reflects kinetic isotope effects due to the rapid precipitation of magnetite by the bacteria (JOHNSON et al., 2004). Brantley et al. (2004) investigated enhanced dissolution of hornblende in experiments with siderophore-producing bacteria, which is likely a common path of dissolution of mineral Fe in soils. The Fe released in the biologically enhanced dissolution experiments was isotopically lighter (-0.8‰) than Fe released in inorganic abiotic leaching experiments.

In addition to large biological fractionations, significant abiotic fractionations of Fe have also been documented in laboratory studies (Table 1.1). Whether the observed fractionations are due to equilibrium or kinetic mechanisms is difficult to determine because obtaining and retaining equilibrium conditions in experiments can be difficult to prove. Isotopic equilibrium fractionation has been demonstrated by Johnson et al. (2002) and Welch et al. (2003) between Fe(II) and Fe(III) aquo-complexes. The Fe(II) species is isotopically lighter than Fe(III) species (-2.9‰). Their results agree well with theoretically predicted fractionation (SCHAUBLE et al., 2001; ANBAR et al., submitted), which lends support that the experiment reached and retained Fe(II)-Fe(III) isotopic equilibrium during the chemical separation of Fe(II) and Fe(III). Skulen et al. (2002) observed that rapidly precipitated hematite was isotopically light (-1.3‰). However, estimated equilibrium fractionation from experiments with lower precipitation rates was much smaller (-0.1‰). This experiment demonstrates how kinetic fractionation processes can mask equilibrium fractionation based on how the experiment is designed.

Several laboratory experiments have been designed to mimic and isolate mechanisms of isotopic fractionation observed in nature or in laboratory studies. Bullen et al. (2001) observed that ferrihydrite deposits from a hydrothermal spring were isotopically heavy compared to the aqueous Fe(II) in the spring water, and that the stream water and deposits became isotopically lighter downstream until most of the dissolved Fe had precipitated (Figure 1.4). Similar fractionations were reproduced in laboratory experiments by precipitation of Fe(II) in steady-state batch experiments, and results

followed a Rayleigh fractionation trend. From the observation that the precipitate was isotopically heavier than the reactant, Bullen et al. (2001) suggested that equilibrium fractionation between co-existing aqueous species might be responsible for the observed fractionation. Brantley et al. (2001) leached hornblende with organic chelators and found that released Fe was also isotopically depleted (-0.6‰) after observing isotopic fractionation (-0.8‰) in biologically enhanced dissolution of hornblende and no fractionation in abiotic dissolution (discussed above). A trend in δ^{56}Fe with the strength of the chelator was observed with more isotopically depleted Fe released by stronger ligands. The organic leaching experiments suggest that the fractionation observed in the biotically enhanced dissolution experiments may be due to the organic (siderophore) leaching step in the biotic experiments.

Many of the observed fractionations in laboratory studies are between aqueous Fe species and solid phases. Another important consideration for aqueous Fe and mineral interactions, which is also relevant to natural systems, is adsorption of the aqueous Fe onto mineral surfaces. Icopini et al. (2004) found that Fe(II) in solution was isotopically depleted (-0.8‰) after a significant fraction of the Fe(II) had adsorbed onto goethite.

Process studies are important for understanding the potential pathways of Fe isotope fractionation and the expected magnitudes and direction of isotopic fractionation in nature. A range of nearly 4‰ is observed for natural samples that are formed at the Earth's surface (Figure 1.4) (reviews: BEARD et al., 2003; BEARD AND JOHNSON, 2004). This is in contrast to the ultimate source of iron; igneous rock, which shows very little isotopic variability, ± 0.10‰ (2σ standard deviation) (BEARD et al., 2003a). Some of the largest variations observed in Fe isotopes are found in samples deposited or altered in the marine environment. Banded Iron Formations (BEARD and JOHNSON, 1999; JOHNSON et al., 2003) and organic-rich black shales (YAMAGUCHI et al., 2003; MATTHEWS et al., 2004) have δ^{56}Fe values spanning almost the entire observed range. The isotopically heaviest natural samples have been found in hydrothermally altered mid-ocean ridge basalts where >80% of the Fe has been leached from the basalt (ROUXEL et al., 2003). Vent fluids from mid-ocean ridge systems are isotopically light (-0.2 to -0.3‰)

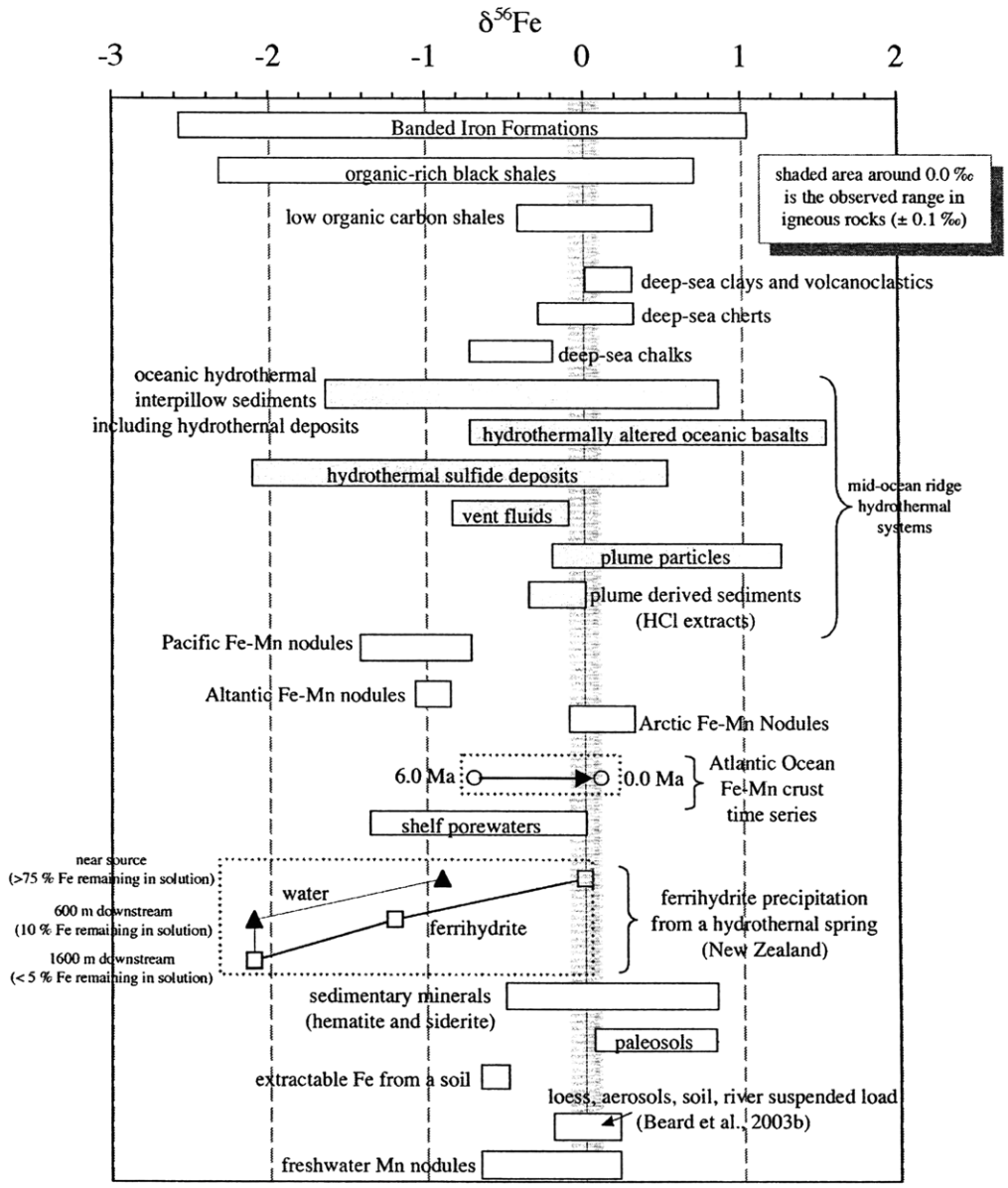

Figure 1.4: Compilation of observed Fe isotopic compositions of natural samples formed at the Earth's surface. Data sources are: Banded Iron Formation data from Beard and Johnson (1999) and Johnson et al. (2003); organic-rich black shale data from Yamaguchi et al. (2003) and Matthews et al. (2004); deep-sea sediment and hydrothermal deposit data from Rouxel et al. (2003, 2004); hydrothermal vent fluid data from Sharma et al. (2001), Beard et al. (2003b), and Severmann, et al. (in press); hydrothermal plume particle and plume derived sediment data from Severmann et al. (in press); Pacific, Atlantic, Arctic, and freshwater nodule data from Beard and Johnson (1999) and Beard et al. (1999); Shelf porewater data from Severmann et al. (2003); natural spring ferrihydrite data from Bullen et al. (2001); sedimentary mineral data from Belshaw et al. (2000); paleosol data from Zhu et al. (2000) and Arnold et al. (2004); extractable Fe from soil data from Brantley et al. (2001); summation of loess, aerosols, soil, and river suspended load taken from Beard et al. (2003b).

(SHARMA, 2001; BEARD et al., 2003b; SEVERMANN et al., in press) and may reflect preferential leaching of isotopically light Fe from the basalts. Fe-Mn nodules and crusts formed in the marine environment also have a large range in δ^{56}Fe values with values as light as -1.36‰ observed in the Pacific Ocean (BEARD and JOHNSON, 1999; ZHU et al., 2000; CHU et al., 2003). Two time-series of Fe isotopes have been reconstructed using Fe-Mn crusts and nodules from the marine environment. Zhu et al. (2000) observed a trend of increasing δ^{56}Fe values towards the present over the last 6 Ma in a crust from the North Atlantic. Variations in δ^{56}Fe values with time were also observed in a Fe-Mn nodule in the Pacific near hydrothermal inputs (CHU et al., 2003). If the Fe deposited in Fe-Mn crusts and nodules precipitated from seawater and has not been diagenetically altered, then these records might serve as a proxy for the Fe isotopic composition of the deep ocean. However, an understanding of the mechanisms that control the iron isotopic composition of the seawater and deposition of Fe isotopes in Fe-Mn crusts is necessary to interpret the Fe isotope records.

Although it is thought that most of the fractionation in the environment occurs in the aqueous and biological phases, only a few studies report δ^{56}Fe values for aqueous iron isotopes in natural systems and non-laboratory biological samples. As stated before, Fe from mid-ocean ridge hydrothermal vents is isotopically depleted relative to igneous sources (-0.2 to -0.7‰) (SHARMA, 2001; BEARD et al., 2003b; SEVERMANN et al., in press). Porewater Fe from the California margin shows isotopic variability with observed isotopic values as light as -1.3 ‰ (SEVERMANN et al., 2003). A terrestrial hot spring Fe(III) deposit was +0.9‰ heavier than the dissolved Fe(II) (-0.9 to +2.1‰) from which it precipitated (BULLEN et al., 2001). Human blood and haemoglobin from animals are also isotopically variable and depleted compared with dietary sources (WALYCZYK and VON BLANCKENBURG, 2002; ZHU et al., 2002; OHNO et al., 2004).

Iron isotopic studies are early in their development; therefore few studies are conclusive about the controls of iron isotope fractionation in the environment. However, they demonstrate that there are measurable fractionations and some observable trends in the data. The challenge now is to use the observed Fe isotope fractionations in nature to

obtain information about Fe cycling in the environment. The variability of $\delta^{56}Fe$ observed in marine deposits suggests that Fe isotopes may be a powerful tool to study Fe cycling in the marine system. Also, laboratory experiments have shown that redox changes, organic leaching, and biological cycling can all lead to Fe isotopic fractionation. The cycle of Fe in the ocean was shown in Figure 1.1 and potential pathways for biological Fe uptake and utilizaion were shown in Figure 1.3. It seems likely from all these pathways, that Fe isotopic fractionation occurs in the marine system. In order to illustrate this, two hypothetical applications of Fe isotopes in the upper ocean are shown in Figure 1.4 and discussed below. The first is a steady-state model and the second is a model based on Rayleigh fractionation.

Over certain time periods and conditions, steady-state assumptions might be applicable to the upper ocean Fe cycle (e.g., oligotropic gyres). A schematic of this model is shown in Figure 1.5a. A question that might be addressed with a steady-state model of Fe in the upper open ocean is what fraction of aerosol iron becomes bioavailable. The main inputs of iron to the upper ocean are from the dissolution of atmospheric dust and the upwelling/vertical mixing of nutrient rich waters from below the euphotic zone. The major output of iron is through biogenic export and scavenging onto particulate material. If lateral and downward mixing are neglected, a simple isotopic mass balance can be made where the flux of dissolved Fe from atmospheric deposition (F_{atm} and $\delta^{56}Fe_{atm}$) plus the flux of Fe from upward mixing (F_{up} and $\delta^{56}Fe_{up}$) equals the flux of the exported material excluding the refractory dust (F_{exp} and $\delta^{56}Fe_{exp}$). Therefore an isotopic mass balance can written:

$$F_{atm} = F_{up}*(\delta^{56}Fe_{exp} - \delta^{56}Fe_{up})/(\delta^{56}Fe_{atm} - \delta^{56}Fe_{exp})$$

If all of the $\delta^{56}Fe$ values are measured and the F_{up} estimated from nitrate upwelling and Fe:NO_3 ratios in the water below the euphotic zone, then F_{atm} can be solved for. Or one could make an independent estimate F_{atm} using the dissolved Fe input values of Duce and Tindale (1991) or Fung et al. (2000) and solve for F_{up}. Also, if the $\delta^{56}Fe$ of the mixed layer could then be estimated based on dissolved seawater samples or biomass, and the $\delta^{56}Fe_{exp}$ and $\delta^{56}Fe_{atm}$ were known, F_{up} and F_{atm} could be solved for directly. In order to

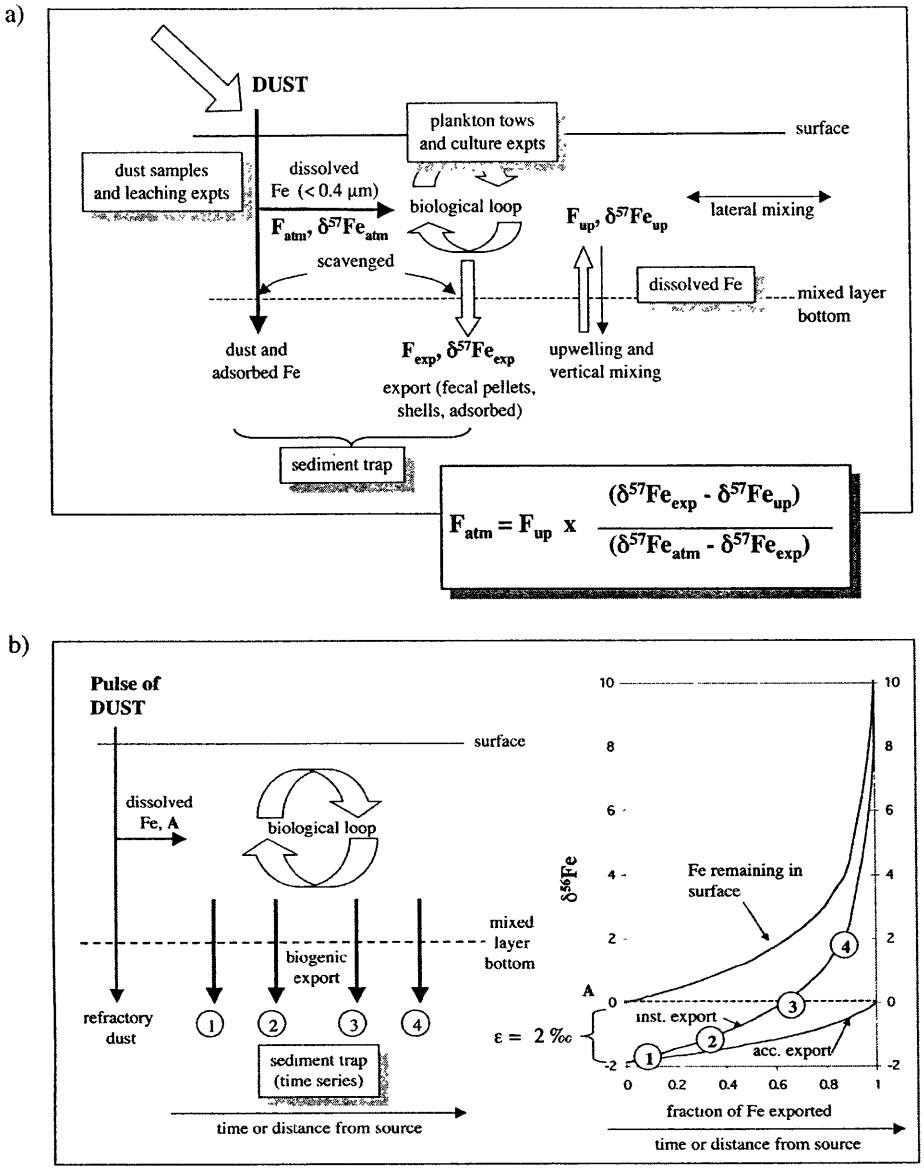

Figure 1.5: 1.5a) Hypothetical schematic of a steady state model for a Fe isotope application in the upper open ocean. The shadowed boxes highlight the type of samples that should be collected and measured for iron concentration and isotopic analysis. 1.5b) Hypothetical schematic of how Rayleigh fractionation could control the $\delta^{56}Fe$ of different pools of Fe in the upper ocean. This model assumes a pulse of dust as the primary source of Fe to a region of the upper ocean. Iron is taken up by organisms and isotopically fractionated with an assumed fractionation of -2‰. As Fe is removed from surface waters over time by biologic export, the dissolved pool in the upper ocean becomes heavier. The graph shows the link between the fraction of the Fe from the pulse removed from the surface ocean and the $\delta^{56}Fe$ of the remaining Fe in the mixed layer, the instantaneous export material, and the accumulated export. Material collected in sediment traps would reflect some combination of the instantaneous and accumulated products. This type of fractionation might also be observed as one moved laterally away from a source of iron (upwelling).

estimate fluxes, $\delta^{56}Fe_{up}$ and $\delta^{56}Fe_{atm}$ need to be measurably different. This steady state model could yield in situ estimates of dissolved Fe input from atmospheric deposition, which would serve as checks against other estimates based on dust leaching experiments.

Another possible scenario for Fe fractionation in the upper ocean is based on Rayleigh fractionation in response to Fe utilization by organisms in the upper ocean, analogous to the use of $\delta^{15}N$ for nitrate utilization (FRANCOIS et al., 1997; SIGMAN et al., 1999). Two possible questions this model might address are 1) what is the relationship between a dust event and Fe utilization, and 2) what is the residence time of Fe in the surface ocean. If Fe input to the upper ocean is episodic (dust events) or local (upwelling), the Fe will then be taken up by organisms and removed through biological export. This loss of Fe from the euphotic zone will result in decreasing amounts of bioavailable Fe over time in response to a pulse source of Fe such as a dust event (or over space as a water mass moves away from the source of dissolved Fe). If there is fractionation of Fe isotopes by phytoplankton during uptake (preferentially taking up the lighter Fe isotopes) and isotopically light Fe is removed through biological export, this would lead the remaining pool of dissolved Fe in the euphotic zone becoming isotopically heavier (Figure 1.5b). Surface iron ($\delta^{56}Fe_{surface}$) would follow the following equation:

$$\delta^{56}Fe_{surface} = \delta^{56}Fe_{source} - \varepsilon \ln(f)$$

where $\delta^{56}Fe_{source}$ is the isotopic value of the source of the dissolved Fe (value A in Figure 1.5b, set to 0‰), ε is the fractionation associated with biological uptake of Fe (set to 2‰ in Figure 1.5b), and f is the fraction of Fe removed from the surface water (Fe utilization). Exported material will get heavier as Fe utilization increases. It is likely that Rayleigh fractionation behavior does exist for Fe isotopes in regions of highly episodic dust flux or seasonal upwelling. If iron utilization trends exist in nature, they could be correlated with dust flux, productivity, and export for different regions of the ocean. With these data, quantitative relationships could be defined between bioavailable Fe and dust flux, along with residence times of Fe in different regions of the upper ocean. $\delta^{56}Fe$ in particulate-bound Fe collected in sediment traps might also be useful to delineate

between Fe-limited and Fe-replete environments, such as the hypothesized difference between recent and glacial conditions in the Southern Ocean.

1.3. THESIS OUTLINE

This thesis offers several new insights into the biogeochemical cycling of Fe and Fe isotopes in the marine environment. First, detailed profiles and transects of dissolved, colloidal, and soluble Fe in the subtropical and tropical Atlantic Ocean are presented in Chapter 2. Surface DFe concentrations reflect variations in dust deposition over the region sampled. Dissolved Fe profiles generally have nutrient-type profiles, although the profiles have interesting features deviating from classic nutrient-type profiles with surface maxima, intermediate water minima and maxima, and variations clearly associated with water masses. The residence time of dissolved Fe in both the surface and deep ocean was estimated from observations. Detailed profiles of soluble and colloidal Fe extend the work of Wu et al. (2000) and demonstrate that the two pools of Fe have distinct profiles suggesting different biogeochemical behavior. In Chapter 3, aerosol Fe solubility is estimated using natural seawater and freshly collected aerosols from the North Pacific. The next three chapters investigate Fe isotopes in aqueous and biological samples in the environment. First, a method for Fe isotopic measurement was developed on the MIT GV Instruments IsoProbe MC-ICPMS (Chapter 4). Because of the small sample size processed for many marine samples, accuracy and precision on low-level samples needed to be addressed including matrix effects, instrumental mass bias stability, and isobaric interferences. Using the methods discussed in Chapter 4, the Fe isotopic composition of marine plankton tow samples and an aerosol leachate were investigated (Chapter 5). Large variations in the δ^{56}Fe of plankton tow samples were observed with δ^{56}Fe values generally depleted (by up to $\approx 4‰$). One plankton tow was collected in Amazon River plume water in the eastern Atlantic Ocean and had a depleted δ^{56}Fe value. In order to interpret the δ^{56}Fe of this plankton tow, knowledge of the isotopic composition of the source of Fe was needed (Amazon River and shelf region). In Chapter 6, a variety of samples from the Amazon system were analyzed for δ^{56}Fe including filtered river

water, suspended sediment from the river water, and an Amazon shelf porewater. River water-seawater mixing experiments were also performed to investigate potential fractionation during flocculation of Fe in the estuary. Chapter 5 and 6 demonstrate that aqueous and biological samples in the environment have measurable ranges in $\delta^{56}Fe$ and might be useful in understanding the Fe cycle.

References for Chapter 1

Anbar A. D., Arnold G. L., Rye R., and Weyer S. (2002) Iron isotopes in an Archean paleosol. *Geochimica et Cosmochimica Acta* **66**(15A), A18-A18.

Anbar A. D., Jarzecki A., and Spiro T. (submitted) Theoretical investigation of equilibrium iron isotope fractionation between $Fe(H2O)_6^{+2}$ and $Fe(H2O)_6^{+3}$. *Geochimica et Cosmochimica Acta.*

Anbar A. D., Roe J. E., Barling J., and Nealson K. H. (2000) Nonbiological fractionation of iron isotopes. *Science* **288**(5463), 126-128.

Anbar A. D., Roe J. E., Holman E. S., Barling J., and Zhuang C. (1999) Biotic and abiotic fractionations of iron isotopes. *AGU Abstracts with Programs* **1999 AGU Fall Meeting**(B32A-20).

Archer D. E. and Johnson K. (2000) A model of the iron cycle in the ocean. *Global Biogeochemical Cycles* **14**, 269-279.

Arnold G. L., Weyer S., and Anbar A. D. (2004) Fe isotope variations in natural materials measured using high mass resolution multiple collector ICPMS. *Analytical Chemistry* **76**(2), 322-327.

Barbeau K. and Moffett J. W. (1998) Dissolution of iron oxides by phagotropic protists: using a novel method to quantify reaction rates. *Environmental Science and Technology* **32**, 2969-2975.

Barbeau K. and Moffett J. W. (2000) Laboratory and field studies of colloidal iron oxide dissolution as mediated by phagotrophy and photolysis. *Limnology and Oceanography* **45**, 827-835.

Barbeau K., Moffett J. W., Caron M. A., Croot P. L., and Erdner D. L. (1996) Role of protozoan grazing in relieving iron limitation of phytoplankton. *Nature* **380**, 61-64.

Beard B. L. and Johnson C. L. (1999) High precision iron isotope measurements of terrestrial and lunar materials. *Geochimica et Cosmochimica Acta* **63**, 1653-1660.

Beard B. L., Johnson C. L., Cox L., Sun H., Nealson K. H., and Aguilar C. (1999) Iron isotope biosignatures. *Science* **285**, 1889-1892.

Beard B. L., Johnson C. M., Skulen K. H., Nealson K. H., Cox L., and Sun H. (2003a) Application of Fe isotopes to tracing the geochemical and biological cycling of Fe. *Chemical Geology* **195**, 87-117.

Beard B. L., Johnson C. M., Von Damm K. L., and Poulson R. (2003b) Iron isotope constraints on Fe cycling and mass balanced oxygenated Earth. *Geology* **31**, 629-632.

Belshaw N. S., Zhu X. K., Guo Y., and O'Nions R. K. (2000) High precision measurement of iron isotopes by plasma source mass spectrometry. *International Journal of Mass Spectrometry* **197**, 191-195.

Bonnet S. and Guieu C. (2004) Dissolution of atmospheric iron in seawater. *Geophysical Research Letters* **31**, LO3303.

Boyd P. W., Law C. S., Wong C. S., Nojiri Y., Tsuda A., Levasseur M., Takeda S., Rivkin R., Harrison P. J., Strzepek R., Gower J., McKay R. M., Abraham E., Arychuk M., Barwell-Clarke J., Crawford W., Crawford D., Hale M., Harada K.,

Johnson K., Kiyosawa H., Kudo I., Marchetti A., Miller W., Needoba J., Nishioka J., Ogawa H., Page J., Robert M., Saito H., Sastri A., Sherry N., Soutar T., Sutherland N., Taira Y., Whitney F., Wong S. K. E., and Yoshimura T. (2004) The decline and fate of an iron-induced subarctic phytoplankton bloom. *Nature* **428**(6982), 549-553.

Boyd P. W., Watson A. J., Law C. S., Abraham E. R., Trull T., Murdoch R., Bakker D. C. E., Bowie A. R., Buesseler K. O., Chang H., Charette M., Croot P., and al e. (2000) A mesoscale phytoplankton bloom in the polar Southern Ocean stimulated by iron fertilization. *Nature* **407**, 695-702.

Boyle E. A. (1997) What controls dissolved iron concentrations in the world ocean - a comment. *Marine Chemistry* **57**, 163-167.

Boyle E. A., Bergquist B. A., and Kayser R. (submitted) Iron, manganese, and lead at Hawaii Ocean Time Series Station ALOHA: temporal variability and an intermediate water hydrothermal plum. *Geochimica et Cosmochimica Acta.*

Brantley S. L., Liermann L., and Bullen T. D. (2001) Fractionation of Fe isotopes by soil microbes and organic acids. *Geology* **29**(6), 535-538.

Brantley S. L., Liermann L., Wu S., and Bullen T. D. (1999) Concentration and isotopic signature of trace metal release during abiotic and biotic dissolution of hornblende. *AGU Abstracts with Programs, 1999 AGU Fall Meeting*, H521-03.

Bruland K. W., Orians K. J., and Cowen J. P. (1994) Reactive trace metals in the stratified central North Pacific. *Geochimica et Cosmochimica Acta* **58**, 3171-3182.

Bruland K. W. and Rue E. L. (2001) Analytical methods for the determination of concentrations and speciation of iron. In *The Biogeochemistry of Iron in Seawater*, Vol. 7 (ed. K. A. Hunter and D. Turner), pp. 255-289. John Wiley & Sons, Ltd.

Buesseler K. O., Andrews J. E., Pike S. M., and Charette M. A. (2004) The effects of iron fertilization on carbon sequestration in the Southern Ocean. *Science* **304**, 414-417.

Bullen T. D. and McMahon P. M. (1998) Using stable isotopes to assess microbially-mediated Fe^{+3} reduction in a jet-fuel contaminated aquifer. *Mineralogical Magazine* **62A**, 255-256.

Bullen T. D., White A. F., Childs C. W., Vivit D. V., and Schulz M. S. (2001) Demonstration of significant abiotic iron isotope fractionation in nature. *Geology* **29**(8), 699-702.

Butler I. P., Archer C., Rickard D., Vance D., and Oldroyd A. (2003) Fe isotope fractionation during Fe(II) monosulfide precipitation from aqueous Fe solutions at pH 8 and ambient temperature. *Geochimica et Cosmochimica Acta* **67**, A51.

Chen M., Dei R. C. H., Wang W., and Guo L. (2003) Marine diatom uptake of iron bound with natural colloids of different origins. *Marine Chemistry* **81**, 177-189.

Chu N. C., Johnson C. M., Beard B. L., German C. R., Nesbitt R. W., and Usui A. (2003) Secular Fe isotope variations in the NW and Central Pacific Ocean. *Geochimica et Cosmochimica Acta* **67**, A66.

Coale K. H., Johnson K. S., Chavez F. P., Buesseler K. O., Barber R. T., Brzezinski M. A., Cochlan W. P., Millero F. J., Falkowski P. G., Bauer J. E., Wanninkhof R. H.,

Kudela R. M., Altabet M. A., Hales B. E., Takahashi T., Landry M. R., Bidigare R. R., Wang X. J., Chase Z., Strutton P. G., Friederich G. E., Gorbunov M. Y., Lance V. P., Hilting A. K., Hiscock M. R., Demarest M., Hiscock W. T., Sullivan K. F., Tanner S. J., Gordon R. M., Hunter C. N., Elrod V. A., Fitzwater S. E., Jones J. L., Tozzi S., Koblizek M., Roberts A. E., Herndon J., Brewster J., Ladizinsky N., Smith G., Cooper D., Timothy D., Brown S. L., Selph K. E., Sheridan C. C., Twining B. S., and Johnson Z. I. (2004) Southern ocean iron enrichment experiment: Carbon cycling in high- and low-Si waters. *Science* **304**(5669), 408-414.

Coale K. H., Johnson K. S., Fitzwater S. E., Gordon R. M., Tanner S., Chavez F. P., Ferioli L., Sakamoto C., Rogers P., and Millero F., Steinberg, P., Nightingale, P., Cooper, D., Cochlan, W.P., Landry, M.R., Constantinou, J., Rollwagen, G., Trasvina, A., Kudela, R. (1996) A massive phytoplankton bloom induced by an ecosystem-scale iron fertilization experiment in the equatorial Pacific Ocean. *Nature* **383**, 495-501.

Croal L. R., Johnson C. M., Beard B. L., and Newman D. K. (in press) Iron isotope fractionation by Fe(II)-oxidizing photoautotrophic bacteria. *Geochimica et Cosmochimica Acta.*

de Baar H. J. W. and de Jong J. T. M. (2001) Distributions, sources and sinks of iron in seawater. In *The Biogeochemistry of Iron in Seawater*, Vol. 7 (ed. K. A. Hunter and D. Turner), pp. 123-253. John Wiley & Sons, Ltd.

de Baar H. J. W., de Jong J. T. M., Notling R. F., Timmermans K. R., van Leeuwe M. A., Bathmann U., van der Loeff M. R., and Sildman J. (1999) Low dissolved Fe and the absence of diatom blooms in the remote Pacific waters of the Southern Ocean. *Marine Chemistry* **66**, 1-34.

Duce R. A. and Tindale N. W. (1991) Atmospheric transport of iron and its deposition in the ocean. *Limnology and Oceanography* **36**, 1715-1726.

Falkowski P. G. (1998) Evolution of the nitrogen cycle and its influence on the biological sequestration of CO_2 in the ocean. *Nature* **387**, 272-275.

Francois R. F., Altabet M. A., Yu E. F., Sigman D. M., Bacon M. P., Frank M., Bohrmann G., Bareille G., and Labeyrie L. D. (1997) Water column stratification in the Southern Ocean contributed to the lowering of glacial atmospheric CO_2. *Nature* **389**, 929-935.

Fung I. Y., Meyn S. K., Tegen I., Doney S. C., John J. G., and Bishop K. B. (2000) Iron supply and demand in the upper ocean. *Global Biogeochemical Cycles* **14**, 281-295.

Gao Y., Kaufman Y. J., Tanre D., Kolber D., and Falkowski P. G. (2001) Seasonal distributions of aeolian iron fluxes to the global ocean. *Geophysical Research Letters* **28**, 29-32.

Gledhill M. and van den Berg C. M. G. (1994) Determination of complexation of iron(III) with natural organic complexing ligands in seawater using cathodic stripping voltammetry. *Marine Chemistry* **47**, 41-54.

Granger J. and Price N. M. (1999) Importance of siderophores in iron nutrition of heterotrophic marine bacteria. *Limnology and Oceanography* **44**, 541-555.

Gregg W. W., Ginoux P., Schopf P. S., and Casey N. W. (2003) Phytoplankton and iron: validation of a global three-dimensional ocean biogeochemical model. *Deep-Sea Research II* **50**, 3143-3169.

Hayes J. (1993) Factors controlling the ^{13}C contents of sedimentary organic compounds. *Marine Geology* **113**, 111-125.

Hudson R. J. M. and Morel F. M. M. (1990) Iron transport in marine phytoplankton: kinetics of cellular and medium coordination reactions. *Limnology and Oceanography* **35**, 1002-1020.

Hutchins D. A. and Bruland K. W. (1998) Iron-limited diatom growth and Si : N uptake ratios in a coastal upwelling regime. *Nature* **393**(6685), 561-564.

Hutchins D. A., Witter A. E., Butler A., and Luther G. W. (1999) Competition among marine phytoplankton for different chelated iron species. *Nature* **400**, 858-861.

Icopini G. A., Anbar A. D., Ruebush S. S., Tien M., and Brantley S. L. (2004) Iron isotope fractionation during microbial reduction of iron: the importance of adsorption. *Geology* **32**, 205-208.

Jickells T. D. and Spokes L. J. (2001) Atmospheric iron inputs to the oceans. In *The Biogeochemistry of Iron in Seawater*, Vol. 7 (ed. K. A. Hunter and D. Turner), pp. 85-121. John Wiley & Sons, Ltd.

Johnson C. M., Beard B. L., Beukes C., Klein C., and O'Leary J. M. (2003) Ancient geochemical cycling in the Earth as inferred from Fe isotope studies of banded iron formations from Transvaal Craton. *Contributions to Mineral Petrology* **144**, 523-547.

Johnson C. M., Beard B. L., Roden E. E., Newman D. K., and Nealson K. H. (2004) Isotopic constraints on the biogeochemical cycling of Fe. In *Geochemistry of Non-Traditional Stable Isotopes.*, Vol. 55 (ed. C. M. Johnson, B. L. Beard, and F. Albarede), pp. 359-408. The Mineralogical Society of America.

Johnson C. M., Skulan J. L., Beard B. L., Sun H., Nealson K. H., and Braterman P. S. (2002) Isotopic fractionation between Fe(III) and Fe(II) in aqueous solutions. *Earth and Planetary Science Letters* **195**(1-2), 141-153.

Johnson K. S., Gordon R. M., and Coale K. H. (1997) What controls dissolved iron concentrations in the world ocean. *Marine Chemistry* **57**, 137-161.

Karl D. M., Letelier R. D., Tupas L., Dore J., Christian J., and Hebel D. (1997) The role of nitrogen fixation in biogeochemical cycling in the subtropical North Pacific Ocean. *Nature* **388**, 533-537.

Kuma K., Nishioka J., and Matsunaga K. (1996) Controls on the iron(III) hydroxide solubility in seawater: the influences of pH and natural organic chelators. *Limnology and Oceanography* **41**, 396-407.

Kumar N., Anderson R. F., Mortlock R. A., Froelich P. N., Kubik P., Dittrich-Hannon B., and Suter M. (1995) Increased biological productivity and export production in the glacial Southern Ocean. *Nature* **378**, 675-680.

Lefevre N. and Watson A. J. (1999) Modeling the geochemical cycle of iron in the oceans and its impact on atmospheric CO_2 concentrations. *Global Biogeochemical Cycles* **13**, 727-736.

Letelier R. M. and Karl D. M. (1996) The role of Trichodesmium spp. in the productivity of the subtropical North Pacific. *Marine Ecology Progress Series* **57**, 173-179.

Luther G. W. I. and Wu J. (1997) What controls dissolved iron concentrations in the world ocean? – A comment. *Marine Chemistry* **57**, 173-179.

Mahowald N., Kohfeld K., Hansson M., Balkanski Y., Harrison S. P., Prentice I. C., Schulz M., and Rodhe H. (1999) Dust sources and deposition during the last glacial maximum and current climate: a comparison of model results with paleodata from ice cores and marine sediments. *Journal of Geophysical Research* **104**, 15895-15916.

Maldonado M. T. and Price N. B. (2001) Reduction and transport of organically bound iron by Thalassiosira oceanica. *Journal of Phycology* **37**, 298-310.

Mandernack K. W., Bazylinski D. A., Shanks W. C., and Bullen T. D. (1999) Oxygen and iron isotope studies of magnetite produced by magnetotactic bacteria. *Science* **285**(5435), 1892-1896.

Marcrellis H. M., Trick C. G., Rue E. L., Smith G., and Bruland K. W. (2001) Collection and detection of natural iron-binding ligands from seawater. *Marine Chemistry* **76**, 175-187.

Martin J. H. (1990) Glacial-interglacial CO_2 change: the iron hypothesis. *Paleoceanography* **5**, 1-13.

Martin J. H., Coale K. H., Johnson K. S., Fitzwater S. E., Gordon R. M., and Tanner S. J., Hunter, C.N., Elrod, V.A., Nowicki, J.L., Coely, T.L., Barber, R.T., Lindley, S., Watson, A.J., van Scoy, K., Law, C.S., Liddicoat, M.I., Ling, R., Stanton, T., Stockel, J., Collins, C., Anderson, A., Bidigare, R., Ondrusek, M., Latasa, M., Millero, F.J., Lee, K., Yao, W., Zhang, J.Z., Friederich, G., Sakamoto, C., Chevez, F., Buck, K., Kolber, Z., Greene, R., Falkowski, P., Chisholm, S.W., Hoge, F., Swift, R., Yungel, J., Turner, S., Nightingale, P., Hatton, A., Liss, P., Tindale, N.W. (1994) Testing the iron hypothesis in ecosystems of the equatorial Pacific Ocean. *Nature* **371**, 123-129.

Martin J. H. and Fitzwater S. E. (1988) Iron deficiency limits phytoplankton growth in the north-east Pacific subarctic. *Nature* **331**, 341-343.

Martin J. H., Fitzwater S. E., and Gordon R. M. (1990) Iron deficiency limits phytoplankton growth in Antarctic waters. *Global Biogeochemical Cycles* **4**, 5-12.

Matthews A., Morgans-Bell H. S., Emmanuel S., Jenkyns H. C., Erel Y., and Halicz L. (2004) Controls on iron-isotope fractionation in organic-rich sediments. *Geochimica et Cosmochimica Acta*, in press.

Matthews A., Zhu X. K., and O'Nions K. (2001) Kinetic iron stable isotope fractionation between iron (II) and iron (III) complexes in solution. *Earth and Planetary Science Letters* **192**, 81-92.

Michaels A. F., Olson D., Sarmiento J. L., Ammerman J. W., Fanning K., Jahnke R., Knap A. H., Lipschultz F., and Prospero J. M. (1996) Inputs, losses and transformation of nitrogen and phosphorus in the pelagic North Atlantic Ocean. *Biogeochemistry* **35**, 181-226.

Millero F. J. (1998) Solubility of Fe III in seawater. *Earth and Planetary Science Letters* **154**, 323-329.

Moffett J. W. (2001) Transformations Among Different Froms of Iron in the Ocean. In *The Biogeochemistry of Iron in Seawater*, Vol. 7 (ed. K. A. Hunter and D. Turner), pp. 343-372. John Wiley & Sons, Ltd.

Ohno T., Kouge I., and Hirata T. (2004) Iron isotopes in human blood. *Geochimica et Cosmochimica Acta* **66**(15A), A569-A569.

Parekh P., Follows M. J., and Boyle E. A. (2004) Modeling the global ocean iron cycle. *Global Biogeochemical Cycles* **18**(GB1002), 1-15.

Parekh P., Follows M. J., and Boyle E. A. (submitted) Decoupling of iron and phosphate in the global ocean. *Global Biogeochemical Cycles.*

Polyakov V. B. (1997) Equilibrium fractionation of the iron isotopes: Estimation from Mossbauer spectroscopy data. *Geochimica et Cosmochimica Acta* **61**(19), 4213-4217.

Powell R. and Donat J. (2001) Organic complexation and speciation of iron in the South and Equatorial Atlantic. *Deep-Sea Research Part II* **48**, 2877-2893.

Ried R. T., Live D. H., Faulkner D. J., and Butler A. (1993) A siderophore from a marine bacterium with an exceptional ferric ion affinity constant. *Nature* **366**, 455-458.

Rouxel O., Dobbek N., Ludden J., and Fouquet Y. (2003) Iron isotope fractionation during oceanic crust alteration. *Chemical Geology* **202**(1-2), 155-182.

Rouxel O., Fouquet Y., and Ludden J. N. (2004) Subsurface processes at the Lucky Strike hydrothermal field, Mid-Atlantic Ridge: evidence from sulfur, selenium, and iron isotopes. *Geochimica et Cosmochimica Acta* **68**, 2295-2311.

Rue E. L. and Bruland K. W. (1995) Complexation of iron(III) by natural ligands in the central North Pacific as determined by a new competitive ligand equilibrium/adsorptive cathodic stripping voltammetric method. *Marine Chemistry* **50**, 117-138.

Rueter J. G. and Ades D. R. (1987) The role of iron nutrition in photosynthesis and nitrogen assimilation in Scenedesmus quadeicauda (Chlorophyceae). *Journal of Phycology* **23**, 452-457.

Sarthou G., Baker A. R., Blain S., Achterberg E. P., Boye M., Bowie A. R., Croot P., Laan P., de Baar H. J. W., Jickells T. D., and Worsfold P. J. (2003) Atmospheric iron deposition and sea-surface dissolved iron concentrations in the eastern Atlantic Ocean. *Deep-Sea Research I* **50**, 1339-1352.

Schauble E. A., Rossman G. R., and Taylor H. P. (2001) Theoretical estimates of equilibrium Fe-isotope fractionations from vibrational spectroscopy. *Geochimica et Cosmochimica Acta* **65**(15), 2487-2497.

Severmann S., Johnson C. M., Beard B. L., German C. R., Edmonds H. N., Chiba H., and Green D. H. (in press) Origin of the Fe isotope composition of the oceans as inferred by Rainbow vent site, Mid-Atlantic Ridge, 36deg14'N. *Earth and Planetary Science Letters.*

Severmann S., McManus J., Johnson C. M., and Beard B. L. (2003) Iron isotope geochemistry in California Margin sediments and porewaters. *Eos Trans. AGU, Ocean Science Meeting Supplement* **84**, Abstract#OS31L-019.

Sharma. (2001) Iron isotopes in hot springs along the Juan de Fuca Ridge. *Earth and Planetary Science Letters* **194**, 39-51.

Sigman D. M., Altabet M. A., Francois R., McCorkle D. C., and Gaillard J.-F. (1999) The isotopic composition of diatom-bound nitrogen in Southern Ocean sediments. *Paleoceanography* **14**, 118-134.

Sigman D. M. and Boyle E. A. (2000) Glacial/Interglacial variations in atmospheric carbon dioxide: searching for a cause. *Nature* **407**, 859-868.

Skulan J. L., Beard B. L., and Johnson C. M. (2002) Kinetic and equilibrium Fe isotope fractionation between aqueous Fe(III) and hematite. *Geochimica et Cosmochimica Acta* **66**(17), 2995-3015.

Spokes L. J. and Jickells T. D. (1996) Factors controlling the solubility of aerosol trace metals in the atmosphere and on mixing into seawater. *Aquatic Geochemistry* **1**, 355-374.

Taylor P. D. P., Maeck R., and Debievre P. (1992) Determination of the absolute isotopic composition and atomic-weight of a reference sample of natural iron. *International Journal of Mass Spectrometry Ion Processes* **121**, 111-115.

Walyczyk T. and von Blanckenburg F. (2002) Natural iron isotope variations in human blood. *Science* **295**, 2065-2066.

Welch S. A., Beard B. L., Johnson C. M., and Braterman P. S. (2003) Kinetic and equilibrium Fe isotope fractionation between aqueous Fe(II) and Fe(III). *Geochimica et Cosmochimica Acta* **67**(22), 4231-4250.

Wells M. L., Price N. M., and Bruland K. W. (1995) Iron chemistry in seawater and its relationship to phytoplankton. *Marine Chemistry* **48**, 157-182.

Wiesli R. A., Beard B. L., and Johnson C. M. (2003) Experimental determination of Fe isotope fractionation between aq. Fe(II), "green rust", and siderite. *Geochimica et Cosmochimica Acta* **67**, A533.

Witter A. E., Hutchins D. A., Butler A., and Luther G. W. (2000) Determination of conditional stability constants and kinetic constants for strong model Fe-binding ligands in seawater. *Marine Chemistry* **69**, 1-17.

Witter A. E. and Luther G. W. (1998) Variation in Fe-organic complexation with depth in the Northwestern Atlantic Ocean as determined using a kinetic approach. *Marine Chemistry*, 241-258.

Wu J., Boyle E. A., Sunda W., and Wen L. (2001) Soluble and colloidal iron in the oligotrophic North Atlantic and North Pacific. *Science* **293**, 847-849.

Wu J. and Luther G. W. (1996) Spatial and temporal distribution of iron in surface water of the northwest Atlantic Ocean. *Geochimica et Cosmochimica Acta* **60**, 2729-2741.

Wu J. and Luther G. W. I. (1995) Complexation of iron(III) by natural organic ligands in the Northwest Atlantic Ocean by competitive ligand equilibration method and a kinetic approach. *Marine Chemistry* **50**, 159-177.

Yamaguchi K. E., Beard B. L., Johnson C. M., Ohkouchi N., and Ohmoto H. (2003) Iron isotope evidence for redox stratification of the Archean oceans. *Geochimica et Cosmochimica Acta* **67**, A550.

Zhu X. K., Guo Y., Williams R. J. P., O'Nions R. K., Matthews A., Belshaw N. S., Canters G. W., de Waal E. C., Weser U., Burgess B. K., and Salvato B. (2002)

Mass fractionation processes of transition metal isotopes. *Earth and Planetary Science Letters* **200**(1-2), 47-62.

Zhu X. K., O'Nions R. K., Guo Y. L., and Reynolds B. C. (2000) Secular variation of iron isotopes in North Atlantic Deep Water. *Science* **287**(5460), 2000-2002.

Chapter 2

Iron (Soluble and Colloidal), Manganese, and Chromium in the Tropical and Subtropical Atlantic Ocean

B.A. Bergquist, MIT/WHOI Joint Program in Oceanography

E.A. Boyle, MIT/WHOI Joint Program in Oceanography

J. Wu, University of Alaska-Fairbanks, International Arctic Research Center

2.1. INTRODUCTION

Studies of trace metals in the marine environment are essential because of the roles metals play as trace nutrients (e.g., Fe), toxins (e.g., Cr (VI)), and for the understanding of large scale biogeochemical cycling (e.g., using Mn to locate hydrothermal vents). However, many of these metals are difficult to study due to their complex chemistry and the difficulty of obtaining measurements without contamination. It was not until the mid-1970s that reliable profiles of many trace metals were produced. Despite a decade or two of research on trace metals and a growing awareness of their importance in ocean biogeochemistry, there are still limited data on the distribution, speciation, and behavior of many important metals in the environment.

Iron is an essential micronutrient on both land and in the oceans, and is proposed to play a role in climate change by influencing primary production in the ocean (MARTIN, 1990; KUMAR et al., 1995; FALKOWSKI, 1998). In Chapter 1, the distribution and biogeochemical cycle of Fe was reviewed. Briefly, it is believed that atmospheric dust deposition is the main source of Fe to the open ocean (DUCE and TINDALE, 1991). Changes in dust flux to the ocean may affect concentrations of bioavailable iron in the upper ocean by both changing the amount of aerosol iron that directly dissolves in the upper ocean and by affecting the amount of Fe delivered to the deep ocean via sinking

organic matter (and hence upwelled Fe). The residence time of Fe in both the surface and deep ocean, cycling of Fe in the upper ocean, the relationship between dust deposition and bioavailable Fe (e.g., percent of aerosol dissolution), and changes in productivity and export due to Fe input need to be better constrained in order to include Fe in biological pump and climate models.

Another complication in understanding the dissolved Fe cycle is that a significant fraction of "dissolved" Fe (DFe) is not truly dissolved, which may have consequences for the amount of DFe that is available to organisms. Wu et al. (2001) found that a substantial fraction (30 to 70% in deep-water) of DFe was colloidal in the North Atlantic and North Pacific, and the two pools of DFe (colloidal, >0.02 μm and <0.4 μm; soluble, <0.02 μm) did not have the same concentration profiles. The operationally defined "dissolved" fraction of Fe (0.2 or 0.4 μm filtered) is based on the minimum size needed to remove most organisms and particles as well as the availability of acid cleanable filters with trusted pore sizes (review: BRULAND and RUE, 2001). There is evidence that marine organisms can grow utilizing colloidal Fe, although growth rates are usually lower than organisms grown on free Fe (BARBEAU and MOFFETT, 1998; NORDWELL and PRICE, 2001; CHEN et al., 2003). The different biogeochemical behaviors and of colloidal and soluble Fe have yet to be rigorously studied along with the consequences that a significant fraction of the DFe in the ocean is colloidal.

Comparisons of Fe with other trace metals may be useful in understanding and quantifying certain aspects of the Fe cycle in the ocean. In this study, Mn and Cr were measured along with Fe. Published Al data is also available along a transect near our transect in the western Atlantic from June 1996 (VINK and MEASURES, 2001). Manganese and Al are two other trace metals that are particle reactive and have distributions in the ocean that reflect their sources. Aeolian deposition is a main source for both in the open ocean (like Fe); however, unlike Fe, neither of these elements have profiles and distributions indicative of biological cycling (KLINKHAMMER and BENDER, 1980; LANDING and BRULAND, 1980; ORIANS and BRULAND, 1986; BRULAND et al., 1994). Aluminum is considered an excellent tracer of atmospheric deposition in the

surface ocean (MEASURES and E.T., 1996; MEASURES and VINK, 2000). It has elevated surface concentrations and decreases with depth due to scavenging with residence times of 3-5 years in the surface ocean (ORIANS and BRULAND, 1986) and <100 years in the deep ocean (BRULAND et al., 1994).

Manganese also has a surface maximum and decreases with depth, but surface values are higher than what would be predicted from atmospheric deposition and removal via scavenging (BRULAND et al., 1994). Manganese has two oxidation states in the ocean (II and IV) where the reduced form is soluble and the oxidized form is easily scavenged from the water column (WEISS, 1977; KLINKHAMMER and BENDER, 1980). However in surface waters, particulate MnO_2 is photochemically reduced to Mn(II) (SUNDA and HUNTSMAN, 1988). Photochemical cycling maintains higher concentrations and results in a longer residence time of ≤20 years in surface waters (LANDING and BRULAND, 1980; LANDING and BRULAND, 1987; SUNDA and HUNTSMAN, 1988). Deep-water Mn concentrations are generally very low (0.1 to 0.6 nmol/kg) and decrease with the age of the deep-water due to progressive scavenging (STATHAM et al., 1998) except near hydrothermal sources (KLINKHAMMER et al., 1977; EDMOND et al., 1979) or suboxic boundary regions where Mn(II) is present (LANDING and BRULAND, 1987). The residence time of Mn in the deep ocean is estimated to be very short, <50 years (WEISS, 1977; BRULAND et al., 1994). The short residence time of Mn in deep-water leads to the Mn distribution being very sensitive to its external sources such as hydrothermal sources.

Very little is known about Cr in the ocean, but it is considered a nutrient-type element with a residence time of ≈10,000 years (WHITFIELD and TURNER, 1987; SIRINAWIN et al., 2000). River input is considered to be the main source (>99%) to the ocean (JEANDEL and MINSTER, 1984). Cr has two oxidation states, (III) and (VI), in seawater with most of the Cr present in the thermodynamically favored oxidized form in the open ocean (CRANSTON and MURRAY, 1978; CAMPBELL and YEATS, 1981; CRANSTON, 1983). Generally, Cr concentrations are lower in the surface ocean than deep-water by 10 to 45% and increase to values of 2-10 nmol/kg in deep-water. Cranston (1983) found that Cr correlated best with silica in the northeast Pacific Ocean and

suggested that the Cr profile could possibly be explained by release of Cr with dissolution of biogenic silicate and organic matter.

The idea that Cr is dominantly a nutrient-type element has been recently challenged. Sirinawin et al. (2000) found that although Cr is correlated with macronutrients at individual stations, there was no global correlation of Cr concentrations with phosphate for samples deeper than 200 m in the Atlantic and Pacific. Chromium concentrations were slightly higher or about the same for deep-water samples from the Atlantic compared to the Pacific. They suggested that the behavior of Cr could best be described as intermediate between a nutrient- and conservative-type element. A conservative element is mostly non-reactive in seawater and varies with physical parameters such as salinity. The Cr (VI) anion is in the same group as other conservative elements that form non-reactive oxyanions (e.g., Mo, S). More data on the distribution of Cr in the open ocean is needed to assess the Cr cycle and its potential to be used as a tracer or for comparative studies with other metals or nutrients.

The aim of this study was to investigate Fe distribution, speciation, and dissolution in areas of varying atmospheric dust inputs in the Atlantic Ocean. Iron concentrations were measured by a new isotope dilution multi-collector inductively coupled plasma mass spectrometry (MC-ICPMS) method, which allows Mn and Cr concentrations to be measured simultaneously. We present Fe and Mn data from three cruises in the sub-tropical and tropical Atlantic Ocean (30°N to 30°S) including both surface data and profiles of Fe. One profile of Cr was measured in the South Atlantic. For Fe, we also measured the different pools of dissolved Fe (soluble and colloidal) and, in particular, we present high-density profiles of dissolved (<0.4 μm) and soluble Fe (<0.02 μm) in the upper 200 m. In this study, the terminology for dissolved Fe species put forth in Wu et al. (2001) will be adopted: (a) "dissolved" Fe (DFe) is defined as the Fe that passes though the 0.4 μm filter, (b) "soluble" Fe (SFe) is the Fe that passes through the 0.02 μm filter, and (c) colloidal Fe (CFe) is the difference between the DFe and the SFe (0.02 μm to 0.4 μm).

2.2. Sampling and Methods

2.2.1. Sampling Sites

Between January 2001 and March 2002, trace metal clean seawater samples were collected on three cruises in the sub-tropical and tropical Atlantic Ocean (Figure 2.1): 1) January 2001 (R/V Seward Johnson, SJ0101, surface sampling and deep profiles), 2) June/July 2001 (R/V Knorr, Knr162, surface sampling and detailed euphotic zone profiles), 3) March 2002 (R/V Endeavor, En367, surface sampling, detailed euphotic zone and deep profiles). The two 2001 cruises focused on the North Atlantic sub-tropics and tropics and were part of the NSF-sponsored Biocomplexity MANTRA program (A. Michaels et al.) in which sampling sites were chosen based on variations in dust input and possible connections with N_2 fixation. Two sites were visited in both the winter and summer of 2001 (30°N, 45°W and 10°N, 45°W), which allowed for sampling at both times of year in the upper 200 m. The northern site at 30°N is in the subtropical gyre and is characterized by oligotrophic conditions, a deep pycnocline, and lower atmospheric dust inputs than the 10°N site. The 10°N site is on the edge of the subtropical gyre and equatorial system and has a shallow pycnocline and higher atmospheric dust inputs. The March 2002 cruise followed along the western part of the Atlantic basin from Barbados to Rio de Janeiro, Brazil. The deep South Atlantic profile presented in this study was taken at the southernmost extent of the cruise (24.5°S, 37°W) in the subtropical gyre of the South Atlantic.

The sampling sites cover an area in the Atlantic where estimated dust deposition rates vary by orders of magnitude both from north to south and seasonally (Duce and Tindale, 1991; Mahowald et al., 1999; Fung et al., 2000; Gao et al., 2001; Vink and Measures, 2001; Chen and Siefert, 2004). Dust deposition rates are highest in the North Atlantic downwind from the Sahara and decrease rapidly south of the inter-tropical convergence zone (ITZC) based on satellite data. Generally, more dust is deposited in the winter than in the summer in the Atlantic. The maximum dust transport off North Africa is at 5°N in the winter and moves to 20°N in the summer due to the seasonal migration of the ITCZ (Husar et al., 1997; Moulin et al., 1997). Particulate Fe and

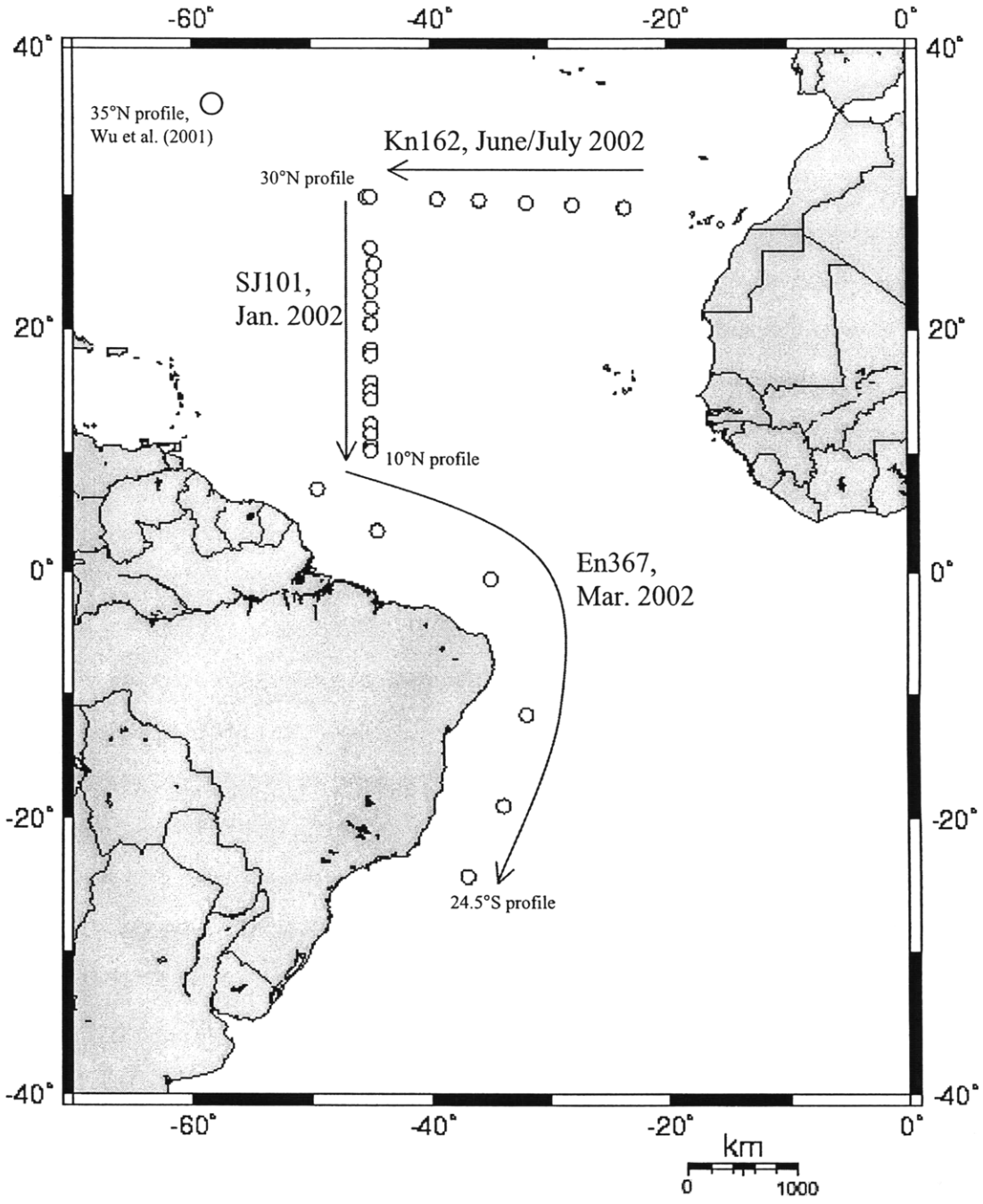

Figure 2.1: Sample location map for the three cruises discussed in this study. Surface samples are marked by circles, and profile sites are marked with their latitude. The northwest Atlantic profile site from Wu et al. (2001) is also shown.

labile Fe (90-minute, pH 4.5, reducing leach) atmospheric concentrations were measured concurrently at sea on the North Atlantic cruises by Y. Chen and R. Siefert (University of Maryland) and the data can be found in Chen and Siefert (2004). Using the atmospheric particulate Fe concentrations (CHEN and SIEFERT, 2004), a crustal average abundance of 4.3% for Fe (WEDEPOHL, 1995), and a settling velocity of 1 cm d^{-1}, in situ dust deposition rates can be estimated for the North Atlantic sites. Dust deposition rates varied from 0.02 g $m^{-2} y^{-1}$ at 30°N to 6 g $m^{-2} y^{-1}$ at 10°N in the winter, and from 2 g $m^{-2} y^{-1}$ at 30°N to 2.5 g $m^{-2} y^{-1}$ at 10°N in the summer. Contemporaneous dust deposition rates are not available for the South Atlantic cruise in March 2002. However, Vink and Measures (2001) derived deposition estimates based on measured dissolved Al along a similar transect in June 1996 and calculated very low dust deposition rates in the western South Atlantic around 25°S of <1 g $m^{-2} y^{-1}$. The Al derived rates of deposition for their 1996 North Atlantic sites agree reasonably with Chen and Siefert (2004) estimates and are also in general agreement with model derived deposition estimates.

2.2.2. Sampling Methods

The trace metal clean seawater samples collected in this study were collected using a variety of methods. Many of the samples collected on the cruise were taken with the Moored In situ Trace Element Serial Sampler (MITESS) water sampler or with a single MITESS "ATE" (Automated Trace Element) module (BELL et al., 2002). Each MITESS module opens and closes an acid-cleaned 500 ml polyethylene bottle while underwater in order to minimize chances for contamination. Near surface samples were collected by (a) "ATE/Vane", a single MITESS module attached to a "weather-vane" that is free to rotate around the hydrowire and orients itself such that the module is upstream of the wire while ship moves forward at 1-2 knots placing the sampler upstream of the wire and wire contamination, (b) an underway "towed fish" device (VINK et al., 2000) deployed while the ship is steaming up to ≈10 knots or (c) "pole" sampling, extending a sample bottle from the side of a ship using a long pole while the ship is moving forward at 1-2 knots. "Pole" samples and "towed fish" samples are collected in the upper meter

of the water column. The shallow "ATE/Vane" samplers are deployed with a shallow depth recorder (less than ± 0.5 m precision), or depths are estimated by measuring wire out and the wire angle (± 1 m precision). Profile samples were collected using either the "ATE/Vane" device with a single MITESS module for shallow samples (<200 m) or the full 12 unit MITESS for deeper samples (>30 m). In order to reconstruct sampling depths on deeper profiles, MITESS was deployed with a temperature-recording device and depths were estimated by comparison to a CTD deployed just before MITESS for the July 2001 and March 2002 cruises. The precision of the depths estimated by this method is ± 5 m. For the January 2001 cruise, a CTD was deployed prior to MITESS and the depths were marked on the hydrowire. The precision and accuracy of the depth estimates by this method are not known, but are probably within 50 m for the deeper samples (>1000 m) and better for shallower depths.

For profile work, it is especially challenging to collect trace metal clean samples in the upper 30 m of the water column while maintaining good depth control. Near surface techniques such as the "towed fish" device or "pole" sampling only allow samples to be collected in the upper couple meters of the water column, and trace metal clean Go-Flow collectors and MITESS might be suspect in shallow depths where ship contamination might occur. Therefore, detailed shallow water profiles for Fe are rare. In this study, high density profile samples in the upper 200 m were collected on the July 2001 cruise using multiple "ATE/Vane" samplers and the same principle as the "towed fish" and "pole" sampling methods. Five "ATE/Vane" devices were attached to a hydrowire running off a winch/crane that extended 3-4 meters off the side of the ship (Figure 2.2). To reconstruct depths, the spacing between each "ATE/Vane" was measured, a depth recorder attached to the deepest sampler, and the wire angle measured for each deployment. All samplers were lowered into the water, and the ship was moved forward at 1-2 knots. Thus the samplers were being towed along the side of the ship and the "weather vanes" pointed the samplers upstream of the hydrowire. The forward movement of the ship insured that the samplers collected water moving parallel to the ship's path and not water that was in contact with the ship. After a minimum of

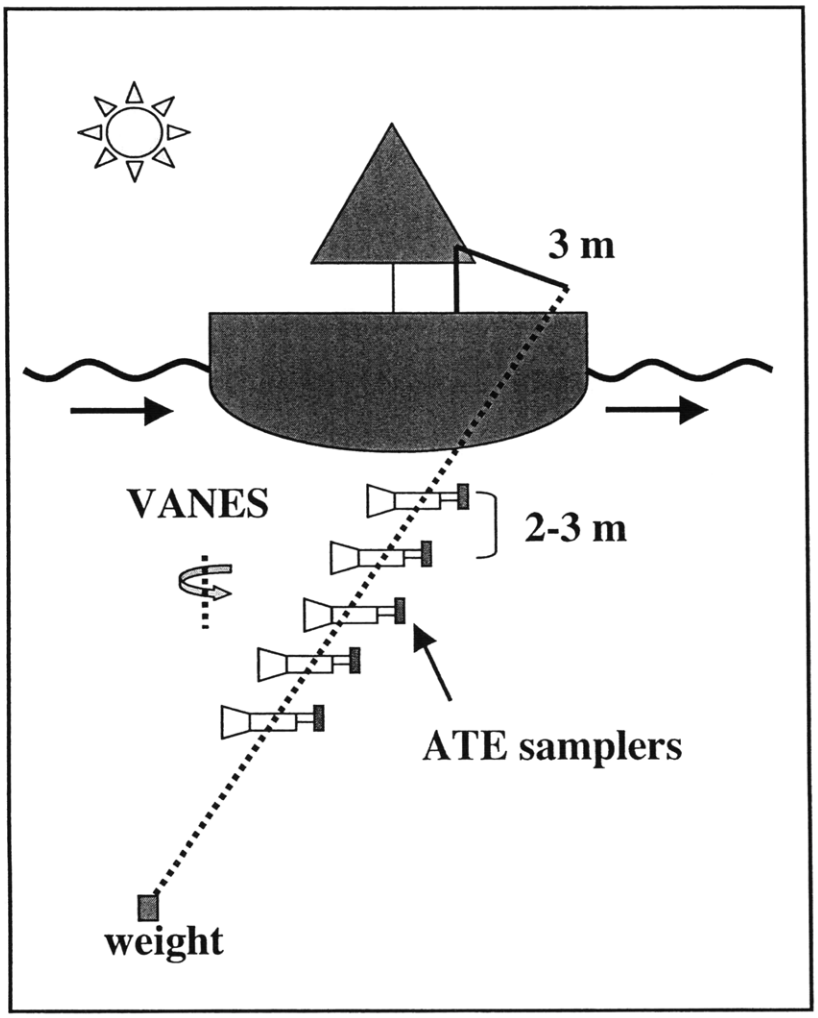

Figure 2.2: Schematic of upper water column sample collection technique used to collect high-density euphotic zone Fe samples on the summer 2001 cruise in the North Atlantic.

20 minutes in the water and rinsing by seawater, the samplers open and close after flushing for 10 minutes. The largest uncertainty of the depth reconstruction in the "ATE/Vane" sampling technique is the wire angle estimate at the surface. It is not known how constant the wire angle was under the water. Therefore, the relative difference between the samples is known better (less than ± 0.5 m) than the absolute depth (± 1 to 2 m).

After sample collection, sealed sample bottles were taken into a class 100 clean air flow environment for filtration within 12-24 hours of collection in order to avoid Fe loss to bottle walls. Splits of each sample were vacuum filtered through acid cleaned 0.4 μm Nuclepore® filters and syringe filtered though acid cleaned 0.02 μm Anotop® alumina filters (details of 0.02 μm filtration in WU ET AL., 2001). Prior to each filtration, acid cleaned filters and the filter rig were thoroughly rinsed with dilute trace metal clean HCl and then several aliquots of seawater. The acid cleaned collection bottles were also rinsed several times with filtered seawater prior to the final sample collection. Two to three separate aliquots of the filtrates were collected and the sequence noted on bottles. The last aliquot is the sample usually measured for Fe concentration because it is considered to be least likely to have been contaminated during filtration. Random bottle contamination happened infrequently (less than 10%) and high values were checked against measurements of earlier filtrates. Filtrates were acidified at sea in a class 100 clean environment to pH 2.5 by addition of triply distilled Vycor 6 N HCl in a ratio of 1 ml acid to 500 ml of seawater.

2.2.3. Fe, Mn, and Cr Measurement

Iron, Mn, and Cr concentrations on filtrates were measured by a modified version of the method by Wu and Boyle (1998), which utilizes isotope dilution followed by $Mg(OH)_2$ co-precipitation and measurement by ICPMS (Bergquist and Boyle, in prep). The main differences of the technique used in this study are the use of a ^{54}Fe isotope spike and a GV Instruments (formerly Micromass) IsoProbe MC-ICPMS. The IsoProbe incorporates a hexapole collision cell prior to the magnet that eliminates ArO^+ and ArN^+

interferences on masses 56 and 54, which allows samples to be measured in low mass resolution. The multi-collection feature permits simultaneous collection of masses 52 (monitor Cr and correct for Cr interference on 54), 54, 55 (Mn), 56, and 57. The largest interference correction for Fe is CaO^+ on mass 56. The CaO^+ interference is monitored by measuring $CaOH^+$ on mass 57, measuring the CaO/CaOH ratio on a trace metal clean Ca solution throughout the run, and correcting mass 56 for the CaO^+ interference. Mn and Cr concentrations are calculated by measuring a recovery efficiency (from spiked samples) compared to the ^{54}Fe spike and by measuring the relative ionization efficiency of Mn, Cr, and Fe in the plasma. The recovery efficiency for Mn and Cr is calculated by measuring several samples with standard addition spikes throughout a run. The recovery efficiency is a function of time before the precipitate is centrifuged for Cr than Mn. Therefore, each step in the precipitation procedure was timed and kept as constant as possible. Typical recovery efficiencies for Mn and Cr are 50 ± 7% and 60 ± 8% (1σ standard deviation (SD)) respectively.

In more detail, 1.3 ml sample aliquots were measured for Fe, Mn, and Cr after a minimum of several months after acidification. A ^{54}Fe isotope spike was added to each sub-sample. The Fe and Mn were then co-precipitated with $Mg(OH)_2$ by adding a small amount of vapor distilled (sub-boiling) NH_4OH. Only enough NH_4OH was added to precipitate a small fraction of the Mg in the sample (WU and BOYLE, 1998). The samples were then centrifuged and the liquid discarded. The precipitate was dissolved in 150 to 200 µl of 0.3 N Optima HNO_3 for analysis on the MC-ICPMS. Procedural blanks for Fe ranged from 0.08 to 0.17 nmol/kg from run to run with typical precisions of ± 0.03 nmol/kg (1σ SD) for individual runs. For Mn, procedural blanks ranged from 0.4 to 1.0 nmol/kg with typical precisions of ± 0.1 nmol/kg (1σ SD) for individual runs. Only one data set was analyzed for Cr. For that run, the Cr blank was 2.16 ± 0.20 nmol/kg (1σ SD). Replicate analysis of samples yield precisions of less than ± 0.05 nmol/kg for Fe, ± 0.10 nmol/kg for Mn, and ± 0.15 nmol/kg for Cr (1σ SD). Error bars reported in this study represent the 1σ standard deviation of replicate analysis of samples.

There are two components to the blank in the method described above: (1) a reagent blank and (2) an instrument blank. Reagent blanks are assessed by processing a 50 µl aliquot of a low-Fe seawater sample though the same procedure as the samples. However, most of the Fe, Mn, and Cr blanks in this method are due to instrument blank (blanks released from the hardware of the instrument), and not due to reagents. The 0.3 M HNO_3 blank can be measured directly, and the blank associated with the NH_4OH is negligible (doubling or tripling of NH_4OH does not change blank). Because the samples and procedural blanks have slightly different matrices, the reagent blank does not correctly characterize the instrument blank. Therefore, multiple consistency samples are analyzed at the beginning, middle, and end of each analytical session. Consistency samples are in-house seawater samples with a defined concentration. The reagent blank is then slightly adjusted (less than 0.1 nmol/kg) in order to bring the consistency samples into agreement with their defined concentration. The adjusted reagent blank is considered the full procedural blank of the method (including both the reagent and instrument blank).

Based on the reagent blank alone, samples can only be compared with confidence using their individual sample replication within a given analytical session (e.g., less than ± 0.05 nmol/kg (1SD) for Fe). However, in order to compare samples from different analytical sessions (e.g., to better than ± 0.1 nmol/kg for Fe), the changes in the instrument blank must also be included. Offsets (up to 0.1 nmol/kg for Fe) from analytical session to session due to changes in the instrument blank are corrected by using the consistency samples, which better mimic the matrix of an actual sample. Therefore, we feel differences between samples in our extended data set are comparable to within the analytical session sample replication. Comparisons of our data to other published data sets within 0.1 nmol/kg for Fe should be made with caution, as no inter-lab consistency sample exists. However, agreement between deep-water concentrations in DFe in the North Pacific measured in our lab (BOYLE et al., submitted) and concentrations observed at a nearby station by Bruland et al. (1994) suggest that our consistency samples are reasonably well defined. No such consistency sample correction

was used for the Mn data, and the consistency samples were reproduced for Mn to within ± 15%. Chromium was only analyzed in one set of samples, thus analysis session comparisons cannot be made and no estimate of external precision exists yet.

Periodic contamination still remains a problem in sample analysis (≈ 10%), therefore samples were always analyzed in triplicate. When at least two replicates agreed within expected reproducibility, the average of two or three replicates was taken as the sample concentration. If no replicates agree or two replicates were high and one low, the sample was re-analyzed. If all the sample replicates seem high based on "oceanographic consistency", then a second filtrate was measured. If the new result was lower and "consistent", then the contaminated bottle data was discarded. If both replicate filtrates are high or no replicate exists, then the sample data is reported in the attached data tables with a question mark. Data is omitted from figures and the discussion where a clear judgment could be made that the sample was contaminated.

2.3. Results and Discussion

2.3.1. Surface Water Fe and Mn Variability and Distribution

2.3.1.1. N-S Transect

The surface distributions of DFe, SFe, and dissolved Mn (DMn) from 30°N to 25°S are shown in Figure 2.3 along with published dissolved Al and DFe data from a similar transect from June 1996 (Vink and Measures, 2001). The data are given in Appendix 2.1. The N-S transects from the January 2001 (north section) and the March 2002 (south section) cruises were combined to make the figure. Although the two transects are a year apart and are from slightly different times of the year, the DFe values are in good agreement where the two transects approach eachother. DFe values are highest in the North Atlantic (0.60 ± 0.17 nmol/kg, 1 SD, n=16) and decrease by a factor of 3 south the equator (0.29 ± 0.07 nmol/kg, 1 SD, n=3). SFe does not show such a dramatic trend as DFe, but also decreases slightly from the North Atlantic (0.36 ± 0.10 nmol/kg, 1 SD, n=6) to South Atlantic (0.25 ± 0.02 nmol/kg, 1 SD, n=3). A maximum in DFe is seen at 20°N with a peak value of 0.89 nmol/kg.

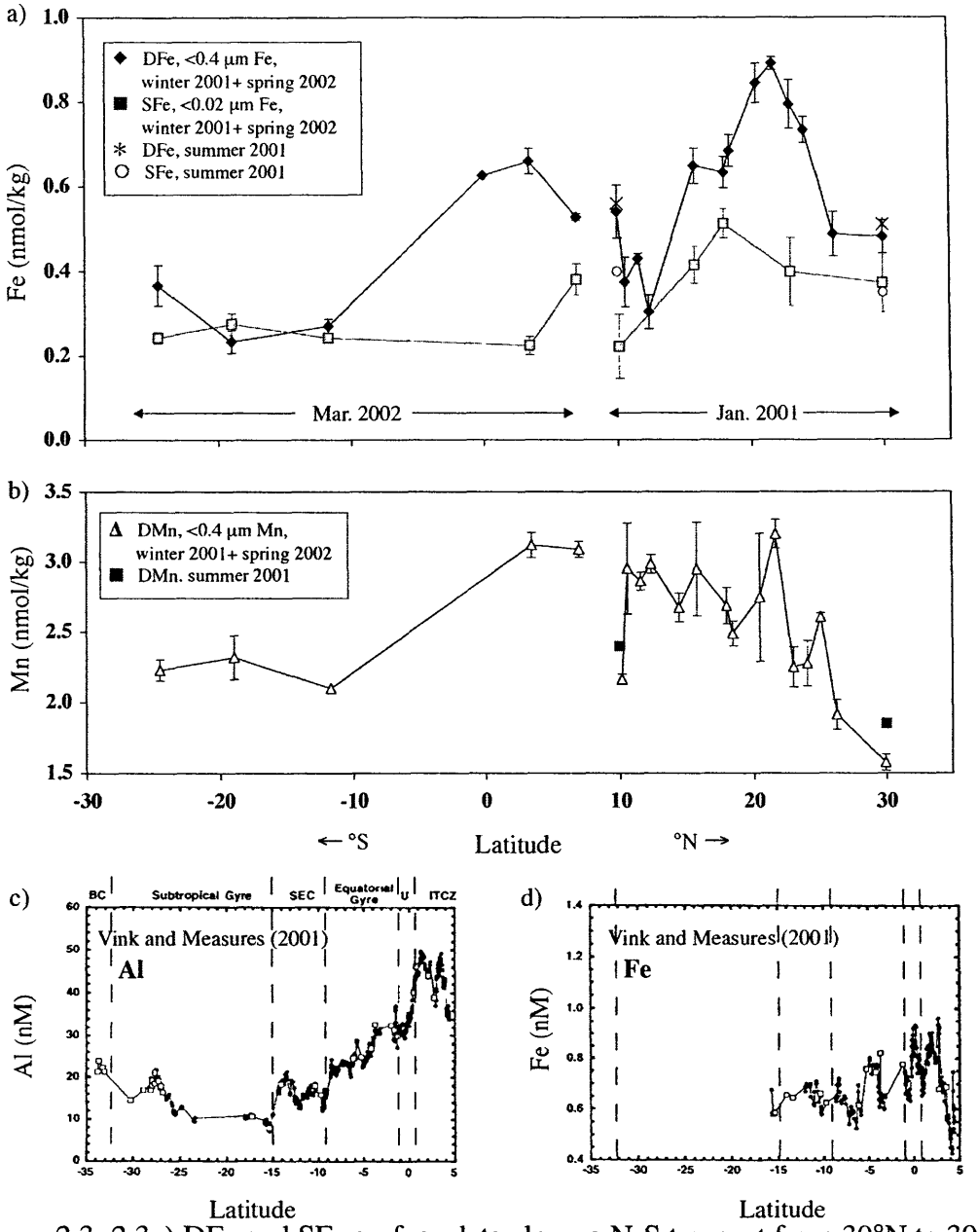

Figure 2.3: 2.3a) DFe and SFe surface data along a N-S transect from 30°N to 30°S in the western Atlantic. Transects from the January 2001 and March 2002 cruises were combined and are marked by a break in the transect. DFe and SFe data for the stations re-sampled on the summer, 2001, cruise are also shown (30°N and 10°N). 2.3b) DMn data from the surface samples as in Figure 2.3a. 2.3c&2.3d) Surface transect data from a similar transect in the western Atlantic from Vink and Measures, 2001. Dissolved Al data shown in Figure 2.3c, and dissolved Fe data in Figure 2.3d. Error bars are 1σ standard deviation of sample replicates (external reproducibility is typically less than ± 0.05 nmol/kg (1 SD) for DFe and less than ± 0.08 nmol/kg (1 SD) for DMn).

In general, the observed trend in DFe is similar to trends of other dust derived trace metals (e.g., Mn and Al). DMn measured along the same transect shows a similar pattern with average values of 2.62 ± 0.45 nmol/kg (1 SD, n=18) in the North Atlantic and 2.22 ± 0.11 nmol/kg (1 SD, n=3) in the South Atlantic. A broader maximum is observed for Mn between 0 and 25°N with a peak value of 3.20 nmol/kg. Our distribution of DMn compares well with previously published surface Mn for the Atlantic Ocean (SHILLER, 1997). Dissolved Al data along a similar transect from Vink and Measures (2001) also shows higher values in the North Atlantic (40-50 nmol/kg) and decrease in the South Atlantic to concentrations less than 10 nmol/kg in the subtropical gyre (Figure 2.3c). Dust deposition rates derived from the dissolved Al data from Vink and Measures (2001) agree well with other model results in the Atlantic.

The general similarity of DFe and DMn with the Al data from Vink and Measures (2001) indicates that the observed trends in DFe and DMn are also probably due to variations in dust input along the transect. However, dissolved Al values decrease by more than a factor of 5 between the North and South Atlantic. DFe values only decrease by a factor of 3 and DMn decrease only slightly (25%). For DFe, factors such as biological uptake, biological export, and scavenging result in a shorter residence time of less than a year in the surface ocean compared to Al (3-5 years). Solubility limits may also play a role in surface DFe profiles (VINK and MEASURES, 2001; WU and BOYLE, 2002). If a proportional amount of Fe to Al was dissolved from atmospheric particles based on the composition of continental crust (8.0% Al, 4.3% Fe (WEDEPOHL, 1995)), then one would expect higher DFe concentrations (20-25 nmol/kg) in the North Atlantic. Therefore, the short residence time of Fe in surface waters and solubility limits lead to DFe values that are more variable than Al and do not have comparably high values as Al does in the North Atlantic. As for Mn, the photochemical cycling leads to a longer surface residence time (≤20 years) than Al (LANDING and BRULAND, 1980; SUNDA and HUNTSMAN, 1988). Thus, enhanced cycling and lateral transport erases large flux variations.

Our surface DFe data is in general agreement with published DFe concentrations reported for the subtropical and tropical Atlantic. North of the equator, our DFe values are similar to concentrations (0.4 to 0.8 nmol/kg) measured by Vink and Measures (2001). However, they did not observe a decrease in DFe values south of the equator. Their transect extends to 15°S with DFe values remaining high and mostly invariant (0.6 to 0.8 nmol/kg). We only have one data point between 0-15°S with a value of 0.27 nmol/kg, which is quite a bit lower. This sample could be isolated and un-representative, or illustrate the potential temporal variability of DFe. The Vink and Measures (2001) transect also may not have sampled far enough south to observe a decrease in DFe. A transect of DFe in the eastern Atlantic (October 2000) from 28°N to 20°S was recently published (SARTHOU et al., 2003) and shows a similar trend as our transect with average values of DFe of 0.40 ± 0.18 μmol/kg in the North Atlantic and 0.11 ± 0.07 nmol/kg in the South Atlantic. The observed eastern Atlantic concentrations were typically lower than our values and may represent values to be expected in the fall. The dustiest season for the Atlantic is in the winter (CHIAPELLO et al., 1995), and by October DFe values would be expected to be lower based on the short residence time of DFe. Sarthou et al. (2003) reported very low DFe south of equatorial upwelling zone (≈ 0.02 nmol/kg), which is an order of magnitude lower than our lowest value from the western transect.

Both our DFe and DMn transect data show maxima in the North Atlantic near 20°N. This is in agreement with estimated surface DFe derived from dust deposition models (FUNG et al., 2000; GREGG et al., 2003; PAREKH et al., submitted). These models use dust deposition models (based on satellite data, observations, and/or climatological dust parameters) and assume some constant dust solubility for Fe in aerosol particles across all particle size classes, usually 1 or 10%. In Fung et al. (2000) the upwelling/vertical mixing component of DFe to the upper ocean was also modeled using dissolved nitrate and a Fe:NO_3 ratio based on available data. For the tropical and subtropical North Atlantic, the modeled aeolian contribution to DFe to the upper ocean was predicted to be more than an order of magnitude higher than the vertical upwelling/mixing component. The maximum dust deposition also occurred between 0-

20°N decreasing to the north at ≈ 25-30°N and south of the equator. In the western South Atlantic, the modeled atmospheric contribution to DFe was still higher than the upwelling/vertical-mixing component. However, it was not as dramatically higher than the upwelling component as the North Atlantic modeled estimates. In the eastern South Atlantic, the atmospheric component and the upwelling/vertical mixing terms were more comparable. Although the deposition flux patterns modeled by Fung et al. (2000) are similar to our DFe distribution, Fung et al. (2000) did not estimate DFe in surface waters.

Surface DFe distributions were modeled seasonally in Gregg et al. (2003), although only an atmospheric Fe flux to surface water was included (no upwelling flux). There is good agreement between our measured DFe trend along the N-S transect and the modeled derived DFe. However, the modeled DFe in the winter are higher (>1 nmol/kg) than our measured values and the maximum around 20°N was much broader. The modeled DFe decrease in the South Atlantic to values of 0.2-0.3 nmol/kg in the subtropical gyre, which agrees well with our data. Differences between the model and measured DFe may be due to model assumptions, such as constant dust dissolution percentages and constant scavenging rates, but the general pattern and reasonably good agreement for the DFe values indicates that a 3-D general circulation model including dust dissolution, scavenging, and biological uptake for Fe is capturing many of the processes controlling surface DFe in this region of the ocean. Part of the good agreement between modeled DFe and observed DFe may be due to the dominance of the atmospheric flux of Fe over the upwelling flux in the Atlantic sub-tropics and tropics. In other regions where dust deposition is low, models with an upwelling flux will be needed to better estimate the DFe in surface waters (PAREKH et al., submitted).

The north and south endpoints of the North Atlantic transect were sampled both on the January 2001 and the July 2001 cruises. The 30°N station had a peak surface DFe of 0.68 nmol/kg in the winter and 0.50 nmol/kg in the summer. The peak value at 30°N is part of a well-defined surface maximum. The integrated mixed layer value for this station was 0.51 nmol/kg, therefore the winter and summer surface DFe are similar at this site. Large differences in the DFe from winter to summer are also not observed at the

higher dust site, 10°N, with winter surface DFe at 0.59 nmol/kg and summer at 0.56 nmol/kg. The climatological trend of higher dust input in the winter than in the summer is not reflected in our DFe data. Chen and Siefert (2004) measured total dust, total Fe, and labile Fe (90 min, pH=4.5, reducing leach) concentrations in the atmosphere concurrently with our DFe on the same cruises. At the 10°N station, total and labile atmospheric Fe flux estimates show the overall climatological trend of more dust in the winter than in the summer with 30 ± 16 $\mu g\ m^{-2}\ d^{-1}$ of labile Fe in the winter and 6.1 ± 3.3 $\mu g\ m^{-2}\ d^{-1}$ in the summer. However at the 30 °N station, concurrent dust measurements are actually higher in the summer than in the winter with labile Fe fluxes only at 0.7 ± 0.3 $\mu g\ m^{-2}\ d^{-1}$ in the winter and 3.2 ± 3.0 $\mu g\ m^{-2}\ d^{-1}$ in the summer.

The poor correlation of our sea surface DFe concentrations and the concurrent dust flux estimates demonstrates the problem of trying to compare in situ atmospheric measurements with sea-surface DFe measurements. DFe integrates over weeks to months of dust deposition events and is biologically cycled with possible solubility controls. Dust deposition measurements at sea are made daily and may not represent the regional or seasonal input because of the episodic and spatially inhomogeneous nature of dust events (PROSPERO, 1996; JICKELLS and SPOKES, 2001). Some models use satellite data and average over multiple years to constrain their dust deposition fields (GREGG et al., 2003) or use seasonally averaged climatological data (MAHOWALD et al., 1999), therefore they probably capture a more integrated picture.

Although dust deposition models provide more temporally integrated dust deposition estimates, satellite- and climatological- based dust deposition models still need more ground-truthing from observations in order for modeled estimates of DFe distributions to be more quantitative. Both the models and the in situ (field) measurements assume depositional velocities in order to estimate deposition fluxes from atmospheric concentrations (usually 1 cm d^{-1} (CHEN and SIEFERT, 2004)). Because field measurements are made near the sea-surface, they may capture what actually gets deposited better than the models. Models also assume a constant fraction of Fe dissolved into seawater from atmospheric particles. In situ measurement studies such as Chen and

Siefert (2004) and Sarthou et al. (2003) include estimates of labile Fe from chemical leaching experiments. In the Chen and Siefert (2004) study, the percentage of labile Fe to total Fe varied from 2 to 5% at the 10°N station from summer to winter, and from 28 to 3% from winter to summer at the 30°N station. The large percent of labile Fe in aerosols, 28%, at 30°N winter occupation was associated with particles in which the Fe was correlated with Cu, Ni, and V instead of Al indicating that the Fe was not associated with crustal material and likely was of anthropogenic origin (CHEN and SIEFERT, submitted). Not only does the amount of dissolution vary with aerosol type, but it also varies with particle size with more labile Fe in the finer fractions (SIEFERT et al., 1999; JOHANSEN et al., 2000; CHEN and SIEFERT, submitted). Atmospheric cycling and lifetime in the atmosphere will also affect the potential amount of Fe that is dissolvable in the surface ocean. All these factors need to be incorporated into dust deposition models.

Because most of the N-S variation is seen in the DFe and not in the SFe, much of the structure seen in the DFe transect is due to CFe. Wu et al. (2001) suggested that most atmospherically derived DFe was preferentially released into the colloidal pool. This assumption was based on profiles from oligotrophic gyre sites in the North Atlantic and North Pacific where surface maxima in the DFe were observed without corresponding maxima SFe. Our CFe and SFe distributions support that interpretation; CFe follows the dust deposition variations and the Al distribution from Vink and Measures (2001). In the southern part of the transect where dust deposition is the lowest, the colloidal fraction of Fe disappears and then increases slightly at the southernmost station where the Al data also starts to increase again. It is interesting that SFe does not show a strong trend from north to south. This observation implies that the SFe distribution is not strongly influenced by dust inputs directly and may be controlled by other mechanisms (possibly solubility).

2.3.1.2. E-W Transect

DFe and DMn were measured along an E-W transect (23°W to 45°W) along 30°N on the July 2001 cruise (Figure 2.4, Appendix 2.1). DFe shows a relatively minor E-W

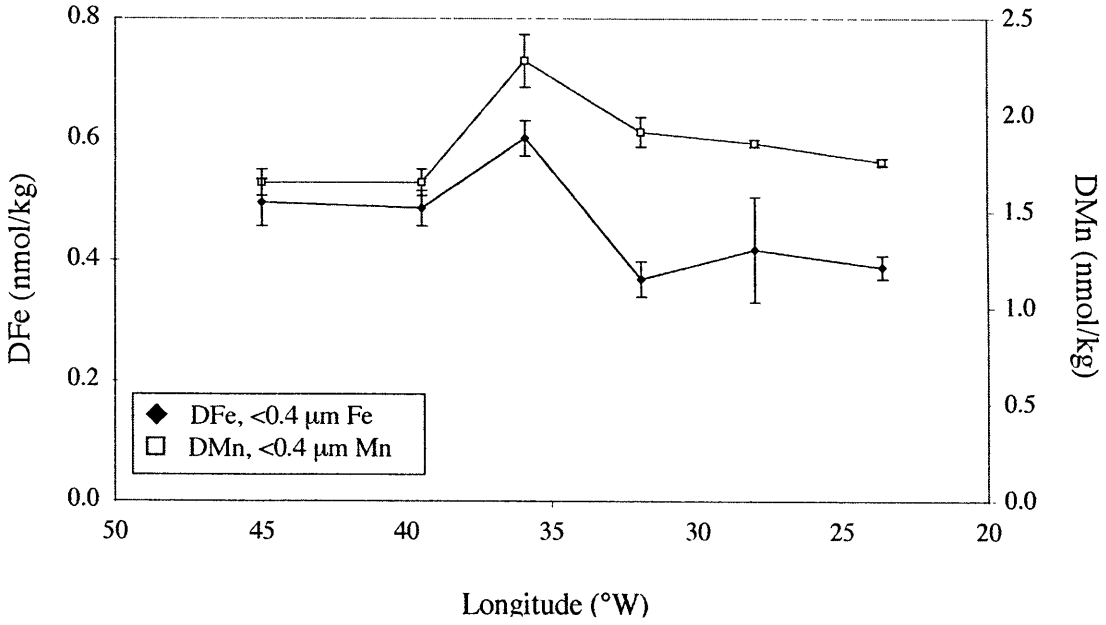

Figure 2.4: DFe and DMn along an E-W transect at ≈ 30°N in the North Atlantic from the June/July 2001 cruise. Error bars are 1σ standard deviation of sample replicates (external reproducibility is typically less than ± 0.05 nmol/kg (1 SD) for DFe and less than ± 0.08 nmol/kg (1 SD) for DMn).

trend with slightly higher values towards the west. The easternmost stations had an average DFe of 0.39 ± 0.02 nmol/kg (1 SD, n=3) and the westernmost samples had 0.53 ± 0.06 nmol/kg (1 SD, n=3) (difference is significant at the 95% confidence level using a t-test). DMn remained relatively invariant along the transect with an average concentration of 1.93 ± 0.23 nmol/kg (1 SD, n=6). The concurrent atmospheric Fe measurements made by Chen and Siefert (2004) also show an increase in dust deposition toward the west, which is reflected in the DFe transect and not in the DMn concentration data. Once again, dust deposition events are episodic and sea-surface DFe and DMn integrate over different periods (months for Fe and years for Mn).

Strong E-W gradients in dust deposition or DFe at 30°N are not predicted by models except for very high values close to the African continent where most of the larger particles are deposited (MAHOWALD et al., 1999; FUNG et al., 2000; GREGG et al., 2003). 30°N is north of the zone of maximum dust transport, and the E-W transect was sampled the summer when there is generally lower dust deposition. Sarthou et al. (2003) measured surface DFe of greater than 1 nmol/kg closer to the African continent at 15°W and 28°N. Our easternmost sample is at 23.6°W and had a DFe concentration of 0.40 nmol/kg suggesting that a longitudinal gradient may exist, but only to the east of our easternmost sample. Generally, our DFe and DMn E-W distributions suggest that finer particles transported to the west of ≈ 20°W are not preferentially deposited closer to Africa in the summer.

2.3.2. Surface Aerosol Solubility

On the summer 2001 cruise, trace metal clean incubation experiments were performed by D. Capone and coworkers (University of Southern California) in order to investigate the effects of dust and Fe additions for phytoplankton at both the 10°N and 30°N stations. The mesocosm experiments were done in large carboys (20 L) in incubation chambers on deck, allowed to incubate for varying amounts of time (0 to 5 days), and sampled by our group for DFe. A summary of the Fe data is given in Table 2.1. Atmospheric dust was collected for several days on large volume acid-cleaned

Table 2.1: Fe Data from Surface Solubility and Mesocosm Experiments

Mesocosm Experiments[a]	days of expt	DFe (nmol/kg)	1 SD[d]	n	SFe (nmol/kg)	1 SD	n	Excess DFe[b] (nmol/kg)	1 SD	Excess SFe[c] (nmol/kg)	1 SD
30°N station											
surface water-0.2 m		0.51	0.04	3							
surface water-3.7 m		0.54	0.03	2	0.43	0.03	3				
surface water-5.5 m		0.56	0.03	3	0.29	0.02	2				
mesocosm-control#1	5	0.53	0.02	3							
mesocosm-control #12	5	0.54	0.02	2							
mesocosm-control #8	5	0.46	0.02	2							
mesocosm-filter control #20	5	0.54		1							
mesocosm-filter control #4	5	0.50		1							
average of controls and blanks:		0.52	0.03	8	0.36	0.10	2				
mesocosm-dust addition #13	5	0.62	0.03	2	0.33	0.02	3	0.08	0.04	-0.04	0.10
mesocosm-dust addition #22	5	0.52	0.00	2	0.33	0.02	3	-0.02	0.03	-0.04	0.10
mesocosm-dust addition #7	5	0.50		1	0.46	0.02	3	-0.04	0.03	0.09	0.10
10°N station											
surface water-0.2 m		0.60	0.03	3	0.41	0.05	2				
surface water-1.8 m		0.71	0.04	3	0.37	0.04	3				
mesocosm-filter control #4	5	0.61	0.03	2							
mesocosm-control #16	5	0.66	0.01	2							
mesocosm-control #18	5	0.75		1							
mesocosm-control #6	3	0.56	0.03	2							
average of controls and blanks:		0.65	0.07	6	0.39	0.03	2				
mesocosm-dust addition #13	5	1.10		2				0.43	0.09		
mesocosm-dust addition #21	5	1.20		1				0.54	0.09		
mesocosm-dust addition #23	3	0.48	0.02	2				-0.19	0.08		

Fe (II) addition experiments		DFe (nmol/kg)	1 SD	n	SFe (nmol/kg)	1 SD	n	Fe addition[e] SFe (nmol/kg)	1 SD	n	Excess SFe[e] (nmol/kg)	1 SD
10°N Fe(II) solubility experiment	24 hour	0.48	0.05	3	0.40	0.05	3	0.62	0.04	5	0.22	0.06

a) Mesocosm experiments were coducted by D. Capone and coworkers (University of Southern California) on the summer 2001 cruise. Trace metal clean large volume seawater incubations (20 L) were performed in carboys in incubation chambers on deck. Dust was collected for several days on acid cleaned filters (by R. Siefert and Y. Chen, University of Maryland), and then was sectioned and added to individual carboys. Mesocosm experiments were allowed to incubate for several days (3-5 days) before samples were collected for Fe analysis. DFe, and in some cases SFe, were collected and processed in the same way as surface and profile samples.

b) Excess DFe is the difference between the sample DFe measured for an individual dust addition experiment and the average of the blanks and controls.

c) Excess SFe is the difference between the sample SFe measured for an individual dust addition experiment and the average of the blanks and controls.

d) 1 SD is the standard deviation of sample replicates. A representative 1 SD of 0.05 was used for error propagation for samples where only one measurement was reported.

e) Fe addition SFe is the SFe measured in samples in which 20 nmo/kg of Fe(II) was added and allowed to equilibrate for 24 hours.

e) Excess SFe is the difference between the SFe measured in the Fe addition sub-sample and the SFe of the unperturbed sub-sample.

filters (by R. Siefert and Y. Chen), and then the filters were sectioned and added to the mesocosm experiments. Chen and Siefert (personal communication) estimated that each section of dust filter had about 100 μg total Fe at the 30°N station and 900 μg total Fe at the 10°N station based on sections kept for later analysis. Fe samples were collected at the end of each experiment and processed for DFe and periodically for SFe.

Excess DFe from the dust filter additions was observed at the 10°N station for the two 5-day incubation experiments. At the 30°N station and for the 3-day incubation experiment at 10°N, no detectable amounts of additional DFe dissolved from the dust filters. The 5-day 10°N experiments reached total concentrations of ≈ 1.15 nmol/kg with an excess DFe of ≈ 0.50 nmol/kg. Although a large amount of aerosol Fe was added to these experiments (900 μg), the amount of Fe released into the dissolved pool was very small (<0.1%). The upper concentration reached in these experiments may represent the saturation of the organic ligand in the dissolved pool. Excess dissolved organic ligand concentrations were measured by Wu and Luther (1995) and Luther and Wu (1997) in surface water of the northwestern Atlantic Ocean. Excess ligand concentrations of 0.45-0.60 ± 0.20 nM were observed, which agrees well with our observed excess DFe for the 5-day mesocosm experiments. It is unclear why no excess DFe was observed at the 30°N station and in the 3-day dust addition experiment at 10°N. Dust concentrations were much lower at the 30°N station, and perhaps there is a kinetic barrier to dissolving the Fe off the dust filters.

Unfortunately we did not measure the SFe at the 10°N station, so we cannot calculate how much of the excess DFe is CFe. However, a solubility experiment was performed on a 10 m sample from the station. Fe(II) was added to an aliquot of seawater and allowed to equilibrate for 24 hours, and then was filtered through a 0.02 μm filter in order to determine how much excess SFe could be put into solution (Wu et al., 2001). This excess SFe is interpreted to represent the amount of excess strong ligand that is present in the soluble fraction. An excess SFe of ≈ 0.2 nmol/kg was observed arguing that perhaps 60% of the excess dissolved DFe from dust observed in the mesocosms experiments was colloidal.

2.3.3. Fe Water Column Profiles

Figures 2.5 to 2.8 show water column profiles of DFe and SFe at three sites along the N-S transect: 1) 30°N, 45°W, 2) 10°N, 45°W, and 3) 24.5°S, 36°W. DFe and SFe profiles from a station near the Bermuda Rise (35°N, 58°W) from Wu et al. (2001) are shown for comparison in Figure 2.7 and 2.9. The 30°N and 10°N stations were sampled both on the January and the July cruises. Deep-water profiles were collected in the winter (Figures 2.5a and 2.5c) and high-density euphotic zone profiles collected in the summer (Figures 2.5b and 2.5d). The South Atlantic site was sampled on the March 2002 cruise (Figures 2.6a and 2.6b). Tables 2.2 and Appendix 2.2 summarize the data from the profiles. The DFe concentration profiles generally have nutrient-type profiles with lower concentrations in surface waters than in deep-water, although the profiles have interesting features deviating from classic nutrient-type profiles with some surface maxima, intermediate water minima and maxima, and variations clearly associated with water masses. Also, the different pools of DFe (CFe and SFe) have distinct vertical profiles. Profiles will be discussed in terms of their upper and deep-water column profiles. Residence time calculations were made for surface Fe where steady-state assumptions could be made and also for deep-water Fe.

2.3.3.1. Upper (Surface to ~ 1000 m) Water Column Fe Profiles

The two subtropical gyre sites (30°N and 24.5°S) along with the profile from Wu et al. (2001) near Bermuda have very different upper water column profiles of Fe compared with the 10°N site (Figures 2.5 through 2.8). The pycnocline extends deeper at the gyre sites (≈ 750 m), whereas the pycnocline at 10°N is much shallower (<250 m). At all three gyre sites, surface maxima in DFe are observed followed by broad minima in the pycnocline before DFe increases below depths greater than 600 m (Figure 2.7a). At the 10°N station (on the edge of the equatorial system), a surface maximum in DFe is observed in the summer and not in the winter (Figure 2.5c and 2.5d). DFe values increase dramatically at this site to values >1 nmol/kg below the mixed layer and remain

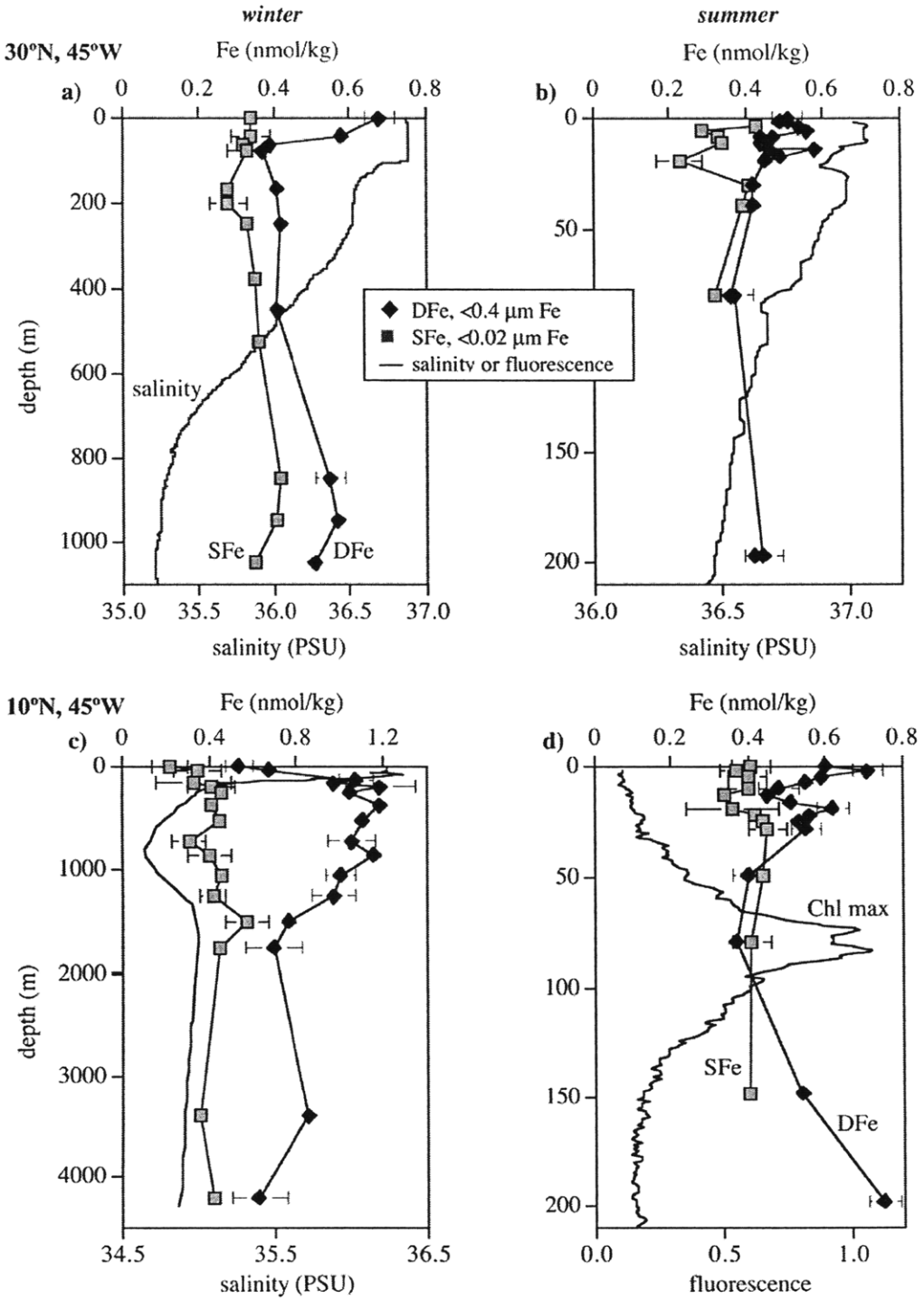

Figure 2.5: DFe and SFe water column data at the 30°N, 45°W and 10°N, 45°W stations from both the winter and summer cruises, 2001. 2.5a) The winter 30°N station is plotted with salinity. 2.5b) The summer 30°N station is plotted with salinity. 2.5c) The winter 10°N station is plotted with salinity. 2.5d) The summer 10°N station is plotted with chlorophyll fluorescence. Error bars are 1σ standard deviation of sample replicates (external reproducibility is typically less than ± 0.05 nmol/kg (1 SD) for Fe).

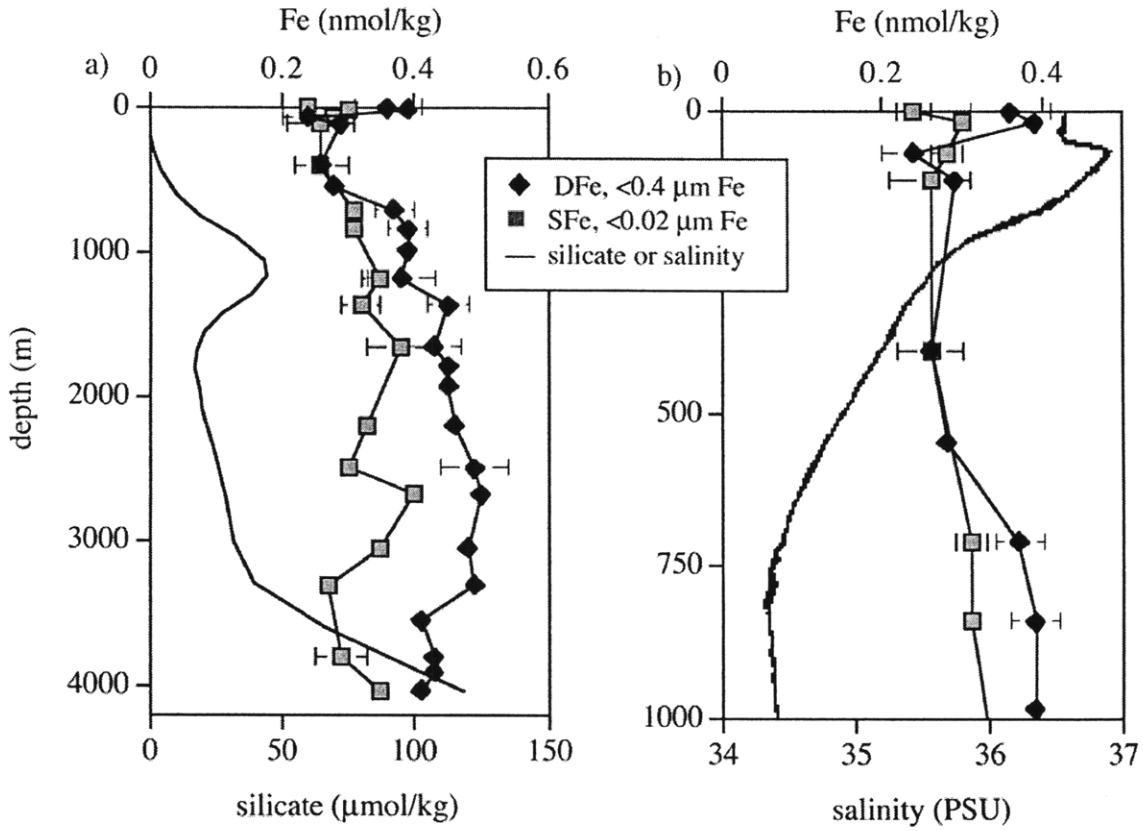

Figure 2.6: DFe and SFe profiles for the South Atlantic station at 24.5°S, 37°W occupied in March 2002. Figure 2.6a is the full Fe profile to 4000 m plotted along with silicate data measured on the same cruise. Figure 2.6b is a blow up of the upper 1000 m plotted along with CTD salinity data. Error bars are 1σ standard deviation of sample replicates (external reproducibility typically less than ± 0.05 nmol/kg (1 SD) for Fe).

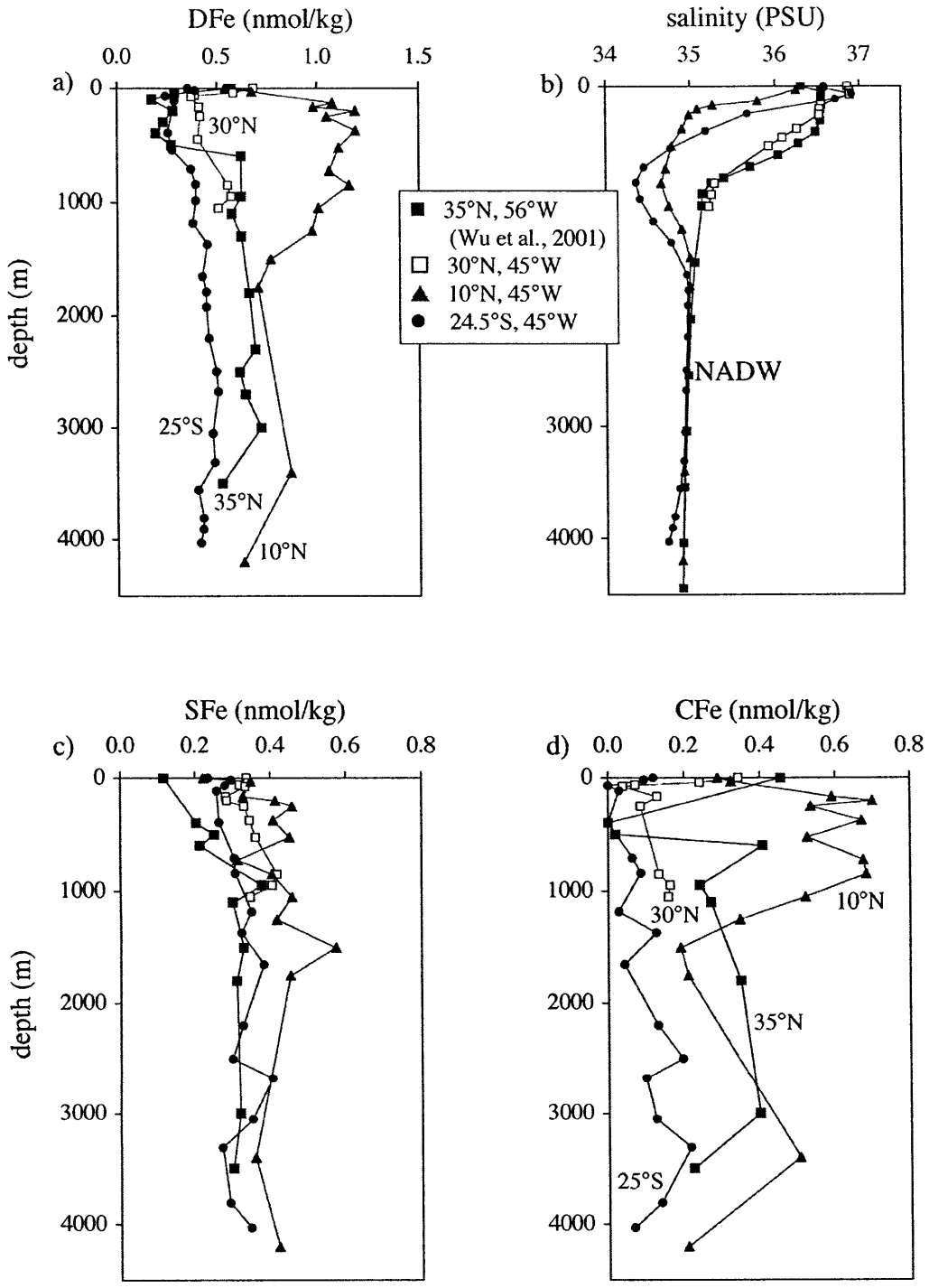

Figure 2.7: Fe water column data for the three deep stations sampled in this study (30°N, 45°W; 10°N, 45°W; 24.5°N, 36°W) along with a station sampled near the Bermuda Rise from Wu et al., 2001 (35 °N, 56 °W). The DFe (<0.4 μm Fe) profiles are shown in figure 2.7a, the salinity in figure 2.7b, the SFe (<0.02 μm Fe) profiles in figure 2.7c, and the CFe (0.02 to 0.4 μm) profiles in figure 7d. In figure 2.7b, the core of North Atlantic Deep Water (NADW) is marked.

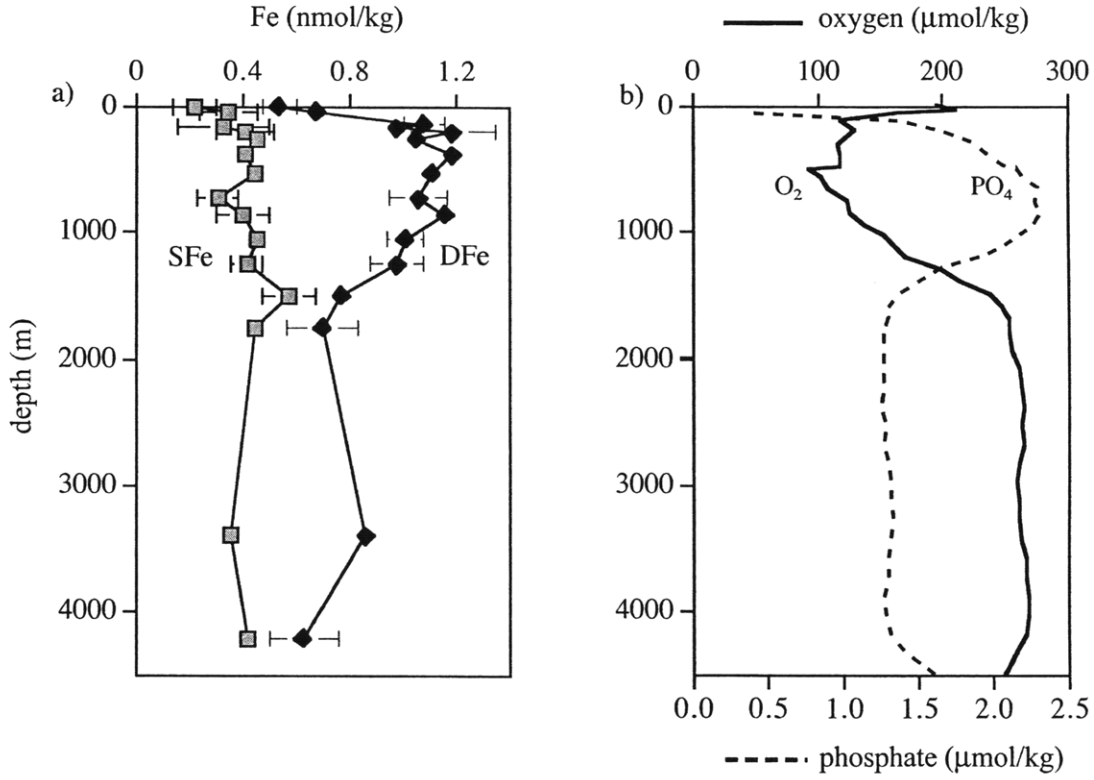

Figure 2.8: 2.8a) DFe and SFe from the winter 10°N, 45°W station. Error bars are 1σ standard deviation of sample replicates (external reproducibility is typically less than ± 0.05 nmol/kg (1 SD) for Fe). 2.8b) Phosphate and AOU data from the nearby GEOSECS station 39 (7.8 °N, 43.9 °W). Temperature and salinity overlays for our station and the GEOSECS station were nearly identical.

Table 2.2: Summary of Fe Water Column Data

depth (m)	DFe (nmol/kg)	1 SD (a)	n (b)	SFe (nmol/kg)	1 SD (a)	n (b)	CFe (nmol/kg)	1 SD (a)	n (b)	CFe/DFe (%)[c]	Fe* (nmol/kg)[d]	1 SD (a)	AOU calc. Fe:C (μmol/mol)[e]	1 SD (a)
35°N, 58°W (Wu et al., 2001)														
mixed layer, <20 m	0.57		1	0.12		1	0.46		1	81%				
pycnocline, 50-500 m	0.24	0.05	6	0.24	0.04	2	0.01	0.01	2	≈0%				
deep, >1500 m	0.64	0.05	6	0.32	0.01	4	0.32	0.09	3	50%	0.04	0.07		
30°N, 45°W														
winter mixed layer, 0-100 m	0.51	0.15	4	0.33	0.01	4	0.17	0.17	4	34%				
winter mixed layer peak, 0m	0.68		1	0.34		1	0.34		1	50%				
summer mixed layer, 0-11 m	0.50	0.05	8	0.35	0.06	4	0.16	0.08	4	32%				
pycnocline, 165-525 m	0.41	0.02	3	0.32	0.03	5	0.11	0.03	2	27%				
deep, 850-1050 m	0.54	0.03	3	0.39	0.04	3	0.15	0.02	3	28%				
10°N, 45°W														
winter mixed layer, 0-55 m	0.59	0.13	2	0.28	0.10	2	0.31	0.03	2	53%				
summer mixed layer, 0-32 m	0.56	0.07	11	0.40	0.04	9	0.17	0.09	9	30%				
O2 minimum, 150-1050 m	1.09	0.08	9	0.40	0.06	8	0.61	0.08	8	63%	0.17	0.15	11	1
deep, 1600-4200 m	0.73	0.12	3	0.41	0.05	3	0.31	0.07	3	42%	0.13	0.12	17	3
24.5°S, 36°W														
mixed layer, 0-52 m	0.37	0.03	2	0.27	0.04	2	0.11	0.02	2	30%				
pycnocline, 60-550 m	0.27	0.02	4	0.27	0.01	3	0.01	0.02	3	≈0%				
AAIW, 700-1200 m	0.38	0.01	4	0.32	0.03	3	0.06	0.03	3	16%	-0.57	0.09	5.4	0.8
NADW, 1700-3350 m	0.47	0.02	7	0.33	0.05	4	0.15	0.05	4	32%	-0.15	0.02	11	1
AABW, > 3500 m	0.42	0.01	4	0.32	0.04	2	0.10	0.05	2	24%	-0.43	0.10	6.7	0.9

a) 1σ standard deviation of depths used in sample grouping (not the same as analysis replicates).

b) Number of depths used in sample grouping.

c) CFe/DFe is the percentage of DFe that is CFe. Uncertainty in this estimate is ± 5-10%.

d) Fe* is defined by Parekh et al (submitted) and is calculated with the following formula: $[DFe] - [PO_4^{-}]*(Fe/P)_{uptake\ ratio}$. Phosphate data from nearby GEOSECS stations 39 and 57 was used respectively for the 10°N and 24.5°S stations . For the Wu et al., 2001, station, Bermuda time series data was used from the winter of 2001. A biological uptake Fe:P ratio of 0.47 mmol/mol was used (Parekh et al., submitted). Fe* is a measure of the Fe deficiency of the water for biological growth with negative values indicating that there is not enough Fe to support the growth that could be sustatined by phosphate.

e) Fe:C ratios are calculated using the measured AOU from nearby GEOSECS stations (above) and a organic re-mineralization ratio of O_2:C of –1.6 (similar to the method used by Sunda (1997)).

f) North Atlantic Deep Water (NADW) values. The deep profile samples from >1500 m at the 35°N (Wu et al., 2001) and 10 °N stations. The mid-depth samples from the 24.5°S stations were chosen based on salinity, oxygen, and nutrient profiles.

high to a depth of 1050 m before decreasing to an average of 0.73 nmol/kg in deep water (Figure 2.5c and 2.8).

One of the most striking features of the upper ocean profiles is the different vertical distribution of DFe and SFe suggesting distinct biogeochemical behaviors for the SFe and CFe pools. At all sites with surface maxima in DFe, the surface maxima are due to CFe. This is shown in Figures 2.7c and 2.7d where maxima are observed in the CFe profiles, but not in the SFe profiles. A pronounced surface maximum in CFe was observed at the 30°N site in the winter, where a peak value of CFe was observed at the surface of 0.34 nmol/kg (Figure 2.5a). CFe decreased within the mixed layer to negligible amounts (0.04 ± 0.05 nmol/kg) by 77 m. The disappearance of CFe was observed at all sites with surface maxima at depths of 30 to 80 m (Figure 2.7d). At depths greater than the minima, CFe values increased to 30% of the DFe pool at 150 m at the 30°N station in the winter and the 10°N station in the summer. At the South Atlantic site in contrast, the CFe pool remained negligible throughout the pycnocline to depths greater than 550 m (Figure 2.6). The northwestern Atlantic site at 35°N that was sampled by Wu et al. (2001) may be similar to the South Atlantic site in that the CFe is also negligible at 400 and 500 m (Figure 2.7d). In general, the SFe profiles show much less structure than the CFe profiles indicating that much of the structure in the DFe profiles is due to CFe (Figure 2.9). SFe concentrations do increase with depth with most of the increase occurring below the pycnocline.

High sample density profiles in the upper 200 m were collected at the North Atlantic sites in the summer of 2001. The goal of this sampling protocol was to examine the upper water column Fe pools in more detail. At both sites, CFe had a surface maximum and decreased to negligible amounts at 30 to 50 m. The DFe and SFe for the 30°N site are plotted with salinity in Figure 2.5b. The mixed layer was very shallow at the time of sampling (11 m) and distinct salinity features in the upper 30 m are present. The DFe and SFe profiles show similar patterns to the salinity profile suggesting that the Fe values are correlated with shallow water mass properties. A similar correlation was observed along a transect in the Sargasso Sea for DFe and temperature (WU and BOYLE,

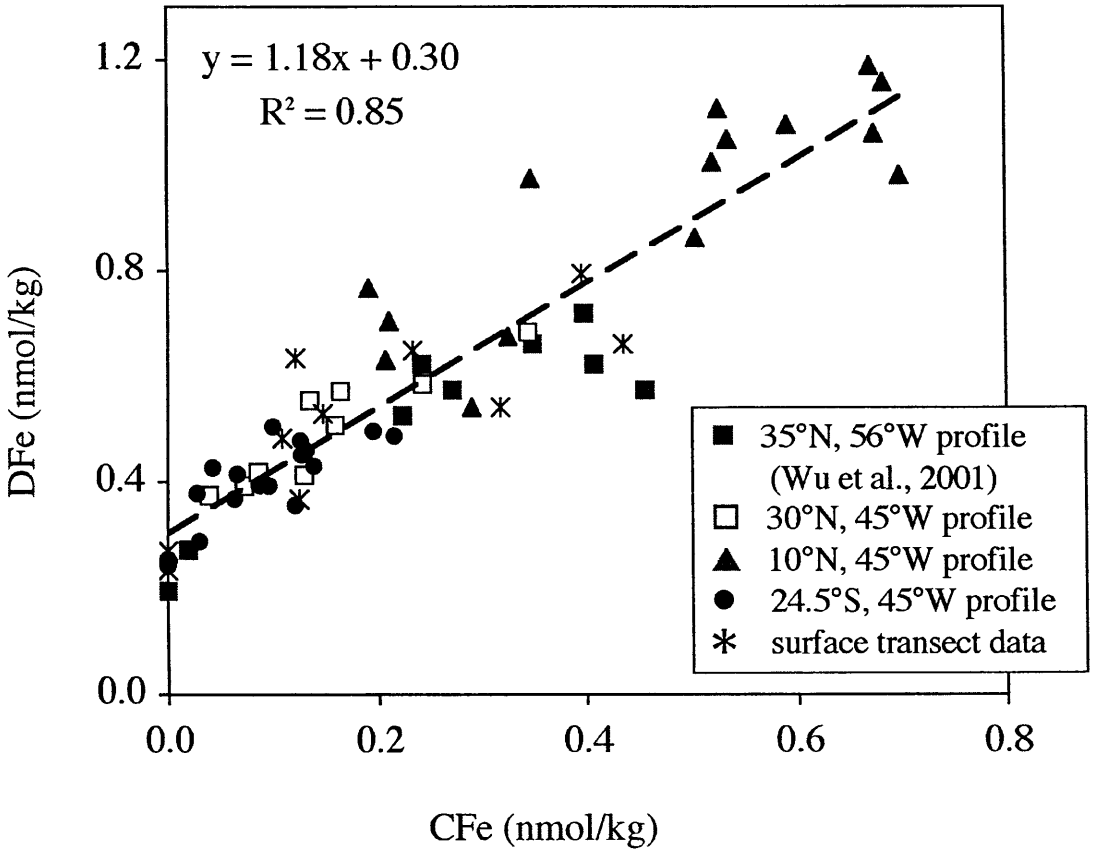

Figure 2.9: CFe plotted against DFe. This plot illustrates that much of the structure observed in DFe data is due to variations in CFe, especially at DFe concentrations above 0.3 nmol/kg.

2002). Although the residence time of Fe in surface waters is probably less than a year, it must be sufficiently long enough that young, shallow water masses retain a memory of their original surface Fe conditions. The same station in the winter was characterized by a deep mixed layer of 100 m; CFe concentrations exhibited a surface maximum and decreased to negligible levels within the mixed layer. This observation contrasts with the summer profile implying that the residence time of CFe is less than the mixing time of the mixed layer during the winter. The winter surface maximum in CFe may be due to a dust deposition event prior to our sampling, as very low atmospheric dust concentrations were measured concurrently at the station (CHEN and SIEFERT, 2004). The 30°N station in the winter is also where a large fraction of labile Fe was measured in the aerosol Fe with a possible anthropogenic source.

The summer high-density profile at the 10°N station is plotted along with chlorophyll fluorescence in Figure 2.5d. The mixed layer depth at the time of sampling was 32 m. The SFe profile shows little variation over the entire depth profile to 150 m (0.40 ± 0.03 nmol/kg, 1 SD), whereas the CFe exhibits a surface maximum and variability within the mixed layer, disappears from 50 to 100 m, and increases with depth to 200 m. The same station in the winter was characterized by a deeper mixed layer (55 m). The DFe concentration increased with depth with most of the increase in the CFe pool in the upper 200 m. This station only had 5 depths sampled in the upper 200 m and may have not sampled a CFe minimum, but likely a DFe and CFe minimum did not have occured at this time of year due to winter vertical mixing of high DFe deeper waters into the mixed layer. DFe values increased to high levels at shallower depths in the winter than in the summer reaching levels of 1 nmol/kg at 130 m versus 0.54 nmol/kg at 148 m in the summer (Figure 2.5c and 2.5d).

Below the depth where CFe and DFe minima occur (30 to 70 m), DFe concentrations do not increase much in the deep pycnocline at the subtropical gyre sites (Figure 2.7a). DFe values reach very low concentrations (<0.3 nmol/kg) with no CFe present in the pycnocline at both the South Atlantic site (Figure 2.6b) and the 35°N site (WU et al., 2001). The DFe minimum at the 30°N station remains low throughout the

pycnocline as well, but DFe concentrations are higher (0.41 nmol/kg) than the other gyre sites with 27% of the DFe present as CFe. The pycnocline water in the subtropical gyres is formed at higher latitudes (40°N) in the gyres and spreads along isopycnals (TCHERNIA, 1980). In the South Atlantic, this water forms in an area of very low dust deposition. Therefore, the pycnocline waters at the 24.5°S station are probably ventilated by water that sinks with very low DFe and negligible CFe. The reason for the difference between the pycnocline waters of the station near Bermuda and the 30 °N station from this study is less clear, but may reflect differences in the sources of the pycnocline water.

The station at 10°N is different from the gyre stations in that the pycnocline is very shallow and high levels of DFe are observed in the upper 1000 m. The zone of high Fe concentration persists from 130 to 1050 m with an average DFe of 1.09 ± 0.08 nmol/kg (1 SD, n=9) with 60% of the DFe present as CFe. The Fe maximum is associated with an oxygen minimum zone (OMZ) and maximum in phosphate (Figure 2.8). The OMZ in the tropical Atlantic is due to enhanced re-mineralization of organic matter sinking from the high productivity upwelling region off Northwest Africa (CHESTER, 1992). The oxygen depletion below the euphotic zone to intermediate depth is strongest in the eastern basin and becomes weaker westward. The Fe maximum is also associated with a salinity minimum (Figure 2.5c) of northward moving Antarctic Intermediate Water (AAIW) (TCHERNIA, 1980), which may be assumed to have low Fe concentrations based on the 24.5°S profile (<0.40 nmol/kg). Therefore, the high Fe concentrations in the upper 1000 m at the 10°N site is likely from re-mineralization of organic matter sinking from the high productivity eastern equatorial region and spreading of this water westward (FUKUMORI and WUNSCH, 1991). There are other observations that DFe in the OMZ in the eastern tropical Atlantic is very high, on the order of 2 nmol/kg (LANDING et al., 2003).

One can calculate the Fe:C ratio for the re-mineralized organic matter in the oxygen minimum zone using the same method as Sunda (1997). An Fe:C ratio of 11 ± 1 μmol/mol was calculated using the DFe concentrations, apparent oxygen utilization (AOU) from GEOSECS station 39 (8°N, 44°W), and an O_2:C ratio of –1.6 (MARTIN et

al., 1987). Our ratio falls within the range of Fe:C ratios estimated by Sunda (1997) for the North Atlantic (7 to 12 μmol/mol) calculated using the Johnson et al. (1997) data compilation. The North Atlantic estimates of re-mineralized Fe:C ratios are higher than values for the Pacific or Southern Ocean regions (usually <6 μmol/mol). Sunda (1997) interpreted this difference to indicate that the organic matter sinking in the North Atlantic may have elevated Fe:C ratios compared with most of the ocean due to the higher surface DFe and luxury Fe uptake by organisms (SUNDA and HUNTSMAN, 1995). It must be kept in mind that this Fe:C ratio could be over estimating the Fe:C ratio if the water had pre-formed DFe (meaning it sank with a significant amount of DFe). Finally, we note that more of the DFe in the oxygen minimum zone is CFe suggesting that re-mineralization of organic matter may preferentially be released into the colloidal fraction.

Although surface maxima with subsequent minima in DFe have been measured before (BRULAND et al., 1994; WU et al., 2001), only the Wu et al. (2001) study measured CFe and SFe and observed the CFe pool disappearing completely. Our study is the first to measure DFe, SFe, and CFe in the upper water column at sufficiently high sample density to document the disappearance of the CFe at multiple stations. There are two possible explanations for the disappearance of CFe: (1) atmospheric dust deposition and downward mixing and/or (2) some removal mechanism for the CFe between ≈ 30 to 80 m. There are several possible removal mechanisms for CFe: (1) colloidal aggregation and settling, (2) dissociation of colloidal ligand complexes and subsequent uptake by organisms or scavenging onto particles, and (3) direct use of colloidal Fe by organisms (i.e., ingestion). The second mechanism can be written in the following manner.

$$\text{Colloidal-Fe} \leftrightarrow \text{Colloidal} + \text{Fe} \rightarrow \text{uptake or scavenging of Fe}$$

This pathway could be driven to the right if some mechanism existed that enhanced dissociation of the Fe from the colloid (such as photochemistry or bioreduction at cell membranes, Chapter 1) at approximately ≈ 50 m. As discussed in Chapter 1 (Figure 1.3), there is evidence that marine organisms can grow utilizing colloidal Fe, although growth rates are usually lower than organisms grown on free Fe (BARBEAU et al., 1996; BARBEAU and MOFFETT, 1998; BARBEAU and MOFFETT, 2000; CHEN and WANG, 2001;

NORDWELL and PRICE, 2001; CHEN et al., 2003). However, with our data it is impossible to distinguish a biological removal mechanism from a scavenging/aggregation removal term at a similar depth (near where there are biological particles and export). The reappearance of CFe in deeper waters does suggest that CFe is regenerated at depth probably through re-mineralization of organic matter.

2.3.3.2. Surface Residence Time Estimates

Surface residence time calculations were made at the profile sites for which reasonable assumptions of steady-state could be made (Table 2.3). DFe concentrations were integrated over the depth of the mixed layer and concurrent labile Fe deposition estimates (90-minute, pH 4.5, reducing leach) were used as an input flux of DFe where available (CHEN and SIEFERT, 2004). This method assumes that atmospheric deposition is the dominant source of DFe to the mixed layer, that the labile Fe flux estimates are representative of the atmospheric input, and the DFe concentrations are at steady-state.

Excluding the 30°N site, estimates of surface residence times in the North Atlantic were 1.5 to 5 months (± 50%). This agrees with other estimates of surface residence times of weeks to a few months (DE BAAR and DE JONG, 2001; SARTHOU et al., 2003). The atmospheric Fe concentrations at the 30°N station were very low (despite the high solubility) and the residence time calculation gave unrealistic results. For the 24.5°S station, concurrent measurements of dust were not available. Estimates of dust deposition from Vink and Measures (2001) were used from a similar transect in June 1996. Because of the variability of dust dissolution, two cases (3% and 10%) were chosen based on the observations from Chen and Siefert (2004) and residence times of 14 and 4 months were calculated respectfully. The only way to reduce the residence time to a few months using our method is to increase the estimated flux to the surface ocean. In our method, this can be done assuming higher aerosol dissolution. It is also possible that our estimate of total atmospheric input is too low or some other significant source is being neglected (i.e. surface water advection from areas with higher DFe). In either of these cases, our estimate would be an upper limit. Another possibility is that surface

Table 2.3: Surface Residence Time Estimates*

Site	mixed layer depth (m)	total Fe flux ($\mu g/m^2/d$)	1 SD[f]	total labile Fe flux[c] ($\mu g/m^2/d$)	1 SD	% dust dissolution	integrated DFe (μg)	residence time (days)	1 SD
10°N winter	55	630[a]	350	30[a]	16	5%	2055	69	37
10°N summer	32	278[a]	171	6.1[a]	3.3	2%	1000	164	89
30°N summer	11	203[a]	122	6.9[a]	5	3%	318	46	32
30°N winter	100	2.5[a]	1.4	0.7[a]	0.5	28%	2937	*4196*[e]	*2997*
24.5°S (varying	52	88[b]		2.7[d]	1.7	3%	1122	424	297
dissolution	52	88[b]		8.8[d]	6.2	10%	1122	128	89

*Residence time calculations in this table were made using measured Fe concentrations in the mixed layer and mixed layer depths. This estimate assumes steady state and that atmospheric deposition is the only input flux into the system. It does not consider vertical mixing or advection.

a) Total Fe fluxes and total labile Fe fluxes measured concurrently at sea assuming a 1 cm d^{-1} deposition rate (Chen and Siefert, submitted).

b) Based on an estimate of dust flux for this station from June 1996 (Vink and Measures, 2001). A total atmospheric dust deposition flux was calculated from dissolved Al data. Total Fe deposition flux was calculated using an average continental crustal abundance for Fe of 4.3%. Standard deviation estimate made using typical Chen and Siefert, submitted, estimates of variablilty.

c) Total labile Fe flux is the Fe that was released from a reducing, slighty acidic (pH 4.5) leaching solution (Chen and Siefert, submitted) measured concurrently at sea on fresh aerosols.

d) Since no estimate of total labile Fe exists for this station exists, three % dust dissolution values were chosen that are in the range of the observed values from the North Atlantic data.

e) The 30°N had a surface maximum in the mixed layer and decreasing values of Fe in the mixed layer. The in situ measured dust flux for this region is too low to explain the Fe maximum and/or the steady-state assumption for the DFe is incorrect. Thus, residence time calculations for this station are unrealistically long.

f) Standard deviation estimates from Chen and Siefert, submitted, are the 1σ variability of many stations within each region.

residence time is longer in areas without large atmospheric input and low CFe concentrations.

2.3.3.3. Deep-water Column Fe Profiles

Two deep-water profiles were collected at 10°N and 30°N during the winter 2001 North Atlantic cruise and one deep profile was sampled at 24.5°S on the March 2002 South Atlantic cruise. The 10°N station profile was sampled to 4200 m. Below the high DFe of the OMZ, DFe values decrease to an average value of 0.73 ± 0.12 nmol/kg (1 SD, n=3) below 1600 m. The decrease in the DFe concentration is entirely due to a decrease in the fraction of CFe from ≈ 60% of the DFe in the OMZ to 40% at depths greater than 1600 m. SFe concentrations do not change with depth throughout the OMZ and deeper at this site. From the salinity profile (Figures 2.5c and 2.7b), the water from 1600 m to 4200 m can be identified as North Atlantic Deep Water (NADW). The Wu et al. (2001) 35°N station also sampled NADW (see salinity profile, Figure 2.7b) and had an average value of 0.64 ± 0.05 nmol/kg (n=6) at depths greater than 1600 m, which is lower than our observed value. However, we only have three samples below 1600 m and the 3400 m sample yielded high concentrations (0.86 nmol/kg) and hence is potentially contaminated. The concentration was measured in analyses from both filtrate bottles, so the datum is retained in the sample plots and calculations. Without the 3400 m point, the 10°N NADW average for DFe would be 0.67 ± 0.05 nmol/kg (n=2) and indistinguishable from the Wu et al. (2001) 35°N NADW value. The 30°N station was only sampled to 1050 m and did not sample NADW, but both DFe and SFe concentrations increase below the pycnocline (Figure 2.5a).

The South Atlantic water column profile Fe data are the first reported and includes all the major water masses. In Figure 2.6a, the DFe and SFe profiles are shown along with reactive silicate data. Antarctic Intermediate Water (AAIW) is the high-Si water just below the pycnocline from 700 to 1200 m and has a DFe value of 0.38 ± 0.01 nmol/kg (1 SD, n=4). NADW has lower Si concentration and forms the core of the deep water from 1700 to 3350 m with higher DFe concentrations (0.47

± 0.02 nmol/kg, 1SD, n=7). Below 3500 m, Si levels increase to very high levels at 4040 m (118 μmol/kg) indicative of Antarctic Bottom Water (AABW). The DFe in the AABW was 0.42 ± 0.01 nmol/kg (1 SD, n=4). There are few measurements of DFe in the Atlantic sector of the Southern Ocean and those data are mostly from surface water. Surface waters vary from 0.1 to 0.5 nmol/kg (MARTIN et al., 1990; DE BAAR et al., 1995; LOSCHER et al., 1997), and DFe concentrations from a profile near the Drake Passage were 0.10 to 0.16 nmol/kg at the surface and increased to 0.40 nmol/kg at 550 m (MARTIN et al., 1990). These Antarctic DFe concentrations, which represent the source water for the Antarctic water masses, are comparable with our observations of DFe concentrations for AAIW and AABW at our site.

All of the structure in the observed deep-water DFe profile at 24.5°S and in most of the DFe data in this study is due to CFe (Figure 2.7c, 2.7d, 2.9). The SFe at the South Atlantic site is invariant at depths greater than 700 m (0.33 ± 0.04 nmol/kg, 1 SD, n=12). The average value of deep-water SFe from the North Atlantic sites (0.38 ± 0.08 nmol/kg, 1 SD, n=14) is only slightly higher than the deep-water SFe at the South Atlantic site. In contrast, the deep-water CFe decreases from 0.26 ± 0.11 nmol/kg (1 SD, n=13) in the North Atlantic to 0.11 ± 0.06 nmol/kg (1 SD, n=12) in the South Atlantic. The difference is significant at the 95% confidence level using both the t-test and a distribution-free test, the Kolmogorov-Smirnov test (HOLLANDER and WOLFE, 1973). If one looks only at the NADW, the CFe fraction decreases from 40-50% of the DFe in the North Atlantic to 30% at the South Atlantic site. This loss in CFe along the flowpath suggests that CFe is preferentially lost along the flow path of this water. Despite having lower CFe concentrations than further north, the NADW at 24.5°S still has a larger fraction of CFe than the Antarctic water masses. The CFe fraction of the DFe is slightly lower in the AAIW and AABW (≈ 20% of DFe) compared to the NADW (≈ 30% of DFe) at the South Atlantic site. This difference between the NADW and Antartic derived water masses is probably due to high dust input to North Atlantic surface waters and regeneration of Fe-replete sinking organic matter compared to the very low initial Fe concentrations of Antarctic surface waters. The relatively invariant concentrations of SFe

are suggestive of some solubility control (perhaps limited organic ligand concentrations in the soluble fraction).

In Figure 2.9, all of the DFe and CFe concentration data from the Atlantic are plotted and a positive correlation between DFe and CFe is observed. The y-intercept of the data is at a DFe concentration of ≈ 0.30 nmol/kg. The CFe fraction of the DFe disappears below DFe concentrations of less than 0.30 nmol/kg, and there is approximately a 1:1 relationship between DFe and CFe above 0.30 nmol/kg (r^2=0.85). Not only does this relationship illustrate that higher DFe concentrations are usually due to CFe, but also suggests that there is some limit on SFe concentrations or that CFe only exists when SFe reaches a certain concentration. Unfortunately not much is known about the distribution of organic ligands in the CFe and SFe pool, but it is probable that organic ligands may play a role in establishing this relationship in the Atlantic Ocean. Excess organic ligands were measured and observed in both the colloidal and soluble fraction of surface and deep water in the northwest Atlantic and in the subtropical and tropical Atlantic on the March 2002 cruise (unpublished, CULLEN AND MOFFET, 2003). How the distributions of these organic ligands relates to the distribution of SFe and CFe still remains an open question that needs to be explored.

Two qualitatively useful parameters (Fe* and AOU estimated Fe:C ratios) were estimated for the various water masses sampled in the deep-water at our sites (Table 2.2). Fe* is defined by Parekh et al. (submitted) and is calculated with the following formula: $Fe^* = [Fe] - (Fe/P)_{uptake\ ratio} * [PO4^-]$. Fe* is a measure of the Fe deficiency of the water for biological growth with negative values indicating that there is insufficient Fe to support growth based on the available phosphate. The Fe:P uptake ratio (0.47 mmol/mol) used in this estimation corresponds to a Fe:C ratio of 4 μmol/mol (SUNDA and HUNTSMAN, 1995) and a Redfield C:P of 117 (ANDERSON and SARMIENTO, 1994). The Fe:C ratio is a reasonable value for a minimum amount of Fe needed for growth by oceanic species (SUNDA and HUNTSMAN, 1995). Fe* values for the North Atlantic sites are mostly slightly positive, whereas Fe* is negative for all the water masses at the South Atlantic site. The most severe Fe deficiencies are observed in the Antarctic-derived water masses.

The general pattern of Fe* agrees well with model derived estimates of Fe* by Parekh et al. (submitted).

The NADW, a major source of water upwelling in the Southern Ocean (TCHERNIA, 1980), is already deficient in DFe relative to phosphate at 24.5°S due to removal of Fe by scavenging (Fe* of -0.15 nmol/kg). The severe deficiency of Fe relative to phosphate in waters derived from the Southern Ocean is caused by upwelling water already being deficient in Fe as well as the low dust supply to the Southern Ocean, which does not supply enough Fe for the biological pump to utilize the entire phosphate pool. Therefore, a large excess of phosphate is left in the surface waters when it sinks. The excess phosphate combined with progressive scavenging of Fe as the Antarctic water masses move north leads to the low Fe* values observed (-0.43 to -0.57 nmol/kg). It is interesting that the Fe* values in the North Atlantic are positive. This lends support to arguments by Sunda (1997) that sinking organic matter in the North Atlantic has higher Fe:C ratios due to luxury uptake of Fe when more Fe is available.

The other quantity estimated from our data set was Fe:C ratios based on AOU measurements and an O_2:C ratio of -1.6 (MARTIN et al., 1987; SUNDA, 1997). The AOU derived Fe:C ratios represents the Fe:C ratio of re-mineralized organic matter, but is only valid in water masses that sank with very little preformed Fe and have not had significant loss of DFe due to scavenging (young water masses). The Fe:C ratio of 11 μmol/mol estimated for the OMZ at the 10°N site may be representative of Fe:C ratios of sinking organic matter in the North Atlantic due to the high levels of re-mineralized DFe in the OMZ and the relatively young age of this water. The NADW at 10°N has elevated Fe:C ratios of ≈ 17 μmol/mol, which may be due to higher Fe:C ratios in sinking organic matter or preformed Fe in the NADW when it sank the in the North Atlantic. A preformed DFe of 0.3 nmol/kg would lower the Fe:C ratio estimate to ≈ 10 μmol/mol. At 24.5°S, the NADW Fe:C ratio decreases from to 11 μmol/mol indicating net loss of Fe by scavenging. The two Antarctic derived water masses (AAIW and AABW) at 24.5°S have significantly lower AOU-derived Fe:C ratios of 5 to 7 μmol/mol, which could

indicate that re-mineralized organic matter in the South Atlantic and Southern Ocean has lower Fe:C values than the North Atlantic re-mineralized organic matter.

2.3.3.4. Deep-water Residence Time Estimate

The scavenging residence time of DFe in the NADW can be estimated from the difference between DFe in the North Atlantic sites and the South Atlantic site. The NADW at the South Atlantic site (0.47 ± 0.02 nmol/kg, 1 SD, n=4) has significantly less DFe than the average of NADW from the northern sites (0.67 ± 0.09 nmol/kg, 1 SD, n=9). Salinity and silicate data indicate that the NADW has not been significantly diluted with Antarctic water sources during transit from the North Atlantic to 24.5°S station. The NADW value for the North Atlantic is an average of the DFe concentrations from depths greater than 1600 m from the 10°N site from this study and the 35°N site from Wu et al. (2001). Neither North Atlantic site sampled deep enough to include AABW (see salinity plot, Fig. 2.7b), so all sample depths are included in the average. Again, most of the decrease from the North Atlantic to the South Atlantic site in the DFe pool occurs in the CFe pool. The average SFe for the North Atlantic (0.36 ± 0.05 nmol/kg, n=7) is the same as the SFe at the South Atlantic site (0.33 ± 0.05 nmol/kg, n=4). However, the CFe in NADW decreases from 0.32 ± 0.12 nmol/kg (1 SD, n=6) to 0.15 ± 0.05 nmol/kg (1 SD, n=4). Both measured differences in the DFe and CFe between the North Atlantic sites to South Atlantic site are significant at the 95% confidence level using the t-test and a distribution-free test, the Kolmogorov-Smirnov test (HOLLANDER and WOLFE, 1973)

In order to calculate a scavenging residence time for the DFe in the NADW, several factors were considered including (1) dilution of the NADW with low Fe Antarctic water, (2) re-mineralization of organic bound Fe along the flow path, and (3) the transit time of NADW from the North Atlantic (at 10°N) to the South Atlantic site (24.5°S). As can be seen by the salinity profile (Figure 2.7b), the core of the NADW salinity from all sites is nearly the same indicating very little dilution of the NADW from lower salinity Antarctic water. However, if one assumes that the small increase in Si in NADW observed at GEOSECS stations near our stations (station 39: 8°N, 44°W; station

Table 2.4: Deep-water Scavenging Residence Time Estimates

IRON

	depth range (m)	DFe (nmol/kg)	1 SD (a)	n (b)	SFe (nmol/kg)	1 SD. (a)	n (b)	CFe (nmol/kg)	1 SD (a)	n (b)
10°N and 35°N[c]	>1600	0.67	0.09	9	0.36	0.05	7	0.31	0.10	6
24.5°S	1700-3310	0.47	0.02	7	0.33	0.05	4	0.15	0.05	4
gain or loss due to re-mineralization or dilution from 10°N to 24.5°S										
gain (re-mineralization)[d]:		0.04	0.02[f]		0.02[h]	0.01		0.02[h]	0.01	
loss (dilution)[e]:		-0.01	0.01[g]		-0.01[i]	0.01		0.00[i]	0.00	
net::		0.03	0.02		0.01	0.01		0.02	0.01	
scavenging residence time	**net DFe (nmol/kg)**	**DFe (yr)**	**unc.[l]**					**CFe (yr)**	**unc.[l]**	
low net gain (56 yr)[j]	0.01	300	160					160	110	
mid net gain (56 yr)[j]	0.03	270	140					140	100	
high net gain (56 yr)[j]	0.05	250	130					130	90	
mid net gain (40 yr)[k]	0.03	200	100					100	70	

MANGANESE

	depth range (m)	DMn (nmol/kg)	stdev (a)	n (b)		transit time (yr)	DMn (yr)	unc.[l]
10°N	>300 m	0.50	0.04	10	**residence time:**	56[j]	130	50
24.5°S	>300 m	0.20	0.08	19		40[k]	90	35

a) 1 SD is the standard deviation of the concentration measurements at the depths used in sample grouping (not the same as analysis replicates).

b) Number of depths used in sample grouping.

c) Fe values were combined from the 10°N site from this study and the 35°N site from Wu et al. (2001). This was done because the 10°N site only had three samples in the NADW and one of them was suspect (see text). Without the one sample, the deep water between the two sites was indistinquishable.

d) The gain due to re-mineralization in NADW from 10°N to 24.5°S was calculated using phosphate data from GEOSECS stations near our sites (st. 39 and 57 respectively) after correcting for dilution of NADW with Antarctic waters. A Fe:P ratio of 1 mmol/mol (which corresponds to an Fe:C ratio of 10 μmol/mol and a C:P of 117) was used to calulate the Fe gain.

e) The loss due to dilution of NADW with low Fe Antarctic waters was calculated by assuming all of the increase in silicate in NADW from 10°N to 24.5°S was due to dilution of low silicate NADW with high silicate Antarctic waters. 0.4 nmol/kg was used for the Antarctic water Fe concentration.

f) The standard deviation of this estimate is based on changing the Fe:C ratio and changing the dilution factor by a factor of 2.

g) This is an assumed uncertainty in this estimate. However based on salinity and the small increase in silicate (2 μmol/kg), very little dilution has occured in the core of the NADW.

h) The CFe and SFe from re-mineralization was assumed to be 60% CFe and 40% SFe based on the large re-mineralization zone measured at 10°N in the oxygen minimum zone.

i) The CFe and SFe loss from dilution was assumed to be 20% CFe and 80% based on the observed ratio of these two pools in the AAIW and AABW at the 24.5°S site.

j) The difference in age from 10°N to 24.5°S was calculated to be ≈ 56 years based on radiocarbon age estimates from Broecker and Virgilio (1991).

k) Residence times were also calculated for an assumed transit time of 40 years between 10°N to 24.5°S. This was the age needed to bring the Mn residence time to under 100 years.

l) Uncertainties in residence time calculations are determined by the the uncertainty in the difference between the north and south Fe concentrations and an assumed uncertainty of 30% in the transit time estimattion.

57: 24°S, 35°W) is due to dilution of low-Si NADW with high-Si Antarctic water, a modest dilution factor of 3.5% can be estimated. Dilution could then account for 0.01 nmol/kg of the DFe decrease from the North to South Atlantic assuming 0.40 nmol/kg DFe for Antarctic deep-water. DFe from re-mineralization of organic matter was considered by using the phosphate and AOU data from the two GEOSECS sites. There is a small increase in phosphate from the northern to southern site. If one accounts for dilution of low-P Antarctic water with the higher-P NADW and uses a Fe:P re-mineralization ratio of ≈ 1 mmol/mol (corresponds to an Fe:C of 10 μmol/mol and a C:P of 117), a regeneration input of 0.04 nmol/kg DFe can be estimated for the transit from the northern to the southern station. Combining the dilution loss and the regeneration gain, an increase of DFe of 0.03 ± 0.02 nmol/kg was estimated between the two stations. The uncertainty in this estimate is large because both the Fe:C ratio and the dilution factor also could be a factor of 2 different. The transit time of NADW was estimated using radiocarbon age estimates for western Atlantic deep water (STUIVER, 1976; BROECKER and VIRGILIO, 1991). Averaging multiple stations around our 10°N and 25°S stations from Broecker and Virgilio (1991) resulted in an age difference of ≈ 56 ± 18 years. This estimate is probably reasonable as a simple linear age model assuming an age difference of 160 years between 42°N and 30°S (STUIVER, 1976), results in an age difference of ≈ 75 years. Stuiver (1976) inferred that more of the 160 year aging occured in the North Atlantic, therefore 75 years would be an upper limit.

A summary of the data used and estimated scavenging residence times are given in Table 2.4. An estimate of 270 ± 140 years was calculated for deep-water DFe based on the observed loss of DFe (0.20 nmol/kg) and the estimated input of 0.03 nmol/kg DFe from regeneration minus dilution in the transit from the northern to southern station. Changing the regenerative- and mixing-induced input to lower and higher estimates of 0.01 and 0.05 nmol/kg does not significantly change the scavenging residence time estimate (300 ± 150 years and 250 ± 130 years, respectively). Our derived scavenging residence time is very sensitive to the difference in DFe from north to south and the transit time estimate. Lowering the transit time to 40 years changes our estimate of

scavenging residence time to 200 ± 100 years. Our estimate of scavenging residence time agrees with published estimates of residence time (BRULAND et al., 1994; JOHNSON et al., 1997; PAREKH et al., submitted), but there is a large uncertainty due to the uncertainties in the difference between the DFe between the North Atlantic sites and South Atlantic site and the transit time.

Assuming there is no exchange between the SFe and CFe, it is possible to estimate a scavenging residence time for the CFe fraction of DFe as well. It was assumed that 60% of the re-mineralized DFe was released into the CFe fraction (based on the CFe/DFe of the OMZ at the 10°N site) and that 20% of the DFe from Antarctic sources diluting NADW was CFe (based on AAIW and AABW from 24.5°S profile). From these assumptions, a deep-water scavenging residence time for CFe of 140 ± 100 years was estimated indicating that CFe has a shorter residence time than DFe and SFe. However, it is not known how the two pools of DFe interact.

2.3.4. Mn Water Column Profiles

Deep-water column profiles of DMn for the 30°N, the 10°N, and the 24.5°S sites are shown in Figure 2.10a and the data is given in Appendix 2.2. DMn concentrations are highest in surface waters, well mixed within the mixed layer, and decrease rapidly below the mixed layer. The surface water DMn levels were discussed in the surface transect section and follow atmospheric input trends with high levels being maintained by photochemical cycling in the upper euphotic zone and mixed layer (SUNDA and HUNTSMAN, 1988). Below the zone of photochemical cycling, the deep-water DMn (>300 m) decreased to values of 0.51 ± 0.05 nmol/kg (n=16) at the North Atlantic sites and 0.20 ± 0.08 nmol/kg (n=19) at the South Atlantic sites. The values in the deep-water of the South Atlantic were near or at our detection limit for Mn. Our values in North Atlantic deep-waters are slightly higher than previously published values, 0.3 to 0.4 nmol/kg, for mid-latitude sites from 10°N to 35°N (YEATS and BEWERS, 1985; STATHAM and BURTON, 1986; STATHAM et al., 1998). Higher DMn values (0.6 to 0.7 nmol/kg) have been observed at North Atlantic sites at higher latitudes, 45°N to 53°N

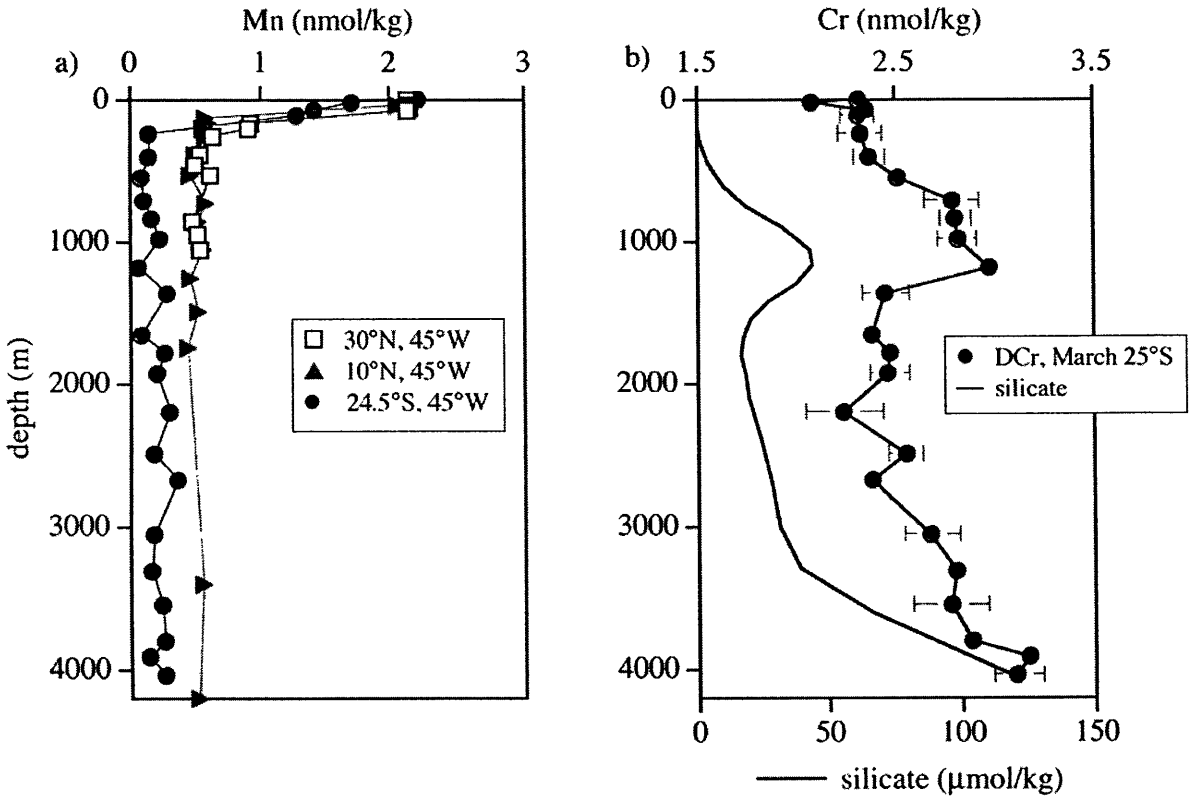

Figure 2.10: 2.10a) Dissolved Mn data for the profile stations in the Atlantic. Values are high in surface waters and decrease with depth. The external reproducibity of the Mn data is typically ± 0.08 nmol/kg (1 SD). 2.10b) Dissolved Cr profile from the South Atlantic station at 24.5°S plotted along with silicate. Error bars are 1σ standard deviations of sample replicates. The external reproducibility of the Cr measurement is ± 0.15 nmol/kg (1 SD).

(YEATS and BEWERS, 1985). There are only two previously published profiles from the South Atlantic at 15°S and 30°S in the eastern basin. DMn from greater than 300 m at those sites was 0.2 to 0.3 nmol/kg, which is similar to our observed deep-water DMn in the western basin of the South Atlantic.

Because Mn is a scavenged element in oxygenated deep-water, DMn concentrations in deep-water tend to decrease with increasing age of deep-water unless there is an input of DMn (e.g., hydrothermal vents, suboxic boundary layer) (LANDING and BRULAND, 1987; STATHAM et al., 1998). Our data follows this trend with decreasing DMn in the deep-water from the North Atlantic to South Atlantic. We did not observe elevated DMn levels in the OMZ at 10°N. Elevated levels of DMn have been observed in the OMZ of the Pacific (KLINKHAMMER and BENDER, 1980; LANDING and BRULAND, 1980; LANDING and BRULAND, 1987), but much lower levels of oxygen (<50 μmol/kg) are observed in the Pacific OMZ than the minimum oxygen levels at our site (≈ 100 μmol/kg). Klinkhammer and Bender (1980) proposed three possible mechanisms for the Mn maximum observed in the OMZ of the Pacific: (1) reduction of MnO_2 to soluble Mn(II) in reducing sediments of the continental margin, contact of OMZ water with these sediments, followed by lateral transport of Mn(II) with the OMZ water, (2) reduction of MnO_2 particles within the OMZ due to low oxygen and lower pH conditions, and (3) release of Mn(II) from sinking organic matter. The first mechanism has been argued against due to the low observed Mn fluxes from sediments in the OMZ of the continental margin of the Pacific (JOHNSON et al., 1992; JOHNSON et al., 1996). Johnson et al. (1996) modeled the dissolved Mn(II) maxima in oxygen minimum zones using a model where Mn(II) was released from sinking organic matter and the rate of Mn(II) oxidation to MnO_2 followed by scavenging was reduced within the OMZ. The reduction in Mn(II) oxidation and scavenging leads to formation of the dissolved Mn maximum in the OMZ. However, the model predicts that Mn maxima would only exist in OMZs with more severe oxygen depletions (<100 umol/kg) than our station.

Deep-water scavenging residence time estimates were made for DMn (Table 2.4) using concentrations in NADW at 10°N and 24.5°S and a transit time of 56 years, similar

to the method used for DFe. No gain or dilution factors were considered for Mn because it does not have a significant source from re-mineralization of organic matter nor is there a difference between the Antarctic water masses and NADW at the South Atlantic site. We estimated a scavenging residence time of 130 ± 50 years, which is longer than previous estimates of <50 years (WEISS, 1977; BRULAND et al., 1994). In order to reduce the scavenging residence time, the transit time of the NADW from 10°N and 24.5°S would need to be decreased or another input of Mn would need to be included. It is possible that there could be lateral advection of Mn from the shelf to mid-depth water, although no variations with depth are observed. If the transit time were shortened to 40 years, the residence time of DMn would be less than 100 years.

2.3.5. Cr Water Column Profile

Only one profile was processed for dissolved Cr (DCr) at the 24.5°S station (Figure 2.10b and Appendix 2.3). DCr concentrations range from 2.2 nmol/kg in the surface water to 3 nmol/kg in deep-waters and show a correlation with Si (r^2=0.69) and thus water mass units. The Antarctic water masses have higher DCr (AAIW: 2.85 ± 0.08 nmol/kg, 1 SD, n=4; AABW: 2.98 ± 0.19 nmol/kg, 1 SD, n=4), and the NADW values are slightly lower (2.52 ± 0.19 nmol/kg, 1 SD, n=7). A correlation of Cr with Si (and slightly less pronounced correlation with other nutrients such as P) for individual profiles has been observed before (CRANSTON, 1983). However, unlike Si, Cr does not seem to increase from the North Atlantic to the South Atlantic or to the Pacific with increasing age of deep-water. Observed values in the deep-water of the North Atlantic range from 3 to 5 nmol/kg (and higher) at open ocean sites (CAMPBELL and YEATS, 1981; JEANDEL and MINSTER, 1987; SIRINAWIN et al., 2000), and one profile from the eastern South Atlantic had measured deep-water DCr of ≈ 5 nmol/kg (SIRINAWIN et al., 2000). Comparable, if not somewhat lower, concentrations have been observed in the Pacific (CRANSTON, 1983; MURRAY et al., 1983; JEANDEL and MINSTER, 1987). It is unclear from the data sets how much of the variation in observed measurements is due to real variability and how much is due to differences in measurement technique. Our method

suffers from a large blank correction, and we have not assessed our accuracy with external consistency samples or standards. Therefore, it is difficult to compare our DCr concentrations with other published data sets. However, our concentrations do fall within (towards the low end) the range of observed values published for the Atlantic. Our DCr observations support earlier observations that Cr is involved in biogeochemical cycling to a limited extent.

2.4. CONCLUSIONS

In the subtropical and tropical Atlantic, surface DFe and DMn concentrations follow dust deposition trends. The coupling of dust deposition and dissolved concentrations of these elements is modified by their chemistry in the surface waters. For DFe, biological uptake and scavenging cause DFe levels to be variable and have residence times in surface waters on the order of a few months (1 to 5 months). Based on dust solubility experiments (mesocosm incubation experiments), lower DFe compared to dissolved Al, and observed excess ligand concentrations in the North Atlantic, there may be a solubility limit to how much atmospheric Fe can dissolve in the North Atlantic surface waters ($\approx$ 1.15 nmol/kg). DMn has a longer residence time in surface waters (decades) due to photochemical cycling, therefore the correlation of DMn and dust deposition is erroded due to cycling and lateral advection.

Two fractions of DFe, soluble and colloidal, were considered in this study. The CFe followed dust deposition trends more strongly than the SFe, and observed surface maxima in DFe profiles were always associated with maxima in CFe. These observations support arguments by Wu et al. (2001) that atmospheric Fe is preferentially released into the colloidal fraction. Where dust deposition is low and CFe is low (i.e. the South Atlantic), the residence time of DFe may be longer because of a smaller fraction of CFe.

SFe and CFe profiles had distinct profiles both in the upper water column and in deeper waters. SFe profiles were always depleted in surface waters (and also in the deep pycnocline of the gyre sites) and gradually increased to relatively uniform concentrations in deep-water ($\approx$ 0.3 to 0.4 nmol/kg). CFe profiles showed significantly more variability.

At sites with surface maxima in CFe, the CFe always decreased to negligible levels at depths of 30-80 m either in the mixed layer or below. At two gyre sites (24.5°S and likely the Wu et al. (2001) 35°N site near the Bermuda Rise), the CFe pool remained negligible throughout the deep pycnocline. At the 30°N gyre station, which also had a deep pycnocline, DFe and CFe also remained low throughout the pycnocline with CFe accounting for 30% of the DFe. The low DFe and CFe in the deep pycnocline of the gyre sites may be due to ventilation with water from higher latitiudes with lower dust input (and thus low CFe).

In contrast to the gyre sites, the 10°N station was located on the edge of the equatorial system and had a very shallow pycnocline (<250 m). It was the only station that did not have a surface maximum in DFe or CFe, but only in the winter when the mixed layer was deep. DFe increased rapidly within the shallow pycnocline to concentrations >1 nmol/kg associated with an OMZ at depths of 130 to 1050 m. A majority of the increase in DFe (60%) resulted from increasing CFe. The increased DFe in the OMZ is likely due to re-mineralization of organic matter under the high-productivity eastern equatorial upwelling region and then lateral westward spreading. Under the more stratified summer conditions, the 10°N site had a surface maximum followed by a minimum from 50 to 100 m in the CFe. We have not established the mechanisms that cause the shallow minima in CFe, but it may be due to (1) atmospheric deposition and downward mixing and/or (2) a Fe sink within the euphotic zone such as scavenging or an indirect biological utilization mechanism.

Deep-water DFe and CFe concentrations show variability with water mass and with the source, age, and path of the water masses. DFe concentrations in NADW decrease by 30% from the North Atlantic to South Atlantic with most of the decrease associated with the colloidal pool. Despite the loss in CFe, the NADW CFe and DFe concentrations at 24.5°S are still higher than the concentrations of Antarctic derived water masses (AAIW and AABW). DFe in AAIW and AABW is low ($\approx$ 0.4 nmol/kg), which is consistent with observations of DFe in the Southern Ocean. Approximately 20% of the DFe in the Antarctic water masses is colloidal, which may reflect their low-

dust and low DFe source region. SFe in the deep-water in the Atlantic is relatively uniform, therefore most of the variability observed is due to CFe. This was illustrated by positive correlation between DFe and CFe above a DFe concentration of ≈ 0.3 nmol/kg. A deep-water scavenging residence time for DFe of 270 ± 140 years was estimated from the DFe decrease in NADW from the North Atlantic to South Atlantic. If one assumes there is no exchange from the SFe pool to the CFe pool, then a scavenging residence time for CFe ws also estimated (140 ± 100 years).

DMn concentrations were also measured at all the profile sites, and a DCr profile measured only the South Atlantic site. DMn profiles are consistent with observations with high surface water values (≈ 2 to 3 nmol/kg) in the mixed layer and euphotic zone where there is atmospheric input and photochemically cycling. Concentrations drop off rapidly to low values at depths greater than 300 m. Concentrations decrease with the age of deep-water with higher values in the North Atlantic (≈ 0.5 nmol/kg) than at the South Atlantic site (≈ 0.2 nmol/kg). From this decrease, a scavenging residence time of 130 ± 50 years was estimated. The South Atlantic DCr profile had depleted surface values (2.1 nmol/kg) and increased with depth to values between 2.3 and 3.2 nmol/kg. Concentrations varied with water mass unit with higher concentrations associated with the Antarctic water masses (≈ 3 nmol/kg) and lower values in NADW (≈ 2.5 nmol/kg). With only one profile, it is difficult to contribute to the discussion on the controls of the Cr distribution in the ocean. However, our data falls within the range of observed values and supports earlier observations that Cr is involved in biogeochemical cycling to a limited extent.

Appendix 2.1: Surface Transect Data

Cruise	date	Lat. (°N, neg. °S)	Long. (°W)	DFe[a] (nmol/ kg)	1 SD[d]	n	SFe[b] (nmol/ kg)	1 SD	n	DMn[c] (nmol/ kg)	1 SD	n
SJ0101	1/14/01	30.0	45.3	0.48	0.04	2	0.37	0.07		1.58	0.06	6
Jan. 2001	1/16/01	26.2	45.0	0.49	0.05	3				1.92	0.11	3
	1/17/01	25.1	44.7	? 1.13	0.07	2				2.60	0.03	2
	1/17/01	24.0	45.0	0.73	0.03	2				2.28	0.16	3
	1/17/01	23.0	45.0	0.79	0.06	4	0.40	0.08		2.25	0.14	9
	1/18/01	21.7	45.0	0.89	0.02	2				3.20	0.10	3
	1/18/01	20.5	45.0	0.84	0.05	4				2.75	0.45	6
	1/18/01	18.4	45.0	0.68	0.04	3				2.49	0.09	3
	1/19/01	18.0	45.0	0.63	0.04	4	0.51	0.03		2.68	0.13	6
	1/19/01	15.8	45.0	0.65	0.04	6	0.42	0.04		2.95	0.33	9
	1/20/01	14.4	45.0	? 0.91	0.05	3				2.67	0.10	3
	1/20/01	12.3	45.0	0.30	0.04	3				2.98	0.07	3
	1/20/01	11.6	45.0	0.43	0.01	2	? 0.74	0.02		2.86	0.07	3
	1/20/01	10.6	45.0	0.37	0.06	3				2.95	0.33	3
	1/21/01	10.2	45.0	0.54	0.06	6	0.22	0.08		2.17	0.04	6
Kn162	6/27/01	29.2	23.6	0.39	0.02	3				1.76	0.02	3
June/July	6/28/01	29.3	28.0	0.42	0.09	4				1.85	0.02	3
2001	6/29/01	29.6	31.9	0.37	0.03	3				1.91	0.08	3
	6/30/01	29.7	35.9	0.60	0.03	5				2.28	0.14	3
	7/1/01	29.8	39.4	0.49	0.03	4				1.65	0.07	6
	7/2/01	30.0	45.0	0.50	0.04	3				1.70	0.07	3
En367	3/4/02	7.0	49.5	0.53	0.01	2	0.38	0.04	3	2.67	0.06	3
Mar. 2002	3/6/02	3.5	44.5	0.66	0.03	3	0.23	0.02	8	2.72	0.09	3
	3/9/02	-0.5	35.0	0.63	0.00	3				2.77	0.11	9
	3/13/02	-11.7	32.0	0.27	0.02	2	0.24	0.03	2	3.18	0.16	3
	3/16/02	-19.0	34.0	0.23	0.03	2	0.28	0.01	3	3.40	0.07	3
	3/18/02	-24.5	37.0	0.37	0.05	3	0.24	0.02	3	2.76	0.05	3

? Sample data is suspected to be contamination and is not considered in figures and discussion.

a) DFe is the Fe that passes through a 0.4 μm filter.

b) SFe is the Fe that passes through a 0.02 μm filter.

c) DMn is the Mn that passes through a 0.4 μm filter.

d) 1 SD is the standard deviation of sample replicates.

Appendix 2.2: Water Column Profile Data

Cruise-St	date	Lat.	Long.	depth (m)	DFe (nmol/kg)	1 SD[d]	n	SFe (nmol/kg)	1 SD	n	DMn (nmol/kg)	1 SD	n
30°N profile	1/14/01	30.0°N	45.3°W	0.2	0.68	0.04	3	0.34	0.02	3	2.13	0.04	3
SJ0101,				41	0.58	0.03	3	0.34		1	2.13	0.08	3
Jan. 2001				63	0.39	0.01	3	0.32	0.03	3	2.16	0.05	3
				77	0.37	0.01	2	0.33	0.05	3	2.14	0.10	3
				165	0.41	0.02	2	0.28	0.01	3	0.93	0.07	3
				200	? 0.63	0.04	3	0.28	0.05	3	0.90	0.24	3
				250	0.42	0.03	3	0.33	0.03	3	0.63	0.02	3
				375	? 1.19	0.08	3	0.35	0.01	3	0.54	0.13	3
				450	0.41	0.01	2	? 0.48	0.03	3	0.49	0.09	3
				525	? 0.74	0.03	3	0.36	0.03	2	0.61	0.09	3
				850	0.55	0.04	3	0.42	0.01	3	0.47	0.06	3
				950	0.57	0.02	3	0.41	0.00	2	0.51	0.09	3
				1050	0.51	0.01	2	0.35	0.01	2	0.53	0.04	3
10°N profile	1/21/01	10.2°N	45.0°W	0	0.54	0.06	6	0.22	0.08	3	2.17	0.04	6
SJ0101,				30	0.68	0.01	2	0.35	0.11	3	2.06	0.07	3
Jan. 2001				130	1.08	0.08	4	? 2.98	0.03	2	0.58	0.06	3
				165	0.98	0.04	2	0.33	0.17	2	0.59	0.06	3
				200	1.19	0.16	3	0.41	0.11	3	0.56	0.07	3
				250	1.05	0.01	2	0.46	0.01	3	0.57	0.07	3
				375	1.19	0.02	2	0.41	0.05	4	0.49	0.04	3
				525	1.11	0.03	2	0.45	0.02	2	0.46	0.03	3
				725	1.06	0.11	2	0.31	0.08	3	0.57	0.09	3
				850	1.16	0.03	4	0.40	0.10	3	0.51	0.01	3
				1050	1.01	0.07	3	0.46	0.02	2	0.56	0.07	8
				1250	0.98	0.10	3	0.42	0.06	2	0.46	0.06	3
				1500	0.77	0.02	3	0.58	0.10	3	0.51	0.03	3
				1750	0.70	0.13	6	0.45	0.02	3	0.43	0.01	3
				3400	0.86	0.05	4	0.36	0.02	2	0.55	0.08	8
				4200	0.63	0.13	2	0.42	0.05	2	0.51	0.08	9
30°N profile	7/2/01	30.0°N	45.0°W	0	0.51	0.04	3				1.70	0.07	3
Kn162,				2	0.49	0.03	2	? 0.60	0.01	3	1.94	0.12	3
July 2001				2	0.51	0.02	3				1.79	0.03	3
				4	0.54	0.03	2	0.43	0.03	3	1.86	0.06	3
				6	0.56	0.03	3	0.29	0.02	2	1.94	0.02	3
				8	0.47	0.02	3	0.33	0.01	2	1.70	0.00	3
				8	0.44	0.02	3				1.73	0.02	3
				11	0.44	0.02	3	0.34	0.02	2	1.75	0.01	3
				14	0.46	0.02	3	0.48	0.03	3	1.80	0.05	3
				17	0.49	0.01	2	? 0.68	0.03	3	1.88	0.17	3
				19	0.45	0.03	2	0.23	0.06	2	1.84	0.08	3
				30	0.42	0.02	3	0.41	0.03	4	1.92	0.09	3
				39	0.42	0.03	4	0.39	0.02	3	1.86	0.02	3
				79	0.36	0.02	3	0.32	0.03	3	1.79	0.03	3
				79	0.37	0.05	2				1.69	0.05	3

				197	0.44	0.05	2	?0.49	0.00	2	0.90	0.02	3
				197	0.42	0.03	2				0.84	0.01	3
10°N profile	7/12/01	10.1°N	45.5°W	0	0.60	0.03	3	0.41	0.05	2	2.40	0.13	3
Kn162,				2	0.71	0.04	3	0.37	0.04	3	2.41	0.08	3
July 2001				5	0.59	0.03	3	0.40	0.05	3	2.28	0.12	3
				7	0.55	0.02	3	0.65	0.03	2	2.51	0.12	3
				10	0.48	0.05	3	0.40	0.05	3	2.32	0.06	3
				13	0.45	0.02	3	0.34	0.01	2	2.40	0.10	3
				16	0.51	0.00	2	?2.96	0.27	3	2.55	0.13	3
				19	0.62	0.04	3	0.36	0.12	3	2.33	0.07	3
				22	0.56	0.01	3	0.42	0.00	2	2.21	0.11	3
				25	0.53	0.02	2	0.44	0.01	2	2.33	0.07	3
				28	0.55	0.04	3	0.45	0.05	3	2.24	0.25	3
				49	0.40	0.04	3	0.44	0.03	3	2.12	0.06	3
				79	0.37	0.03	3	0.41	0.05	3	1.91	0.09	3
				148	0.54	0.03	3	0.40	0.01	3	0.77	0.07	3
				198	0.75	0.04	3	0.82	0.02	3	0.73	0.02	3
24.5°S profile	3/18/02	24.5°S	37.0°W	1	0.36	0.05	3	0.24	0.02	3	2.21	0.12	3
En367,				18	0.39	0.02	2	0.30	0.01	3	1.71	0.39	3
Mar. 2002				69	0.24	0.04	2	0.28	0.02	2	1.42	0.07	3
				113	0.29	0.02	3	0.26	0.05	3	1.28	0.04	3
				239	?0.50	0.01	2	?0.61	0.01	2	0.15	0.09	3
				394	0.26	0.04	3	0.26	0.04	2	0.14	0.17	3
				544	0.28	0.00	2	?0.46		1	0.08	0.04	3
				709	0.37	0.03	2	0.31	0.02	3	0.10	0.20	3
				841	0.39	0.03	3	0.31	0.01	3	0.16	0.03	3
				985	0.39	0.01	3	?0.45	0.03	3	0.23	0.10	3
				1181	0.38		1	0.35	0.03	3	0.06	0.07	2
				1366	0.45	0.03	3	0.32	0.03	3	0.28	0.11	3
				1649	0.43	0.04	2	0.38	0.05	3	0.08	0.24	2
				1787	0.45	0.01	3	?3.83	0.29	2	0.26	0.05	3
				1920	0.45	0.02	2	?0.55	0.05	2	0.21	0.16	3
				2198	0.46	0.03	3	0.33	0.01	3	0.31	0.17	3
				2494	0.49	0.05	2	0.30	0.00	2	0.19	0.08	3
				2676	0.50	0.02	2	0.40	0.01	3	0.36	0.11	3
				3051	0.48	0.02	3	0.35	0.01	3	0.18	0.05	3
				3308	0.49	0.02	3	0.27	0.02	2	0.16	0.07	3
				3556	0.41	0.02	3	?0.48		1	0.25	0.19	3
				3806	0.43	0.03	3	0.29	0.04	3	0.27	0.05	3
				3905	0.43	0.02	3				0.15	0.16	3
				4029	0.41	0.02	2	0.35	0.01	3	0.26	0.18	3

? Sample data is suspected to be contamination and is not considered in figures and discussion.

a) DFe is the Fe that passes through a 0.4 μm filter.

b) SFe is the Fe that passes through a 0.02 μm filter.

c) DMn is the Mn that passes through a 0.4 μm filter.

d) 1 SD is the standard deviation of sample replicates.

Appendix 2.3: En367, 24.5 °S Station Dissolved Cr and Silicate Data								
date	Lat.	Long.	Cr depth (m)	DCr[a] (nmol/ kg)	1 SD[c]	n	Si depth (m)	SiO_3[b] (µmol/ kg)
3/18/02	24.5°S	37.0°W	1	2.32	0.07	3	48	0.3
			18	2.09	0.08	2	102	0.2
			69	2.36	0.05	3	202	0.8
			113	2.32	0.08	3	303	1.5
			239	2.33	0.11	3	450	4.3
			394	2.37	0.08	3	601	9.9
			544	2.51	0.03	3	750	18.8
			709	2.79	0.14	3	900	32.7
			841	2.81	0.08	3	1051	43.3
			985	2.81	0.10	3	1176	43.9
			1181	2.97	0.04	2	1299	38.8
			1366	2.45	0.12	3	1426	28.1
			1649	2.38	0.06	2	1549	21.1
			1787	2.48	0.01	3	1673	17.8
			1920	2.47	0.10	3	1800	17.4
			2198	2.25	0.19	3	1949	18.5
			2494	2.55	0.09	3	2100	20.2
			2676	2.39	0.03	3	2397	24.3
			3051	2.68	0.14	3	2699	28.7
			3308	2.81	0.05	3	2998	31.9
			3556	2.77	0.18	3	3298	39.0
			3806	2.88	0.05	3	3599	66.2
			3905	3.17	0.07	2	3898	101
			4029	3.11	0.12	3	4041	118

a) DCr is the Cr that passes through a 0.4 µm filter.

b) Silicate measurements were made at sea by UV-VIS spectrometry (by M. Reuer and A. Lima) on unfiltered samples collected from a CTD rosette. Typical sample precisions were ± 2%.

c) 1 SD is the standard deviation of sample replicates.

References for Chapter 2

Anderson L. and Sarmiento J. (1994) Redfield ratios of remineralization determined by nutrient data analysis. *Global Biogeochemical Cycles* **8**, 65-80.

Barbeau K. and Moffett J. W. (1998) Dissolution of iron oxides by phagotropic protists: using a novel method to quantify reaction rates. *Environmental Science and Technology* **32**, 2969-2975.

Barbeau K. and Moffett J. W. (2000) Laboratory and field studies of colloidal iron oxide dissolution as mediated by phagotrophy and photolysis. *Limnology and Oceanography* **45**, 827-835.

Barbeau K., Moffett J. W., Caron M. A., Croot P. L., and Erdner D. L. (1996) Role of protozoan grazing in relieving iron limitation of phytoplankton. *Nature* **380**, 61-64.

Bell J., Betts. J., and Boyle E. A. (2002) MITESS: A Moored In-situ Trace Element Serial Sampler for Deep-Sea Moorings. *Deep-Sea Research I* **49**, 2103-2118.

Boyle E. A., Bergquist B. A., and Kayser R. (submitted) Iron, manganese, and lead at Hawaii Ocean Time Series Station ALOHA: temporal variability and an intermediate water hydrothermal plum. *Geochimica et Cosmochimica Acta.*

Broecker W. S. and Virgilio A. (1991) Radiocarbon age of waters in the deep Atlantic revisited. *Geophysical Research Letters* **18**(1), 1-3.

Bruland K. W., Orians K. J., and Cowen J. P. (1994) Reactive trace metals in the stratified central North Pacific. *Geochimica et Cosmochimica Acta* **58**, 3171-3182.

Bruland K. W. and Rue E. L. (2001) Analytical methods for the determination of concentrations and speciation of iron. In *The Biogeochemistry of Iron in Seawater*, Vol. 7 (ed. K. A. Hunter and D. Turner), pp. 255-289. John Wiley & Sons, Ltd.

Campbell J. A. and Yeats P. A. (1981) Dissolved chromium in the northwest Atlantic Ocean. *Earth and Planetary Science Letters* **53**, 427-433.

Chen M., Dei R. C. H., Wang W., and Guo L. (2003) Marine diatom uptake of iron bound with natural colloids of different origins. *Marine Chemistry* **81**, 177-189.

Chen M. and Wang W. X. (2001) Bioavailability of natural colloidal Fe to marine plankton: influence of colloidal size and aging. *Limnology and Oceanography* **46**, 1956-1960.

Chen Y. and Siefert R. (2004) Seasonal and spatial distributions of dry deposition fluxes of atmospheric total and labile iron over the tropical and sub-tropical North Atlantic Ocean. *Journal of Geophysical Research-Atmosphere* **109**, Art. No. D09305.

Chester R. (1992) *Marine Geochemistry.* Unwin Hyman Ltd.

Chiapello I., Bergametti G., Gomes L., Chatenet B., Dulac F., Pimenta J., and Soares E. S. (1995) An additional low layer transport of Shaelian and Saharan dust of the North-eastern Tropical Atlantic. *Geophysical Research Letters* **22**, 3191-3194.

Cranston R. E. (1983) Chromium in Cascadia Basin, Northeast Pacific Ocean. *Marine Chemistry* **13**, 109-125.

Cranston R. E. and Murray J. W. (1978) The determination of chromium species in natural waters. *Analyitca Chimica Acta* **99**, 275-282.

Cullen J. T. and Moffett J. W. (2003) The phyhsicochemical speciaton of Fe in the tropical and northwest Atlantic. *ASLO Aquatic Sciences Meeting.*, Abstract #CS08.

de Baar H. J. W. and de Jong J. T. M. (2001) Distributions, sources and sinks of iron in seawater. In *The Biogeochemistry of Iron in Seawater*, Vol. 7 (ed. K. A. Hunter and D. Turner), pp. 123-253. John Wiley & Sons, Ltd.

de Baar H. J. W., de Jong J. T. M., Bakker D. C. E., Loscher B. M., Veth C., Bathmann U., and Smetacek V. (1995) The importance of iron for plankton blooms and carbon dioxide drawdown in the Southern Ocean. *Nature* **373**, 412-415.

Duce R. A. and Tindale N. W. (1991) Atmospheric transport of iron and its deposition in the ocean. *Limnology and Oceanography* **36**, 1715-1726.

Edmond J. M., Measures C. I., Magnum B., Grant B., Sclater F. R., Collier R., Hudson A., Gordon L. I., and Corliss J. B. (1979) On the formation of metal-rich deposits at the ridge crests. *Earth and Planetary Science Letters* **46**, 19-30.

Falkowski P. G. (1998) Evolution of the nitrogen cycle and its influence on the biological sequestration of CO_2 in the ocean. *Nature* **387**, 272-275.

Fukumori I. and Wunsch C. (1991) Efficient representation of the North Atlantic Hydrographic and Chemical Distributions. *Progress in Oceanography* **27**, 111-195.

Fung I. Y., Meyn S. K., Tegen I., Doney S. C., John J. G., and Bishop K. B. (2000) Iron supply and demand in the upper ocean. *Global Biogeochemical Cycles* **14**, 281-295.

Gao Y., Kaufman Y. J., Tanre D., Kolber D., and Falkowski P. G. (2001) Seasonal distributions of aeolian iron fluxes to the global ocean. *Geophysical Research Letters* **28**, 29-32.

Gregg W. W., Ginoux P., Schopf P. S., and Casey N. W. (2003) Phytoplankton and iron: validation of a global three-dimensional ocean biogeochemical model. *Deep-Sea Research II* **50**, 3143-3169.

Hollander M. and Wolfe D. A. (1973) *Nonparametric Statistical Methods.* John Wiley & Sons, Inc.

Husar R. B., Prospero J. M., and Stowe L. L. (1997) Characterization of tropospheric aerosols over the oceans with the NOAA advanced very high resolution radiometer optical thickness operational product. *Journal of Geophysical Research* **102**, 16889-16909.

Jeandel C. and Minster J. F. (1984) Isotope dilution measurement of inorganic Cr (III) and total chromium in seawater. *Marine Chemistry* **14**, 347-364.

Jeandel C. and Minster J. F. (1987) Chromium behavior in the ocean: global versus regional processes. *Global Biogeochemical Cycles* **1**, 131-154.

Jickells T. D. and Spokes L. J. (2001) Atmospheric iron inputs to the oceans. In *The Biogeochemistry of Iron in Seawater*, Vol. 7 (ed. K. A. Hunter and D. Turner), pp. 85-121. John Wiley & Sons, Ltd.

Johansen A. M., Siefert R. L., and Hoffmann M. R. (2000) Chemical composition of aerosols collected over the tropical North Atlantic Ocean. *Journal of Geophysical Research* **105**, 15277-15321.

Johnson K. S., Berelson W. M., Coale K. H., Coley T. L., Elrod V. A., Fairey W. R., Iams H. D., Kilgore T. E., and Nowicki J. L. (1992) Manganese flux from continental margin sediments in a transect through the oxygen minimum. *Science* **257**, 1242-1245.

Johnson K. S., Coale K. H., Berelson W. M., and Gordon R. M. (1996) On the formation of manganese maximum in the oxygen minimum. *Geochimica et Cosmochimica Acta* **60**, 1291-1299.

Johnson K. S., Gordon R. M., and Coale K. H. (1997) What controls dissolved iron concentrations in the world ocean. *Marine Chemistry* **57**, 137-161.

Klinkhammer G. P. and Bender M. L. (1980) The distribution of manganese in the Pacific Ocean. *Earth and Planetary Science Letters* **46**, 361-384.

Klinkhammer G. P., Bender M. L., and Weiss R. F. (1977) Hydrothermal manganese in the Galapagos Rift. *Nature* **269**, 319-320.

Kumar N., Anderson R. F., Mortlock R. A., Froelich P. N., Kubik P., Dittrich-Hannon B., and Suter M. (1995) Increased biological productivity and export production in the glacial Southern Ocean. *Nature* **378**, 675-680.

Landing W. M. and Bruland K. W. (1980) Manganese in the North Pacific. *Earth and Planetary Science Letters* **49**, 45-56.

Landing W. M. and Bruland K. W. (1987) The contrasting biogeochemistry of iron and manganese in the Pacific Ocean. *Geochimica et Cosmochimica Acta* **51**, 29-43.

Landing W. M., Measures C. I., Buck C. S., and Brown M. (2003) Sections of dissolved iron and aluminum from the 2003 repeat hydrography A16N expedition. *Eos Trans. AGU* **84 (52)**(Ocean Sci. Meet. Suppl., Abstract OS31L-07).

Loscher B. M., de Baar H. J. W., de Jong J. T. M., Veth C., and Dehairs F. (1997) The distribution of Fe in the Antarctic circumpolar current. *Deep-Sea Research Part II* **44**, 143-187.

Mahowald N., Kohfeld K., Hansson M., Balkanski Y., Harrison S. P., Prentice I. C., Schulz M., and Rodhe H. (1999) Dust sources and deposition during the last glacial maximum and current climate: a comparison of model results with paleodata from ice cores and marine sediments. *Journal of Geophysical Research* **104**, 15895-15916.

Martin J. H. (1990) Glacial-interglacial CO_2 change: the iron hypothesis. *Paleoceanography* **5**, 1-13.

Martin J. H., Gordon R. M., and Fitzwater S. E. (1990) Iron in Antarctic waters. *Nature* **345**, 156-158.

Martin J. H., Knauer G. A., Karl D. M., and Broenkow W. W. (1987) VERTEX: Carbon cycling in the northeast Pacific. *Deep-Sea Research* **34**, 267-285.

Moulin C., Lambert C. E., Dulac F., and Dayan U. (1997) Control of the atmospheric export of dust from North Africa by the North Atlantic Oscillation. *Nature* **387**, 691-694.

Murray J. W., Spell B., and Paul B. (1983) The contrasting geochemistry of manganese and chromium in the Eastern Tropical Pacific Ocean. In *Trace Metals in Sea Water* (ed. C. S. Wong, E. A. Boyle, K. W. Bruland, J. D. Burton, and E. D. Goldberg), pp. 643-669. Plenum.

Nordwell L. M. and Price N. B. (2001) Direct use of inorganic colloidal iron by marine mixotrophic phytoplankton. *Limnology and Oceanography* **46**(4), 765-777.

Orians K. J. and Bruland K. W. (1986) The biogeochemistry of aluminum in the Pacific Ocean. *Earth and Planetary Science Letters* **78**, 397-410.

Parekh P., Follows M. J., and Boyle E. A. (submitted) Decoupling of iron and phosphate in the global ocean. *Global Biogeochemical Cycles.*

Prospero J. M. (1996) The atmospheric transport of particles to the ocean. In *Particle Flux in the Ocean*, Vol. SCOPE Rep. 57 (ed. V. Ittekkott, P. Schafer, S. Honjo, and P. J. Depestris), pp. 19-52. John Wiley.

Sarthou G., Baker A. R., Blain S., Achterberg E. P., Boye M., Bowie A. R., Croot P., Laan P., de Baar H. J. W., Jickells T. D., and Worsfold P. J. (2003) Atmospheric iron deposition and sea-surface dissolved iron concentrations in the eastern Atlantic Ocean. *Deep-Sea Research I* **50**, 1339-1352.

Shiller A. M. (1997) Manganese in surface waters of the Atlantic Ocean. *Geophysical Research Letters* **24**(12), 1495-1498.

Siefert R. L., Johanson A. M., and Hoffmann M. R. (1999) Chemical characterization of ambient aerosol collected during the southwest monsoon and intermonsoon seasons over the Arabian Sea: labile-Fe(II) and other trace metals. *Journal of Geophysical Research-Atmosphere* **104**, 3511-3526.

Sirinawin W., Turner D. R., and Westerlund S. (2000) Chromium (VI) distributions in the Arctic and the Atlantic Oceans and a reassessment of the oceanic Cr cycle. *Marine Chemistry* **71**, 265-282.

Statham P. J. and Burton J. D. (1986) Dissolved manganese in the North Atlantic Ocean, 0-35°N. *Earth and Planetary Science Letters* **79**, 55-65.

Statham P. J., Yeats P. A., and Landing W. M. (1998) Manganese in the eastern Atlantic Ocean: processes influencing deep and surface water distributions. *Marine Chemistry* **61**, 55-68.

Stuiver M. (1976) The C-14 distribution in west Atlantic abyssal waters. *Earth and Planetary Science Letters* **32**, 322-330.

Sunda W. G. (1997) Control of dissolved iron concentrations in the world ocean: a comment. *Marine Chemistry* **57**, 169-172.

Sunda W. G. and Huntsman S. A. (1988) Effects of sunlight on redox cycles of manganese in the southwestern Sargasso Sea. *Deep-Sea Research* **35**, 1297-1317.

Sunda W. G. and Huntsman S. A. (1995) Iron uptake and growth limitation in oceanic and coastal phytoplankton. *Marine Chemistry* **50**(189-206).

Tchernia P. (1980) *Descriptive Regional Oceanography*. Pergamon Press Inc.

Vink S., Boyle E. A., Measures C. I., and Yuan J. (2000) Automated high resolution determination of the trace elements iron and aluminum in the surface ocean using towed Fish coupled to a flow injection analysis. *Deep-Sea Research I* **47**, 1141-1156.

Vink S. and Measures C. I. (2001) The role of dust deposition in determining surface water distributions of Al and Fe in the South West Atlantic. *Deep-Sea Research II* **48**, 2787-2809.

Wedepohl K. H. (1995) The composition of the continental crust. *Geochimica et Cosmochimica Acta* **59**, 1217-1232.

Weiss R. F. (1977) Hydrothermal manganese in the deep sea: scavenging residence time and Mn/He-3 relationships. *Earth and Planetary Science Letters* **37**, 257-262.

Whitfield M. and Turner D. R. (1987) The role of particles in regulating the composition of seawater. In *Aquatic Surface Chemistry* (ed. W. Stumm), pp. 457-493. Wiley.

Wu J. and Boyle E. A. (1998) Determination of iron in seawater by high resolution isotope dilution inductively coupled plasma mass spectrometry after $Mg(OH)_2$ coprecipitation. *Analyitca Chimica Acta* **367**, 183-191.

Wu J. and Boyle E. A. (2002) Iron in the Sargasso Sea: implications for the processes controlling dissolved Fe distribution in the ocean. *Global Biogeochemical Cycles* **16**(4), 1086-1094.

Wu J., Boyle E. A., Sunda W., and Wen L. (2001) Soluble and colloidal iron in the oligotrophic North Atlantic and North Pacific. *Science* **293**, 847-849.

Yeats P. A. and Bewers J. M. (1985) Manganese in the western North Atlantic. *Marine Chemistry* **17**, 255-263.

Chapter 3

Dissolution of Aerosol Iron in Seawater

3.1. Introduction

In order to estimate the effects of changing fluxes of iron to the ocean using biological pump and climate change models, an improved understanding of the relationship between iron sources to the ocean, biological productivity and export is necessary. The dominant source of Fe to the open ocean is atmospheric deposition, mostly of aluminosilicate mineral soil sources from arid and semi-arid regions (Duce and Tindale, 1991). There are a few models of total atmospheric Fe deposition to the oceans that incorporate observational data, long term satellite observations, and/or climatological data (Duce and Tindale, 1991; Mahowald et al., 1999; Fung et al., 2000; Gao et al., 2001; Hand et al., submitted). Given the estimated total aerosol iron flux, models must then estimate the fraction of Fe that becomes bioavailable in seawater (e.g., dissolves).

Aerosol iron solubility is a function of aerosol type and chemical processing in the atmosphere (reviews: Jickells, 1999; Jickells and Spokes, 2001). Particles are subject to multiple wetting and drying cycles in the atmosphere, and therefore experience large chemical variations before being deposited. Cloud droplets can be acidic due to SO_2 and NO_x oxidation reactions and can have high and variable ionic strengths. Iron solubility in aerosols is very sensitive to pH with Fe being much more soluble under acidic conditions (Zhuang et al., 1992; Spokes et al., 1994; Spokes and Jickells, 1996). Photochemistry is another process that may increase the amount of labile Fe by photoreduction of Fe(III) to more soluble Fe(II) in the atmosphere (Behra and Sigg, 1990; Siefert et al., 1996; Zhu et al., 1997). All of these processes act to increase the amount of labile Fe as particles are transported to the ocean by altering the chemical species of Fe present and the aerosol solubility in seawater.

The composition of aerosol particles is also important in determining the amount of Fe released into seawater. Urban aerosols of anthropogenic origin have more labile Fe than lithogenic crustal-type aerosols (ZHU et al., 1993; SPOKES et al., 1994; BONNET and GUIEU, 2004). It is thought that some of the increased labile Fe might be due to higher organic concentrations (such as oxalic acid) in anthropogenic aerosol and the increased photolability of the organically bound Fe species (ZHU ET AL., 1993). Also, Fe in anthropogenic particles is associated with more reactive phases and more acidic conditions in the aerosol cloud waters (SPOKES et al., 1994; JICKELLS and SPOKES, 2001). Differences in the composition of crustal aerosols are also reflected in the amount of Fe that becomes bioavailable in seawater. In laboratory culture experiments, marine organisms had higher growth rates when grown with lithogenic particles with a higher fraction of amorphous Fe hydroxides (VISSER et al., 2003). It has been proposed that up to 50% of the dust in the atmosphere today is from human disturbed soil (TEGAN et al., 1996). Therefore, the crustal-type aerosols we observe today (perhaps with more soil material) may not be representative of past aerosol types. Other potential sources of aerosol particles such as volcanic emissions or extraterrestrial dust may have higher fractions of labile Fe than crustal-type aerosols (JOHNSON, 2001).

Aerosol particles are deposited onto the ocean surface either by gravitational settling (dry deposition) or scavenging during rain events (wet deposition), and the amount of Fe released into seawater from wet and dry deposition is likely different. Aerosol iron solubility from dry dust has been estimated by leaching experiments under a variety of pH conditions. Only a few studies have assessed dissolution under high pH conditions either with artificial seawater or natural seawater, and only one study has investigated the solubilization of remote oceanic aerosols in natural seawater. Generally, the amount of crustal aerosol Fe dissolved in laboratory experiments at pH 8 and in seawater is low. In experiments where Saharan dust was cycled from low pH 2 conditions to high pH 8, high ionic strength conditions, less than 0.3% of the total Fe remained dissolved in the final solution (SPOKES and JICKELLS, 1996). For Saharan soil leached with natural seawater, the fraction of Fe dissolved ranged from 0.001 to 2.2%

and was dependent on particle concentration (BONNET and GUIEU, 2004). The observation of aerosol solubility decreasing with increasing particle loading may be due to enhanced scavenging of Fe onto particle surfaces (SPOKES and JICKELLS, 1996; BONNET and GUIEU, 2004). One study with aerosols collected in the remote Pacific ocean found that ≈ 50% of aerosol Fe could be dissolved at aerosol Fe concentrations of less than 2 nmol/kg using natural seawater (ZHUANG et al., 1990).

Instead of using high pH seawater conditions, many researchers use leaching solutions that mimic cloud conditions. The argument is that the low solubilization observed for crustal material (as for the Saharan dust) does not represent the bioavailable, labile fraction of Fe from dust. Aerosols leached under low pH (1-5) conditions mimicking cloud solutions have found leachable fractions of Fe ranging from 2 to 7% for open ocean Atlantic aerosols (ZHU et al., 1997; CHEN and SIEFERT, 2004) to more than 50% in remote North Pacific aerosols (ZHUANG et al., 1990; ZHUANG et al., 1992). Zhuang et al. (1992) also found that Chinese loess leached under the same conditions as remote Pacific aerosols released less Fe to solution than the remote aerosols suggesting that atmospheric cycling increased the solubility of the aerosol material compared with its source. Particle size also plays a role in how much Fe can be released from aerosol particles. More labile Fe is consistently observed in the finer fraction of aerosols (SIEFERT et al., 1999; JOHANSEN et al., 2000; CHEN and SIEFERT, 2004; CHEN, 2004, in preparation).

Using a 90-minute, pH 4.5, reducing (hydroxylamine) leach to estimate the labile fraction of Fe, the leachable fraction of Fe from freshly collected aerosols from the tropical and subtropical Atlantic ocean was typically 2 to 5% (CHEN and SIEFERT, 2004). Higher solubility was observed in aerosols collected in the central North Pacific in the summer of 2002 (2 to 16%) (CHEN, 2004, in preparation). However, lower fractions of labile Fe were observed for Pacific aerosols in the same region in April 2001 (1 to 3%) (CHEN, 2004, in preparation; HAND et al., submitted). Dust concentrations in the atmosphere during April in the North Pacific are much higher than in the summer (PROSPERO, 1996). Recent studies have argued for higher solubilization of Pacific

aerosols based on DFe budgets in surface water (JOHNSON et al., 2003; BOYLE et al., submitted). It takes approximately one week for an aerosol particle to cross the Atlantic from African sources, whereas it takes 8 to 14 days for a particle to reach the central Pacific from China (JICKELLS and SPOKES, 2001). Higher solubilization of Pacific aerosols may be related to longer transit times and/or differences in the composition of source material.

The compositional ranges in material used in experiments (e.g., remote weathered aerosols versus soil or loess) and in leaching conditions have lead to a large range in reported soluble fractions for atmospheric Fe. Jickells and Spokes (2001) suggested that the overall solubility of Fe from dry Fe deposition was less than 1%. Because of the low solubility of dry deposition and much higher observed soluble fraction of Fe in rainwater ($\approx$ 14%), they suggested that wet deposition may dominate the input of dissolved Fe to the ocean although dry deposition dominates total Fe input. Reported soluble Fe in rainwater (pH 4 to 7) ranges from 4 to 48% with an average of 14% (references in (JICKELLS and SPOKES, 2001)). As a droplet falls, low pH solutions are neutralized by entrainment of NH_3 and other species. When deposited in the ocean, large chemical gradients are encountered going from mildly acidic pH to basic pH, and low to high ionic strength. How much of the rainwater Fe remains dissolved as it is neutralized and mixes with seawater is unknown, but some fraction of it may form complexes with organic ligands (GLEDHILL and VAN DEN BERG, 1994; RUE and BRULAND, 1995; WU and LUTHER, 1995; WITTER and LUTHER, 1998) or precipitate as hydrated Fe oxides which may be bioavailable (review: SUNDA, 2001).

The fraction of aerosol Fe released into seawater is an important variable in models of the Fe cycle, yet is very poorly constrained. In this chapter, aerosol dissolution experiments were performed using freshly collected aerosols and natural seawater from the North Pacific subtropical gyre in July 2002. These experiments differ from other studies in that the amount of aerosol dust added to the seawater was low and the seawater was changed every 24 hours to minimize saturation of the seawater or Fe loss to bottle walls. For the same aerosols, estimates of labile Fe using the 90-minute, pH 4.5,

reducing leaching method by Chen and Siefert (2003) are also available for comparison (CHEN, 2004, in preparation).

3.2. SAMPLING SITES, COLLECTION, AND METHODS

3.2.1. Sites and Sample Collection

North Pacific aerosol samples and surface seawater were collected in July 2002 on the R/V Ka'imikai-o-Kanaloa (KOK0210 cruise) along a transect northwest from Hawaii (Figure 3.1) from west (25.6°N, 173°W) to east (Station ALOHA, 22.8 N, 158°W). Aerosol samples were collected at sea by Y. Chen and Dr. R. Siefert (University of Maryland) on 47 mm polycarbonate 0.4 μm Nuclepore® filters using a low-volume dichotomous virtual impactor collector (1.3 m^3 hr^{-1}) with a sector sampling system, which only allowed collection when the wind direction was ±70° off the bow. The low volume collectors only collected the fine fraction of aerosol (< 2.5 μm). Filters were acid cleaned and rinsed with trace metal clean water prior to aerosol collection. Collection technique details and trace metal considerations are discussed in Chen and Siefert (2003, 2004). The two aerosol samples used in the dissolution experiments were collected on July 13 (9 hr) and July 14 (6 hr). The end points of collection were 25.6°N, 173°W and 24.2°N, 168.6°W respectively. A modeled 2 week back trajectory for the air mass sampled at the sea surface during the aerosol collection time is plotted in Figure 3.2 (HYSPLIT model, (DRAXLER and ROLPH, 2003) using the 1948-2002 NCAR reanalysis data. Atmospheric dust concentrations vary seasonally in the North Pacific with the dustiest season in the late winter/early spring and much lower levels in the summer when the aerosol samples were collected (PARRINGTON et al., 1983; PROSPERO, 1996). March and April concentrations of Fe in the atmosphere can be greater than 300 ng m^{-3}, based on measurements of Al in oceanic air at Midway Island from 1981 to 1993 (PROSPERO, 1996). Fe concentrations in the atmosphere measured during July 2002 were much lower than winter values, and quite different on the two sampling dates with observed values of 3.72 ng m^{-3} for July 13 and 86.8 ng m^{-3} for July 14 (CHEN, 2004, in preparation).

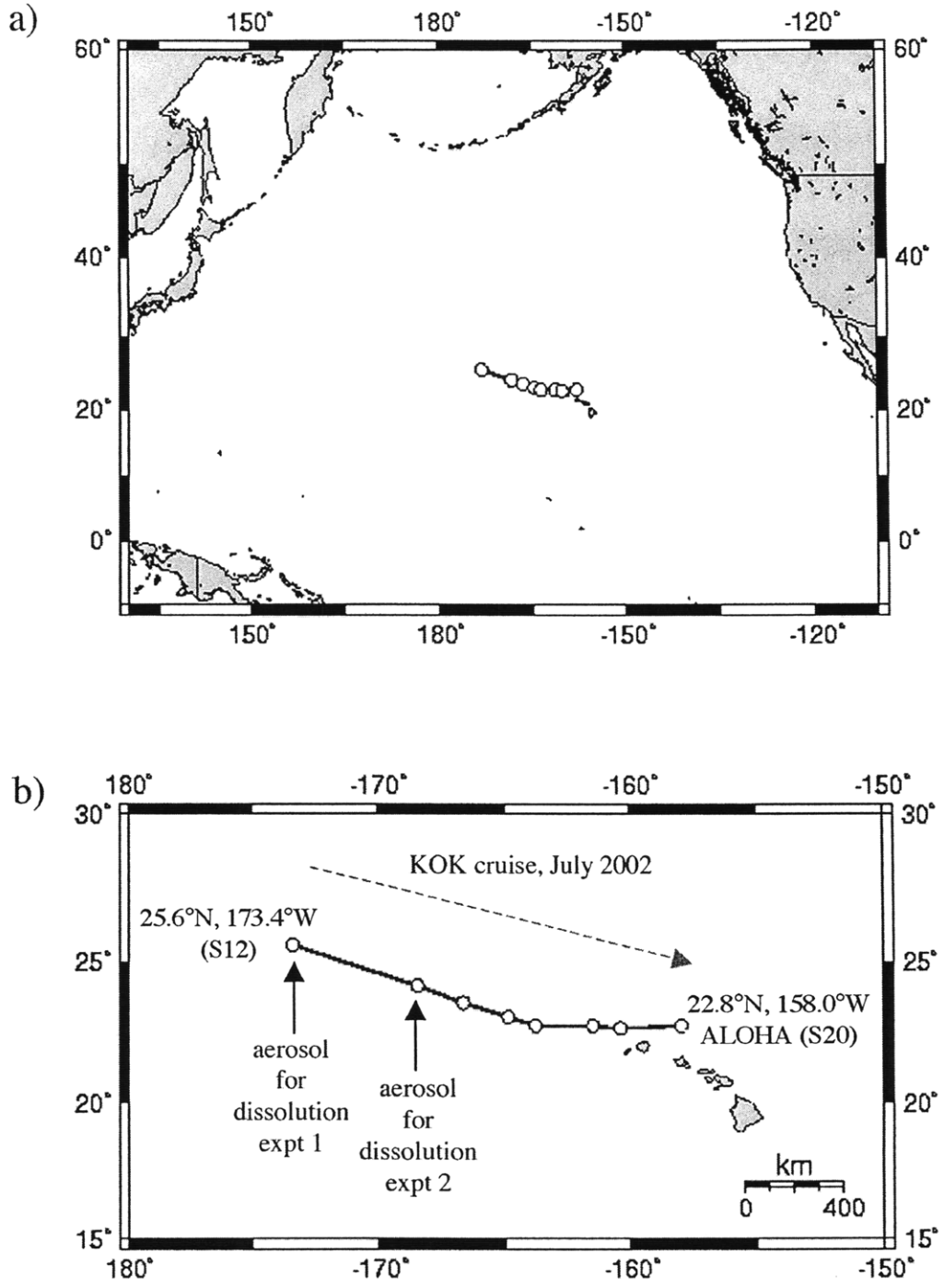

Figure 3.1: Sample location map in the North Pacific. The circles are the locations where trace metal clean surface samples were collected. Aerosol samples were collected at the first two stations along the transect. Arrows denote the end point of the aerosol collection period, which were 6 to 9 hours prior to the stations.

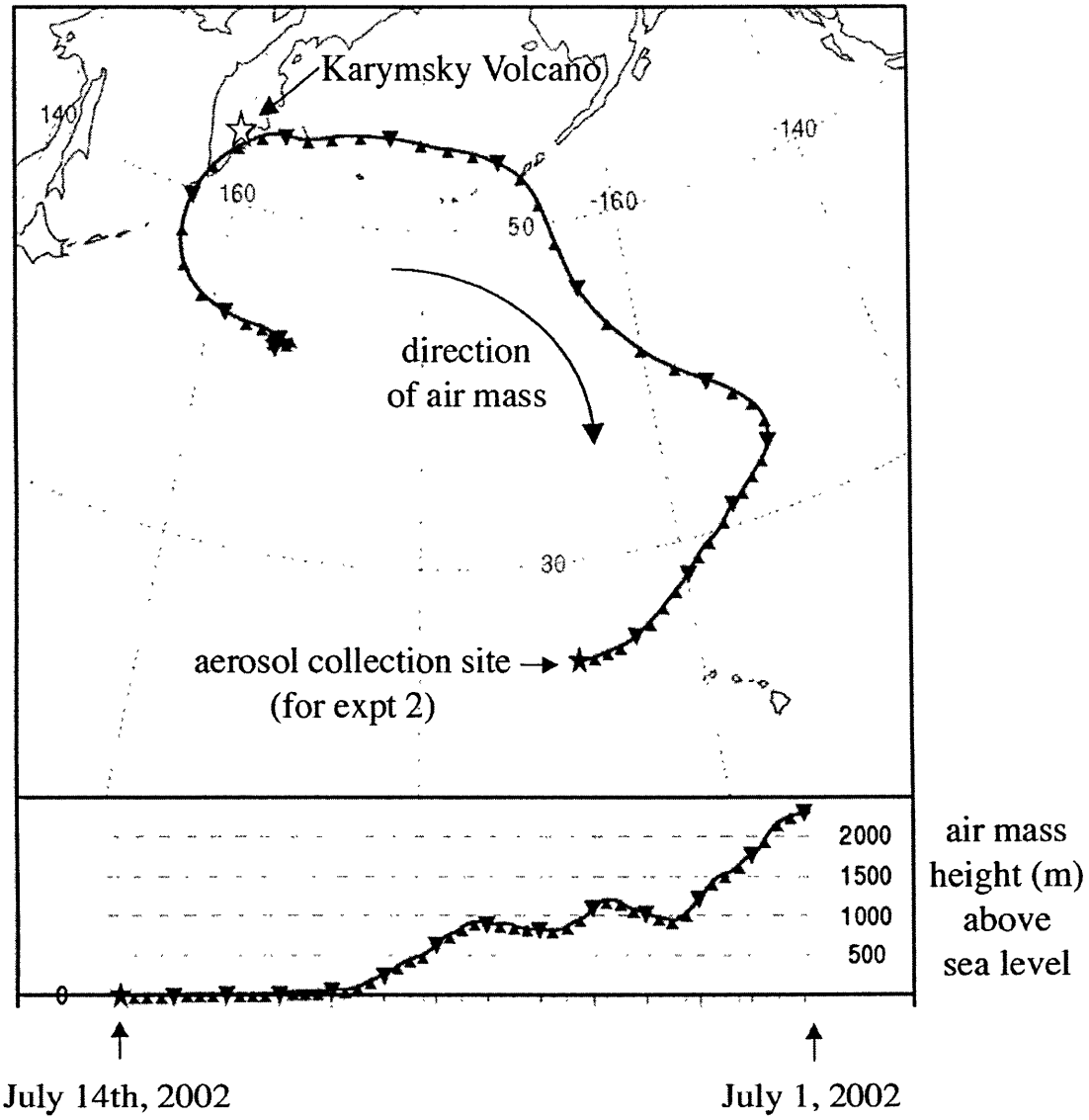

Figure 3.2: A two week modeled back trajectory for the aerosol sample used in the dissolution experiment #2. The aerosol sample was collected for 9 hours on July 14, 2002 by Y. Chen and R. Siefert (University of Maryland). The aerosol sample collection end point was 24.2°N, 168.6°W. Modeled back trajectories for the aerosol sampled used in experiment 2 were very similar (July 13th; 25.6°N, 173.4°W). Back trajectories were calculated by the HYSPLIT (HYbrid Single-Particle Lagrangian Integrated Trajectory) Model (DRAXLER and ROLPH, 2003). The author gratefully acknowledges the NOAA Air Resources Laboratory (ARL) for the provision of the HYSPLIT transport and dispersion model and/or READY website used in this publication (http://www.arl.noaa.gov/ready/hysplit4.html). The location of a volcano that was active just before the sampling period (June 28 to July 1, 2002) is also shown (Karymsky Volcano).

Surface seawater samples were collected at 10 m depth along the transect using a single MITESS module (BELL et al., 2002) attached to a "weather-vane" deployed on the hydrowire on the side of the ship ("ATE/Vane", see Chapter 2 for more details). The vane rotates around the hydrowire orientating itself such that the module is upstream of the wire while ship moves forward at 1-2 knots (placing the sampler upstream of the wire and wire contamination). Each MITESS module opens and closes an acid-cleaned 500 ml polyethylene bottle while underwater in order to minimize chances for contamination.

3.2.2. Aerosol Solubility Experiments

Two dust dissolution experiments were performed for 3 to 4 days. For each experiment, the time zero soluble Fe estimate was made by placing the 47 mm filter with dust into a Teflon filter rig with the dust side up. A known amount of seawater ($\approx$ 225 ml) was cycled through the filter 10 times. Volumes were estimated by marking the bottles at sea and measuring the volumes after the cruise. In order to measure "dissolved" Fe (DFe, < 0.4 μm) and "soluble" Fe (SFe, < 0.02 μm), splits of the filtrate were vacuum filtered through an acid cleaned 0.4 μm Nuclepore® filter and syringe-filtered though an acid cleaned 0.02 μm Anotop® alumina filter (more details of this 0.02 μm filtration are given in Wu et al., 2001). Prior to each filtration, acid cleaned filters and the filter rig were thoroughly rinsed with dilute trace metal clean HCl and several aliquots of seawater. The acid cleaned collection bottles were also rinsed several times with filtered seawater prior to the final sample collection. Two 30 ml aliquots of the 0.4 μm and 0.02 μm filtrates were collected, and a 30 ml aliquot of the original filtrate was also archived.

After the time zero point, the filter was placed in a 250 ml acid cleaned polyethylene bottle. Prior to the experiment, the bottle was rinsed with seawater to remove any residual acid. A known volume ($\approx$ 225 ml) of freshly collected unfiltered seawater was added and the bottle gently swirled. Shaking was kept to a minimum to minimize dust particles from being lost from the dust filter. The dust filter and seawater

were left in contact with each other for 24 hours under laboratory light and room temperature. The mixture was gently swirled periodically. After 24 hours, the seawater was removed leaving the dust filter behind and fresh seawater was added. Splits of the removed seawater were vacuum filtered through an acid cleaned 0.4 μm Nuclepore® filter and syringe-filtered though an acid cleaned 0.02 μm Anotop® alumina filter similar to methods described above. Two separate aliquots of the 0.4 μm and 0.02 μm filtrates were collected, and a 30 ml aliquot of the original removed seawater was also archived. This process was repeated for each sequential 24-hour time point. Sub-samples and filtered splits of the original seawater used for each time point were also collected for DFe and SFe concentration measurements. Seawater and seawater leachate Fe and Mn concentrations were analyzed by isotope dilution MC-ICPMS [$Mg(OH)_2$ co-precipitation] using a modified version of a method developed by Wu et al. (2001) (BERGQUIST AND BOYLE, in prep). See chapter 2 for more details.

3.3. Results and Discussion

3.3.1. Aerosol Solubility Experiments

Iron released from the aerosol dissolution experiments is plotted in Figure 3.3. The amount of excess DFe released from the aerosols into seawater in each 24-hour time point was generally very low (< 65 pmol), and the excess DFe ($DFe_{sw+dust\ leach} - DFe_{sw}$) measured in the seawater leaches of the dust filter ranged from 0.00 to 0.29 nmol/kg. Ambient DFe concentrations ranged from 0.24 to 0.36 nmol/kg (Figure 3.4, Appendix 3.1) and the measured DFe in seawater leaches (ambient DFe + aerosol released DFe) never exceeded 0.7 nmol/kg. It is not believed that the excess DFe is due to contamination based on the absence of excess DFe in the first two time points of experiment 1. If the filter with dust was contaminated, then the first leaches should also be susceptible to contamination. However, no filter blanks were performed and therefore contamination may be responsible for some of the observed increases in DFe. Future experiments involving filter blanks will hopefully rectify this issue.

Total Fe concentrations in the atmosphere were measured by Chen (2004) in the

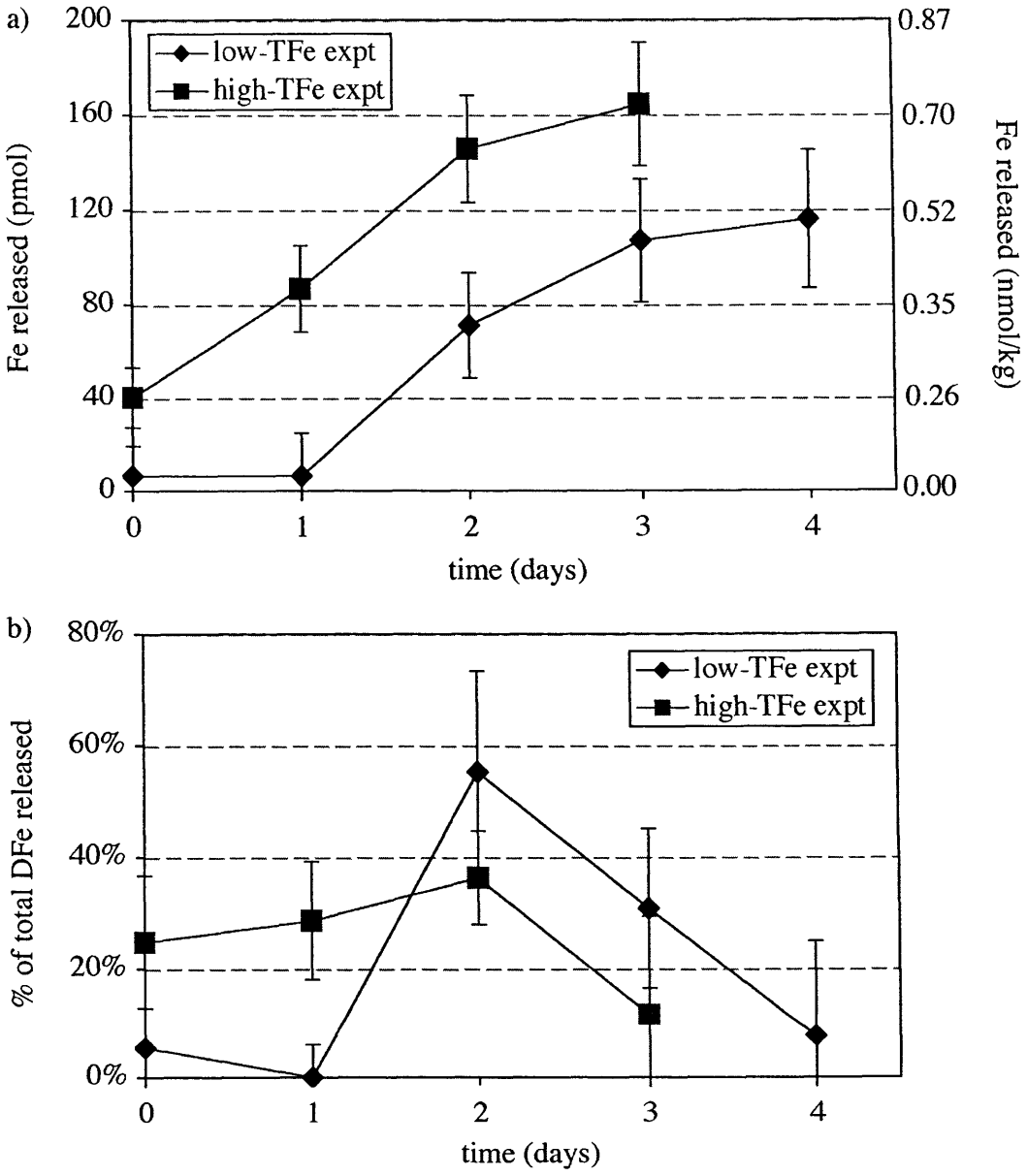

Figure 3.3: Aerosol Fe dissolution with time in natural seawater for freshly collected aerosols from the North Pacific. The seawater was changed every 24 hours in order to avoid saturation or Fe loss to bottle walls. The zero time measurement was processed by cycling seawater through the filter 10 times before starting the first 24-hour leaching experiment. 3.3a) The cumulative Fe released (pmol) from the aerosols over the course of the experiment. The Fe released is the DFe (<0.4 μm) measured in the seawater leachate after correction for the ambient seawater DFe. The Fe released in nmol/kg on the secondary axis is the Fe released divided by the mean volume of the experiments. 3.3b) The fraction of the total excess Fe released by the aerosols in each time interval (excess $Fe_{individual\ expt}$/excess $Fe_{total\ (cumulative\ of\ all\ time\ intervals)}$ where excess Fe is the difference between the Fe measured in the seawater+dust filter and the Fe in the ambient seawater).

fine fraction (< 2.5 m) over the periods of aerosol collection from simultaneous collection of aerosols on 90 mm Teflon filters mounted high volume collectors (experiment 1: 1.97 ng m^{-3}; experiment 2: 22.89 ng m^{-3}). Using the flow rate through the low volume polycarbonate filter and the aerosol collecting time, total Fe (TFe) on the filters used in the dissolution experiments was estimated to be 0.31 nmol for experiment 1 (low-TFe) and 2.36 nmol for experiment 2 (high-TFe). This is equivalent to aerosol Fe concentrations of 1.38 and 10.05 nmol/kg in the seawater and final solubilities of 37% and 6.6% for the low-TFe and high-TFe experiments respectively. The higher solubility was observed in the experiment with much lower aerosol concentration, which has been observed in other aerosol dissolution experiments (SPOKES and JICKELLS, 1996; BONNET and GUIEU, 2004).

In both our dissolution experiments, a significant time dependent dissolution trend was observed with >90% of the dissolution in the low-TFe experiment and 50% for the high-TFe experiment occurring after the 24 hour time point. For remote Pacific aerosols leached with natural seawater, Zhuang et al. (1990) found no difference in the fraction dissolved after 2 minutes up to 35 hours. However, a large amount of aerosol Fe (>200 nmol/kg) was used in the time series experiment with dissolved Fe concentrations reaching 12 to 13 nmol/kg almost immediately. Because this concentration is much higher than observations of excess dissolved ligand in surface waters (RUE and BRULAND, 1995; WU and LUTHER, 1995) and also higher than the inorganic solubility of Fe(III) in seawater (<0.1 nmol/kg) (KUMA et al., 1996; MILLERO, 1998), it could be that a large portion of the observed excess DFe was in the colloidal phase. Bonnet and Guieu (2004) observed very low dissolution of Saharan soil leach in seawater after 24 hours, but but the solubilized fraction of Fe increased to 1.6 and 2.2% after seven days in contact with the same seawater for their lowest particle concentration experiments. They also suggested that the observed Fe released may have been lower than the actual Fe solubilized due to scavenging of released DFe by particles. Iron loss to bottle walls may have occurred after seven days.

By changing the seawater every 24 hours, wall loss of Fe and saturation of the

organic ligands were hopefully minimized in our experiments. If enough TFe is added to a small volume of seawater in a laboratory experiment, it might be possible to saturate the seawater (i.e., the excess ligands present). As observed in the Atlantic Ocean, DFe released during incubation experiments with large amounts of atmospheric dust reached levels of ≈ 1.15 nmol/kg (Chapter 2). It was speculated in Chapter 2 that this might represent the limit of organic ligands present to keep Fe dissolved. In both experiments, a decrease in the amount of excess DFe released is observed after 48 hours (Figure 3.3b). However, particle loss from the filter may have decreased the aerosol concentration for the later time points. Whether the decrease is due to loss of particles or decreasing labile Fe is not known. The large amount of Fe solubilized in both experiments (37 and 7%) support the notion that there was still a significant amount of the aerosol Fe left at the later time points.

Aerosol Fe was released only after 24 hours of conditioning in seawater in the low-TFe experiment, whereas the aerosol in the high-TFe experiment continually released Fe throughout the experiment including the zero time point (cycling of seawater through the filter 10 times). These observations indicate that the two aerosol samples collected were different although the modeled back trajectories for both aerosol air masses were similar (Figure 3.2). Both aerosol samples were transported westward through the North Pacific for about 2 weeks before they were collected. However, the July 13 aerosol was collected in an air mass with much lower aerosol concentrations than the aerosol collected on July 14. One potential source of aerosol Fe during the collection period besides particles from Asia is particles from volcanic emissions. Just before the sampling period for our aerosol particles (June 28 to July 5, 2002), seismicity reports for the Karymksy Volcano on the Kamchatka Peninsula (Russia, 54.1°N, 159.4°E, plotted on Figure 3.2) suggested that weak gas and ash blow-outs had occurred and that explosions may have rose to levels of ≈ 4 km (BGVN, 2002). Volcanic particles may have higher fractions of labile Fe than crustal particles.

If these experiments had only been performed for 24 hours, it would have appeared that negligible amounts of Fe was released in low-TFe experiment and only

3.7% (half of the end percentage) released in the high-TFe experiment. Despite the large difference in TFe present on the filters, both experiments released similar amounts of DFe by the final time point (low-TFe experiment: 116 pmol; high-TFe experiment: 164 pmol). As both experiments were still releasing DFe at the end of the experiment, the fraction of aerosol Fe solubilized represents minima for these experiments. The continual release for up to 4 days in these experiments is relevant to natural conditions as aerosol particles have an estimated residence time in the surface water on the order of weeks (JICKELLS, 1999).

The continual release of Fe from the remote ocean aerosols suggests that a large fraction of the Fe in these aerosols was present in a labile form. The seawater used for leaching the aerosols was not filtered and therefore organisms were present. Both the Zhang et al. (1990) and the Bonnet and Guieu (2004) used filtered seawater and the Spokes and Jickells (1996) experiments used artificial seawater. Therefore some of the DFe released in the experiments in this study may have been due to biological processes. Potential mechanisms of biological enhancement of particulate Fe solubilization were discussed in Chapter 1 (Figure 1.3). Organisms may produce Fe binding ligands, reduce particulate or colloidal Fe at cell membranes, or ingest and mobilize Fe internally (review: SUNDA, 2001). Because the seawater was not filtered, another potential source of DFe in the experiments might be from cell lysis or degradation of particulate organic matter. However, the lack of DFe released in the first time point of the low-TFe experiment argues against this being a significant source of DFe. Also, the same seawater was used for different time points of the two experiments. No similarities were observed for the amount of Fe released in the two experiments when the same seawater was used. Future experiments involving filter blanks should be performed to fully rectify this issue. Photochemistry was likely not very significant also because the experiments were done in the laboratory under artificial light. Manganese, which has an active photochemistry in surface waters (SUNDA and HUNTSMAN, 1988), was not released in any of our experiments. Under natural light, photochemical reduction of Fe(III) on the surface of particles may enhance solubilization of Fe (MOFFETT, 2001; SUNDA, 2001).

Chen (2004) performed dissolution experiments on simultaneously collected aerosols using a reducing pH 4.5 leach solution (formate-acetate buffer with hydroxylamine) and a 90-minute contact time with the aerosols. This approach is interpreted to release labile Fe (LFe) (CHEN and SIEFERT, 2003). The fraction of Fe measured as LFe by Chen (2004) was lower than the observed released of DFe in natural seawater measured in this study for similar aerosol samples. For the low-TFe aerosol, the Chen (2004) measurement of LFe was 10% compared to our 4-day seawater solubilized fraction of 37%. For the high-TFe aerosol, only 1.4% of the TFe was released as LFe in Chen (2004) as opposed to 6.6% observed in this study's 3-day seawater experiment.

Recent observations of surface water DFe concentrations and aerosol flux estimates in the North Pacific have lead authors to argue that aerosol solubility must be higher than 10% to maintain the observed DFe concentrations (JOHNSON et al., 2003; BOYLE et al., submitted). The observations of high solubility in this study and Zhuang et al. (1990) lend support to the notion that the fraction of solubilized Fe for Pacific dry aerosols can be higher than 10%. The dissolution is likely quite variable and dependent on aerosol source, particle size, aerosol concentration, and chemical processing in the atmosphere. This is illustrated by the differences in the observed range in solubility for the two aerosol sampling periods in the Pacific with higher fractions of LFe observed in the summer of 2002 than in April of 2001 (CHEN and SIEFERT, 2004; CHEN, 2004, in preparation; HAND et al., submitted). More LFe appears to be present in the North Pacific aerosols in the summer of 2002 (2 to 16%) when the seawater leaching experiments were performed than LFe in Atlantic aerosols (2 to 5%) (CHEN and SIEFERT, 2004; CHEN, 2004, in preparation). Chen (2004) measured LFe fraction in both the fine (<2.5 μm) and coarse (>2.5 μm) fraction of aerosol Fe for the equivalent aerosols used in the seawater leaching experiments, which only used the fine fraction. During the collection period, more Fe and LFe was present in the fine fraction than the coarse. For July 13, the coarse fraction had only 0.6% of LFe versus 1.4% for the fine fraction. In the July 14 aerosol sample, the coarse fraction had 6.3% LFe versus 10% for the fine fraction. Therefore, our estimates of dissolvable Fe from the seawater leaching

experiments may be over-estimating the overall fraction of leachable Fe from dry aerosols by excluding the coarse fraction.

Jickells (1999) and Jickells and Spokes (2001) speculated that the flux of DFe to the ocean might be dominated by wet deposition due to the high solubility of aerosols in rainwater. Jickells (1999) estimated a residence time of 200 to 300 days for DFe in the Sargasso Sea using estimates of wet and dry deposition and their solubilities, the upwelling flux of DFe to the surface water mixed layer, and the inventory of DFe in the mixed layer. Although wet deposition was estimated to only account for 15% of the total deposition, it dominated the flux of DFe to the surface ocean (>90%) because of the high fraction of solubilized Fe used for wet deposition (14%) and the low dissolution used for dry deposition (<0.1%). Newer estimates for the fraction of Fe dissolved in dry deposition in the Atlantic Ocean suggest that it is greater than 1% (BONNET and GUIEU, 2004; CHEN and SIEFERT, 2004). If the experiments in this study apply to the Atlantic, all and possibly more of the LFe measured by Chen and Siefert (2004) in Atlantic aerosols (2 to 5%) may become DFe in surface seawater. If the Jickells (1999) estimates are redone using a higher solubility for Atlantic dry deposition (≈ 3%), the estimate of the residence time of DFe in the surface seawater decreases to 120 to 150 days and the amount of DFe delivered by wet and dry deposition becomes approximately equivalent. This estimate of 120 to 150 days is more consistent with residence time estimates of surface DFe in the North Atlantic estimated in Chapter 2 of this thesis and estimates by de Baar and de Jong (2001) and Sarthou et al. (2003). Sarthou et al. (2003) also estimated that dry deposition dominated the flux of DFe (>80%) north of the ITCZ in the eastern Atlantic Ocean, although wet deposition dominated in the ITCZ. Estimates were made based on surface seawater observations and concurrent estimates of labile Fe (pH 4.7) in dry deposition as well as measurements of filtered and unfiltered rainwater. The newer estimates of residence time including the ones made in Chapter 2 are all based on higher solubilities of dry deposition, so it is not surprising that these methods tend to agree. However, seasonal and shorter-term changes in surface DFe and the relation between these changes with dust deposition at Station ALOHA in the North Pacific

suggest that the residence time of DFe is on the order of months (BOYLE et al., submitted).

3.3.2. Soluble (< 0.02 μm) Excess Fe from Dust Solubility Experiments

In Figure 3.4, soluble Fe (SFe) concentrations in the seawater along the transect from this study are plotted along with DFe (data given in Appendix 3.1). Although DFe decreases from east to west, the SFe fraction is invariant with a mean concentration of 0.27 ± 0.03 nmol/kg. The SFe fraction was measured for four of the aerosol solubility time points, one for low-TFe experiment and three for the high-TFe experiment. No excess SFe was observed in the low-TFe experiment sample, but all of the measured high-TFe time points had a mean excess SFe of 0.17 ± 0.03 nmol/kg (1 SD). This represented 30 to 100% of the excess DFe released by the dust for those time points. The total SFe (ambient seawater + dust released SFe) measured in the dust dissolution experiments including the sample with no excess SFe had a mean SFe concentration of 0.32 ± 0.02 nmol/kg (1 SD). The relatively constant amount of SFe suggests that a maximum concentration in the soluble fraction was reached. The observed maximum concentration of SFe released in the dissolution experiments is similar to the value of DFe at which no CFe is present in Atlantic seawater samples (Chapter 2, Figure 2.9).

The processes that control whether DFe from aerosol Fe is released into the soluble or colloidal fraction are not clear. From the surface distribution and shallow water column profiles of SFe and CFe in Chapter 2, it was inferred that DFe from dust dissolution was preferentially released into the colloidal fraction in the Atlantic. The observation of excess SFe from the dust dissolution experiments from the Pacific indicate that aerosol Fe can enter the soluble fraction, at least under low aerosol Fe concentrations in the remote Pacific Ocean and up to 0.32 nmol/kg. In order to understand why the SFe fraction in the Atlantic is not strongly correlated with dust inputs, similar dust dissolution experiments as performed in this study are needed for the Atlantic Ocean. Also, information on the distribution of SFe and CFe in areas of varying dust deposition is

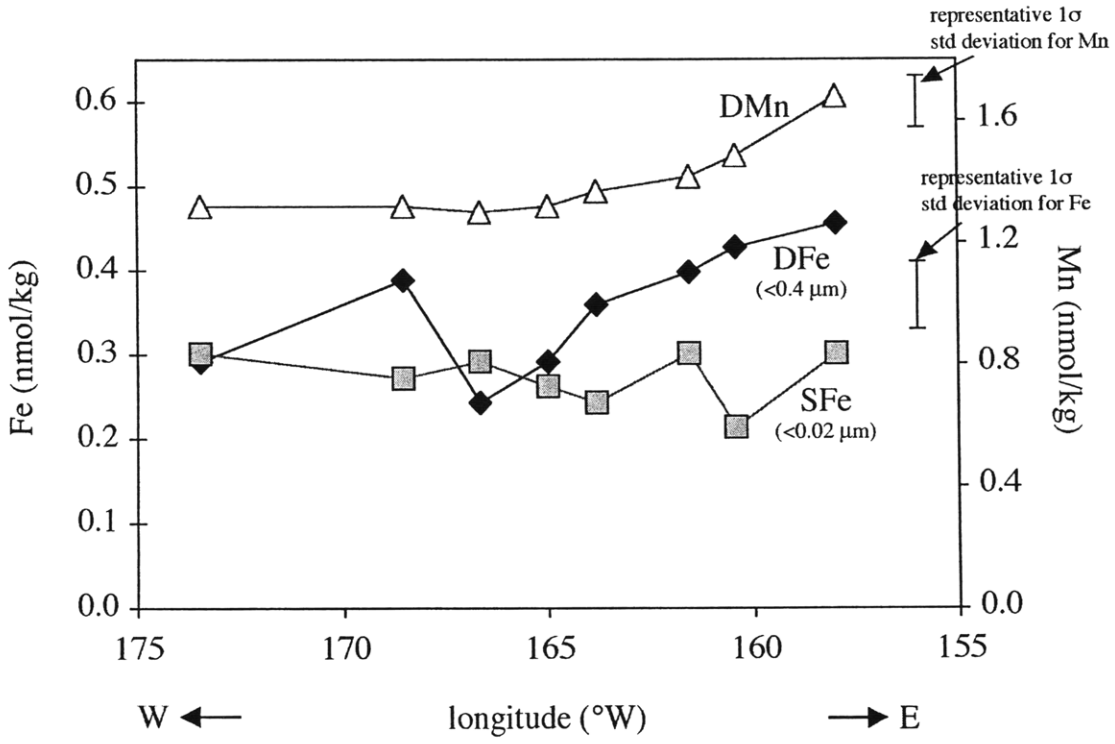

Figure 3.4: E-W transect of DFe, SFe, and DMn northwest from Station ALOHA (22.8°N, 158°W) in the North Pacific subtropical gyre. The surface seawater measured along the transect was the seawater used in the aerosol dissolution experiments.

needed to study how the different fractions of DFe are influenced by atmospheric inputs in the Pacific Ocean.

3.4. CONCLUSIONS

Aerosol dissolution experiments were performed with freshly collected remote Pacific aerosols and natural seawater. The seawater was changed every 24 hours to avoid saturation of the seawater and to avoid Fe loss to the bottle walls. Iron was continually released from the aerosols for up to four days. For the experiment with lower amounts of TFe (0.31 nmol), negligible amounts of DFe were released within the first 24 hours. Continual release was observed for the experiment with higher levels of TFe (2.36 nmol). Despite the slow start for low-TFe experiment, almost as much DFe was released over four days for the low-TFe experiment (116 pmol) than was released after three days in the high-TFe experiment (164 pmol). Based on estimates of TFe, the total amount of DFe released was 37% for the low-TFe experiment and 6.6% for the high-TFe experiment. These estimates are likely minimum estimates because DFe was still being released at the end of both experiments and particles from the dust filters were likely lost when the seawater was changed every 24 hours.

Comparable LFe measurements (90-minute, pH 4.5, reducing conditions) by Chen (2004) yielded lower percentages of LFe for equivalent aerosol samples, although a similar pattern of more labile Fe in the low-TFe aerosols was observed. The high solubilization observed in the remote Pacific aerosols suggest that Pacific aerosols may release a higher fraction of their Fe than Atlantic aerosols. Current estimates of the fraction of dissolvable Atlantic aerosol Fe are low, but pH 8 estimates are based on experiments in artificial seawater (< 0.1%) (SPOKES and JICKELLS, 1996) or Saharan soil with natural seawater where the seawater was not changed for 7 days (up to 2.2%) (BONNET and GUIEU, 2004). Labile Fe estimates from Chen (2004) and Chen and Siefert (2004) are lower for the Atlantic compared with the Pacific in July 2002. Studies with open ocean Atlantic aerosols and natural seawater are needed to better constrain the dissolvable fraction of dry deposition in the Atlantic. Estimates of aerosol solubilization

have important consequences for models of the Fe cycle because the amount of Fe released from dust determines the flux of DFe to the surface ocean. Currently the fraction of Fe released from both dry and wet aerosols is being treated as a constant (usually 1 or 10%) because of the limited and variable estimates available (FUNG et al., 2000; PAREKH et al., 2004).

Appendix 3.1. E-W Transect Measurements from KOK Cruise (July 2002)

Fe Measurements

St. #	Lat. (°N)	Long. (°W)	date	DFe[a] (nmol/kg)	1 SD[b]	n	SFe[c] (nmol/kg)	1 SD	n
S12	25.6	173.4	7/12/02	0.29	0.03	2	0.30	0.06	2
S13	24.2	168.6	7/13/02	0.39		1[d]	0.27	0.01	3
S15	23.6	166.7	7/14/02	0.24	0.05	2	0.29		1
S16	23.1	164.9	7/15/02	0.29	0.05	3	0.26	0.05	3
S17	22.8	163.8	7/15/02	0.36		1	0.24	0.04	2
S18	22.8	161.6	7/16/02	0.40		1	0.30	0.07	3
S19	22.7	160.4	7/16/02	0.43	0.06	2	0.21	0.03	2
S20	22.8	158.0	7/17/02	0.46	0.02	2	0.30		1

Mn Measurements

St. #	Lat. (°N)	Long. (°W)	date	DMn[e] (nmol/kg)	1 SD	n
S12	25.6	173.4	7/12/02	1.32	0.02	3
S13	24.2	168.6	7/13/02	1.32	0.01	3
S15	23.6	166.7	7/14/02	1.30	0.06	3
S16	23.1	164.9	7/15/02	1.32	0.03	6
S17	22.8	163.8	7/15/02	1.37	0.07	3
S18	22.8	161.6	7/16/02	1.42	0.04	3
S19	22.7	160.4	7/16/02	1.49	0.01	2
S20	22.8	158.0	7/17/02	1.68	0.01	3

a) DFe is the Fe that passes through a 0.4 μm filter.
b) 1 SD is the standard deviation of sample replicates.
c) SFe is the Fe that passes through a 0.02 μm filter.
d) If only one replicate is reported, then an uncertainty of 0.05 nmol/kg was used for error propragation.
e) DMn if the Mn that passes through a 0.4 μm filter.

References for Chapter 3

Behra P. and Sigg L. (1990) Evidence for redox cycling of iron in atmospheric water droplets. *Nature* **344**, 419-421.

Bell J., Betts. J., and Boyle E. A. (2002) MITESS: A Moored In-situ Trace Element Serial Sampler for Deep-Sea Moorings. *Deep-Sea Research I* **49**, 2103-2118.

BGVN. (2002) Karymsky. Smithsonian Institution, Bulletin of the Global Volcanism Network, BGVN v.27, no.6. (http://www.volcano.si.edu/gvp/reports/).

Bonnet S. and Guieu C. (2004) Dissolution of atmospheric iron in seawater. *Geophysical Research Letters* **31**, LO3303.

Boyle E. A., Bergquist B. A., and Kayser R. (submitted) Iron, manganese, and lead at Hawaii Ocean Time Series Station ALOHA: temporal variability and an intermediate water hydrothermal plum. *Geochimica et Cosmochimica Acta.*

Chen M. (2004, in preparation) Aerosol inputs of labile iron and other nutrient species and its influences on nitrogen-fixing microorganisms over the remote ocean. PhD, University of Maryland.

Chen Y. and Siefert R. (2004) Seasonal and spatial distributions of dry deposition fluxes of atmospheric total and labile iron over the tropical and sub-tropical North Atlantic Ocean. *Journal of Geophysical Research-Atmosphere* **109**, Art. No. D09305.

Chen Y. and Siefert R. L. (2003) Determination of various types of labile atmospheric iron over remote oceans. *Journal of Geophysical Research* **108**, No. D24, 4774.

Draxler R. R. and Rolph G. D. (2003) HYSPLIT (HYbrid Single-Particle Lagrangian Integrated Trajectory) Model access via NOAA ARL READY Website (http://www.arl.noaa.gov/ready/hysplit4.html). *NOAA Air Resources Laboratory*, Silver Spring, MD.

Duce R. A. and Tindale N. W. (1991) Atmospheric transport of iron and its deposition in the ocean. *Limnology and Oceanography* **36**, 1715-1726.

Fung I. Y., Meyn S. K., Tegen I., Doney S. C., John J. G., and Bishop K. B. (2000) Iron supply and demand in the upper ocean. *Global Biogeochemical Cycles* **14**, 281-295.

Gao Y., Kaufman Y. J., Tanre D., Kolber D., and Falkowski P. G. (2001) Seasonal distributions of aeolian iron fluxes to the global ocean. *Geophysical Research Letters* **28**, 29-32.

Gledhill M. and van den Berg C. M. G. (1994) Determination of complexation of iron(III) with natural organic complexing ligands in seawater using cathodic stripping voltammetry. *Marine Chemistry* **47**, 41-54.

Hand J. L., Mahowald N. M., Chen Y., Siefert R. L., and Luo C. (submitted) Estimates of soluble iron from observations and a global mineral aerosol model: biogeochemical implications. *Journal of Geophysical Research.*

Jickells T. D. (1999) The inputs of dust derived elements to the Sargasso Sea: a synthesis. *Marine Chemistry* **68**, 5-14.

Jickells T. D. and Spokes L. J. (2001) Atmospheric iron inputs to the oceans. In *The Biogeochemistry of Iron in Seawater*, Vol. 7 (ed. K. A. Hunter and D. Turner), pp. 85-121. John Wiley & Sons, Ltd.

Johansen A. M., Siefert R. L., and Hoffmann M. R. (2000) Chemical composition of aerosols collected over the tropical North Atlantic Ocean. *Journal of Geophysical Research* **105**, 15277-15321.

Johnson K. S. (2001) Iron supply and demand in the upper ocean: Is extraterrestrial dust a significant source of bioavailable iron? *Global Biogeochemical Cycles* **15**(1), 61-63.

Johnson K. S., Elrod V. A., Fitzwater S. E., Plant J. N., Chavez F. P., Tanner S. J., Gordon R. M., Westphal D. L., Perry K. D., Wu J., and Karl D. M. (2003) Surface ocean-lower atmosphere interactions in the Northeast Pacific Ocean gyre: aerosols, iron, and the ecosystem response. *Global Biogeochemical Cycles* **17**, Art. No. 1063.

Kuma K., Nishioka J., and Matsunaga K. (1996) Controls on the iron(III) hydroxide solubility in seawater: the influences of pH and natural organic chelators. *Limnology and Oceanography* **41**, 396-407.

Mahowald N., Kohfeld K., Hansson M., Balkanski Y., Harrison S. P., Prentice I. C., Schulz M., and Rodhe H. (1999) Dust sources and deposition during the last glacial maximum and current climate: a comparison of model results with paleodata from ice cores and marine sediments. *Journal of Geophysical Research* **104**, 15895-15916.

Millero F. J. (1998) Solubility of Fe III in seawater. *Earth and Planetary Science Letters* **154**, 323-329.

Moffett J. W. (2001) Transformations Among Different Froms of Iron in the Ocean. In *The Biogeochemistry of Iron in Seawater*, Vol. 7 (ed. K. A. Hunter and D. Turner), pp. 343-372. John Wiley & Sons, Ltd.

Parekh P., Follows M. J., and Boyle E. A. (2004) Modeling the global ocean iron cycle. *Global Biogeochemical Cycles* **18**(GB1002), 1-15.

Parrington J. R., Zoller W. H., and Aras N. K. (1983) Asian dust: seasonal transport to the Hawaiian Islands. *Science* **220**, 195-198.

Prospero J. M. (1996) The atmospheric transport of particles to the ocean. In *Particle Flux in the Ocean*, Vol. SCOPE Rep. 57 (ed. V. Ittekkott, P. Schafer, S. Honjo, and P. J. Depestris), pp. 19-52. John Wiley.

Rue E. L. and Bruland K. W. (1995) Complexation of iron(III) by natural ligands in the central North Pacific as determined by a new competitive ligand equilibrium/adsorptive cathodic stripping voltammetric method. *Marine Chemistry* **50**, 117-138.

Siefert R. L., Johanson A. M., and Hoffmann M. R. (1999) Chemical characterization of ambient aerosol collected during the southwest monsoon and intermonsoon seasons over the Arabian Sea: labile-Fe(II) and other trace metals. *Journal of Geophysical Research-Atmosphere* **104**, 3511-3526.

Siefert R. L., Webb S. M., and Hoffmann M. R. (1996) Determination of photochemically available iron in ambient aerosols. *Journal of Geophysical Research* **101**, 14441-14449.

Spokes L. J. and Jickells T. D. (1996) Factors controlling the solubility of aerosol trace metals in the atmosphere and on mixing into seawater. *Aquatic Geochemistry* **1**, 355-374.

Spokes L. J., Jickells T. D., and Lim B. (1994) Solubilization of aerosol trace metals by cloud processing: A laboratory study. *Geochimica et Cosmochimica Acta* **58**, 3281-3287.

Sunda W. (2001) Bioavailability and bioaccumulation of iron in the sea. In *The Biogeochemistry of Iron in Seawater*, Vol. 7 (ed. K. A. Hunter and D. Turner), pp. 123-253. John Wiley & Sons, Ltd.

Sunda W. G. and Huntsman S. A. (1988) Effects of sunlight on redox cycles of manganese in the southwestern Sargasso Sea. *Deep-Sea Research* **35**, 1297-1317.

Tegan I., Lacis A. A., and Fung I. Y. (1996) The influence on climate forcing of mineral aerosol from disturbed soil. *Nature* **380**, 419-422.

Visser F., Gerringa L. J. A., Van der Gaast S. J., de Baar H. J. W., and Timmermans K. R. (2003) The role of the reactivity and content of iron of aerosol dust on growth rates of two Antarctic diatom species. *Journal of Phycology* **39**, 1085-1094.

Witter A. E. and Luther G. W. (1998) Variation in Fe-organic complexation with depth in the Northwestern Atlantic Ocean as determined using a kinetic approach. *Marine Chemistry*, 241-258.

Wu J. and Luther G. W. I. (1995) Complexation of iron(III) by natural organic ligands in the Northwest Atlantic Ocean by competitive ligand equilibration method and a kinetic approach. *Marine Chemistry* **50**, 159-177.

Zhu X., Prospero J. M., Savoie D. L., Millero F. J., Zika R. G., and Satlzman E. S. (1993) Photoreduction of iron(III) in marine mineral aerosol solutions. *Journal of Geophysical Research* **98**, 21297-21305.

Zhu X. R., Prospero J. M., and Millero F. J. (1997) Diel variability of soluble Fe(II) and soluble total Fe in North African dust in the trade winds at Barbados. *Journal of Geophysical Research* **102**, 21297-21305.

Zhuang G. S., Duce R. A., and Kester D. R. (1990) The solubility of atmospheric iron in surface seawater of the open ocean. *Journal of Geophysical Research* **95**, 16207-16216.

Zhuang G. S., Yi Z., Duce R. A., and Brown P. R. (1992) Chemistry of iron in marine aerosols. *Global Biogeochemical Cycles* **6**, 161-173.

CHAPTER 4

Measurement of Iron Isotopes by Hexapole Collision Cell MC-ICPMS in Natural Samples with Low Concentrations of Iron

4.1. INTRODUCTION

Iron is a vital micronutrient, the 4th most abundant element in the crust, and has active redox chemistry at the surface of the earth. This makes studies of Fe important for processes of life, weathering, and earth chemistry. For example, iron's geochemical role changed drastically during the oxygenation of the earth's atmosphere and ocean. Because Fe is much more soluble under anoxic conditions, the availability of dissolved Fe for biological processes decreased greatly when oxygen built up in the atmosphere and ocean. In the modern ocean, the low solubility of Fe and the great demand for Fe by organisms (e.g., photosynthesis and nitrogen fixation) leads to Fe limitation of primary productivity in large regions of the ocean (MARTIN and GORDON, 1988; MARTIN, 1990; MARTIN et al., 1994). Although the importance of iron is recognized, it is difficult element to study because of its complicated biogeochemical cycling in the environment and the ease of contamination in natural samples with low concentrations of Fe.

Fractionation of Fe isotopes could be a useful tool to investigate and quantify Fe cycling in the environment. Stable isotope fractionation of light elements (e.g., C, O, N, H, S) is commonly used to study environmental processes. For example, stable isotope fractionation in $^{13}C/^{12}C$ of natural samples is employed to study carbon pathways and ocean circulation (DUPLESSY et al., 1988; HAYES, 1993). There are four stable isotopes of Fe (^{54}Fe, 5.84%; ^{56}Fe, 91.76%; ^{57}Fe, 2.12%; ^{58}Fe 0.28% (TAYLOR et al., 1992)) with a relative mass difference of 7% from ^{54}Fe to ^{58}Fe, which is large enough to predict that natural fractionation of Fe isotopes would occur (POLYAKOV, 1997; SCHAUBLE et al.,

2001; ANBAR et al., submitted). One of the hurdles in searching for natural variations of Fe isotopes was the development of analytical tools that could measure the isotopic ratio with high enough precision. This is because Fe is not amenable to gas source mass spectrometry, and thermal ionization mass spectrometry (TIMS) is difficult because of the high ionization potential of Fe. However, Bullen and McMahon (1998) and Beard and Johnson (1999) provided the first high precision iron isotope measurements by TIMS that demonstrated natural variability. More promising is the recent development of multi-collector inductively coupled plasma mass spectrometry (MC-ICPMS), which combines the high ionization efficiency of the plasma source (≈7000 K) and ease of ICPMS with simultaneous measurement of isotopes on multiple collectors (HALLIDAY et al., 1995). Instabilities in the plasma source in ICPMS (single detector instruments) made it impossible to reach similar precision in isotopic ratios as TIMS. This problem was overcome by the introduction of multiple-collector (MC)-ICPMS. Instabilities in the ion beam due to the plasma are effectively cancelled out by simultaneous collection of the isotopes. MC-ICPMS has opened the door to search for variations in the isotopic composition of previously unexplored elements. Measurable differences in the isotopic composition of elements using MC-ICPMS have been observed for several elements in natural samples including Cr, Cu, Zn, Se, Mo, and Fe (review: JOHNSON et al., 2004).

Although there are many advantages, there are two main challenges that need to be considered when making high precision Fe isotope measurements by MC-ICPMS: (1) correction of instrumental mass bias and (2) correcting for or eliminating isobaric interferences produced in the Ar plasma. Both TIMS and MC-ICPMS introduce mass fractionation that is greater than the fractionation produced in nature (in the case of Fe). Therefore, to make high precision isotope measurements, the instrumental mass bias must be well characterized in order to separate the instrumental mass bias from natural fractionation. In the following discussions, instrumental mass fractionation will be referred to as instrumental mass bias in order to keep it clearly distinct from natural isotopic fractionation. In TIMS, instrumental mass bias follows Rayleigh fractionation as the sample is consumed. Iron isotope measurement techniques by TIMS use a double

spiking technique to correct for the variable instrument mass bias, and are limited to a precision of ± 0.2 ‰ (2σ) per mass unit (dalton) for Fe isotopic analysis (BULLEN and MCMAHON, 1998; BEARD and JOHNSON, 1999; JOHNSON and BEARD, 1999; BULLEN et al., 2001).

Instrumental mass fractionation in MC-ICPMS (3-5%/dalton) is an order of magnitude larger than in TIMS. However, the large instrument mass bias is relatively constant making it possible to correct for instrument mass bias and still retain high precision in isotopic measurements. The mass bias in MC-ICPMS appears to dominantly be a function of mass caused by space-charge effects that result in the preferential loss of lighter isotopes as the ion beam is extracted through small apertures (sampling and skimmer cones) from the plasma at atmospheric pressure into the high vacuum environment of the mass analyzer (LEE and HALLIDAY, 1995; NIU and HOUK, 1996; MARÉCHAL et al., 1999; ALBAREDE and BEARD, 2004). The instrumental mass bias for Fe in MC-ICPMS is typically corrected for by sample-standard bracketing (SSB) and/or internal standards. SSB assumes that the instrumental mass bias of the sample is identical to the mass bias of two bracketing standards. The instrumental mass bias for the sample is corrected for by a simple linear interpolation between the bracketing standards. In internal standardization, the sample is spiked with another element in the similar mass range (e.g., Cu for Fe). The mass bias of the instrument is then calculated using a known isotopic composition of the elemental spike, and this instrumental mass bias is used to correct the element of interest. This method assumes that the mass bias of the instrument is only a function of mass (and not the element chemistry) and that the mass bias is some predictable function of mass (e.g., exponential or power law).

Both techniques have been explored for Fe, and several studies have found no significant improvement in precision of Fe isotope measurements using Cu internal spiking compared with SSB (BELSHAW et al., 2000; BEARD et al., 2003). However, recent studies have highlighted potential pitfalls in relying solely on SSB or solely on internal spiking (CARLSON et al., 2001; ALBAREDE and BEARD, 2004; ARNOLD et al., 2004). One potential problem in SSB is the possibility of matrix-induced variability in

instrumental mass bias. This is a particularly hard problem to assess in real samples, as instrumental mass bias shifts will not be discernable with traditional checks on data quality such as double isotopic ratio plots. Both instrumental mass bias and natural mass fractionation follow similar mass-dependent functions; therefore, samples with altered instrument mass bias will plot along mass-dependent fractionation trends on double isotopic ratio plots. Potential changes in MC-ICPMS instrumental mass bias due to matrix have been discussed and documented in a few studies (MARÉCHAL et al., 1999; ANBAR et al., 2001; CARLSON et al., 2001; ROE et al., 2003; ALBAREDE and BEARD, 2004; ARNOLD et al., 2004). Arnold et al. (2004) compared SSB corrected Fe isotope data with internal standard corrected Fe isotope data and found that one of three paleosol samples had significantly different calculated Fe isotopic composition ($\approx 0.6‰$) with the two mass bias correction schemes. This was interpreted to reflect a change in the instrumental mass bias for that one sample due to its matrix. They also found that the precision on all of the paleosol samples was degraded when only SSB correction was used suggesting that instrumental mass bias was more variable in the real samples. It should be noted that no extra chemical purification techniques were used to remove organic matter other than one-stage anion exchange.

Albarede and Beard (2004) looked at both the effect of trace constituents and sample concentration on instrumental mass bias. Increasing shifts in the calculated Fe isotope values (by SSB) were observed with increasing amounts of trace elements (e.g., Mg and La). 70 ppb (ng/g) additions of Mg to sample matrices produced significant shifts in the calculated $^{56}Fe/^{54}Fe$ isotopic composition ($\pm 0.2‰$ in the $^{56}Fe/^{54}Fe$ ratio), and the relationship of concentration of the doped element and induced isotopic shift were not the same (magnitude or direction) from one analysis session to another. They also observed a signal-size dependent trend in the calculated Fe isotopic values over a large concentration range (200 to 600 ppb) with a slope of 0.03‰ per volt (^{56}Fe signal). Calculated iron isotope bias due to signal differences of bracketing standards and samples of less than 10% are relatively small (less than 0.1‰), so careful matching of sample and standard concentrations should avoid this problem. Albarede and Beard (2004) inferred

from their observations that the matrix-induced variations in mass bias resulted from changing the space-charge effects or ionization properties of the plasma. Despite the potential complications with SSB, it is the most common technique employed in Fe isotopic analysis by MC-ICPMS with reported precisions of 0.05 to 0.15 ‰ (2σ, $^{56}Fe/^{54}Fe$ ratio) (BELSHAW et al., 2000; ZHU et al., 2002; BEARD et al., 2003). It is believed that rigorous sample purification can avoid many matrix problems, although one must be aware of potential problems when only using SSB to define instrument mass bias.

Arnold et al. (2004) found improved precision in Fe isotopic measurements by using a Cu internal standard for instrument mass bias correction rather than SSB. Although it would seem that an elemental spike should be the preferred method, it assumes that the mass bias of the instrument is only a function of mass and not element chemistry. Several studies have suggested that elements do not necessarily follow the same mass bias trends at high precision in ICPMS (MARÉCHAL et al., 1999; ANBAR et al., 2001; CARLSON et al., 2001; KEHM et al., 2003; ROE et al., 2003; ALBAREDE and BEARD, 2004). Albarede and Beard (2004) measured mixed Cu and Zn solutions and found that Cu was more strongly fractionated than Zn suggesting that the two elements did not experience the same instrument mass bias. Kehm et al. (2003) found that the relationship between Cu and Fe isotopic ratios changed from one analysis session to another, and the Cu spike in the sample matrix could induce changes in calculated Fe isotopic values. Therefore, Kehm et al. (2003) adopted a method of using both SSB and internal spiking where care was taken to match the concentrations of Fe and Cu in both the samples and the bracketing standards. It is also very important that the sample be free of the element that is being used as an elemental spike. For Fe, the most commonly used ion exchange chromatographic separation method used for purification will separate Fe from Cu if the correct procedure is used. Copper slowly elutes off the column at higher eluent concentrations than Fe. If caution is not taken to insure that all of the Cu is eluted prior to elution of Fe, then the remaining Cu will co-elute with Fe. High precision isotope measurement protocols by MC-ICPMS are still in the early stage of development, and

care should be taken to reduce residual sample matrices and evaluate potential matrix-induced variability in instrument mass bias.

Another important challenge with MC-ICPMS is the molecular interferences that form in the Ar plasma and interface. For Fe, many of these interferences are polyatomic interferences due to the combination of Ar and atmospheric gases. Polyatomic interferences can also form if significant amounts of Ca or C are present. Some of the critical interferences on the Fe masses are listed in Table 4.1. Several approaches are used to reduce the polyatomic interferences including (1) desolvating nebulizers, (2) cold plasma conditions, (3) high mass resolution, and (4) hexapole collision cells.

Desolvating nebulizers reduce the amount of water that is injected into the plasma and minimize oxide interferences. Several studies have demonstrated that Ar oxide interferences can adequately be reduced for high precision Fe isotope analysis using desolvating nebulizers, and ArN^+ can be reduced by preparing samples in dilute HCl solutions instead of the more commonly used HNO_3 (ANBAR et al., 2000; BELSHAW et al., 2000; ZHU et al., 2000). Desolvating nebulizers also have the advantage of increasing analyte transport to the plasma (50 to 90%) as compared to conventional nebulizers (1 to 4%) (Olesik, 2000). However, oxide interferences can still be significant and high concentrations of Fe (20 ppm) are needed to overwhelm the interferences (BELSHAW et al., 2000). "Cold plasma" conditions (lower RF power used to maintain the Ar plasma) also reduce molecular interferences, but high concentrations (30 ppm) are still necessary due to the overall loss in sensitivity (KEHM et al., 2003). High mass resolution MC-ICPMS resolves the polyatomic interferences at the Fe masses (WEYER and SCHWIETERS, 2003; ARNOLD et al., 2004). The ThermoFinnigan Neptune MC-ICPMS has the capability to make high mass resolution measurements on multiple collectors and maintain good peak shape. High resolution reduces the transmission of analyte, and solutions with 1 to 3 ppm Fe are currently used for Fe isotope analysis (although the use of lower concentrations is possible) (WEYER and SCHWIETERS, 2003; ARNOLD et al., 2004). The use of a collision cell with MC-ICPMS will be discussed in the next paragraph. The ^{54}Cr interference can not be resolved from ^{54}Fe even at high resolution.

Table 4.1: Important Isobaric Interferences on Fe Isotopes			
Fe isotope	^{54}Fe	^{56}Fe	^{57}Fe
Fe mass	53.93961	55.93494	56.93540
% abundance	5.80%	91.72%	2.20%
interference	$^{40}Ar^{14}N^{+}$	$^{40}Ar^{16}O^{+}$	$^{40}Ar^{16}O^{1}H^{+}$
mass	53.96546	55.9573	56.96512
% abundance	99.24%	99.36%	99.35%
interference	^{54}Cr	$^{40}Ca^{16}O^{+}$	$^{40}Ca^{16}O^{1}H^{+}$
mass	53.93888	55.95751	56.96533
% abundance	2.37%	96.71%	96.70%
interference	$^{37}Cl^{16}O^{1}H^{+}$	$^{44}Ca^{12}C^{+}$	$^{56}Fe^{1}H^{+}$
mass	53.96864	55.95548	56.94277
% abundance	24.17%	2.07%	91.71%

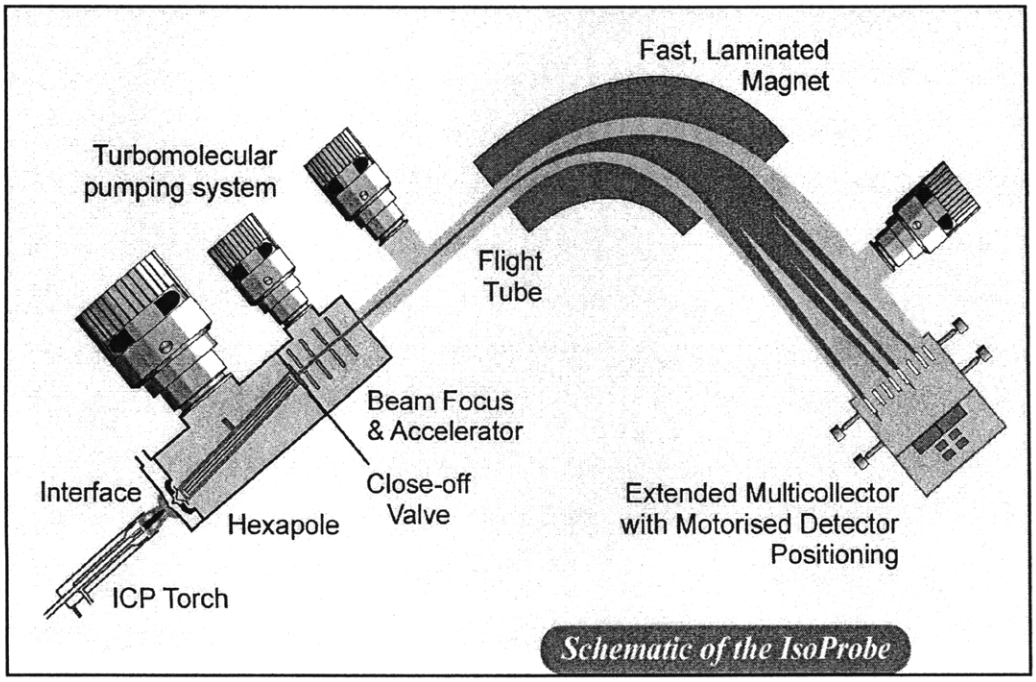

Figure 4.1: Schematic of the GV Instruments IsoProbe MC-ICPMS.

Therefore the Cr interference has to be chemically separated from Fe by ion exchange chromatography, and either ^{52}Cr or ^{53}Cr have to be monitored to correct for Cr on ^{54}Fe.

Iron isotope analysis in this study was done on the MIT GV Instruments (formerly Micromass) IsoProbe MC-ICPMS (Figure 4.1). The IsoProbe is a single focusing instrument that incorporates a hexapole collision cell behind the collimating cone and before the magnetic sector. The hexapole collision cell has two main advantages: (1) high transmission of ions to the mass analyzer and (2) destruction of many molecular interferences. Hexapole collision cells are not new in ICPMS, and have been incorporated into quadrupole-based ICPMS systems (reviews: FELDMANN et al., 1999a; FELDMANN et al., 1999b). Usually both a buffer gas and reaction gas are injected into the hexapole cell. Collisions with the buffer gas (e.g., Ar) thermalize the ions to the energy of the gas used (collisional focusing), which leads to a small energy spread in the ion beam ($\approx$ 1 eV). In other instruments, electrostatic analyzers are used to reduce the energy spread of the beam. This leads to reduced transmission of the ions, whereas transmission of ions is not reduced in the hexapole collision cell. In addition to energy focusing, gas phase reactions are important in destroying and reducing molecular interferences. Several reaction gases have been employed in collision cells (H_2, Xe, N_2, O_2, NH_3, CH_4) depending on which molecular species need to be removed. Most of the Ar polyatomic interferences are essentially eliminated with the addition of H_2 as a reaction gas including ArN^+ and ArO^+ (Figure 4.2). The only Ar interference that remains a problem is $ArOH^+$, which may form in the hexapole by a protonation reaction. Because of the virtual elimination of Ar polyatomic interferences and the high transmission of ions, Fe isotopic analysis can easily be achieved on solutions of 200 to 400 ppb Fe (BERGQUIST and BOYLE, 2002; JOHNSON et al., 2002; BEARD et al., 2003).

In this chapter, the methods used for Fe isotope analysis in this thesis are discussed along with the various tests used to evaluate the precision and accuracy of the measurements. Precision and accuracy were assessed through the measurement of

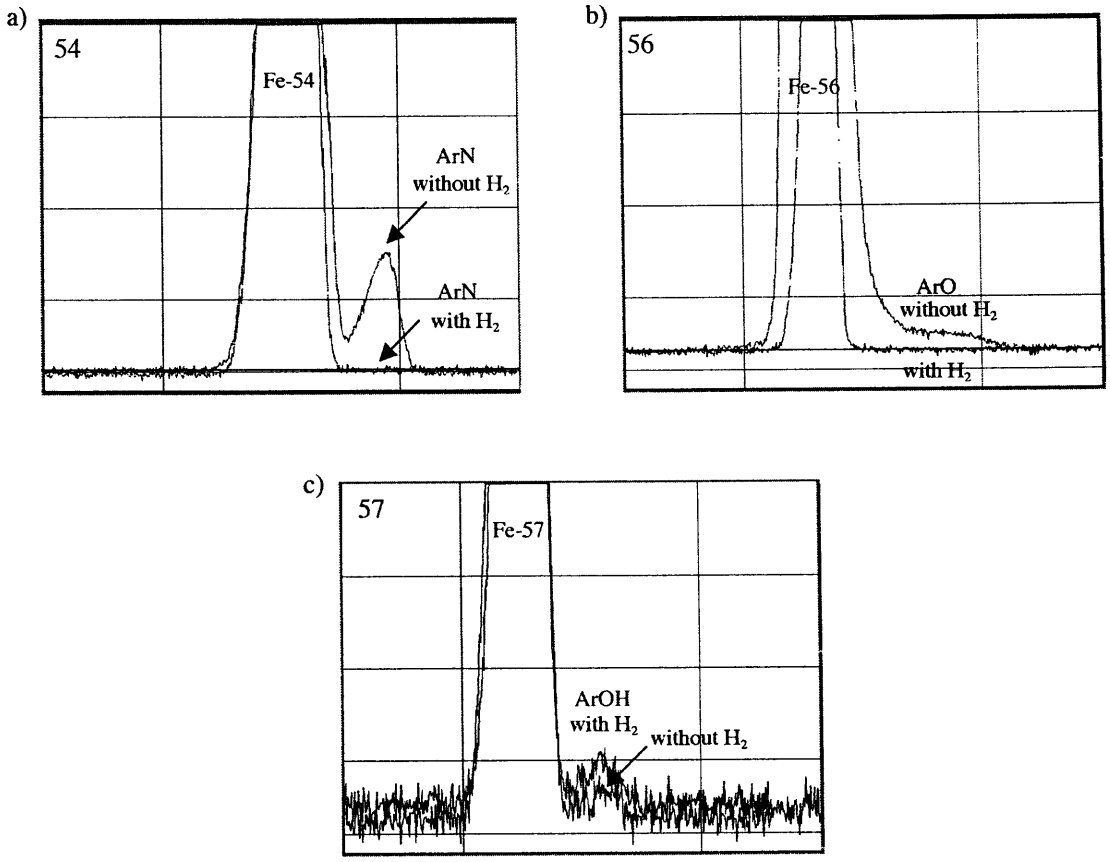

Figure 4.2: "High resolution" scans of the different masses of the Fe isotopes on the MIT GV Instruments IsoProbe MC-ICPMS with 1.8 ml/min of Ar gas in the collision cell. 4.2a) A scan of a 250 ppt (pg/g) ^{54}Fe solution is shown with and without 2 ml/min H_2 gas in the hexapole collision cell. ArN^+ was eliminated with the addition of the H_2 reaction gas. 4.2b) A scan of a 250 ppt ^{56}Fe solution is shown with and without 2 ml/min H_2 gas in the hexapole collision cell. In order to create a significant amount of ArO^+, no H_2 gas was used and the Ar collision gas needed to be reduced to 0.5 ml/min. The ArO^+ was significantly reduced by using 1.8 ml/min of Ar in the collision chamber and eliminated with the addition of the H_2 reaction gas. 4.2c) A scan of a 125 ppt ^{57}Fe solution is shown with and without 2 ml/min H_2 gas in the hexapole collision cell. The $ArOH^+$ interference actually increased slightly with addition of H_2 reaction gas in the hexapole chamber. $ArOH^+$ can be created in the hexapole by protonation of ArO^+. The "high resolution" scans were done by narrowing the source slit and setting the detector slit to the "high resolution" slit, which has a resolving power of $\approx$ 5000 ($m/\Delta m$).

standards including isotopically shifted standards. Process standards were run at various concentrations and with different isotopic compositions to test for fractionation in the separation chemistry and significant blank contributions. Proper interference correction was evaluated by measuring both the $^{56}Fe/^{54}Fe$ and $^{57}Fe/^{54}Fe$ ratios when possible. Finally, an "isotope standard addition" method was developed to investigate matrix-induced variability of the instrument mass bias. This method avoids the complications of using another element by spiking a sample with a very small amount of highly isotopically modified Fe. The concentration of the sample is not changed, but the isotopic composition of the sample is shifted. If the instrument mass bias is corrected properly, the measured isotopic composition of the spiked sample agrees well with predicted values based on simple isotopic mass balance. It is especially important to this study to evaluate the Fe isotope measurement method because samples with low concentrations of Fe were processed for isotopic analysis. Therefore, matrix effects and interferences are potentially more severe due to the low analyte concentrations.

4.2. METHODS

4.2.1. Fe Purification and Separation

Iron isotope analysis requires clean sample matrices and approximately 200-300 ng of Fe per analysis. Therefore, Fe needs to be appropriately pre-concentrated, and purified from each sample matrix-type. Iron was extracted from a variety of samples with varying concentrations. Short descriptions of the basic methods are discussed in this chapter with more details (e.g., sample collection) given in the chapters in which the sample isotopic composition is discussed. It should be noted that sample preparation was performed in class 100 clean laminar flow environments as much as possible. When samples were taken out of the clean environment, the samples were kept covered. Only trace-metal clean reagents were used and all lab-ware in contact with samples was thoroughly acid cleaned.

Rock samples and suspended sediments (<50 mg) were dissolved in a 4:1 HF:HNO_3 solution (trace metal grade Seastar or Optima). Complete dissolution usually

took 4 to 5 days in a sealed Teflon beaker under low heat (≈ 80°C). Samples were then evaporated to dryness with HCl and HNO_3 several times to drive off excess HF, transferred to covered quartz beakers, and placed in a muffle furnace for 8 hours at 550°C to destroy organic matter. Samples were then re-dissolved in 7 M HCl (Optima grade) with heat (60-80°C) prior to Fe separation by anion exchange chromatography.

Trace metal clean plankton tow samples were collected and filtered at sea, then frozen on their filters for storage in acid cleaned polyethylene Nalgene bottles (HDPE). For Fe extraction, samples were thawed and a split was removed from the filter with a plastic scoop or filter tip. The plankton tow material was placed into a quartz beaker and dried on a hot plate in a class 100 clean laminar flow environment overnight. Samples were placed in a muffle furnace for 8 hours at 550°C to destroy organic matter, and then re-dissolved in 7 M HCl (Optima grade) with heat (60-80°C).

Acidified filtered river water samples, porewater samples, and acidic leaches of samples (e.g., aerosols and flocculants with filters from river water-seawater mixing experiments) were evaporated either directly in acid cleaned quartz beakers or larger volume Teflon beakers in a class 100 clean laminar flow environment. Samples initially evaporated in larger volume Teflon beakers were transferred to a quartz beaker prior to taking samples to complete dryness. River water samples were evaporated with a small amount of concentrated trace metal clean HNO_3 and hydrogen peroxide to create an oxidative environment. After samples were taken to dryness, they were placed in a muffle furnace for 8 hours at 550°C to destroy organic matter and re-dissolved in 7 M HCl (Optima grade) with heat (60-80°C).

At this point in the method, all samples were dissolved in 7 M HCl and the samples were ready for Fe separation chemistry by anion exchange chromatography using a method adapted from Marechal et al. (1999). The resin used in this study was Bio-Rad AG MP-1 resin. In 7 M HCl, the dominant species of Fe^{+3} is $FeCl_4^{-1}$ that binds to the resin. After the sample is loaded and the matrix washed through the column, the Fe is eluted by lowering the molarity of HCl. This shifts the dominant species of Fe to either neutral or positively charged species ($FeCl_3$, $FeCl_2^{+1}$), which elute from the resin.

In more detail, a small amount (< 0.1%) of H_2O_2 (EM Science, reagent grade) was added to samples prior to loading onto the resin to ensure all the Fe was present as Fe^{+3}. Samples were loaded onto a 1.8 ml (3.5 cm long x 0.8 cm wide) column of resin and 15 ml of 6 M HCl (triply distilled Vycor HCl) was used to wash the sample matrix through. Iron was then eluted with 18 ml of 2 M HCl (triply distilled Vycor HCl). It is crucial that all chloride is removed from samples prior to isotopic analysis (to avoid $ClOH^+$ interference on ^{54}Fe). Samples were evaporated to dryness twice in HNO_3 and then finally dissolved in 0.3 M HNO_3. For isotopic analysis, samples were diluted with 0.3 M HNO_3 to match the bracketing standard concentration to within 5%.

Iron concentrations were measured before and after the column for most runs. The solution from the sample matrix wash was also collected, concentrated by evaporation, and the Fe concentration measured to verify that Fe did not leak through the column. Iron concentrations were measured by UV-VIS spectroscopy using the Ferrozine method (STOOKEY, 1970) separating the Ferrozine and hydroxylamine hydrochloride reagents (to avoid precipitation of the Ferrozine with HCl). Using a 1 cm pathlength cell and lab-grade reagents, this method has a detection limit of 0.2 μM. Process blanks were always below the detection limit by the Ferrozine method, therefore blanks were measured on the IsoProbe using a simple two-point linear calibration curve. Examples of typical sample sets are shown in Table 4.2. Generally, recovery of the Fe can be verified to ± 2-3%. Leakage of Fe during the separation chemistry was observed only once (in one of the first sets of samples for a soil sample). The cause of the column leakage is unknown, but may have been due to Fe^{+2} still being present in the sample due to high organic content or leakage of a organically bound fraction of Fe. It was after this sample that the pre-column muffle furnace step was added to the method to oxidize organic matter prior to the separation of Fe by column chromatography.

Table 4.2: Three Examples of Sample Sets with Fe Recovery Verification				
sample	**pre-column Fe (μg)**	**post-column Fe (ug)**	**% loss/gain**	**column wash Fe**
5/03 suspended sed SO-B-1st filter	149.0	150	0.8%	clean
5/03 suspended sed SO-B-2cd filter (+ filter)	120.4	120	0.0%	clean
5/03 suspended sed NE-B-1st filter (+ filter)	7.7	7.7	-0.3%	clean
5/03 suspended sed AM-Macapa-B-1st filter	847.2	831	-1.9%	clean
5/03 basalt E	146.8	144	-1.7%	clean
5/03 HF filter blank A		0.06		clean
5/03 HF filter blank B		0.07		clean
5/03 process std A - 55 ug (0 ‰)	54.8	54.4	-0.8%	clean
5/03 process std B - 55 ug (-1.8 ‰)	54.0	57.0	5.6%	clean
8/02 river water sample AM-Macapa (UF)-1	195.1	190.0	-2.6%	clean
8/02 river water sample AM-Macapa (F)-A	191.6	194.3	1.4%	clean
8/02 river water sample NE-Manaus (F)-B	39.8	39.9	0.4%	clean
8/02 river water sample SO-Manaus (F)-B	6.1	6.4	4.8%	spilled
8/02 granite D	103.3	103.3	0.1%	clean
8/02 basalt D	198.0	201.2	1.6%	clean
8/02 process std A (0 ‰)	100.9	90.9	-9.9%[a]	clean
8/02 process std B (-1.8 ‰)	11.9	12.3	3.4%	clean
8/02 process blank A		0.05		clean
8/02 process blank B		0.06		clean
7/03 river sample SO-Manaus-H (Filtered)	8.9	9.1	1.6%	not run
7/03 river sample SO-Manaus-B (Filtered)	7.6	7.5	-0.3%	not run
7/03 river sample NE-Manaus-C (Filtered)	53.7	55.1	2.6%	not run
7/03 river sample AM-Manaus-B (Filtered)	20.6	20.6	-0.2%	not run
7/03 river sample AM-Macapa-C (Filtered)	26.3	27.1	3.0%	not run
7/03 process std A (0 ‰) + 200 ml H2O	15.8	16.2	2.4%	not run
7/03 process std B (-0.6 ‰) + 200 ml H2O	14.6	14.8	1.1%	not run
7/03 process blank		0.06		

a) Portion of this sample was spilled.

4.2.2. Fe Isotope Analysis

Variations in iron isotope ratios have been reported in variety of ways depending on the ratios laboratories are able to measure. In this study, sample data will be reported using the delta notation:

$$\delta^{56}Fe\ (‰) = \left(\frac{^{56}Fe/^{54}Fe_{sample}}{^{56}Fe/^{54}Fe_{standard}} - 1 \right) \times 1000$$

$$\delta^{57}Fe\ (‰) = \left(\frac{^{57}Fe/^{54}Fe_{sample}}{^{57}Fe/^{54}Fe_{standard}} - 1 \right) \times 1000$$

Samples in this study are usually referenced to the mean of the individual measurements of splits of either the Rhode Island Granite (USGS, G-2) and Hawaiian Basalt (USGS, BVHO-1) rock standard reference material unless otherwise noted. In this chapter, many of the standards and samples are referenced to the bracketing standard and will be reported as such (e.g., $\delta^{56/}Fe_{wrk\ std}$). All samples are originally referenced to the bracketing standard during analytical sessions and SSB correction, and then later converted to the $\delta^{56}Fe$ referenced to igneous rocks from the $\delta^{56}Fe_{wrk\ std}$ of the igneous rock samples. Igneous rocks are a convenient baseline for Fe isotope measurements as the they show very little variation in their isotopic composition (BEARD and JOHNSON, 1999; BEARD et al., 2003). Beard et al. (2003) measured nearly 50 igneous rocks and found a mean $\delta^{56}Fe$ of 0.00 ± 0.10 (2σ standard deviation).

Iron isotope measurements were made on the GV Instruments IsoProbe MC-ICPMS at MIT (Figure 4.1). Analyte aerosols from liquid samples were introduced into the plasma using a Fassal quartz torch (Glass Expansion). The liquid samples were injected (aspirated) using a variety of sample introduction systems (discussed below). The ions from the plasma are sampled through a water-cooled interface including Ni sampling, skimmer, and collimating cones. The IsoProbe can either be run in hard or soft

extraction mode on the collimating cone. Hard extraction applies a negative voltage to the collimating cone (typically hundreds of volts), whereas soft extraction applies a slightly positive voltage (less than 10V). Generally, Fe isotope measurements were made in soft extraction mode due to the lower Fe, Ni, and Cr blanks. After extraction, the ion beam is axial-focused and thermalized within a 6 MHz, RF-only hexapole collision cell followed by focusing by electrostatic lenses with a final acceleration potential of –6000V. The ions are then separated by a stigmatic-focusing, Cross geometry magnet (review: TURNER et al., 2000). The ions were detected with a dynamic multiple collector array consisting of nine Faraday collectors (the MIT IsoProbe also has seven Channeltron electron multipliers and one axial Daley detector). Simultaneous measurements were made at masses 52, 54, 56, and 57. All the Faraday collectors used 10^{11} Ω resistors except for the mass 56 Faraday cup, which used a 10^{10} Ω resistor. Chromium was monitored at mass 52 for correction of ^{54}Cr on mass 54 using a $^{54}Cr/^{52}Cr$ ratio of 0.0237/0.838. Mass 52 is free of interferences except for $ClOH^+$, which is avoided by introducing samples in HNO_3. The Cr correction on 54 was generally very small resulting in a less than 0.1‰ correction on the $\delta^{56}Fe$ measurements. For Fe measurements, Ar and H_2 gasses were used in the hexapole collision cell (2 ml/min for both); the H_2 insures that there is no significant residual ArN^+ and ArO^+.

Samples were introduced to the MC-ICPMS in weak HNO_3 by a variety of inlet systems including a "jacketed twister" cyclonic spray chamber (Glass Expansion), the Aridus desolvation inlet system (Cetac), and the APEX inlet system (Spectron) with and without desolvation. Low-flow, self-aspirating PFA nebulizers (uptake rates of 100-200 µl/min) were used with the spray chamber and APEX system. Teflon nebulizers, specifically designed by Cetac for the Aridus (uptake rates of 50-100 µl/min), were used with the Aridus desolvation system. The APEX inlet system uses a heated cyclonic spray chamber followed by a cooled condensation chamber. This set up allows for a higher transmission of the sample analyte to the plasma compared with the normal cyclonic spray chamber. The sample is evaporated in the heated spray chamber (100°C), and the aerosol and water vapor are then carried into the cooled condensation chamber (2°C)

where the much of the water condenses (but 50 to 90% of the sample aerosol is transferred to the torch). A desolvating membrane can be added to the sample-out line of the APEX to remove any remaining water. Generally a factor of five increased sensitivity was observed over the cyclonic spray chamber. The main advantages of the APEX over the Aridus inlet system are (1) shorter sample wash out times (at least a factor of two) compared with the Aridus inlet system, (2) less spiking compared with the Aridus inlet system, and (3) the option of running with or without the desolvator. A summary of the various running conditions is given in Table 4.3.

A 270 ppb Fe solution introduced to the IsoProbe through the APEX with the desolvator produces a ^{56}Fe signal of $\approx$ 35 V (10^{10} Ω resistor = 3.5×10^{-10} A). With a 3.5-minute wash-in time and 2.5-minute data collection time, approximately 300 ng of Fe is consumed per analysis. Wash-in times and data collection times were optimized by assessing how long it took to reach stable isotopic ratio measurements and obtain isotopic ratio measurements with <50 ppm internal precision. Using the cyclonic spray chamber, high precision $\delta^{56}Fe$ measurements have been made on samples with ^{56}Fe signals as low as 4 V (0.2 V on ^{54}Fe). It is possible to envision that $\delta^{56}Fe$ measurements could be achieved on sample sizes of <50 ng using the APEX inlet system if the precision is limited by signal size. However, the amount of interference correction at these low Fe levels is not known.

Fe isotopic measurements in this study were done using SSB to correct for instrumental mass bias (matrix effects will be discussed later). An in-house ultra-pure Fe standard was used for the working bracketing standard. In each run, several standards (both IRMM-014 and gravimetric standards) and a granite split were run to evaluate external long-term precision and accuracy. The IRMM-014 standard (isotopic reference material available from the Institute for Reference Materials and Measurements, Belgium) is currently being used by some labs as a reference standard for reported Fe isotope measurements instead of igneous rocks. It was measured to allow for comparison of $\delta^{56}Fe$ measurements to other laboratories. Beard et al. (2003) measured the IRMM-014 standard and found that it had a $\delta^{56}Fe$ -0.09 ± 0.10 ‰ (2σ standard deviation)

Table 4.3 IsoProbe Instrumental Conditions		
Instrumental Parameter	**Set Point**	**Unit**
Forward power	1370	W
Reflected power	<3	W
Hexapole Ar gas flow	2	ml min^{-1}
Hexapole H2 gas flow	2	ml min^{-1}
Hexapole ion gauge	$4x10^{-4}$	mbar
Analyzer ion gauge	$2x10^{-7}$	mbar
Cyclonic spray chamber		
Uptake rate	100 to 200	µl/min
Uptake time	2	min
Acquisition time	2.5	min
Nebulizer gas flow	0.9 to 1.0	L min^{-1}
Auxiliary gas flow	0.9 to 1.0	L min^{-1}
Cool gas flow	13.5 to 14.0	L min^{-1}
Aridus inlet system		
Uptake rate	50 to 100	µl/min
Uptake time	5	min
Acquisition time	2.5	min
Nebulizer gas flow	1.0 to 1.1	L min^{-1}
Auxiliary gas flow	0.9 to 1.0	L min^{-1}
Cool gas flow	13.5 to 14.0	L min^{-1}
Sweep Ar gas flow (for desolvator)	2.8 to 3.5	L min^{-1}
APEX inlet system without desolvator		
Uptake rate	100 to 200	µl/min
Uptake time	3.5	min
Acquisition time	2.5	min
Nebulizer gas flow	0.7 to 0.8	L min^{-1}
Auxiliary gas flow	0.9 to 1.0	L min^{-1}
Cool gas flow	13.5 to 14.0	L min^{-1}
Secondary Ar nebulizer gas flow (introduced in between APEX system and torch)	0.25	L min^{-1}
APEX inlet system with desolvator		
Uptake rate	100 to 200	µl/min
Uptake time	3.5	min
Acquisition time	2.5	min
Nebulizer gas flow	0.9 to 1.0	L min^{-1}
Auxiliary gas flow	0.9 to 1.0	L min^{-1}
Cool gas flow	13.5 to 14.0	L min^{-1}
Sweep Ar gas flow (for desolvator)	0.8	L min^{-1}

relative to igneous rocks. Gravimetric Fe standards were also made by adding a known amount of ^{54}Fe (or ^{57}Fe) to a higher concentration split of the working reference standard. All quantities were measured gravimetrically to make accurately shifted standards. Many samples were measured over multiple days and with multiple inlet systems.

The uncertainties in the average $\delta^{56}Fe$ measurements quoted in this thesis are the 2σ standard error (2 standard deviation (SD) divided by the square root of the number of analysis). If multiple measurements were not performed for a sample, an uncertainty of $\pm$ 0.22‰ (2σ) is applied to samples referenced to the working standard and $\pm$ 0.24‰ (2σ) to samples referenced to mean of the igneous rock. There is a slight increase in the uncertainty due to error propagation when the sample $\delta^{56}Fe_{wrk\ std}$ is converted to $\delta^{56}Fe$ referenced to igneous rocks. The estimates of uncertainty are based on the long-term external precision of a single granite sample split ($\pm$ 0.22‰, 2 SD, n=22, Table 4.6, granite D). The standard deviation (1 SD), standard error (2σ), and number of measurements within an analytical session are reported for all samples in the data tables.

4.3. Results and Discussion

As reviewed in the introduction, several issues need to be evaluated to ensure that precise and accurate Fe isotope measurements are made by MC-ICPMS. The discussion is divided into three main sections: (1) standards, (2) double isotope ratio plots, and (3) "standard isotope dilution". The first section assesses the accuracy and precision of the Fe isotope measurement method including both the chemistry, the instrument measurement, and corrections. This work was done using clean standards and purified rock samples with high Fe concentrations. Sections 2 and 3 investigate interference corrections and the instrument mass bias correction more closely on samples with more complex matrices and lower concentrations of Fe.

4.3.1. Standards and Testing of the Method

Both the chemistry and the instrument measurement technique were assessed using a variety of standards and samples. The processing of samples in order to extract

and purify Fe has the potential to bias measured Fe isotopes by either fractionating Fe isotopes or introducing Fe blanks or interferences. For example, ion exchange chromatography techniques fractionate metal isotopes during elution including Fe (ANBAR et al., 2000; ZHU et al., 2002). Therefore, it is important to ensure quantitative yield from the column separation or any step in the chemistry that might potentially fractionate Fe isotopes. It is also important to evaluate whether the chemistry procedure introduces Fe blanks, interferences, or matrix constituents that might affect the measured Fe isotopes or instrument mass bias.

Before addressing samples and standards processed through the Fe purification chemistry, the accuracy and precision of the instrument measurement method will first be discussed. When using SSB to correct for instrument mass bias, one of the factors governing precision in the measured Fe isotopic compositions is the stability of the instrument mass bias between the bracketing standard measurements. During set up and tuning of the instrument, several parameters on the instrument are adjusted to optimize for both high transmission of the analyte and the stability of instrument mass bias (e.g., nebulizer flow, collimating cone extraction, hexapole collision gas flows). A simple way to assess the stability of the instrument mass bias is to measure the bracketing standard itself by SSB at the beginning and during an analytical session (0‰ standard in Table 4.4 and Figure 4.3). This represents the best possible precision that can be achieved for a given analytical session. The stability of the instrumental mass bias varied (± 0.03 to 0.14‰, 1 SD, in the $\delta^{56}Fe$ measurement) from session to session and also within sessions, but was typically better than ± 0.10‰ (1 SD). The overall $\delta^{56}Fe_{wrk\ std}$ average for the bracketing standard itself was 0.00 ± 0.03‰ (2σ, n=32). The concentration of the bracketing standard was also varied by ± 5% to ensure that signal size did not affect the measured isotopic ratio. Within the concentration range measured, no trend was observed. In order to assess the accuracy of the SSB correction technique, several isotopically shifted standards (gravimetric standards) were measured during each analytical session (-0.6, -1.2, -1.8‰ standards in Table 4.4 and Figure 4.3). The average $\delta^{56}Fe_{wrk\ std}$ values for the gravimetric standards agree very well with their nominal values

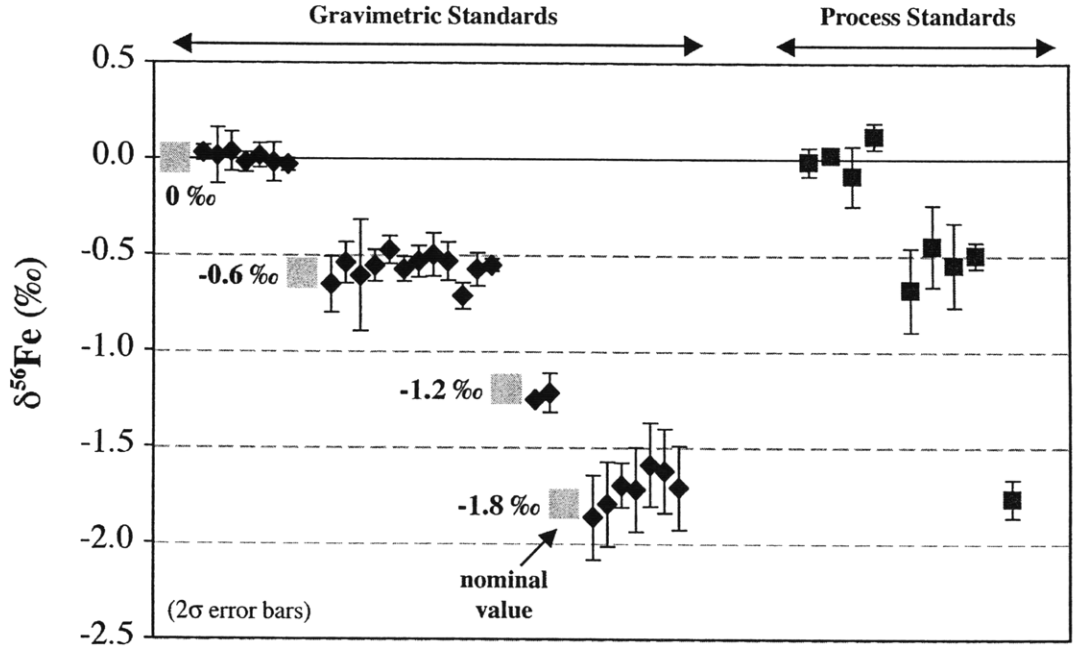

Figure 4.3: Summary of gravimetric standards and process standards analyzed along with samples from October 2001 to April 2004. Gravimetric standards were made by addition of ^{54}Fe to the working standard. $\delta^{56}Fe$ for the standards are referenced to the working standard. Process standards are the gravimetric standards processed through the Fe extraction and separation chemistry. Data with sample descriptions can be found in Table 4.3. The gravimetric standard $\delta^{56}Fe$ measurements for individual analytical sessions are plotted. In contrast, the average $\delta^{56}Fe$ values of the process standards over multiple runs are plotted. Error bars are 2σ standard errors of replicate measurements. If multiple measurements were not made within an analytical session, then a 2σ uncertainty of ± 0.22‰ is used based on the long term external precision of a granite sample (± 0.22‰, 2 SD, n=22, Table 4.6, granite D).

Table 4.4: Summary of Fe Isotopic Data for Gravimetric and Process Standards

Standards	Fe (μg)	analysis date	$\delta^{56}Fe_{wrk\ std}$[a] (‰)	1 SD[b]	2σ unc[c] (2 std error)	n	inlet system[d]
Gravimetric Samples							
nominal, 0‰		11/6/01	0.03	0.03	0.04	3	spray chamber
		5/29/03	0.01	0.10	0.15	2	Aridus
		7/10/03	0.04	0.09	0.10	3	Aridus
		8/1/03	-0.02	0.05	0.05	3	spray chamber
		1/22/04	0.02	0.08	0.06	6	APEX (no des)
		3/31/04	-0.02	0.14	0.10	7	APEX (no des)
		4/24/04	-0.03	0.05	0.03	8	APEX with des.
		all	0.00	0.08	0.03	32	
nominal, -0.6‰		5/15/03	-0.66	0.10	0.15	2	Aridus
		5/28/03	-0.54	0.09	0.11	3	Aridus
		5/29/03	-0.61	0.20	0.29	2	Aridus
		7/10/03	-0.56	0.08	0.08	4	Aridus
		8/1/03	-0.48	0.09	0.07	6	spray chamber
		8/7/03	-0.58	0.06	0.06	4	spray chamber
		8/16/03	-0.53	0.08	0.08	4	spray chamber
		11/5/03	-0.50	0.10	0.11	3	APEX (no des), Cu spike[e]
		1/22/04	-0.53	0.13	0.10	7	APEX (no des)
		3/31/04	-0.72	0.05	0.07	2	APEX (no des)
		4/24/04	-0.58	0.12	0.09	8	APEX with des.
		all	-0.55	0.11	0.03	45	
nominal, -1.2‰		10/24/01	-1.25	0.05	0.02	2	spray chamber
		11/6/01	-1.22	0.07	0.10	2	spray chamber
		all	-1.24	0.05	0.05	4	
nominal, -1.8‰		8/16/03	-1.87	0.11[f]	0.22[f]	1	spray chamber
		8/7/03	-1.80	0.11[f]	0.22[f]	1	spray chamber
		8/1/03	-1.70	0.10	0.12	3	spray chamber
		5/15/03	-1.72	0.11[f]	0.22[f]	1	Aridus
		7/10/03	-1.59	0.11[f]	0.22[f]	1	Aridus
		5/29/03	-1.63	0.11[f]	0.22[f]	1	Aridus
		5/28/03	-1.71	0.11[f]	0.22[f]	1	Aridus
		all	-1.71	0.10	0.06	9	
Process Standards							
0‰, 11/01 column proc. std.	200	11/6/01	-0.02	0.05	0.07	2	spray chamber
0‰, 11/01 muffle proc. std.	100	11/6/01	0.02	0.05	0.03	2	spray chamber
0‰, 8/03 aerosol proc. std.	15	8/16/03	-0.09	0.11	0.16	2	spray chamber
0‰, 11/03 plankton tow proc. std.	10	1/22/04	0.12	0.12	0.17	2	APEX (no des)
0‰ 11/03 plankton tow proc. std.	10	4/24/04	0.13	0.05	0.02	2	APEX with des.
-0.6‰, 8/02 river proc. std.	10	5/28/03	-0.68	0.11[f]	0.22[f]	1	Aridus
-0.6‰, 8/03 aerosol proc. std.	15	8/16/03	-0.45	0.15	0.21	2	spray chamber
-0.6‰, 8/03 mixing expt proc. std.	15	4/24/04	-0.55	0.11[f]	0.22[f]	1	APEX with des.
-0.6‰, 7/03 river proc. std.	15	8/7/03	-0.47	0.05	0.07	2	spray chamber
-0.6‰, 7/03 river proc. std.	15	8/16/03	-0.56	0.11[f]	0.22[f]	1	spray chamber
-1.8‰, 5/03 suspended sed proc. std.	55	8/16/03	-1.82	0.11[f]	0.22[f]	1	spray chamber
-1.8‰, 5/03 suspended sed proc. std.	55	4/24/04	-1.72	0.11[f]	0.22[f]	1	APEX with des.

a) $\delta^{56}Fe$ values of samples in this table are referenced to working standard.

b) SD is the standard deviation of the individual measurements.

c) 2σ uncertainty is the uncertainty in the mean of replicate sample measurements (2 standard error).

d) Several inlet systems were used including a cyclonic spray chamber (spray chamber), the Aridus desolvating system (Aridus), and the APEX system with (APEX with des.) and without a desolvator (APEX (no des)). See text for more details.

e) Cu internal standardization along with SSB was used to correct for instrument mass bias for one session.

f) If only one measurement was made for a sample, a 2σ uncertainty of ± 0.22‰ (2SD) was applied to the sample. The 2σ uncertainty was estimated using the long-term external precision of a granite sample (± 0.22‰, 2 SD, n=22, Table 4.6, granite D).

(-0.55 ± 0.03‰, -1.24 ± 0.05‰, -1.71 ± 0.06‰, 2σ) with overall precisions similar to the 0‰ bracketing standard.

In each sample set, standards were processed through the same chemistry at Fe concentrations similar to samples in order to assess whether there were any artifacts associated with the chemistry. Iron concentrations were monitored throughout the chemistry and Fe was quantitatively recovered from the column separation, the muffle furnace step, and the evaporation steps. Processing both non-shifted and isotopically shifted standards through the chemistry at various concentrations is important when evaluating blank contribution and potential fractionation induced by the chemical separation and purification methods. From the non-shifted process standards, it can be evaluated whether the chemical processing is fractionating the Fe or if an isotopically shifted blank or interference is being introduced. However, the measured isotopic value of a non-shifted Fe process standard would not be affected significantly if the blank was isotopically zero or close to zero. By analyzing isotopically shifted process standards as well, the effect of Fe blanks that are isotopically close to zero can also be assessed. A summary of measured $\delta^{56}Fe_{wrk\ std}$ for process standards is shown along with the corresponding gravimetric standards in Figure 4.3 (data in Table 4.4). Most of the measured $\delta^{56}Fe_{wrk\ std}$ for process standards agree with their nominal values. The one exception was the 11/03 10 μg 0‰ Fe process standard, which was slightly isotopically heavy for the two analytical sessions (0.12 ± 0.07‰, 2σ, n=4). However, the other 10 to 15 μg process standards are not isotopically different from their nominal values.

Process blanks were also measured with each sample set and were found to usually have 0.05 to 0.07 μg of Fe. This amount of Fe contributes less than 0.1% to samples with 100 μg or more of Fe, approximately 0.6% to a 10 μg sample, and 6% to a 1 μg Fe. Even at 6%, a blank would only shift a sample with a $\delta^{56}Fe$ of –0.5‰ sample by 0.03‰ if the blank had an isotopic composition close to 0‰. For the one process standard that is isotopically heavy from its nominal value by 0.12‰, the blank would need to be +20‰ to cause the observed value if the blank were 6% of the sample. Because the other 10 and 15 μg Fe process standards do not support such a large blank

correction, it is likely that there is some other cause for the observed value (e.g., measurement error, matrix induced instrument mass bias variability, or interference). It appears from the process standards and blanks, that the chemistry method generally does not introduce blanks or interferences to an appreciable amount for samples with more than 10 μg of Fe.

Early in the method development for Fe isotopic analysis, an experiment of Fe fractionation by anion exchange chromatography published by Anbar et al. (2000) was reproduced on our instrument as another test of the method. The experiment was done using the same anion exchange resin used by Anbar et al. (2000) and the same resin used for Fe purification in this study. As Fe elutes from the column, the heavier isotope preferentially elutes earlier than the lighter isotope. The elution of Fe and the Fe isotopic composition as Fe elutes is shown Figure 4.4 (data in Table 4.5). For this experiment, a longer column of resin (7 cm long x 1 cm wide, 5.5 ml resin) was used than is used for samples in order to spread out the elution of Fe and isotopic fractionation. The elution curve from this study agrees with the experiment by Anbar et al. (2000) and demonstrates the large fractionation of Fe isotopes on the resin used for purification (+5.3 to –5.4‰). Anbar et al. (2000) suggested that the fractionation was due to equilibrium fractionation between the Fe chloride species. Within the uncertainty of the Fe isotopic analysis and Fe concentration measurement, all of the Fe was eluted with 15 ml and the cumulative isotopic value approached 0‰ (Table 4.4). This experiment highlights the importance of quantitative recovery of Fe from the anion exchange resin. If some of the Fe tail is not collected, the Fe isotopic value of a sample might appear isotopically heavy. For example, a sample would be isotopically shifted 0.3‰ if ≈ 5% of the Fe tail was not collected on the 7 cm column. In this study, a shorter column was used (faster Fe elution, 3.5 cm long x 0.8 cm wide, 1.8 ml resin) and 18 ml of eluent was used to ensure that no isotopic bias was introduced from this step. Also, the process standards support the conclusion that Fe is not being fractionated during the column separation.

Replicate splits of several samples were also processed through the Fe separation chemistry in order to evaluate the reproducibility of the chemistry method for natural

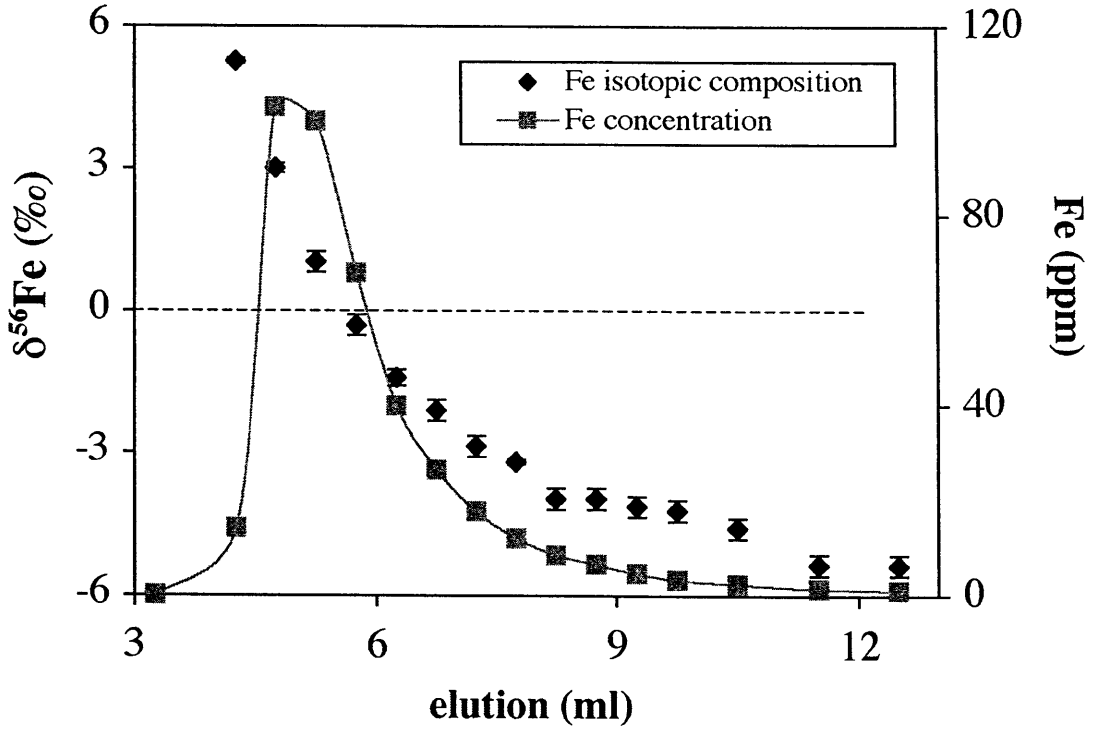

Figure 4.4: Column elution and Fe isotopic fractionation of Fe on the anion exchange resin used in this study (reproduction of an experiment published by Anbar et al. (2000)). The eluent containing the Fe was collected in aliquots as it eluted off the column, and each aliquot was measured for Fe concentration and Fe isotopic composition. In order to spread out the Fe elution, a longer column of resin (7 cm x 1 cm) was used for this experiment than is used for samples (3.5 cm x 0.8 cm). A summary of the data is given in Table 4.5. Error bars are 2σ standard error of multiple measurements. Error bars are 2σ standard errors of replicate measurements. If multiple measurements were not made within an analytical session, then a 2σ uncertainty of ± 0.22‰ is used based on the long term external precision of a granite sample (± 0.22‰, 2 SD, n=22, Table 4.6, granite D).

Table 4.5: Fe Isotopic Data for an Anion Exchange Column
(total Fe loaded on column: 200 μg; column length extended to 7 cm[a])

sample	ml	ppm Fe	fraction Fe	analysis date	$\delta^{56}Fe_{wrk\ std}$[b] (‰)	1 SD[c]	2σ unc[d] (2 std error)	n	cumulative $\delta^{56}Fe$ (‰)
column splits									
5	2.5 to 4	0.0							
6	4 to 4.5	14	0.04	9/25/01	5.27	0.03	0.04	2	0.19
7	4.5 to 5	103	0.26	9/21/01	3.01	0.05	0.08	2	0.96
8	5 to 5.5	100	0.25	9/25/01	1.03	0.11[e]	0.22[e]	1	1.22
9	5.5 to 6	68	0.17	9/25/01	-0.30	0.11[e]	0.22[e]	1	1.17
10	6 to 6.5	40	0.10	9/21/01	-1.41	0.09	0.10	3	1.03
11	6.5 to 7	26	0.07	9/25/01	-2.11	0.11[e]	0.22[e]	1	0.89
12	7 to 7.5	18	0.04	9/25/01	-2.87	0.11[e]	0.22[e]	1	0.76
13	7.5 to 8	12	0.03	9/21/01	-3.20	0.02	0.03	2	0.66
14	8 to 8.5	8.6	0.02	9/25/01	-3.97	0.11[e]	0.22[e]	1	0.58
15	8.5 to 9	6.5	0.02	9/25/01	-3.97	0.11[e]	0.22[e]	1	0.51
16	9 to 9.5	4.6	0.01	9/25/01	-4.13	0.11[e]	0.22[e]	1	0.47
17	9.5 to 10	3.2	0.01	9/25/01	-4.22	0.11[e]	0.22[e]	1	0.43
18	10 to 11	2.4	0.01	9/25/01	-4.59	0.11[e]	0.22[e]	1	0.38
19	11 to 12	1.5	0.01	9/25/01	-5.36	0.11[e]	0.22[e]	1	0.34
20	12 to 13	1.1	0.01	9/25/01	-5.37	0.11[e]	0.22[e]	1	0.31
	Fe accounted for:		103%		cumulative Fe isotopes:				0.31 ‰
	cumulative unc. (1 SD):		5.8%		cumulative unc. (2σ):				0.55 ‰
standards run on same days as column splits									
standard: 0 permil				9/25/01	0.00	0.06	0.09	2	
standard: -1.2 permil				9/25/01	-1.16	0.11[e]	0.22[e]	1	
standard: -1.2 permil				9/21/01	-1.32	0.09	0.16	3	
standard: -5.6 permil				9/25/01	-5.67	0.11[e]	0.22[e]	1	

a) In order to spread out the Fe elution, the resin column was extended to 7 cm long (x 1 cm wide) for this experiment. Normal column length for samples is 3.5 cm (x 0.8 cm wide, internal diameter).
b) $\delta^{56}Fe$ values of samples in this table are referenced to working standard and samples were run using the cyclonic spray chamber inlet system on the MC-ICPMS.
c) SD is the standard deviation (SD) of the individual measurements.
d) 2σ uncertainty is the uncertainty in the mean of replicate sample measurements (2 standard error).
e) If only one measurement was made for a sample, a 2σ uncertainty of ± 0.22‰ (2SD) was applied to the sample. The 2σ uncertainty was estimated using the long-term external precision of a granite sample (± 0.22‰, 2 SD, n=22, Table 4.6, granite D).

samples and methods used for sample digestion. In particular, two samples will be focused on in this discussion: 1) the USGS G-2 granite standard (data in Table 4.6), and 2) a plankton tow sample collected from Amazon plume water in the Atlantic Ocean (10.5°N. 56.6°W; data in Table 4.7). Four splits of the granite were processed through the Fe purification and separation method (100 to 260 μg Fe), and each split measured for its Fe isotopic composition. The average $\delta^{56}Fe_{wrk\ std}$ of all the individual measurements of this granite is -0.23 ± 0.04‰ (2σ, n=27). The 2σ standard deviation (± 0.22‰) of the granite D split measured over multiple sessions using various input techniques to the MC-ICPMS is taken as a reasonable estimate of the overall external reproducibility of the Fe isotopic measurement technique, and is applied to samples only measured once in an analytical session. No systematic differences are seen between the different granite splits or the different inlet systems. The mean igneous rock value used to reference samples to in this study is the mean of the individual measurements of all igneous rock samples ($\delta^{56}Fe_{wrk\ std}$ = -0.23 ± 0.04‰, 2σ, n=30).

Besides igneous rocks, the IRMM-014 standard has been measured and used as a reference standard for $\delta^{56}Fe$ measurements by several laboratories. It was measured during several analytical sessions in this study (Table 4.6). The difference between the mean $\delta^{56}Fe_{wrk\ std}$ of igneous rock and the IRMM-014 standard (-0.13 ± 0.07‰, 2σ, n=12) agrees well with the difference reported by Beard et al. (2003) of -0.09 ± 0.01‰ (2σ, n=52). This is the only test of accuracy (besides the gravimetric standards) available to compare data from this study with results from other laboratories.

In order to evaluate the potential effects of organic matter on Fe isotopic measurement method, a plankton tow sample was processed several ways to remove the organic matter. Different size fractions of the plankton tow (>10 μm and 1 to 10 μm) and replicate tows were also measured to ensure that filtering at sea did not affect the Fe isotopic composition of the sample. It took several hours to completely filter one plankton tow at sea through the 10 μm filter, and then finally through the 1 μm filter before another plankton tow sample could be filtered. If bacterial degradation or organic matter or cell lysis in the plankton tow were affecting the Fe isotopic composition, then

Table 4.6: Summary of Fe Isotopic Data for Igneous Rock Standards and the IRMM-014 Standard

Sample	analysis date	$\delta^{56}Fe_{wrk\ std}$[a] (‰)	1 SD[b]	2σ unc[c] (2 std error)	n	inlet[f]
Basalt, BVHO-1 (USGS standard), Hawaii, 12.2 % (Wt) Fe_2O_3-T						
split B, 1180 μg Fe[d]	11/6/01	-0.13	0.11[e]	0.22[e]	1	spray chamber
split C, 419 μg Fe	11/6/01	-0.24	0.11[e]	0.22[e]	1	spray chamber
split D, 248 μg Fe	4/24/04	-0.32	0.11[e]	0.22[e]	1	APEX des.
average all basalt measurements:		-0.23	0.10	0.11	3	
Granite, G-2 (USGS standard), Rhode Island, 2.66 % (Wt) Fe_2O_3-T						
split A, 113 μg Fe	11/6/01	-0.23	0.05	0.08	2	spray chamber
split B, 140 μg Fe	11/6/01	-0.26	0.03	0.05	2	spray chamber
split C, 230 μg Fe	11/6/01	-0.16	0.11[e]	0.22[e]	1	spray chamber
split D, 263 μg Fe	4/24/04	-0.20	0.10	0.11	3	APEX des.
	8/16/03	-0.14	0.06	0.09	2	spray chamber
	8/7/03	-0.20	0.15	0.21	2	spray chamber
	7/10/03	-0.32	0.00	0.00	2	Aridus
	8/16/03	-0.03	0.11[e]	0.22[e]	1	spray chamber
	5/28/03	-0.38	0.11[e]	0.22[e]	1	Aridus
	4/24/04	-0.34	0.05	0.01	2	APEX des.
	3/31/04	-0.26	0.11[e]	0.22[e]	1	APEX (no des)
	1/22/04	-0.23	0.14	0.13	5	APEX (no des)
	8/16/03	-0.15	0.11[e]	0.22[e]	1	spray chamber
	8/1/03	-0.32	0.05	0.06	2	spray chamber
average of granite split D:		-0.23	0.11[f]	0.05	22	
average all granite measurements:		-0.23	0.10	0.04	27	
average of igneous rock splits:		**-0.23**	**0.10**	**0.04**	**30**	
IRMM-014 Standard						
	4/24/04	-0.35	0.05	0.06	3	APEX des.
	1/22/04	-0.24	0.14	0.20	2	APEX (no des)
	8/16/03	-0.44	0.09	0.13	2	spray chamber
	8/7/03	-0.35	0.11[e]	0.22[e]	1	spray chamber
	8/1/03	-0.41	0.09	0.11	3	spray chamber
	7/10/03	-0.29	0.11[e]	0.22[e]	1	Aridus
average all IRMM-014 std:		-0.36	0.10	0.06	12	
difference between igneous rock mean and IRMM standard[g]:		**-0.13**	**0.14**	**0.07**	12	

a) $\delta^{56}Fe$ values of samples in this table are referenced to working standard.

b) SD is the standard deviation of the individual measurements.

c) 2σ uncertainty is the uncertainty in the mean of replicate sample measurements (2 standard error).

d) Every sample or sub-sample was processed through the Fe separation and purification chemistry separately. The amount of Fe in the rock sample processed through the chemistry is also given.

e) If only one measurement was made for a sample, a 2σ uncertainty of ± 0.22‰ (2SD) was applied to the sample. The 2σ uncertainty was estimated using the long-term external precision of a granite sample (± 0.22‰, 2 SD, n=22, Table 4.6, granite D).

f) The estimate of external precision of ± 0.22‰ (2 SD, n=22) based on this sample set.

g) The difference between the mean of igneous rock samples and IRMM-014 was reported by Beard et al. (2003) to be –0.09 ± 0.01‰ (2σ, n=52).

f) Several inlet systems were used including a cyclonic spray chamber (spray chamber), the Aridus desolvating system (Aridus), and the APEX system with (APEX with des.) and without a desolvator (APEX (no des)). See text for more details.

Table 4.7: Summary of Amazon Plume Plankton Tow Fe Isotope Data								
ID	**digestion method**	**Fe[a] (μg)**	**date**	**$\delta^{56}Fe_{wrk\ std}$[b] (‰)**	**1 SD[c]**	**2σ unc[d] (2 std error)**	**n**	**inlet[i]**
Tow 1 (<10 um[e]), split A	HNO_3 digested, post-col. combusted[g]	?	10/24/03	-0.56	0.11[h]	0.22[h]	1	spray
Tow 1 (<10 um[e]), split B	pre-column combusted	?	10/24/03	-0.63	0.10	0.14	2	spray
Tow 2 (<10 um[e])	pre-column combusted	26	10/24/03	-0.70	0.06	0.08	2	spray
Tow 1 (>10 um[f])	pre-column combusted	68	5/15/03	-0.41	0.11[h]	0.22[h]	1	Aridus
			5/28/03	-0.55	0.11[h]	0.22[h]	1	Aridus
			7/10/03	-0.67	0.12	0.17	2	Aridus
			8/7/03	-0.40	0.03	0.04	2	spray
			1/22/04	-0.59	0.11[h]	0.22[h]	1	APEX (no des)
	average all tow 1 (>10 um):			-0.53	0.13	0.10	7	
	average all individual analysis:			-0.57	0.12	0.07	12	
	difference between mean igneous rock and AM-plume plankton tow:			-0.34	0.13	0.07	12	

a) Amount of Fe extracted from split of plankton tow. Every sample or sub-sample was processed through the Fe separation and purification chemistry separately.
b) $\delta^{56}Fe$ values of samples in this table are referenced to working standard.
c) SD is the Standard deviation of the individual measurements.
d) 2σ uncertainty is the uncertainty in the mean of replicate sample measurements (2 standard error).
e) Plankton tow material that passed through the 10 μm filter and was collected on a 1 μm filter.
f) Plankton tow material that was collected on a 10 μm filter.
g) Samples combusted in a muffle furnace at 550°C for 8 hours.
h) If only one measurement was made for a sample, a 2σ uncertainty of ± 0.22‰ (2SD) was applied to the sample. The 2σ uncertainty was estimated using the long-term external precision of a granite sample (± 0.22‰, 2 SD, n=22, Table 4.6, granite D).
i) Several inlet systems were used including a cyclonic spray chamber (spray chamber), the Aridus desolvating system (Aridus), and the APEX system with (APEX with des.) and without a desolvator (APEX (no des)). See text for more details.

potentially the >10 μm and the 1 to 10 μm samples would have different isotopic compositions. The $\delta^{56}Fe_{wrk\ std}$ data for the Amazon plume plankton tow is given in Table 4.7. The different size fractions and splits of the plankton tow show little isotopic variability ($\delta^{56}Fe_{wrk\ std}$ = -0.57 ± 0.07‰, 2σ, n=12) suggesting that the filtering technique and time did not affect the isotopic composition of the Fe. This sample referenced to igneous rocks gives a $\delta^{56}Fe$ of -0.34 ± 0.07‰ (2σ, n=12).

Organic matter was removed either by nitric acid digestion prior to the column or muffle furnace combustion (550°C). It was found that non-combusted samples caused the stability in the instrument mass bias to degrade. This is illustrated in an example of a SSB analysis session where splits of the Amazon plankton tow sample were measured (Figure 4.4). Although the Fe in the nitric acid digested samples was purified by column separation, residual sample matrix was still present. As can be seen in Figure 4.5, a nitric acid digested sample that was combusted after the column separation did not cause instabilities. However, the nitric acid digested plankton tow that was not combusted post-column caused the isotopic composition of the bracketing standard to shift and become unstable. This behavior was observed in several analytical sessions where organic rich samples were run without combustion. Based on these observations, all samples were combusted prior to the column and combustion was chosen as the preferred method of organic matter digestion. Some samples were combusted both before and after the column separation, but these samples did not behave differently from splits of the same samples that were only combusted prior to column separation.

From the process standards and replicates of a few samples, a reasonable external precision can be estimated of ± 0.22‰ (2 SD) for $\delta^{56}Fe_{wrk\ std}$ and of ± 0.24‰ (2 SD) for $\delta^{56}Fe$ of natural samples referenced to igneous rocks. Samples are usually measured multiple times, which leads to a 2σ uncertainty of better than ± 0.17‰ in the averaged $\delta^{56}Fe$ measurement. This is based on analysis of samples and standards over several days with several inlet systems and also several replicates run through the Fe separation and purification method. The gravimetric standards have external precisions only slightly better than the process standards and samples suggesting that much of the uncertainty in

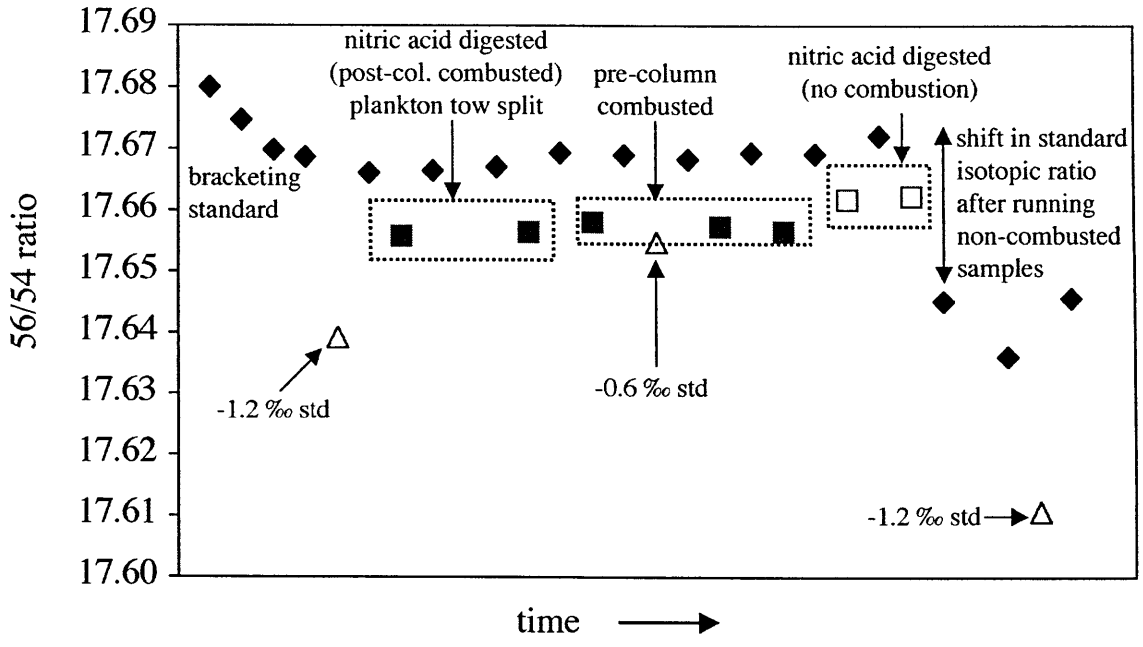

Figure 4.5: An example of a Fe isotopic analysis session by MC-ICPMS (cyclonic spray chamber) demonstrating the importance of removing organic material from the sample matrix. The figure also demonstrates sample-standard bracketing with the plankton tow samples (■, □) and shifted standards (Δ) analyzed between the bracketing standards (♦). Every data point represents 2.5 minutes of data acquisition with approximately 15 minutes in between, which includes blank acquisition (1 min), sample uptake (2 min), and sample washout (12 min). The combusted (550°C) plankton tow samples did not cause problems and the bracketing standard was relatively stable in its Fe isotopic composition. After running two plankton tow samples that were not combusted, the bracketing standard Fe isotopic composition shifted and became unstable. This was observed during several analytical sessions where non-combusted organic-rich samples were analyzed. The recovery to stable conditions took several hours and sometimes cleaning of the glassware.

the isotopic measurement is due to the stability of the instrument mass bias correction by SSB. It can also be concluded that no appreciable blank, interference, or fractionation is being introduced during the Fe separation and purification chemistry for samples with >10 μg of Fe. The accuracy of the method appears to be good based on gravimetric standards and the measured difference between igneous rocks and the IRMM-014 standard. However these conclusions are based on standards and igneous rock samples with high Fe concentrations. Whether or not samples with complex sample matrices (such as the plankton tows) are accurate is more difficult to prove. These samples could be suffering from interferences or variable instrument mass bias associated with their matrices. The next two sections will try to assess the accuracy of the Fe isotopic measurements in natural samples with low concentrations of Fe.

4.3.2. Interference Correction ($^{56}Fe/^{54}Fe$ versus $^{57}Fe/^{54}Fe$)

Mass fractionation of isotopes is predicted to follow a generalized power law function stemming from differences in the vibrational energies of molecules (BIGELEISEN and MAYER, 1947). Two commonly used mathematical descriptions, which are both forms of the generalized power law, are the exponential law and the power law (reviews: MARÉCHAL et al., 1999; ALBAREDE AND BEARD, 2004). Either law predicts that a log-log plot of two isotopic ratios should fall along a linear array. For Fe, a slope of 0.666 for the power law and 0.672 for the exponential is predicted for plots of ln(57/54) versus ln(56/54). When two isotopic ratios of a given element can be measured, plotting the two ratios on a log-log plot and observing a linear trend lends confidence that neither ratio measurement is suffering from incorrect blank or interference corrections. Figure 4.6 is a plot of data for an analytical session on the IsoProbe with the APEX inlet system with desolvation. The best-fit slope for the bracketing standards is 0.683 ± 0.005, which is slightly higher than the slope predicted by the exponential or power law. However, the instrumental mass bias law in ICPMS is not well characterized and deviations from these slopes are observed on other instruments (ALBAREDE and BEARD, 2004; ARNOLD et al., 2004).

A deviation from the predicted slopes could also indicate that there is some unresolvable interference in the standards that is not being corrected. Mass 57 is a difficult measurement on the MIT IsoProbe. Under the best circumstances (desolvation, 1 V signal on mass 57), the $ArOH^+$ interference is 0.4% of the 57 signal and can vary by ± 0.1% over the course of an analytical session. A 25% uncertainty in this correction leads to a minimum uncertainty of ± 0.1‰ in the $\delta^{57}Fe$ measurement. This is compared blank corrections on masses 56 and 54 that are typically less than a 0.01%. Also, the $^{57}Fe/^{54}Fe$ ratio of the bracketing standard is less stable than the bracketing standard $^{56}Fe/^{54}Fe$ ratio. Under the most stable conditions, variations in the bracketing standard $\delta^{57}Fe_{wrk\ std}$ are ± 0.40‰ (2 SD) with APEX desolvation system and ± 0.52‰ (2 SD) with the Aridus desolvation system. Typical 2σ uncertainty for the $\delta^{57}Fe$ measurement is ± 0.35 to 0.40‰. Most analytical sessions in this study were done under wet plasma conditions (no desolvation), because this optimized for the stability of the $^{56}Fe/^{54}Fe$ measurement (but made the $^{57}Fe/^{54}Fe$ less stable). Therefore, typically the $^{57}Fe/^{54}Fe$ ratio is not reported.

A few analytical sessions where desolvation was used were sufficiently stable enough for both the $\delta^{56}Fe$ and $\delta^{57}Fe$ values to be measured with confidence (± 0.22‰ for $\delta^{56}Fe$; ± 0.40‰ for $\delta\ ^{57}Fe$, 2 SD). Measurements made using the APEX inlet system with desolvation are plotted in Figures 4.6 and 4.7a. Bracketing standards are plotted in Figure 4.6a, and samples plotted in Figures 4.6b and 4.7a. Most sample types follow the mass fractionation trend defined by the standards including igneous rock samples, the IRMM-014 standard, Amazon porewater, suspended sediments, the Amazon plume plankton tow, river water-seawater mixing experiments, and the bracketing standard at varying concentrations. The only samples to deviate from significantly from the mass fractionation trend are the 10 μg Fe process standard and the dissolved Fe from river water samples, with the Macapá station showing the largest deviation. The same river water samples were also measured with the Aridus inlet system and follow the mass fractionation trend (Figure 4.7b). The $\delta^{56}Fe$ measurements using the Aridus and APEX agree for the Solimões and Negro River samples, and the measurements also agree with

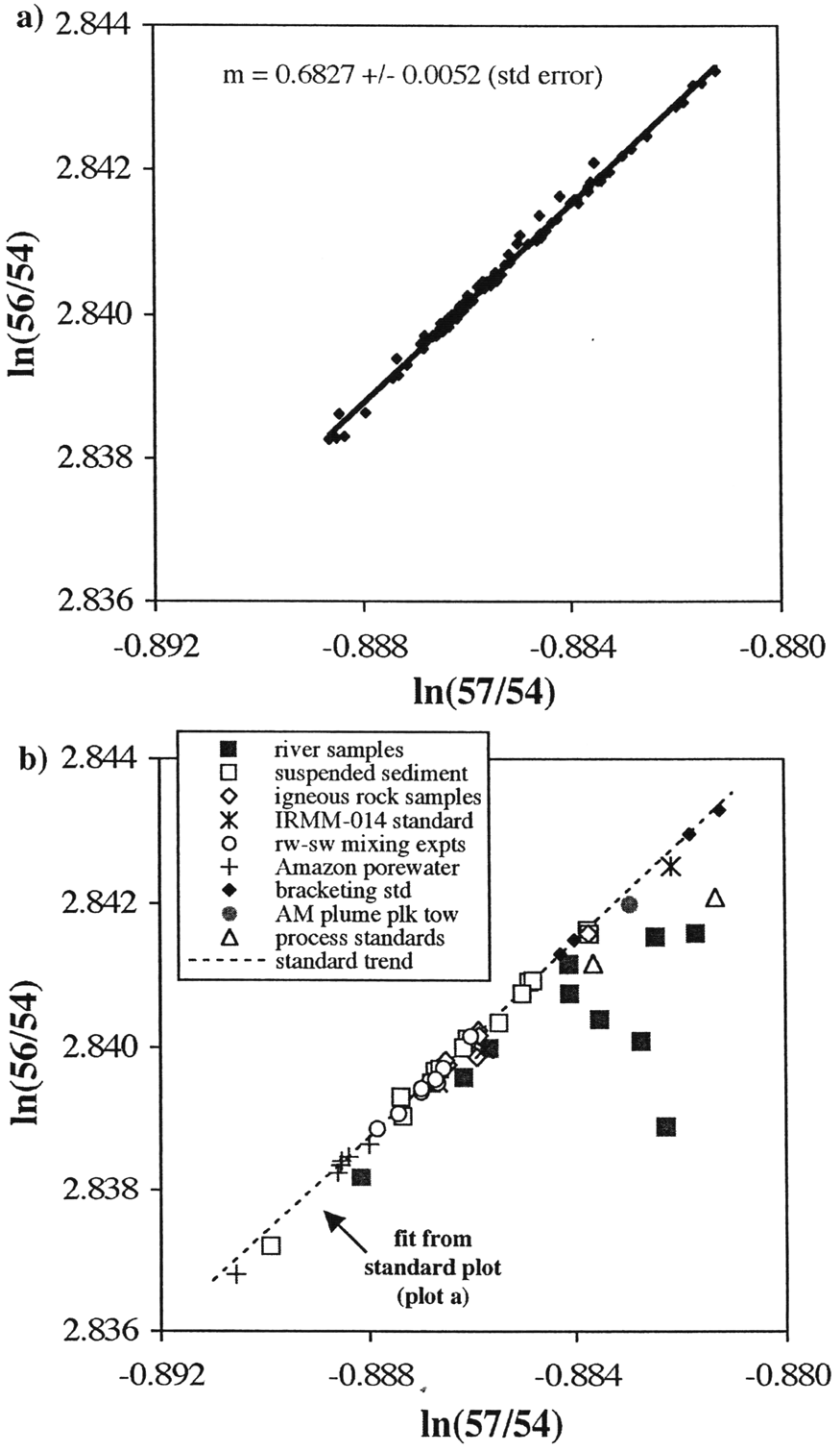

Figure 4.6: Fe isotope data collected with the APEX (with desolvator) inlet system (April 2004). 4.6a) Plot of ln(57/54) versus ln(56/54) for the bracketing standard. 4.6b) Plot of ln(57/54) versus ln(56/54) for the samples measured during the same analytical session as the bracketing standard (Figure 4.6a). The only samples that plot off the mass fractionation trend are the river samples (■) and the 11/03 10 μg Fe process standard measurements (Δ). See text for discussion.

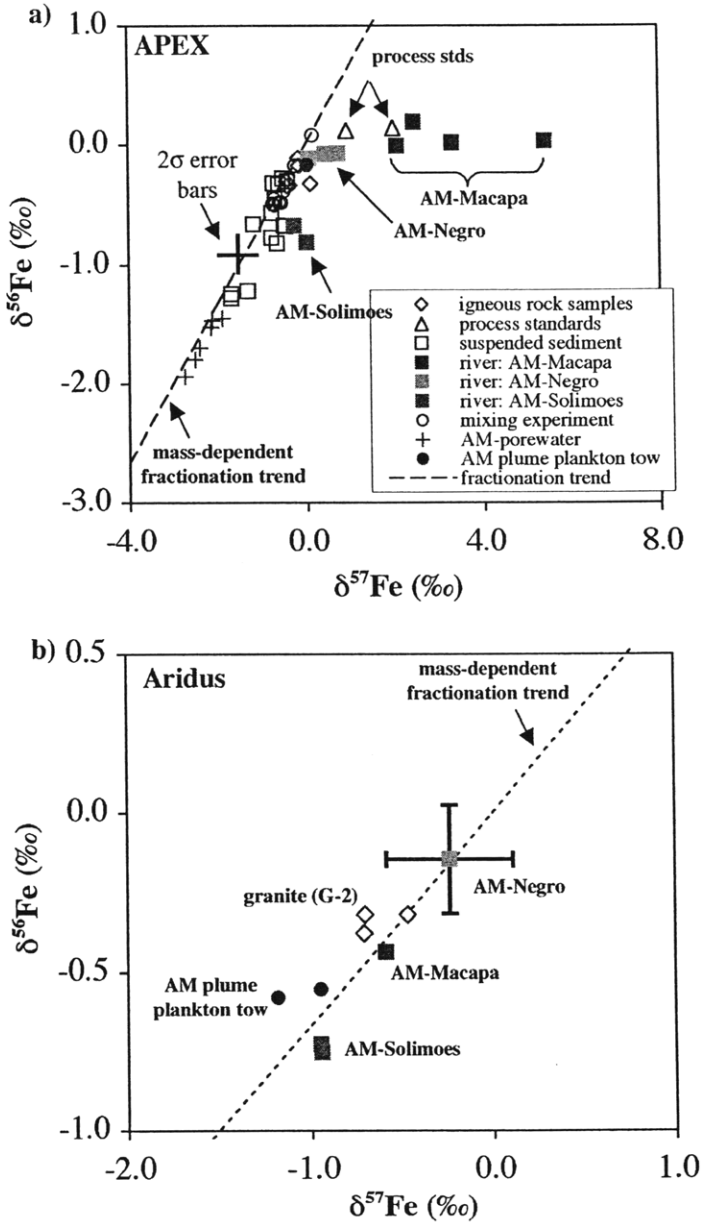

Figure 4.7: Fe isotope data collected with the APEX (with desolvator) inlet system (April 2004) compared with data collected with the Aridus inlet system (summer 2003). 4.7a) APEX data (same data from Figure 4b) plotted as $\delta^{57}Fe_{wrk\ std}$ versus $\delta^{56}Fe_{wrk\ std}$. The samples that deviate from the mass-depended fractionation trend are the river samples (■) and the 0‰ 11/03 10 μg Fe process standard (Δ). The Fe for the 0‰ process standard during the April 2004 run was slightly isotopically heavy, +0.12 ± 0.07‰ (2σ). Whereas, the $\delta^{57}Fe_{wrk\ std}$ measured during the run is very different from predicted values based on mass-dependent fractionation. 4.7b) Aridus data for the same river samples (■) is plotted along with the granite and Amazon plume plankton tow. The river samples follow the mass-dependent fractionation trend and the isotopic compositions from the two data sets are similar for $\delta^{56}Fe_{wrk\ std}$. See text for discussion. 2σ error bars are shown for one sample on each plot (± 0.22‰ for $\delta^{56}Fe$, ± 0.40‰ for $\delta^{57}Fe$, 2 SD).

$\delta^{56}Fe$ data generated with the spray chamber. For the Macapá station river sample, the APEX (with desolvation) $\delta^{56}Fe$ data is isotopically heavy by 0.4‰ compared with the data generated with the Aridus inlet system, the spray chamber, and the APEX (no desolvation) data using Cu internal standardization. The $\delta^{56}Fe$ of the process standard is also shifted by +0.12‰. This suggests that there is some interference associated with the Macapá sample on mass 57 that is present when the sample is analyzed using the APEX (with desolvation) inlet system, and that the $^{56}Fe/^{54}Fe$ measurement is affected as well. Therefore, sample data was discarded with measured $\delta^{57}Fe$ values on the APEX that deviated by more than 1‰ from the predicted $\delta^{57}Fe$ based on stable mass fractionation.

There are two likely interferences on mass 57, $CaOH^+$ and $ArOH^+$, and both could be associated with their non-protonated oxides on mass 56 (CaO^+ and ArO^+). If either interference were present on mass 57, it would still not be obvious that mass 56 should be affected as well. Both CaO^+ and ArO^+ are effectively minimized in the hexapole collision cell, and the ^{56}Fe signal is much larger than the ^{57}Fe signal and thus less sensitive to small interferences. A "high resolution" scan of mass 56 peak in a Fe solution with and without H_2 reaction gas in the hexapole collision cell is shown in Figure 4.2b. A similar scan at mass 56 of a 2.5 ppm Ca solution is shown in Figure 4.8. The CaO^+ interference is effectively destroyed with H_2 gas in the collision cell. For comparison, "high resolution" scans of three samples (including the Macapa station river sample) at masses 54 and 56 are shown in Figure 4.9. The sample peaks are clean without resolvable interferences (CaO^+ and ArO^+ should be resolvable from $^{56}Fe^+$). It is not clear what controls the formation of $CaOH^+$ and $ArOH^+$ in the IsoProbe interface and hexapole regions. The formation could be related to matrix variations, plasma conditions, or reaction conditions in the hexapole. If either CaO^+ or ArO^+ were present in the samples, then the Fe in the measured sample would appear isotopically heavier than its true isotopic value. By screening samples when possible using the $^{57}Fe/^{54}Fe$ ratio and reproducing isotopic measurements under several analytical conditions (e.g., inlet systems, concentrations, wet and dry plasma), it is believed that the reported isotopic

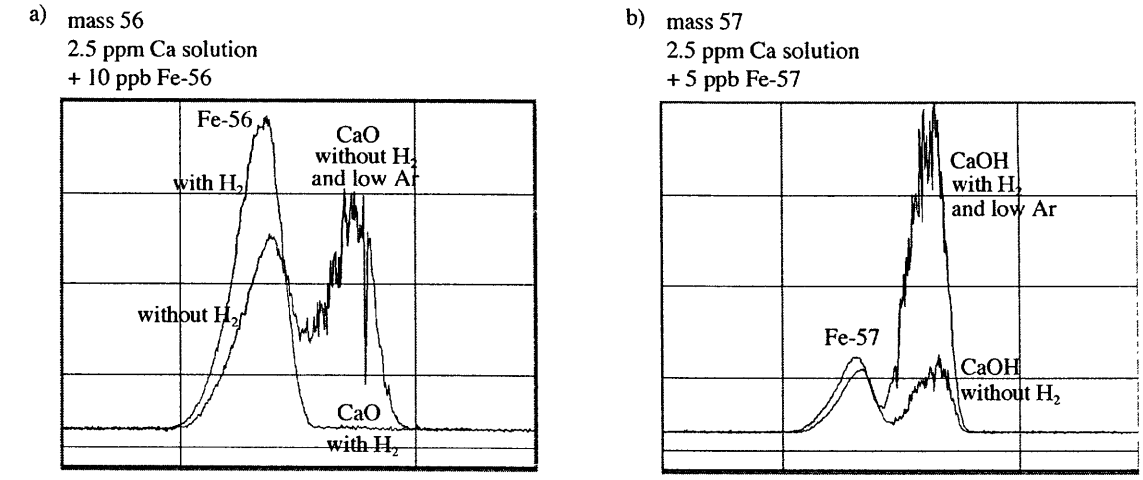

Figure 4.8: "High resolution" scans are shown at mass 56 and mass 57 of a 2.5 ppm Ca solution spiked with Fe. Scans are shown with and without H_2 reaction gas in the hexapole collision cell (2 ml/min). The Ar collision gas was set at 1.8 ml/min. 4.8a) Scans of a Ca solution with 10 ppb of ^{56}Fe are shown with and without H_2 reaction gas in the hexapole collision cell. In order to create a significant amount of CaO^+, no H_2 gas was used and the Ar collision gas was reduced to 0.5 ml/min. The CaO^+ was significantly reduced by using 1.8 ml/min of Ar in the collision chamber and eliminated with the addition of the H_2 reaction gas. 4.8b) Scans of a Ca solution with 5 ppb of ^{57}Fe are shown with and without H_2 reaction gas in the hexapole collision cell. The $CaOH^+$ increased with addition of H_2 reaction gas in the hexapole collision cell. The "high resolution" scan was done by narrowing the source slit and setting the detector slit to the "high resolution" slit, which has a resolving power of $\approx$ 5000 ($m/\Delta m$).

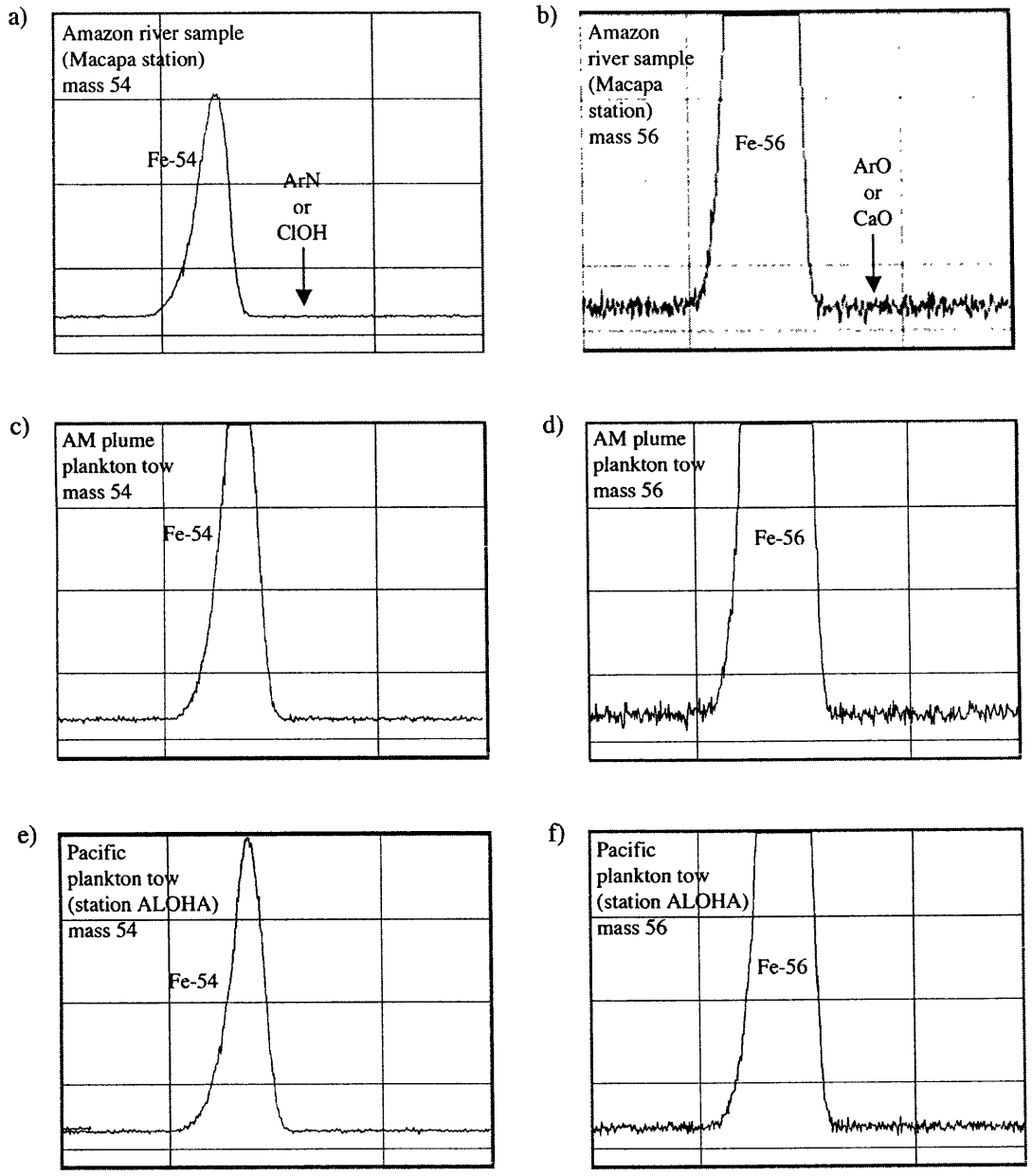

Figure 4.9: "High resolution" scans of mass 54 and 56 of Fe solutions of natural samples with Ar and H_2 gas in the collision cell (2 ml/min for each). Measurements were made with the APEX inlet system without the desolvator. 60 ppb (ng/g) Fe solutions were used for the mass 54 scans and 6 ppb solutions were used for the mass 56 scans. Scans 4.9a and 4.9b are of a Amazon river sample (Macapá station, sample B). 4.9c and 4.9d are scans of the Amazon plume plankton tow sample (tow 1, >10 μm). 4.9e and 4.9f are scans of a Pacific plankton tow (ALOHA, tow 3, >10 μm). All the scans are clean peaks without resolvable interferences (e.g., ArN^+ and $ClOH^+$ on 54; ArO^+ or CaO^+ on 56). The "high resolution" scans were done by narrowing the source slit and setting the detector slit to the "high resolution" slit, which has a resolving power of ≈ 5000 (m/Δm).

values are accurate to within the reported uncertainties (± 0.24‰, 2 SD, for the $\delta^{56}Fe$ value referenced to igneous rocks).

4.3.3. Instrument Mass Bias: Isotope Standard Addition

Besides interferences and blank correction issues, variability in instrument mass bias also needs to be assessed. The common technique used to assess this is Cu internal standardization for Fe isotopic analysis. However due to the potential pitfalls with this technique discussed in the introduction of this chapter and possible Cu co-elution with Fe in our separation chemistry, another approach was used to assess potential changes in instrument mass bias for samples. The technique used in this study is referred to as "standard isotope dilution". A small amount of isotopically shifted Fe was added (0.1 to 0.6 ng of Fe; in a small volume, 25 μl) to a split of a sample (usually 1 to 2 μg of Fe). This changed the Fe isotopic composition of the sample without altering the Fe concentration or matrix of the sample. The ^{54}Fe standard used was calibrated by additions to the working standard and was the same standard used to make the gravimetrically shifted standards. The sample and the sample-standard addition mixture were then both measured for their isotopic composition. If the instrument mass bias is corrected for accurately, then the measured isotopic composition of the sample-standard addition mixture should easily be predicted by simple isotopic mass balance. This technique was applied to a variety of sample types, and the data is given in Table 4.8. In every case, the predicted and measured $\delta^{56}Fe$ values for the sample-standard addition mixtures agree to within the predicted uncertainty and most agree to within the representative 2σ uncertainty (± 0.22‰) in the measurement technique. The good agreement of the predicted and measured $\delta^{56}Fe$ values suggests that the mass bias of the instrument is being characterized correctly by SSB within the uncertainty of the measurement.

Table 4.8: "Standard Isotope Addition" Fe Isotope Data
(all $\delta^{56/54}$Fe referenced to working standard)

Sample Type	Fe from sample (μg)	$\delta^{56/54}$Fe of sample[a]	1 SD	Fe from spike (μg)	$\delta^{56/54}$Fe of spike[b]	predicted $\delta^{56/54}$Fe of sample-spike mixture[c]	pred. unc.[d] (1 SD)	$\delta^{56/54}$Fe of sample-spike mixture[e]	diff from pred.
aerosol leachate – 1 M HCl (Atl 10°N, 45°W)	2.12	-0.22	0.04	0.0006	-11567	**-3.49**	0.32	**-3.40**	0.09
river (AM[f]-Solimoes, split 2)	2.12	-0.63	0.13	0.006	-11567	**-35.00**	0.34	**-35.25**	-0.25
suspended sediment (AM-Solimoes)	0.68	-0.68	0.10	0.0001	-11567	**-1.75**	0.29	**-1.68**	0.07
suspended sediment (AM-Negro)	0.68	-1.25	0.03	0.0001	-11567	**-2.32**	0.20	**-2.26**	0.06
suspended sediment (AM-Macapa)	0.68	-0.43	0.17	0.0001	-11567	**-1.50**	0.52	**-1.52**	-0.02
river water-seawater mixing expt (AM-Solimoes #5)	0.68	-0.48	0.10	0.0001	-11567	**-1.55**	0.34	**-1.56**	-0.01
porewater, split 1 (AM shelf)	0.68	-1.56	0.12	0.0001	-11567	**-2.63**	0.23	**-2.74**	-0.11
AM plume, Atl 10.5°N, 56.5°W plankton tow 1, >10 μm	2.12	-0.53	0.13	0.0006	-11567	**-3.81**	0.37	**-3.73**	0.08
Atl. 10°N, 45°W plankton tow 2, split C	0.54	-0.54	0.11	0.0001	-11567	**-1.88**	0.34	**-1.92**	-0.04
Atl. 10°N, 45°W plankton tow 2, split B	1.06	-0.78	0.07	0.0002	-11567	**-3.40**	0.24	**-3.49**	-0.09
Pac. ALOHA 23°N, 158°W plankton tow 3	0.64	-2.76	0.23	0.0001	-11567	**-3.89**	0.23	**-4.07**	-0.18
Pac. 26°N, 175°W plankton tow 3	0.54	-2.35	0.05	0.0001	-11567	**-3.65**	0.20	**-3.48**	0.17

a) Measured $\delta^{56}Fe_{wrk\ std}$ of sample without isotope standard addition referenced to the working standard.
b) Calculated $\delta^{56}Fe_{wrk\ std}$ of Fe-54 spike referenced to the working standards (confirmed from measurements of spike addition to working standard).
c) Predicted $\delta^{56}Fe_{wrk\ std}$ of mixture of sample and spike (standard addition) referenced to the working standard.
d) Propagated error using the 1σ standard deviation of the isotopic measurements and reasonable estimates of the uncertainty of volumes and concentrations.
e) Measured $\delta^{56}Fe_{wrk\ std}$ of mixture of sample and isotope standard addition referenced to the working standard.
f) AM stands for Amazon.

4.4. CONCLUSION

In this chapter, a technique was presented for Fe isotopic measurements using the GV Instruments IsoProbe MC-ICPMS, which includes a hexapole collision cell. Using SSB and ≈ 300 ng of Fe, this measurement technique yields a representative external precision of ± 0.22‰ (2 SD) in the $\delta^{56/}Fe_{wrk\ std}$ and ± 0.24‰ (2 SD) in the $\delta^{56/}Fe$ of samples referenced to igneous rocks. Because the sample types that will be addressed in the following chapters are natural samples with lower Fe concentrations than previously studied, the potential for elevated levels of residual matrix and interferences in the samples is higher. Precision and accuracy were assessed through the measurement of standards including isotopically shifted standards. Process standards were processed at various concentrations and with different isotopic compositions to test for fractionation in the separation chemistry and significant blank or interference contributions. From the standards, it is concluded that the Fe purification and separation chemistry does not introduce significant fractionation, blanks, or interferences for samples with >10 μg Fe. Also, the gravimetric standards agree with their nominal values and the difference between the IRMM-014 standard and mean igneous rock agreed with published values. Proper interference correction for natural samples was evaluated by measuring both the $^{56}Fe/^{54}Fe$ and $^{57}Fe/^{54}Fe$ ratios when possible. For most sample types, the $^{56}Fe/^{54}Fe$ and $^{57}Fe/^{54}Fe$ followed mass-dependent fractionation trends. There is evidence that variable interferences on 57 (and also potentially 56) need to be addressed (most notably in the river samples). The interferences are not always present and depend on the inlet method suggesting that the interference formation is related to conditions in the plasma. However, the controls over these interferences is not yet understood. By screening samples when possible using the $^{57}Fe/^{54}Fe$ ratio and reproducing isotopic measurements under several analytical conditions (e.g., inlet systems, concentrations, wet and dry plasma), it is believed that the reported isotopic values are accurate to within the reported uncertainties (≈ 0.24‰, 2 SD, for the $\delta^{56}Fe$ relative to igneous rocks). Finally, an "isotope standard addition" method was developed to investigate matrix-induced

variability in the instrument mass bias. Based on the good agreement of the predicted and measured $\delta^{56}Fe$ values of sample-standard addition mixtures, we suggest that the mass bias of the instrument is being characterized correctly by SSB within the external reproducibility of the method.

References for Chapter 4

Albarede F. and Beard B. L. (2004) Analytical methods for non-traditional isotopes. In *Geochemistry of Non-Traditional Stable Isotopes.*, Vol. 55 (ed. C. M. Johnson, B. L. Beard, and F. Albarede), pp. 113-152. The Mineralogical Society of America.

Anbar A. D., Jarzecki A., and Spiro T. (submitted) Theoretical investigation of equilibrium iron isotope fractionation between $Fe(H2O)_6^{+2}$ and $Fe(H2O)_6^{+3}$. *Geochimica et Cosmochimica Acta.*

Anbar A. D., Knab K. A., and Barling J. (2001) Precise determination of mass-dependent variations in the isotopic composition of molybdenum using MC-ICPMS. *Analytical Chemistry* **73**(7), 1425-1431.

Anbar A. D., Roe J. E., Barling J., and Nealson K. H. (2000) Nonbiological fractionation of iron isotopes. *Science* **288**(5463), 126-128.

Arnold G. L., Weyer S., and Anbar A. D. (2004) Fe isotope variations in natural materials measured using high mass resolution multiple collector ICPMS. *Analytical Chemistry* **76**(2), 322-327.

Beard B. L. and Johnson C. L. (1999) High precision iron isotope measurements of terrestrial and lunar materials. *Geochimica et Cosmochimica Acta* **63**, 1653-1660.

Beard B. L., Johnson C. M., Skulen K. H., Nealson K. H., Cox L., and Sun H. (2003) Application of Fe isotopes to tracing the geochemical and biological cycling of Fe. *Chemical Geology* **195**, 87-117.

Belshaw N. S., Zhu X. K., Guo Y., and O'Nions R. K. (2000) High precision measurement of iron isotopes by plasma source mass spectrometry. *International Journal of Mass Spectrometry* **197**, 191-195.

Bergquist B. A. and Boyle E. A. (2002) Iron isotope composition of the Amazon River. *Eos Trans. AGU, Fall Meeting Supplement* **83**(47), Abstract OS12C-0290.

Bigeleisen J. and Mayer M. G. (1947) Calculation of equilibrium constants for isotopic exchange reactions. *Journal of Chemistry and Physics* **15**, 261-267.

Bullen T. D. and McMahon P. M. (1998) Using stable isotopes to assess microbially-mediated Fe^{+3} reduction in a jet-fuel contaminated aquifer. *Mineralogical Magazine* **62A**, 255-256.

Bullen T. D., White A. F., Childs C. W., Vivit D. V., and Schulz M. S. (2001) Demonstration of significant abiotic iron isotope fractionation in nature. *Geology* **29**(8), 699-702.

Carlson R. W., Hauri E. H., and Alexander C. M. O. D. (2001) Matrix-dependent isotope mass fractionation in the ICP-MS. In *Plasma Source Spectrometry: The New Millennium.* (ed. J. G. Holland and S. Tanner), pp. 288-297. The Royal Society of Chemistry.

Duplessy J. C., Schackleton N. J., Fairbanks R. G., Labeyrie L., Oppo D., and Kallel N. (1988) Deepwater source variations during the last climatic cycle and their impact on the global deepwater circulation. *Paleoceanography* **3**, 343-360.

Feldmann I., Jakubowski N., and Stuewer D. (1999a) Application of a hexapole collision and reaction cell in ICP-MS Part I: Instrumental aspects and operational optimization. *Fresenium Journal of Analytical Chemistry* **365**, 415-421.

Feldmann I., Jakubowski N., and Stuewer D. (1999b) Application of a hexapole collision and reaction cell in ICP-MS Part II: Analytical figures of merit and first applications. *Fresenium Journal of Analytical Chemistry* **365**, 422-428.

Halliday A. N., Lee D. C., Christensen J. N., Walder A. J., Freedman P. A., Jones C. E., Hall C. M., Yi W., and Teagle D. (1995) Recent developments in inductively coupled plasma magnetic sector multiple collector mass spectrometry. *International Journal of Mass Spectrometry Ion Proc.* **146**, 21-33.

Hayes J. (1993) Factors controlling the ^{13}C contents of sedimentary organic compounds. *Marine Geology* **113**, 111-125.

Johnson C. M. and Beard B. L. (1999) Correction of instrumentally produced mass fractionation during isotopic analysis of Fe by thermal ionization mass spectrometry. *International Journal of Mass Spectrometry* **193**(1), 87-99.

Johnson C. M., Skulan J. L., Beard B. L., Sun H., Nealson K. H., and Braterman P. S. (2002) Isotopic fractionation between Fe(III) and Fe(II) in aqueous solutions. *Earth and Planetary Science Letters* **195**(1-2), 141-153.

Kehm K., Hauri E. H., Alexander C. M. O., and Carlson R. W. (2003) High precision iron isotope measurements of meteoritic material by cold plasma ICP-MS. *Geochimica et Cosmochimica Acta* **67**, 2879-2891.

Lee D. C. and Halliday A. N. (1995) Precise determinations of the isotopic compositions and atomic weights of molybdenum, tellurium, tin and tungsten using ICP source magnetic sector multiple collector mass spectrometry. *International Journal of Mass Spectrometry and Ion Processes* **146/147**, 35-46.

Maréchal C. N., Telouk P., and Albarede F. (1999) Precise analysis of copper an zinc isotopic compositions by plasma-source mass spectrometry. *Chemical Geology* **156**, 251-273.

Martin J. H. (1990) Glacial-interglacial CO_2 change: the iron hypothesis. *Paleoceanography* **5**, 1-13.

Martin J. H., Coale K. H., Johnson K. S., Fitzwater S. E., Gordon R. M., and Tanner S. J., Hunter, C.N., Elrod, V.A., Nowicki, J.L., Coely, T.L., Barber, R.T., Lindley, S., Watson, A.J., van Scoy, K., Law, C.S., Liddicoat, M.I., Ling, R., Stanton, T., Stockel, J., Collins, C., Anderson, A., Bidigare, R., Ondrusek, M., Latasa, M., Millero, F.J., Lee, K., Yao, W., Zhang, J.Z., Friederich, G., Sakamoto, C., Chevez, F., Buck, K., Kolber, Z., Greene, R., Falkowski, P., Chisholm, S.W., Hoge, F., Swift, R., Yungel, J., Turner, S., Nightingale, P., Hatton, A., Liss, P., Tindale, N.W. (1994) Testing the iron hypothesis in ecosystems of the equatorial Pacific Ocean. *Nature* **371**, 123-129.

Martin J. H. and Gordon R. M. (1988) Northeast Pacific iron distributions in relation to pyhytoplankton productivity. *Deep-Sea Research* **35**, 177-196.

Niu H. and Houk R. S. (1996) Fundamental aspects of ion extraction in inductively coupled plasma mass spectrometry. *Spectrochimica Acta* **51B**, 779-815.

Polyakov V. B. (1997) Equilibrium fractionation of the iron isotopes: Estimation from Mossbauer spectroscopy data. *Geochimica et Cosmochimica Acta* **61**(19), 4213-4217.

Roe J. E., Anbar A. D., and Barling J. (2003) Nonbiological fractionation of Fe isotopes: evidence of an equilibrium isotope effect. *Chemical Geology* **195**(1-4), 69-85.

Schauble E. A., Rossman G. R., and Taylor H. P. (2001) Theoretical estimates of equilibrium Fe-isotope fractionations from vibrational spectroscopy. *Geochimica et Cosmochimica Acta* **65**(15), 2487-2497.

Stookey L. C. (1970) Ferrozine – a new spectrophotometric reagent for iron. *Analytical Chemistry* **42**, 779-781.

Taylor P. D. P., Maeck R., and Debievre P. (1992) Determination of the absolute isotopic composition and atomic-weight of a reference sample of natural iron. *International Journal of Mass Spectrometry Ion Processes* **121**, 111-115.

Turner P. J., Merren T. O., Speakman J., Haines C., Palacz Z., and Meffan-Main S. (2000) Ion optics of multi-collector ICP-MS systems for precise and accurate isotope ratio measurements. Technical Report. GV Instruments, Inc., UK.

Weyer S. and Schwieters J. (2003) High precision Fe isotope measurements with high mass resolution MC-ICPMS. *International Journal of Mass Spectrometry* **226**(3), 355-368.

Zhu X. K., Guo Y., Williams R. J. P., O'Nions R. K., Matthews A., Belshaw N. S., Canters G. W., de Waal E. C., Weser U., Burgess B. K., and Salvato B. (2002) Mass fractionation processes of transition metal isotopes. *Earth and Planetary Science Letters* **200**(1-2), 47-62.

Zhu X. K., O'Nions R. K., Guo Y. L., and Reynolds B. C. (2000) Secular variation of iron isotopes in North Atlantic Deep Water. *Science* **287**(5460), 2000-2002.

Chapter 5

Iron Isotopes in the Marine System: Preliminary Results

5.1. Introduction

Iron is an essential micronutrient in the ocean and a limiting nutrient in high nitrate, low chlorophyll (HNLC) regions of the ocean (Martin and Fitzwater, 1988; Martin et al., 1994; Coale et al., 1996; Boyd et al., 2000). It is also hypothesized to possibly limit nitrogen fixing organisms in the oligotrophic subtropical gyres (Karl et al., 1997; Falkowski, 1998). These observations have led to suggestions that changes in iron input to the upper ocean can lead to climate changes by affecting biological productivity (and thus the carbon cycle) (Martin, 1990). In order to incorporate Fe into models of climate change, it is necessary to understand and quantify the processes that control iron distributions in the ocean. However, our understanding of the Fe cycle is hindered by a paucity of data and every new study significantly improves our understanding of the Fe distribution in the ocean.

Stable isotope studies of light elements (e.g., H, C, O, N, S) are ubiquitous and yield invaluable insights into processes in the environment. For example, carbon isotopes are used to track past changes in ocean circulation (Duplessy et al., 1988) and to study carbon metabolic pathways (Hayes, 1993); nitrogen isotopes can be used to quantify past changes in nitrate utilization (Francois et al., 1997; Sigman et al., 1999). Similarly, fractionation of Fe isotopes could potentially be a useful tool to investigate processes affecting Fe in the marine system. The available Fe isotopic data for both natural samples and laboratory studies was in Chapter 1, and two hypothetical scenarios for the use of Fe isotopic fractionation in the marine system were also discussed. Unfortunately, not enough information about marine Fe isotopes is available to rigorously evaluate potential applications of Fe isotopes to the marine system.

Initial studies of Fe isotopes show promise that useful fractionations exist in nature, and, in particular, in the marine system. A range of 4‰ (δ^{56}Fe, definition in section 5.2.4) is observed for natural samples that formed at the earth's surface (reviews: BEARD et al., 2003a; BEARD and JOHNSON, 2004). This is in contrast to the ultimate source of iron, igneous rock, which shows very little isotopic variability, ± 0.10‰ (2σ standard deviation) (BEARD et al., 2003a). Some of the largest variations observed in Fe isotopes are from samples deposited or altered in the marine environment (Figure 1.3). A 6 Myr paleorecord of iron isotopes was reconstructed from a Fe-Mn crust in the North Atlantic at 1800 m depth (ZHU et al., 2000). δ^{56}Fe increased towards the present from values of -0.7‰ at 6 Ma to +0.1‰ at the present. If the Fe in the Fe-Mn crust precipitated from seawater and has not been diagenetically altered, the record might serve as a proxy for Fe isotopes in the deep ocean. δ^{56}Fe variations through time were also observed in another Fe-Mn crust proximal to hydrothermal inputs in the Pacific, which may be indicative of changing relative fluxes of seawater and hydrothermal dissolved Fe to that site (CHU et al., 2003). Also, deep-sea cherts and chalks also have variable δ^{56}Fe values from +0.23 to -0.66‰ (ROUXEL et al., 2003). These records suggest that useful variations in the Fe isotopic composition of seawater may exist. However, an understanding of the mechanisms that control both the iron concentration and iron isotopic distribution is necessary to interpret the Fe isotope records.

The main sources of Fe to the ocean are rivers, atmospheric deposition, re-suspension of sediments, and hydrothermal vents. Iron concentrations are highest near its sources and decrease rapidly with distance from sources due to the reactivity and insolubility of Fe in seawater (WU and LUTHER, 1996; JOHNSON et al., 1997). Therefore river input and re-suspension of shelf deposits are only considered important sources of Fe to coastal regions. Hydrothermal input is believed to be important only near its sources (mostly in the deep ocean) for the reason that most of the Fe precipitates near the vents and ridge axes. Therefore, a majority of Fe in the open ocean is thought to be from atmospheric deposition. A fraction of this Fe is dissolved in the upper ocean, taken up by organisms, and then exported to the deep ocean by sinking organic material and

scavenging of Fe onto sinking particles. The amount of dissolved Fe in the deep ocean will depend on a balance between the decomposition of sinking organic matter, lateral transport, organic complexation, and removal by scavenging with a residence of ≈ 200 to 300 years (JOHNSON et al., 1997; PAREKH et al., 2004; Chapter 2). Besides atmospheric deposition, upwelling and vertical mixing of nutrient-rich deep-water into the euphotic zone is also an important source of Fe to the biological pump. Therefore understanding atmospheric delivery, dissolution of aerosols, biological cycling in the euphotic zone, and the controls over deep-water Fe concentrations are all vital to understanding biological utilization and cycling of Fe.

Of the four main sources of dissolved Fe to the ocean, only the isotopic composition of dissolved Fe from hydrothermal vents has been measured directly. Dissolved Fe from mid-ocean ridge hydrothermal vents (SHARMA, 2001; BEARD et al., 2003b; SEVERMANN et al., in press) is isotopically light relative to igneous sources (-0.2 to -0.7‰). Heavier isotopic compositions in hydrothermally altered oceanic basalts (where up to 80% of the Fe has been removed by leaching) suggest that isotopically light vent fluid results from preferentially leaching of light isotopes from oceanic basalts (ROUXEL et al., 2003). Precipitation of isotopically heavy minerals (e.g., sulfides) from hydrothermal fluids may also drive hydrothermal Fe input to lighter values (SHARMA, 2001; BEARD et al., 2003b; ROUXEL et al., 2004). When the hydrothermal vent fluid mixes with seawater, a significant fraction of the Fe precipitates from solution forming plume particles. The overall effect of this loss of Fe on the residual dissolved Fe isotopic composition in deep water is still being studied, but an initial study suggests that it may be negligible (SEVERMANN et al., in press).

Although the input of dissolved Fe from rivers, dissolution of atmospheric particles, and re-suspension of shelf sediment have not been measured directly, there are a few studies that hint at the possible Fe isotopic composition of these sources. Shelf sediments along with their porewaters from the California margin show isotopic variability with porewater δ^{56}Fe reaching low values of -1.3‰ relative to igneous rocks (SEVERMANN et al., 2003). Also, organic-rich black shales show a large range in δ^{56}Fe

values from -2.3‰ to +0.6‰ (YAMAGUCHI et al., 2003). These observations suggest that diagenetic processes in marine sediments lead to variations in Fe isotopes, and re-suspension of shelf deposits may lead to input of isotopically light dissolved Fe to coastal and near-shelf areas. There has been some speculation that dissolved Fe inputs to the ocean via rivers or dissolution of lithogenic aerosols might be similar to igneous rocks based on the isotopic homogeneity of continental rocks, river suspended material, soils, loess, and aerosols (BEARD et al., 2003b; BEARD and JOHNSON, 2004). Considering that only a few percent of Fe is mobilized into the dissolved phase in many environments, it would be extremely difficult to detect variations in dissolved Fe inputs from their source rocks and sediments.

Because Fe isotopes might further the understanding of the Fe cycle in the ocean, it is important to continue investigating Fe isotopes in the marine system. Six plankton tow samples from the tropical and subtropical Atlantic and Pacific Oceans were analyzed for their Fe isotopic compositions. An aerosol sample was collected for iron isotopic analysis at a site in the North Atlantic, where atmospheric deposition is the main source of dissolved Fe to the euphotic zone. Biological cycling of Fe in the surface ocean is a significant part of the marine Fe cycle. It is linked to the dissolution of atmospheric particles, biological uptake and recycling, and export to the deep ocean where Fe in sinking organic matter can be re-mineralized. Whether or not planktonic Fe is fractionated from its sources and how it is fractionated are important processes that need to be assessed in order to apply Fe isotopes to the marine system.

5.2. SITES, SAMPLE COLLECTION, AND METHODS

5.2.1. Plankton Tows

Between January 2001 and July 2002, trace metal clean plankton tow samples were collected at ≈ 5 m depth on three cruises in the sub-tropical and tropical Atlantic and Pacific oceans (Figure 5.1): 1) June/July 2001, R/V Knorr, Kn162 cruise (two plankton tows: 10°N, 45°W and 10.5°N, 56.6°W), 2) March 2002, R/V Endeavor, En367 cruise (two plankton tows: 7.4°S, 31.4°W and 24.5°S, 37°W), and 3) July 2002,

R/V Ka'imikai-o-Kanaloa, KOK0210 cruise (two plankton tows: 23°N, 158°W and 26°N, 175°W). The plankton tow sites cover a wide range of oceanic regimes with different organisms represented in the tows. The identification of organisms and their approximate abundance was mainly done by Dr. R. Foster (Dr. E. Carpenter's group at San Francisco State University). The surface dissolved (<0.4 μm Fe) and soluble Fe (<0.02 μm Fe) concentrations along the transects where the plankton tows were collected are plotted for the Atlantic in Figure 2.3 and the Pacific in Figure 3.4.

In the Atlantic, plankton tows were collected at four sites. The open ocean northern site (10°N, 45°W) is on the edge of the subtropical gyre and equatorial system with high surface dissolved Fe (>0.5 nmol/kg) due to higher dust deposition mainly from Saharan sources (DUCE and TINDALE, 1991; MAHOWALD et al., 1999; FUNG et al., 2000; GAO et al., 2001; VINK and MEASURES, 2001). At the time of collection, July 2001, the mixed layer was very shallow (11 m) and surface waters were warm and calm. The dominant plankton collected was the nitrogen fixing cyanobacterium Trichodesmium spp. Similarly, Trichodesmium spp. was the most abundant species collected at the 24.5°S site in the subtropical gyre of the South Atlantic in March 2002. This site was also characterized by a shallow mixed layer (32 m) and warm, calm conditions. However, dissolved Fe levels were much lower at this site (<0.4 nmol/kg) due to the low dust input to the surface ocean in the South Atlantic. The occurrence of Trichodesmium spp. at these sites is likely due to the oligotrophic, warm, shallow mixed layer conditions at the time of collection, which are conditions favorable for Trichodesmium spp. (KARL et al., 2001). The 7.4°S site is located in a oceanographically complicated region of the ocean on the edge of the South Atlantic subtropical gyre and equatorial system where the surface water from the east diverges and either moves southward with the Brazil Current or moves north with the North Brazil Current (BROWN et al., 1989). A CTD cast was not done at this site and dissolved Fe concentrations were not measured. The plankton tow was dominated by both dinoflagellates and diatoms (with intracellular nitrogen fixers). In contrast to the open ocean site described above, the plankton tow from the western tropical Atlantic at 10.5°N, 56.6°W was collected in a 25 m deep low salinity cap

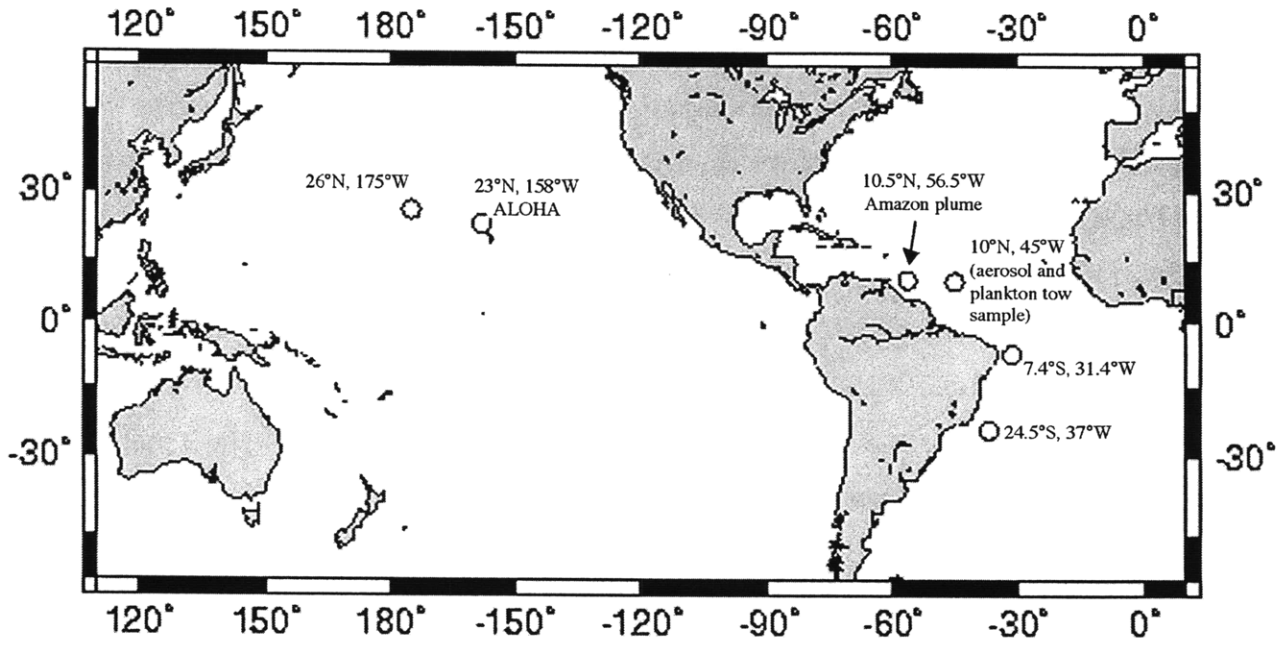

Figure 5.1: Sample location map. Samples were collected on three different cruises from July 2001 to July 2002. The North Atlantic samples were collected in July, 2001. the South Atlantic samples in March 2002, and the North Pacific samples in July 2002. An aerosol sample and plankton tow were collected at the 10°N, 45°W site.

(32 PSU) overlying 36 PSU seawater (Figure 6.1). The plume of fresher water also had high concentrations of total Fe (7 nmol/kg); it is inferred that the source of the freshwater and high Fe levels was the Amazon River System (see Chapter 6 for discussion). The general characterization of this plume water was similar to coastal water with light penetration of only a few meters due to a large bloom of larvaceans ("salps") and diatoms with symbiotic nitrogen fixers.

Both sites in the Pacific were collected in the North Pacific subtropical gyre in July 2002. The 23°N,158°W site is Station ALOHA, which is the part of the Hawaiian Ocean Time-series (HOT) program established in 1988 (see special issues: KARL AND MICHAELS, 1996; SIEGEL et al., 2001). The main source of dissolved Fe to the subtropical gyre is atmospheric input from aeolian transport off the Asian continent (DUCE and TINDALE, 1991; MAHOWALD et al., 1999; FUNG et al., 2000; GAO et al., 2001), which is highest in the late winter/early spring (PARRINGTON et al., 1983; PROSPERO, 1996). Dissolved Fe concentrations were 0.46 nmol/kg at the time of collection, but concentrations vary from 0.2 to 0.7 nmol/kg at Station ALOHA seasonally (BOYLE et al., submitted). At the time of collection, the mixed layer was deep (≈ 80 m) and the plankton tow sample was dominated by diatoms (with symbiotic nitrogen fixing bacteria) with a small amount (10%) Trichodesmium spp. also present. Dissolved Fe concentrations decreased toward the east along with the depth of the mixed layer. At the 26°N,175°W site, dissolved Fe concentrations were less than 0.3 nM (Figure 3.4) and the mixed layer was ≈ 30 m. Similar organisms were found at this site to those at Station ALOHA, but Trichodesmium spp. abundance increased to ≈ 50%.

A 64 μm nylon mesh plankton tow was used to collect organisms at all sites, therefore picoplankton are not represented in our samples. Some organisms smaller than 64 μm are retained by the net due to mesh clogging and turbulent flow in the net, but the abundance of smaller organisms is not known (and organisms smaller than 10 to 20 μm are probably not retained). Picoplankton, such as the cyanobacterium Prochlorococcus (less than 1 μm), make up a significant fraction of the biomass (≈ 50 %) in the open ocean (CHISHOLM et al., 1988; PARTENSKY et al., 1999). For example, it is estimated that

Prochlorococcus dominates the biomass at Station ALOHA (KARL et al., 2001). This is likely the case at the other oligotrophic sites sampled in this study.

Trace metal clean horizontal plankton tows were performed employing techniques similar to those described in Collier and Edmond (1984). A 64 μm nylon mesh plankton tow with a plastic ring and fittings (Sea-Gear Corporation) was deployed from a nylon rope with plastic coated lead weights from the side of the ship. Care was taken to ensure that the plankton net did not contact the side of the ship and was only handled by gloved hands. The lead weights were deployed first and were separated from the plankton tow by 6 m of nylon rope. Plankton tows were performed 3 to 5 m from the side of the ship with the ship steaming at 1 to 2 knots. Therefore, the plankton tow sampled water moving parallel to the ship and not water that had contact with the ship. This technique is commonly used in trace metal surface water sampling (e.g., "towed fish" device [Vink et a., 2000]). In between deployments, the plankton tow was stored in an EDTA solution and deployed without a collection bottle (cod end) for at least 5 minutes to flush the plankton net thoroughly with seawater prior to sampling.

Three half hour tows were carried out at each sampling site to accumulate enough biomass for Fe isotope analysis, except at the Amazon plume site where only 10 minute tows were needed for collection due to high biomass concentration. Two of the plankton tows were immediately vacuum filtered sequentially through acid cleaned and seawater rinsed 10 μm and 1 μm Nuclepore polycarbonate filters in a class 100 clean laminar flow bench. Complete filtration took several hours, and samples were refrigerated until filtered. Plankton material plus filters were frozen and the final filtrate (< 1 μm) acidified and archived. The third plankton tow was split into two 250 ml acid cleaned polycarbonate bottles, frozen, and archived. For Fe isotope analysis, the frozen plankton tow filters were thawed and a split transferred from the filter to a quartz beaker with an acid cleaned plastic scoop or pipette tip. Samples were dried on a hot plate overnight (60 to 80°C) prior to combustion at 550°C in a muffle furnace for 8 hours. Organic carbon estimates (for Fe:C ratios) were made by measuring phosphate and Fe concentrations in the sample prior to column separation. Phosphate was converted to organic carbon using

the Redfield C:P molar ratio for marine organisms of 106:1 (REDFIELD et al., 1963). Organic carbon estimates for a few of the earlier plankton sample replicates from the 10°N, 45°W and 10.5°N, 56.6°W were made by weighing the sample before and after the muffle furnace and assuming complete combustion of organic carbon to CO_2. This method underestimates the amount of organic carbon by approximately 40% (based on a comparison to estimates made from phosphate measurements made on later plankton tow samples), and organic carbon numbers were adjusted for these samples.

5.2.2. Aerosol

An aerosol sample from the North Atlantic (10°N, 45°W) was analyzed for $\delta^{56}Fe$ in this study. The sample was collected at sea by Y. Chen and Dr. R.Siefert (University of Maryland) on acid cleaned cellulose filters using a high-volume dichotomous virtual impactor. Collection techniques and trace metal contamination considerations are discussed in Chen and Siefert (submitted). Splits of the filter with aerosol particles and filter blanks were leached with 5 ml of 1 M HCl (triply distilled Vycor) and 0.5 M HNO_3 (Optima grade); the goal was to preferentially dissolved only the exchangeable Fe (Fe oxides and crusts). The acidic solution was warmed for one hour (60°C) and allowed to sit overnight. The leachate was then transferred to a quartz beaker and taken to dryness in a class 100 clean flow environment prior to combustion. The filter blanks for these samples were higher than typical process blanks (0.16 μg) due to the filter. The blank accounted for 0.4% of the Fe extracted from the aerosol samples.

5.2.3. Fe Concentration Measurements

Sample Fe concentrations and post-column recoveries were measured by UV-VIS spectroscopy using the Ferrozine method (STOOKEY, 1970) separating the Ferrozine and hydroxylamine hydrochloride reagents (to avoid precipitation of the Ferrozine with HCl). Using a 1 cm pathlength cell and lab-grade reagents, this method has a detection limit of 0.2 μM. Process blanks were always below the detection limit by the Ferrozine method, therefore blanks were measured on the IsoProbe using a simple two-point linear

calibration curve. Seawater concentrations were analyzed by isotope dilution MC-ICPMS ($Mg(OH)_2$ co-precipitation) by a modified version of a method developed by Wu et al., (2001) (BERGQUIST AND BOYLE, in prep). See chapter 2 for more details.

5.2.4. Fe Purification and Isotopic analysis

Methods for Fe purification, separation, and Fe isotopic analysis are described in Chapter 4. Briefly, all samples are combusted at 550°C for 8 hours, re-dissolved in 7 M HCl (Optima grade), and purified by anion exchange chromatography. Approximately 300 ng of Fe was used for measurement of Fe isotopic composition on the MIT GV Instruments IsoProbe MC-ICPMS. Instrumental mass bias was corrected for using standard-sample bracketing (SSB), and matrix effects on the instrument mass bias were evaluated using "standard isotope dilution" (also discussed in detail in Chapter 4). All sample Fe isotope data is reported in delta notation:

$$\delta^{56}Fe\ (‰) = \left(\frac{^{56}Fe/^{54}Fe_{sample}}{^{56}Fe/^{54}Fe_{standard}} - 1 \right) \times 1000$$

Samples are referenced to the mean of all the individual analysis of seven splits of Rhode Island Granite (USGS, G-2) and Hawaiian Basalt (USGS, BVHO-1), which had a an average $\delta^{56}Fe_{wrk\ std}$ of -0.23 ± 0.04‰ (2σ, n=30) (see Table 4.6) or a $\delta^{56}Fe$ of 0.00 ± 0.04‰ (2σ, n=30) when referenced to themselves. Some laboratories use the IRMM-014 standard as a reference material instead of igneous rocks. The measured difference between igneous rock and the IRMM-014 standard was -0.13 ± 0.07‰ (2σ, n=12), which agrees well with estimates of -0.09 ± 0.01‰ (2σ, n=52) by Beard et al. (2003a).

The uncertainties in the average $\delta^{56}Fe$ measurements quoted in this thesis are the 2σ standard error (2 standard deviation (SD) divided by the square root of the number of analysis). If multiple measurements were not performed for a sample, an uncertainty of

± 0.22‰ (2σ) is applied to samples referenced to the working standard and ± 0.24‰ (2σ) to samples referenced to mean of the igneous rock. There is a slight increase in the uncertainty due to error propagation when the sample $\delta^{56}Fe_{wrk\ std}$ (sample referenced to the working standard) is converted to $\delta^{56}Fe$ referenced to igneous rocks. The estimates of uncertainty are based on the long-term external precision of a single granite sample split (± 0.22‰, 2 SD, n=22, Table 4.6, granite D). The standard deviation (1 SD), standard error (2σ), and number of measurements within an analytical session are reported for all samples in the data tables. Individual samples listed and plotted in the tables and figures represent samples or sub-samples that were processed through the entire Fe separation and purification chemistry separately.

5.3. Results and Discussion

The $\delta^{56}Fe$ of plankton tow samples vary by over 4‰ from -3.87‰ to +0.36‰, and the aerosol leachate is indistinguishable from igneous rocks (Figure 5.2, Table 5.1). The $\delta^{56}Fe$ of the plankton tow samples span much of the observed range in natural samples (-2.5‰ to +1‰ (Beard et al., 2003a; Beard and Johnson, 2004)) with very isotopically light Fe from the Station ALOHA plankton tow samples (-2.5‰ to -3.9‰) collected in the North Pacific subtropical gyre.

Different size fractions of the plankton tow from the Amazon plume water (>10 μm and 1 to 10 μm) and replicate tows were measured to ensure that the filtering at sea did not affect the Fe isotopic composition of the sample. It took several hours to completely filter one plankton tow at sea through the 10 μm filter, and then finally through the 1 μm filter before starting the filtration of the second tow. The plankton tow samples (collected with a 64 μm mesh) in this study should contain few organisms that are less than 10 μm, therefore the 1 to 10 μm sample should consist of products of degradation or cell lysis. If bacterial degradation or cell lysis in the plankton tow were affecting the isotopic composition, then potentially the different size fractions or replicate tows would be different. The Fe isotopic data for the different size fractions and replicate

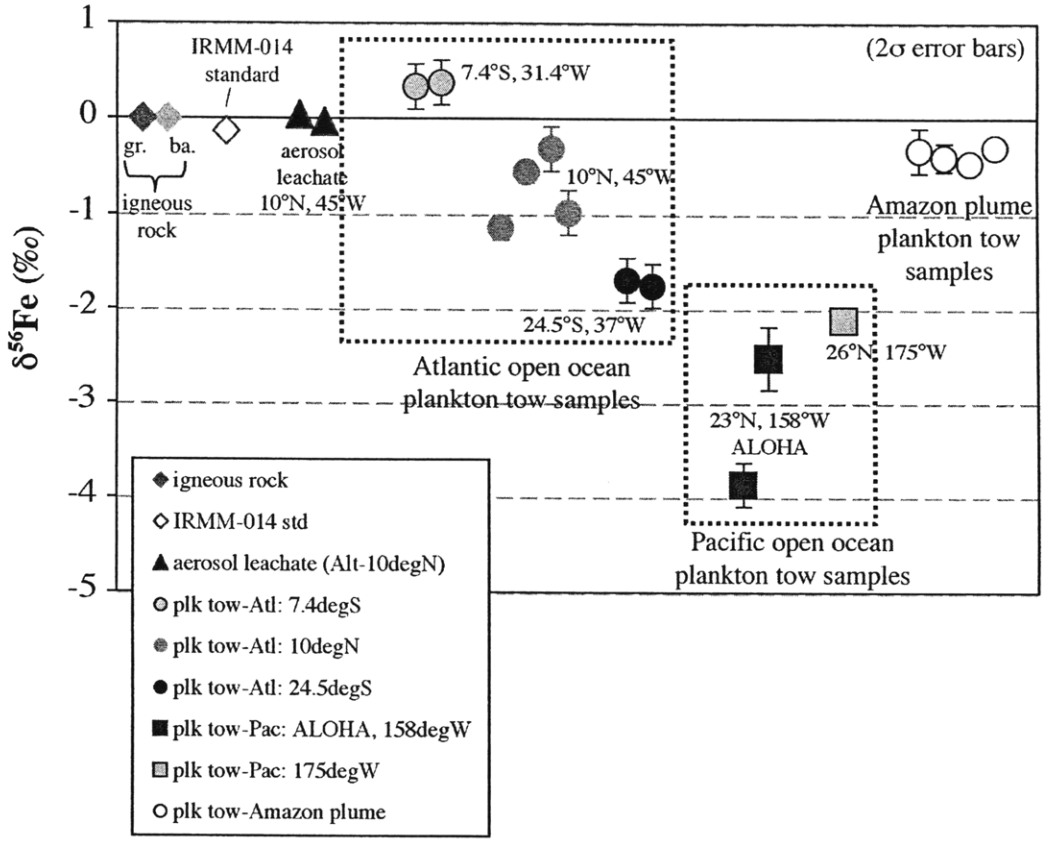

Figure 5.2: Summary of marine $\delta^{56}Fe$ data for marine samples measured in this study. The means of the igneous rock samples (granite (gr.) and basalt (ba.) and the IRMM-014 are shown for reference. The Atlantic plankton tow samples are plotted with circles and the Pacific samples with squares. The replicate points for samples represent the $\delta^{56}Fe$ for a sample or a sub-sample that was processed through the entire Fe separation and purification chemistry. Error bars are 2σ standard errors of replicate measurements. If multiple measurements were not made within an analytical session, then a 2σ uncertainty of ± 0.24‰ is used based on the long term external precision of a granite sample (± 0.22‰, 2 SD, n=22, Table 4.6, granite D). There is a slight increase in the uncertainty due to error propagation when the sample $\delta^{56}Fe_{wrk\ std}$ (sample referenced to the bracketing sample) is converted to $\delta^{56}Fe$ referenced to igneous rocks.

Table 5.1: Summary of $\delta^{56}Fe$ data for Marine Samples

Sample ID	proc. Fe[a] (μg)	Fe:C[b] (μmol/mol)	analysis date	$\delta^{56}Fe$[c] (‰)	1 SD[d]	2σ unc[e] (2 std error)	n	inlet[j]
Aerosol Sample, 1 M HCl leach (10°N, 45°W; July 15, 2001)								
sample 1[f]	51		8/16/03	0.04	0.04	0.06	2	spray
sample 2	50		8/16/03	-0.03[i]	0.04	0.06	2	spray
average of samples:				0.01	0.06	0.06	4	
Atl. Amazon Plume Plankton Tow (10.5°N, 56.5°W; July 20, 2001) (diatoms and larvaceans "salps")								
tow 1 (<10 um) split A	?	?	10/24/03	-0.33	0.12[h]	0.24[h]	1	spray
tow 1 (<10 um) split B	?	?	10/24/03	-0.40	0.11	0.15	2	spray
tow 2 (<10 um) split 1	25	540[g]	10/24/03	-0.47	0.07	0.10	2	spray
tow 1 (>10 um, muffle)	67	620[g]	5/15/03	-0.18	0.12[h]	0.24[h]	1	Aridus
			5/28/03	-0.32	0.12[h]	0.24[h]	1	Aridus
			7/10/03	-0.44	0.13	0.18	2	Aridus
			8/7/03	-0.17	0.05	0.07	2	spray
			1/22/04	-0.36	0.12[h]	0.24[h]	1	APEX (no des)
average of tow 1 (>10 um, muffle):				-0.30[i]	0.14	0.10	7	
average all measurements:				-0.34	0.13	0.08	12	
Alt. Plankton Tow (10°N, 45°W; July 15, 2001) (Trichodesmium)								
tow 2 (>10 um) split A	12	167[g]	8/16/03	-1.14	0.09	0.13	2	spray
tow 2 (>10 um) split B	7	118[g]	8/16/03	-0.55[i]	0.08	0.11	2	spray
tow 2 (>10 um) split C	21	431	1/22/04	-0.31[i]	0.12[h]	0.24[h]	1	APEX (no des)
tow 3 (>10 um) split D	9	295	1/22/04	-0.98	0.12[h]	0.24[h]	1	APEX (no des)
Atl. Plankton Tow (7.4°S, 31.4°W; March 12, 2002) (dinoflagellates and diatoms)								
tow 1 (>10 um)	115	1700	1/22/04	0.34	0.12[h]	0.24[h]	1	APEX (no des)
tow 2 (>10 um)	141	2325	1/22/04	0.38	0.12[h]	0.24[h]	1	APEX (no des)
average:				0.36	0.03	0.04	2	
Atl. Plankton Tow (24.5°S, 37°W; March 17, 2002) (Trichodesmium)								
tow 1 (>10 um)	1	34.7	1/22/04	-1.69	0.12[h]	0.24[h]	1	APEX (no des)
tow 2 (>10 um)	3	57.2	1/22/04	-1.76	0.12[h]	0.24[h]	1	APEX (no des)
average:				-1.73	0.04	0.06	2	
Pac. Plankton Tow (ALOHA, 23°N, 158°W; July 1, 2002) (mostly diatoms with small amounts (10%) Trichodesmium)								
tow 2 (>10 um)	37	166	1/22/04	-3.87	0.12[h]	0.24[h]	1	APEX (no des)
tow 3 (>10 um)	37	261	1/22/04	-2.53[i]	0.24	0.33	2	APEX (no des)
Pac. Plankton Tow (26°N, 175°W; July 11, 2002) (diatoms and Trichodesmium)								
tow 3 (>10 um)	12	65.9	1/22/04	-2.12[i]	0.07	0.09	2	APEX (no des)

a) Amount of Fe processed through the Fe separation and purification chemistry.

b) Fe:C ratio of plankton tow samples calculated by estimating organic carbon either by phosphate measurement assuming a "Redfield" C:P ratio of 106:1 (REDFIELD et al., 1963).

c) Sample $\delta^{56}Fe$ values are referenced to the mean of igneous rocks (0.00 ± 0.04‰, 2σ, n=30).

d) SD is the standard deviation of the individual measurements.

e) 2σ uncertainty is the uncertainty in the mean of replicate sample measurements (2 standard error).

f) Every sample or sub-sample was processed through the Fe separation and purification chemistry separately. Sample number denotes sequence of filtration in the field.

g) Organic carbon estimated made by weighing the sample before and after the muffle furnace, and assuming complete combustion to CO_2. This method was found to underestimate the organic carbon by ~ 40% compared with the phosphate method (b), and the Fe:C were adjusted.

h) If only one measurement was made for a sample, a 2σ uncertainty of ± 0.24‰ (2 SD) was applied to the sample. The 2σ uncertainty was estimated is based on the long term external precision of a granite sample.

i) Sample $\delta^{56}Fe$ measurements tested for potential instrument mass bias shifts by "standard isotope dilution" technique described in Chapter 4.

j) Several inlet systems were used including a cyclonic spray chamber (spray chamber), the Aridus desolvating system (Aridus), and the APEX system with (APEX with des.) and without a desolvator (APEX (no des)). See Chapter 4 for more details.

tows is shown in Table 5.1. The different size fractions and replicates of the Amazon plume plankton tow show little isotopic variability (0.34 ± 0.08‰, 2σ, n=12) suggesting that the filtering technique and time did not affect the isotopic composition of the Fe. At other sites, plankton tow replicates have variable isotopic compositions along with variable and high Fe:C ratios. For example, three splits of the same plankton tow replicate from 10°N, 45°W had Fe:C ratios that varied by a factor of three. This will be discussed in the next section. There are no systematic trends in Fe isotopes or Fe:C ratios based on filtering order. At the South Atlantic site (24.5°S, 37°W) the plankton tow replicates have low Fe:C ratios more indicative of intracellular levels (SUNDA and HUNTSMAN, 1995; HO et al., 2003) and the is δ^{56}Fe of the two are identical.

Fe isolated from the plankton tow samples includes both intracellular Fe and Fe adsorbed (both particulate and dissolved) to the surface of organisms. The measured Fe:C ratios ranged from 35 to 2300 μmol/mol with very high ratios at the –7.4°S, 31.4°W site and at the Amazon plume station. The Fe:C ratio needed for optimal growth determined in laboratory cultures for a variety of marine organisms is typically less 70 μmol/mol and varies by a factor of 8 from species to species and under differing conditions (SUNDA and HUNTSMAN, 1995; HO et al., 2003), which agrees well with field observations (MARTIN and KNAUER, 1973; BRULAND et al., 1991; SCHMIT and HUTCHINS, 1999; KUSTKA et al., 2003; TOVAR-SANCHEZ et al., 2003). Organisms will also take up Fe in excess of what they need if more Fe is available (luxury uptake). In a laboratory cultures of a coastal diatom, Fe:C ratios greater than 100 μmol/mol were observed when available Fe exceeded 1 nM (SUNDA and HUNTSMAN, 1995; HO et al., 2003). The Fe:C continued to rise with increasing Fe, but intracellular Fe:C plateaued at 120 μmol/mol. The increase in Fe:C above 120 μmol/mol was due to extracellular Fe adsorption (HO et al., 2003). The ratio of intracellular Fe to extracellular Fe is difficult to quantify in natural samples because of the variable Fe:C ratios and because plankton wash methods for removing extracellular Fe at sea were not available until recently (TOVAR-SANCHEZ et al., 2003). Tovar-Sanchez et al. (2003) found that 16 to 86% of the Fe measured in plankton tows in the Southern Ocean was extracellular, and intracellular

Fe:C ratios were typically less than 50 μmol/mol. The plankton tow samples in this study were not washed and were collected in surface seawater with range of dissolved Fe concentrations. It is likely that plankton tow samples that have Fe in excess of the Fe predicted from a Fe:C ratio of 70 μmol/mol is extracellular Fe. The δ^{56}Fe of the plankton tow samples will therefore reflect a mixture of Fe adsorbed to the surface of the plankton and intracellular Fe.

The Fe:C ratios versus δ^{56}Fe values of the open ocean plankton tow samples are plotted in Figure 5.3a. The Amazon plume plankton tow samples had high Fe:C ratios (≈ 600 μmol/mol), and it is likely that >80% of the Fe is extracellular. Because of the unique source of Fe for this plankton tow (Amazon River and shelf region), the light δ^{56}Fe composition will be discussed in Chapter 6 along with samples from the Amazon system. The open ocean plankton tow collected at –7.4°S, 31.4°W also had extremely high Fe:C ratios (>1500 μmol/mol) and an isotopically heavy δ^{56}Fe (+0.36‰) compared to igneous rocks and the aerosol leachate. Iron concentrations at this station were not measured, but the dissolved Fe concentrations along the transect where the plankton tow samples were collected do not indicate that Fe concentrations at this station would be much higher than 0.6 nmol/kg (Figure 2.3). Also, dissolved Fe concentrations were less than 0.8 nmol/kg between 5°S to 10°S along a similar transect in June 1996 and estimated atmospheric input to this region is moderate (1 to10 g m^2 yr^{-1}) based on dissolved Al (VINK and MEASURES, 2001). The station is ≈ 400 km from the shelf of Brazil and south of the outflow from the Amazon River. It is not likely that high concentrations of Fe from the coastal region would persist this far into the open ocean (WU and LUTHER, 1996; JOHNSON et al., 1997). Johnson et al. (1997) observed Fe in the open ocean decreases to levels of less than 2% of the high coastal concentrations within 100 km from the continental margin. Also, the surface water in this region is generally coming from the east (BROWN et al., 1989). It is possible that the high Fe:C ratios could be due to contamination (e.g., rust chips from ship). However, it seems unlikely that both tows would be contaminated and another set of plankton tows collected three days later (not measured for Fe isotopes) had measured Fe:C ratios of less than 40 μmol/mol. It is

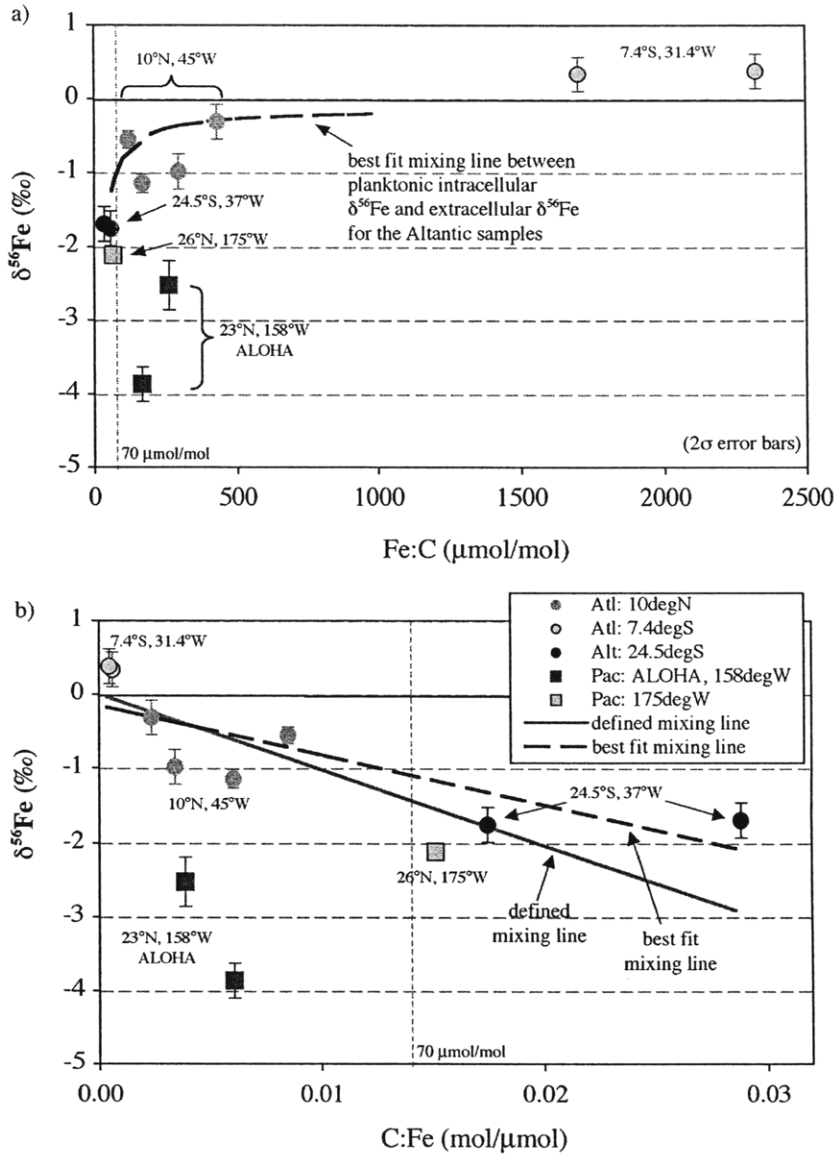

Figure 5.3: The $\delta^{56}Fe$ measurements of plankton tow samples is plotted against their measured Fe:C ratios (µmol/mol) in Figure 5.3a and against C:Fe (mol/µmol) in Figure 5.3b. Hypothetical mixing lines are plotted for the Atlantic Ocean samples between an assumed planktonic intracellular endmember and an extracellular endmember (e.g., Fe/particles/colloids adsorbed to cell surfaces). It was assumed that all Fe in excess of a certain Fe:C ratio was extracellular The best fit mixing line yielded an intracellular $\delta^{56}Fe$ of –1.5‰, an extracellular endmember $\delta^{56}Fe$ of -0.14‰., and a Fe:C threshold of 50 µmol/mol. A defined mixing line is also shown where the intracellular $\delta^{56}Fe$ was set at –1.7‰ (based on measurements of $\delta^{56}Fe$ in plankton samples at 24.5°S) and the extracellular $\delta^{56}Fe$ at 0‰ (based on aerosol leachate measured in this study at 10°N, 45°W). For the defined mixing line, it was assumed that all Fe in excess of a Fe:C ratio of 60 µmol/mol was extracellular. Error bars are 2σ standard errors of replicate measurements. If multiple measurements were not made within an analytical session, then a 2σ uncertainty of ± 0.24‰ is used based on the long-term external precision of a granite sample.

probable that at least 95% of the Fe from this tow is extracellular, and the heavy δ^{56}Fe might reflect the source of the Fe. One possible way to check for ship contamination would be to measure rust chips from the R/V Endeavor to see if they are isotopically heavy as well. With the current data, the source of the isotopically heavy Fe is also unknown.

The rest of the open ocean plankton tow samples have Fe:C ratios of less than 500 μmol/mol, and probably reflect more reasonable mixtures of extracellular and intracellular Fe. Both sites (the Atlantic 10°N, 45°W site and Station ALOHA) collected in surface water with higher levels of dissolved Fe (>0.4 nmol/kg) and colloidal Fe (>0.15 nmol/kg), have higher and more variable Fe:C ratios greater than 100 μmol/mol. The δ^{56}Fe of the replicate tows and splits are different and appear to be isotopically heavier with increasing Fe:C ratios suggesting that the extracellular Fe is isotopically heavy compared with intracellular Fe. At the other two sites (Atlantic 24.5°S, 37°W and Pacific 26°N, 175°W), dissolved and colloidal concentrations of Fe were lower (<0.4 and <0.1 nmol/kg respectively). Fe:C ratios are less than 70 μmol/mol and the δ^{56}Fe of the replicate plankton tows at the South Atlantic site are similar despite a factor of two difference in the Fe:C ratios (35 and 57 μmol/mol). The Fe in these plankton tow samples may represent mostly intracellular Fe.

If it is assumed that all the Fe in excess of Fe predicted by some threshold Fe:C ratio is extracellular, hypothetical mixing lines can be estimated between a planktonic intracellular endmember and an extracellular component for the Atlantic samples. Two mixing lines are plotted in Figure 5.3b where the δ^{56}Fe is plotted against the inverted Fe:C ratios in order for the mixing lines to plot linearly. The best-fit mixing line yielded an intracellular endmember δ^{56}Fe of -1.5‰, an extracellular endmember δ^{56}Fe of -0.14‰, and a threshold Fe:C ratio of 50 μmol/mol. These values are in general agreement with reasonable estimates that can be made based on available data. The intracellular endmember estimate is similar to the South Atlantic (24.5°S) plankton sample δ^{56}Fe value of -1.7‰. This plankton tow had low Fe:C ratios of <60 μmol/mol and the Fe from the sample is likely representative of intracellular Fe. The extracellular endmember δ^{56}Fe

estimate of -0.14‰ is similar to the δ^{56}Fe measured in the aerosol leachate from the Atlantic (+0.01‰). Finally, the estimated threshold Fe:C ratio from the best-fit mixing line (50 μmol/mol) matches well with estimates (<70 μmol/mol) of the intracellular Fe:C ratio of oceanic organisms (SUNDA and HUNTSMAN, 1995; HO et al., 2003; TOVAR-SANCHEZ et al., 2003). Also plotted in Figure 5.3b is a mixing line where the endmember isotopic compositions and the threshold Fe:C ratio were defined based on the available data described above (intracellular δ^{56}Fe of -1.7‰, an extracellular endmember δ^{56}Fe of 0.0‰, and a threshold Fe:C ratio of 60 μmol/mol). If the plankton tow sample data from the 7.4°S station is removed from the best-fit mixing line due to its extremely high (and potentially unrepresentative) Fe:C ratio, then the estimated extracellular endmember δ^{56}Fe becomes more negative (-0.5‰) with the other variables similar to the estimates above.

The data from the Atlantic tows scatter around the mixing line, but do not follow it perfectly. The intracellular Fe:C ratio is not a constant and can vary by a factor of 8 from species to species and in the same species grown under different conditions (SUNDA and HUNTSMAN, 1995; HO et al., 2003). Although Trichodesmium spp. is the dominant organism at two of stations (10°N and 24.5°S), it is likely that the planktonic community at each site is different. Also, different plankton tows at the same site and splits of the same plankton tow are also not likely to be homogenous as reflected in the varying Fe:C ratios measured in the different tow samples and tow sub-samples from 10°N. The Fe:C and isotopic composition differences may be due varying abundances of other plankton and higher trophic level organisms.

The Pacific plankton tow samples are isotopically lighter than those sampled in the Atlantic and do not follow a simple two endmember mixing curve. Although both sites are in the North Pacific subtropical gyre, the two sites had different abundances of plankton along with different Fe concentrations and mixed layer depths. Station ALOHA samples had the isotopically lightest Fe with δ^{56}Fe values of -2.5 and -3.9‰ (corresponding to Fe:C ratios of 261 and 166 μmol/mol respectively). The plankton tow sample with the higher Fe:C had the heavier isotopic composition suggesting that the

extracellular Fe is heavier than the intracellular Fe at Station ALOHA, similar to the Atlantic samples. However, the 175°W site had a lower Fe:C ratio of 66 μmol/mol and a δ^{56}Fe value of -2.1‰. The difference in the observed δ^{56}Fe values of plankton between the two sites is not known, but may be related to the different abundances of organisms represented in the tows at each site (e.g., diatoms at ALOHA and 50:50 mixture of diatoms and Trichodesmium spp. at the 175°W site). It is interesting that δ^{56}Fe for plankton samples from the Pacific are isotopically lighter than plankton samples from the Atlantic. The cause of this difference is unknown, but could be indicative of differences between the two ocean basins such as the ultimate source of Fe (Asian versus Saharan dust), differing amounts of atmospheric processing and dissolution of aerosols, different inputs of deep water Fe to the euphotic zone, or could be a function of the biological cycling and residence time of Fe.

The mechanism responsible for the isotopically light Fe observed in the marine plankton tows is not known. However, one might imagine several possible mechanisms including:

1) fractionation of Fe during uptake and cycling by organisms
2) preferential release of isotopically light Fe during aerosol dissolution
3) preferential loss of heavy isotopes during scavenging and biological export of dissolved Fe from of the euphotic zone
4) input of another source of isotopically light Fe (lateral advection, vertical mixing, or upwelling)

It is not possible to evaluate the various proposed mechanisms with the data in this study. However, all the proposed mechanisms are plausible based on what is known about Fe cycling in the euphotic zone (Figure 1.3) and laboratory experiments of iron isotopic fractionation (Table 1.1). Several of pathways of Fe uptake, utilization, and chemical transformations could lead to isotopic fractionation. Fe is subject to biological uptake, biological recycling, photochemical reduction, ligand exchange chemistry, dissolution from particulate and colloidal phases, and scavenging in the surface ocean (reviews: SUNDA, 2001; MOFFETT, 2001). In culture experiments, organisms have been shown to

preferentially utilize isotopically light Fe with fractionation factors of 1 to 2‰ (BULLEN and MCMAHON, 1998; ANBAR et al., 1999; BEARD et al., 1999; BRANTLEY et al., 2001; BEARD et al., 2003a; ICOPINI et al., 2004; CROAL et al., in press). Although no experiments have been done with marine organisms, it is likely that they will fractionate Fe isotopes as well. Photoreduction and bioreduction pathways might also lead to isotopic fractionation. There is a large equilibrium fractionation between Fe(III) and Fe(II) aquo-complexes of 2.9‰ with the lighter isotope preferentially associated with the Fe(II) complexes (JOHNSON et al., 2002; WELCH et al., 2003).

Because the aerosol leachate measured in this study was isotopically identical to igneous rocks, it might be concluded that the second mechanism from above (Fe isotopic fractionation during aerosol dissolution) is not responsible for the observed light isotopic composition in the plankton samples. However, the aerosol leachate in this study may not be representative of dissolved Fe inputs to the ocean from atmospheric particles in nature. The aerosol leachate measured in this study was a 1 M HCl inorganic leach of an aerosol sample. Significantly more Fe was released by this harsh leach than would be released by seawater, and the mechanism by which the Fe was released does not mimic natural dissolution. Atmospheric particles undergo active redox and pH cycling in the atmosphere, which alters the chemical species and solubility of Fe, before they are deposited by either wet or dry deposition (SPOKES et al., 1994; SPOKES and JICKELLS, 1996; JICKELLS and SPOKES, 2001). Once in seawater, the soluble Fe precipitates quickly as hydrated Fe oxides or is complexed by organic ligands both in the soluble and colloidal size fractions (RUE and BRULAND, 1995; SPOKES and JICKELLS, 1996; WU et al., 2001). Fe in organic complexes or hydrated Fe oxides can be photochemically reduced to soluble Fe(II) and/or utilized by organisms (reviews: SUNDA, 2001; MOFFETT, 2001). Atmospheric Fe delivered in the solid phase is also subject to dissolution by organic ligands, photochemistry, and organisms (i.e. digestion, colonies forming around particles and creating more soluble micro-environments) (reviews: SUNDA, 2001; MOFFETT, 2001). Brantley et al. (2001) demonstrated that organic leaching and biotically enhanced dissolution of hornblende released isotopically light Fe (-0.6 to -0.8‰). There are many

steps in the dissolution of atmospherically derived Fe that may lead to fractionation. It is likely that Fe dissolution from atmospheric particles does not exceed 10% (JICKELLS, 1999). Therefore, it will be difficult to evaluate whether isotopically light Fe is preferentially released by studying the aerosol particles. Studies of dissolved Fe from rainwater may help resolve whether atmospheric cycling leads to fractionation. Dissolution of atmospheric Fe in seawater will be more difficult to assess as it is still an active area of research and the pathways by which dissolution occurs in nature are not well constrained (JICKELLS and SPOKES, 2001; SUNDA, 2001). More realistic leaching conditions (e.g., higher pH, model organic ligands) should be attempted.

The plankton tow δ^{56}Fe observations suggest that dissolved Fe delivered to the deep ocean via biological export might be isotopically light relative to igneous rocks. However most of the Fe in plankton is recycled in the euphotic zone by grazing, cell lysis, bacterial degradation, and excretion (HUTCHINS et al., 1993) prior to eventually being exported. Therefore, it is not necessarily the case that planktonic δ^{56}Fe will be the same as sinking organic matter. Sediment trap material needs to be measured in order to evaluate possible offsets, but preservation of Fe in sediment trap material will first need to be evaluated. Studies of dissolved seawater δ^{56}Fe will be more challenging because of the low concentrations, but they will be necessary in order to assess the mechanisms of fractionation in the marine system. It will be important to evaluate the upwelling/vertical mixing component of dissolved Fe input to the euphotic zone.

5.4. CONCLUSIONS

The δ^{56}Fe of plankton tow samples vary by over 4‰ from -3.87‰ to +0.36‰, and the aerosol leachate is indistinguishable from igneous rocks (Figure 5.2, Table 5.1). The range in the δ^{56}Fe of the plankton tow samples demonstrates that significant and potentially informative fractionation is associated with cycling of Fe in the upper ocean. The Fe in the plankton tow samples in this study is a mixture of intracellular and extracellular Fe adsorbed to the plankton. For plankton samples with Fe:C ratios greater than 70 μmol/mol, the δ^{56}Fe values are more variable and appear to be isotopically

heavier with increasing Fe:C ratios suggesting that extracellular Fe is isotopically heavier than the intracellular Fe. Plankton samples from the Atlantic scatter around a hypothetical mixing line between a planktonic intracellular δ^{56}Fe of ≈ -1.5‰ and an extracellular component of Fe that is isotopically similar to igneous rocks. The open ocean Pacific plankton samples (-2.1‰ to -3.9‰) are isotopically lighter than the Atlantic samples (+0.4‰ to –1.7‰), which may be due differences in the ultimate source of Fe or differences in the cycling and residence times of Fe. In order to find the cause of the observed fractionation in the plankton samples, the δ^{56}Fe of sinking organic matter, surface seawater, upwelled seawater, and more realistic atmospheric dissolution studies are needed. If the δ^{56}Fe of planktonic material is representative of sinking organic matter, then biological export and re-mineralization would be a significant source of isotopically light Fe to the deep ocean.

References for Chapter 5

Anbar A. D., Roe J. E., Holman E. S., Barling J., and Zhuang C. (1999) Biotic and abiotic fractionations of iron isotopes. *AGU Abstracts with Programs* **1999 AGU Fall Meeting**(B32A-20).

Beard B. L., Johnson C. L., Cox L., Sun H., Nealson K. H., and Aguilar C. (1999) Iron isotope biosignatures. *Science* **285**, 1889-1892.

Beard B. L. and Johnson C. M. (2004) Fe isotope variations in the modern and ancient earth and other planetary bodies. In *Geochemistry of Non-Traditional Stable Isotopes.*, Vol. 55 (ed. C. M. Johnson, B. L. Beard, and F. Albarede), pp. 319-357. The Mineralogical Society of America.

Beard B. L., Johnson C. M., Skulen K. H., Nealson K. H., Cox L., and Sun H. (2003a) Application of Fe isotopes to tracing the geochemical and biological cycling of Fe. *Chemical Geology* **195**, 87-117.

Beard B. L., Johnson C. M., Von Damm K. L., and Poulson R. (2003b) Iron isotope constraints on Fe cycling and mass balanced oxygenated Earth. *Geology* **31**, 629-632.

Boyd P. W., Watson A. J., Law C. S., Abraham E. R., Trull T., Murdoch R., Bakker D. C. E., Bowie A. R., Buesseler K. O., Chang H., Charette M., Croot P., and al e. (2000) A mesoscale phytoplankton bloom in the polar Southern Ocean stimulated by iron fertilization. *Nature* **407**, 695-702.

Boyle E. A., Bergquist B. A., and Kayser R. (submitted) Iron, manganese, and lead at Hawaii Ocean Time Series Station ALOHA: temporal variability and an intermediate water hydrothermal plum. *Geochimica et Cosmochimica Acta.*

Brantley S. L., Liermann L., and Bullen T. D. (2001) Fractionation of Fe isotopes by soil microbes and organic acids. *Geology* **29**(6), 535-538.

Brown J., Colling A., Park D., Phillips J., Rothery D., and Wright J. (1989) *Ocean Circulation.* Open University.

Bruland K. W., Donat J. R., and Hutchins D. A. (1991) Interactive influences of bioactive trace metals on biological production in oceanic waters. *Limnology and Oceanography* **36**, 1555-1577.

Bullen T. D. and McMahon P. M. (1998) Using stable isotopes to assess microbially-mediated Fe^{+3} reduction in a jet-fuel contaminated aquifer. *Mineralogical Magazine* **62A**, 255-256.

Chisholm S. W., Olson R. J., Zettler E. R., and Armbrust E. V. (1988) A novel free-living prochlorophyte abundant in the oceanic euphotic zone. *Nature* **334**, 340-343.

Chu N. C., Johnson C. M., Beard B. L., German C. R., Nesbitt R. W., and Usui A. (2003) Secular Fe isotope variations in the NW and Central Pacific Ocean. *Geochimica et Cosmochimica Acta* **67**, A66.

Coale K. H., Johnson K. S., Fitzwater S. E., Gordon R. M., Tanner S., Chavez F. P., Ferioli L., Sakamoto C., Rogers P., and Millero F., Steinberg, P., Nightingale, P., Cooper, D., Cochlan, W.P., Landry, M.R., Constantinou, J., Rollwagen, G., Trasvina, A., Kudela, R. (1996) A massive phytoplankton bloom induced by an

ecosystem-scale iron fertilization experiment in the equatorial Pacific Ocean. *Nature* **383**, 495-501.

Croal L. R., Johnson C. M., Beard B. L., and Newman D. K. (in press) Iron isotope fractionation by Fe(II)-oxidizing photoautotrophic bacteria. *Geochimica et Cosmochimica Acta.*

Duce R. A. and Tindale N. W. (1991) Atmospheric transport of iron and its deposition in the ocean. *Limnology and Oceanography* **36**, 1715-1726.

Duplessy J. C., Schackleton N. J., Fairbanks R. G., Labeyrie L., Oppo D., and Kallel N. (1988) Deepwater source variations during the last climatic cycle and their impact on the global deepwater circulation. *Paleoceanography* **3**, 343-360.

Falkowski P. G. (1998) Evolution of the nitrogen cycle and its influence on the biological sequestration of CO_2 in the ocean. *Nature* **387**, 272-275.

Francois R. F., Altabet M. A., Yu E. F., Sigman D. M., Bacon M. P., Frank M., Bohrmann G., Bareille G., and Labeyrie L. D. (1997) Water column stratification in the Southern Ocean contributed to the lowering of glacial atmospheric CO_2. *Nature* **389**, 929-935.

Fung I. Y., Meyn S. K., Tegen I., Doney S. C., John J. G., and Bishop K. B. (2000) Iron supply and demand in the upper ocean. *Global Biogeochemical Cycles* **14**, 281-295.

Gao Y., Kaufman Y. J., Tanre D., Kolber D., and Falkowski P. G. (2001) Seasonal distributions of aeolian iron fluxes to the global ocean. *Geophysical Research Letters* **28**, 29-32.

Hayes J. (1993) Factors controlling the ^{13}C contents of sedimentary organic compounds. *Marine Geology* **113**, 111-125.

Ho T., Quigg A., Finkel Z. V., Milligan A. J., Wyman K., Falkowski P. G., and Morel F. M. (2003) The elemental composition of some marine phytoplankton. *Journal of Phycology* **39**, 1145-1159.

Hutchins D. A., DiTullio G. R., and Bruland K. W. (1993) Iron and regenerated production: evidence for biological recycling in two marine environments. *Limnology and Oceanography* **38**, 1242-1255.

Icopini G. A., Anbar A. D., Ruebush S. S., Tien M., and Brantley S. L. (2004) Iron isotope fractionation during microbial reduction of iron: the importance of adsorption. *Geology* **32**, 205-208.

Jickells T. D. (1999) The inputs of dust derived elements to the Sargasso Sea: a synthesis. *Marine Chemistry* **68**, 5-14.

Jickells T. D. and Spokes L. J. (2001) Atmospheric iron inputs to the oceans. In *The Biogeochemistry of Iron in Seawater*, Vol. 7 (ed. K. A. Hunter and D. Turner), pp. 85-121. John Wiley & Sons, Ltd.

Johnson C. M., Skulan J. L., Beard B. L., Sun H., Nealson K. H., and Braterman P. S. (2002) Isotopic fractionation between Fe(III) and Fe(II) in aqueous solutions. *Earth and Planetary Science Letters* **195**(1-2), 141-153.

Johnson K. S., Gordon R. M., and Coale K. H. (1997) What controls dissolved iron concentrations in the world ocean. *Marine Chemistry* **57**, 137-161.

Karl D. M., Bidigare R. R., and Letelier R. M. (2001) Long-term changes in the plankton community structure and productivity in the North Pacific Subtropical Gyre: the domain shift hypothesis. *Deep-Sea Research Part II* **48**, 1149-1170.

Karl D. M., Letelier R. D., Tupas L., Dore J., Christian J., and Hebel D. (1997) The role of nitrogen fixation in biogeochemical cycling in the subtropical North Pacific Ocean. *Nature* **388**, 533-537.

Karl D. M. and Michaels A. F. (1996) Preface: The Hawaiian Ocean Time-series (HOT) and Bermuda Atlantic Time-series Study (BATS). *Deep-Sea Research Part II* **43**, 127-128.

Kustka A. B., Sanudo-Wilhelmy S. A., Carpenter E. J., Capone D. G., Burns J., and Sunda W. G. (2003) Iron requirements for dinitrogen- and ammonium-supported growth in cultures of Trichodesmium (IMS 101): comparison with nitrogen fixation rates and iron: carbon ratios of field populations. *Limnology and Oceanography* **48**(5), 1869-1884.

Mahowald N., Kohfeld K., Hansson M., Balkanski Y., Harrison S. P., Prentice I. C., Schulz M., and Rodhe H. (1999) Dust sources and deposition during the last glacial maximum and current climate: a comparison of model results with paleodata from ice cores and marine sediments. *Journal of Geophysical Research* **104**, 15895-15916.

Martin J. H. (1990) Glacial-interglacial CO_2 change: the iron hypothesis. *Paleoceanography* **5**, 1-13.

Martin J. H., Coale K. H., Johnson K. S., Fitzwater S. E., Gordon R. M., and Tanner S. J., Hunter, C.N., Elrod, V.A., Nowicki, J.L., Coely, T.L., Barber, R.T., Lindley, S., Watson, A.J., van Scoy, K., Law, C.S., Liddicoat, M.I., Ling, R., Stanton, T., Stockel, J., Collins, C., Anderson, A., Bidigare, R., Ondrusek, M., Latasa, M., Millero, F.J., Lee, K., Yao, W., Zhang, J.Z., Friederich, G., Sakamoto, C., Chevez, F., Buck, K., Kolber, Z., Greene, R., Falkowski, P., Chisholm, S.W., Hoge, F., Swift, R., Yungel, J., Turner, S., Nightingale, P., Hatton, A., Liss, P., Tindale, N.W. (1994) Testing the iron hypothesis in ecosystems of the equatorial Pacific Ocean. *Nature* **371**, 123-129.

Martin J. H. and Fitzwater S. E. (1988) Iron deficiency limits phytoplankton growth in the north-east Pacific subarctic. *Nature* **331**, 341-343.

Martin J. H. and Knauer G. A. (1973) The elemental composition of plankton. *Geochimica et Cosmochimica Acta* **37**(1639-1653).

Parekh P., Follows M. J., and Boyle E. A. (2004) Modeling the global ocean iron cycle. *Global Biogeochemical Cycles* **18**(GB1002), 1-15.

Parrington J. R., Zoller W. H., and Aras N. K. (1983) Asian dust: seasonal transport to the Hawaiian Islands. *Science* **220**, 195-198.

Partensky F., Hess W. R., and Vaulot D. (1999) Prochlorochoccus, a marine photosynthetic prokaryote of global significance. *Microbial and Molecular Biology Reviews* **63**, 103-127.

Prospero J. M. (1996) The atmospheric transport of particles to the ocean. In *Particle Flux in the Ocean*, Vol. SCOPE Rep. 57 (ed. V. Ittekkott, P. Schafer, S. Honjo, and P. J. Depestris), pp. 19-52. John Wiley.

Redfield A. C., Ketchum B. H., and Richards F. A. (1963) The influence of organisms on the composition of sea-water. In *The Sea* (ed. M. N. Hill), pp. 26-77. Interscience.

Rouxel O., Dobbek N., Ludden J., and Fouquet Y. (2003) Iron isotope fractionation during oceanic crust alteration. *Chemical Geology* **202**(1-2), 155-182.

Rouxel O., Fouquet Y., and Ludden J. N. (2004) Subsurface processes at the Lucky Strike hydrothermal field, Mid-Atlantic Ridge: evidence from sulfur, selenium, and iron isotopes. *Geochimica et Cosmochimica Acta* **68**, 2295-2311.

Rue E. L. and Bruland K. W. (1995) Complexation of iron(III) by natural ligands in the central North Pacific as determined by a new competitive ligand equilibrium/adsorptive cathodic stripping voltammetric method. *Marine Chemistry* **50**, 117-138.

Schmit M. A. and Hutchins D. A. (1999) Size fractionated biological iron and carbon uptake along a coastal to offshore transect in the NE Pacific. *Deep-Sea Research Part II* **46**, 2487-2503.

Severmann S., Johnson C. M., Beard B. L., German C. R., Edmonds H. N., Chiba H., and Green D. H. (in press) Origin of the Fe isotope composition of the oceans as inferred by Rainbow vent site, Mid-Atlantic Ridge, 36deg14'N. *Earth and Planetary Science Letters.*

Severmann S., McManus J., Johnson C. M., and Beard B. L. (2003) Iron isotope geochemistry in California Margin sediments and porewaters. *Eos Trans. AGU, Ocean Science Meeting Supplement* **84**, Abstract#OS31L-019.

Sharma. (2001) Iron isotopes in hot springs along the Juan de Fuca Ridge. *Earth and Planetary Science Letters* **194**, 39-51.

Siegel D. A., Karl D. M., and Michaels A. F. (2001) Interpretations of the biogeochemical processes from the US JGOFS Bermuda and Hawaii time-series sites. *Deep-Sea Research Part II* **48**, 1403-1404.

Sigman D. M., Altabet M. A., Francois R., McCorkle D. C., and Gaillard J.-F. (1999) The isotopic composition of diatom-bound nitrogen in Southern Ocean sediments. *Paleoceanography* **14**, 118-134.

Spokes L. J. and Jickells T. D. (1996) Factors controlling the solubility of aerosol trace metals in the atmosphere and on mixing into seawater. *Aquatic Geochemistry* **1**, 355-374.

Spokes L. J., Jickells T. D., and Lim B. (1994) Solubilization of aerosol trace metals by cloud processing: A laboratory study. *Geochimica et Cosmochimica Acta* **58**, 3281-3287.

Stookey L. C. (1970) Ferrozine – a new spectrophotometric reagent for iron. *Analytical Chemistry* **42**, 779-781.

Sunda W. (2001) Bioavailability and bioaccumulation of iron in the sea. In *The Biogeochemistry of Iron in Seawater*, Vol. 7 (ed. K. A. Hunter and D. Turner), pp. 123-253. John Wiley & Sons, Ltd.

Sunda W. G. and Huntsman S. A. (1995) Iron uptake and growth limitation in oceanic and coastal phytoplankton. *Marine Chemistry* **50**(189-206).

Tovar-Sanchez A., Sanudo-Wilhelmy S. A., Garcia-Vargas M., Weaver R. S., Popels L. C., and Hutchins D. A. (2003) A trace metal clean reagent to remove surface-bound iron from marine phytoplankton. *Marine Chemistry* **82**, 91-99.

Vink S., Boyle E. A., Measures C. I., and Yuan J. (2000) Automated high resolution determination of the trace elements iron and aluminum in the surface ocean using towed Fish coupled to a flow injection analysis. *Deep-Sea Research I* **47**, 1141-1156.

Vink S. and Measures C. I. (2001) The role of dust deposition in determining surface water distributions of Al and Fe in the South West Atlantic. *Deep-Sea Research II* **48**, 2787-2809.

Welch S. A., Beard B. L., Johnson C. M., and Braterman P. S. (2003) Kinetic and equilibrium Fe isotope fractionation between aqueous Fe(II) and Fe(III). *Geochimica et Cosmochimica Acta* **67**(22), 4231-4250.

Wu J., Boyle E. A., Sunda W., and Wen L. (2001) Soluble and colloidal iron in the oligotrophic North Atlantic and North Pacific. *Science* **293**, 847-849.

Wu J. and Luther G. W. (1996) Spatial and temporal distribution of iron in surface water of the northwest Atlantic Ocean. *Geochimica et Cosmochimica Acta* **60**, 2729-2741.

Yamaguchi K. E., Beard B. L., Johnson C. M., Ohkouchi N., and Ohmoto H. (2003) Iron isotope evidence for redox stratification of the Archean oceans. *Geochimica et Cosmochimica Acta* **67**, A550.

Zhu X. K., O'Nions R. K., Guo Y. L., and Reynolds B. C. (2000) Secular variation of iron isotopes in North Atlantic Deep Water. *Science* **287**(5460), 2000-2002.

Chapter 6

Iron Isotopes in the Amazon River System

6.1. Introduction

Current studies of iron isotopes have demonstrated that Fe isotopes can vary up to 4‰ (δ^{56}Fe, section 6.2.6) in natural samples (reviews: Beard et al., 2003a; Beard and Johnson, 2004). Most of the natural samples that show significant Fe isotopic variability are samples that formed at the earth surface where Fe has been in the dissolved phase and likely participated in redox transitions and chemical and/or biological cycling. The variability observed in low temperature samples contrasts the homogeneity observed in igneous rocks, the ultimate source of iron, which show very little isotopic variability, ± 0.10‰ (2σ standard deviation) (Beard et al., 2003a). Much of the variability that has been documented in nature is from samples where Fe is in the solid phase, e.g., banded iron formations, Fe-Mn crusts and nodules, paleosols, black shales, hydrothermal deposits (Beard and Johnson, 1999; Zhu et al., 2000; Beard et al., 2003a; Beard et al., 2003b; Johnson et al., 2003; Rouxel et al., 2003; Arnold et al., 2004; Rouxel et al., 2004). In order to use Fe isotopic signatures to unravel the geochemistry of Fe, we must study and understand how Fe isotopes are mobilized, transported, and fractionated in the dissolved and biological phases. Then it might be possible to interpret past and present iron isotope variations in nature.

Most studies of Fe isotope fractionation in aqueous and biological systems have been controlled laboratory studies (Bullen and McMahon, 1998; Beard et al., 1999; Brantley et al., 1999; Anbar et al., 2000; Brantley et al., 2001; Bullen et al., 2001; Matthews et al., 2001; Johnson et al., 2002; Levasseur et al., 2002; Roe et al., 2003; Welch et al., 2003; Croal et al., in press; Brantley et al., submitted), which are extremely useful in trying to isolate and understand the mechanisms of isotope fractionation. For example, Fe reducing bacteria produce Fe(II) that is isotopically lighter (-1.3‰) than the source Fe(III) (Beard et al., 1999; Beard et al., 2003a;

BRANTLEY et al., submitted). In contrast, there have only been a few studies of aqueous iron isotopes in natural systems and non-laboratory biological samples (where presumably Fe fractionation in the environment occurs). Iron from mid-ocean ridge hydrothermal vents (SHARMA, 2001; BEARD et al., 2003b; SEVERMANN et al., in press) is isotopically light relative to igneous sources (-0.2 to -0.7‰). Porewater Fe from the California margin shows isotopic variability with δ^{56}Fe values as negative as -1.3‰ relative to igneous rocks (SEVERMANN et al., 2003). A terrestrial hot spring Fe(III) deposit was isotopically heavy by +0.8‰ relative to the dissolved Fe(II) from which it precipitated (BULLEN et al., 2001). Human blood and haemoglobin from animals are also isotopically light compared with dietary sources (WALYCZYK and VON BLANCKENBURG, 2002; ZHU et al., 2002; OHNO et al., 2004).

There has been some speculation that dissolved Fe inputs to the ocean via rivers or dissolution of lithogenic aerosols might be isotopically similar to igneous rocks, based on the observed isotopic homogeneity of continental rocks, river suspended material, soils, aerosols, and loess (BEARD et al., 2003b; BEARD and JOHNSON, 2004). Considering that only a few percent of Fe is mobilized into the dissolved phase in many environments, it would be extremely difficult to detect variations in dissolved Fe inputs from their source rocks and sediments. Even if 10% of the Fe was mobilized from a rock source (0‰) and the mobilized Fe was isotopically light by 1‰, the rock phase would be istopically heavier by only 0.1‰ (close to the analytical limits of detection). Brantley et al. (2001) demonstrated that organic leaching of hornblende produced Fe in solution that was up to -0.6‰ lighter than the hornblende Fe and that biotically enhanced dissolution by siderophore producing bacteria resulted in even lighter dissolved Fe (-0.8‰). In highly altered marine oceanic basalts where 80% of the Fe has been leached by mid-ocean ridge hydrothermal fluids, the resulting altered basalts are isotopically heavy compared with unaltered crust (ROUXEL et al., 2003).

Systematic Fe isotope investigations of aqueous systems could potentially provide fundamental constraints and insights into the physical, chemical, and biological cycling of Fe. A potentially interesting region to study for Fe isotopic variations is the Amazon

system, one of the most intense weathering systems in the world (STALLARD, 1980; STALLARD and EDMOND, 1983; GAILLARDET et al., 1997). It is also relatively free of human impact and is ideal for investigating natural processes. The Amazon river supplies approximately 20% of the freshwater flux to the ocean (6×10^{15} L/yr), and Amazon fine-grained material is dispersed along the shelf of South America from the equator to the Orinoco river ($\approx$ 1600 km) (MEADE et al., 1985). Low salinity plumes from the Amazon outflow can be detected as far away as Barbados, Puerto Rico, and $\approx$ 20°N in the western Atlantic Ocean (STEVEN and BROOKS, 1972; DESSIER and DONGUY, 1993; HELLWEGER and GORDON, 2002). The Amazon plume water can also be identified from ocean color satellite images due to the high productivity resulting from the high nutrient concentrations in this water (MULLER-KARGER et al., 1988; SIGNORINI et al., 1999; FROIDEFOND et al., 2002). Tracer studies and models have established that the major source of the freshwater in the low salinity plumes in the western equatorial Atlantic is the Amazon River (STEVEN and BROOKS, 1972; BORSTAD, 1982; KELLY et al., 2000; HELLWEGER and GORDON, 2002). The Orinoco River does not have the required freshwater flow or the right pattern of outflow to explain salinity variations at Barbados (HELLWEGER and GORDON, 2002). The depth penetration of the Amazon plume water in the open ocean is dependent on vertical mixing (e.g., wind), but is usually constrained to the upper 30 m (HELLWEGER and GORDON, 2002). Salinity and fluorescence (measure of chlorophyll) depth profiles from the upper 100 m at the open ocean site sampled in this study (10.5°N, 56.6°W) are shown in Figure 6.1. The low salinity and high chlorophyll plume is evident in the upper 25 m.

Although it is likely that much of the Fe in the Amazon plume water in the open ocean is from Amazon sources, the Fe has undergone a chemically complicated path from dissolution from rock and soil sources to the open ocean. The Amazon drains a variety of geological and weathering regions. A significant fraction (40 to 60%) of the major dissolved load (STALLARD, 1980) and roughly 60% of the suspended sediment load (CALLEDE et al., 1997) of the Amazon River is estimated to be from the Solimões River. The Solimões River is the section of the Amazon River up-stream from Manaus draining

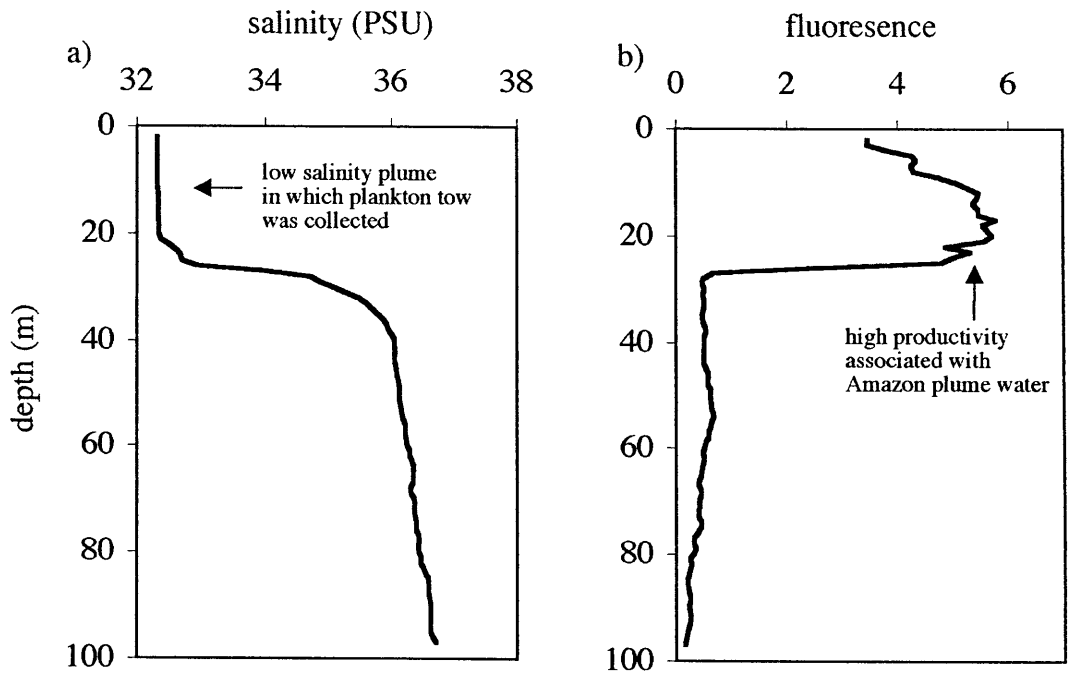

Figure 6.1: Salinity (1a) and fluorescence (1b) depth profile from a sample site (plankton tow) in the eastern tropical Atlantic Ocean at 10.5°N, 56.0°W. The low salinity plume in the upper 25 m is interpreted to be from freshwater input from the Amazon River (≈ 1000 km from the mouth of the Amazon).

Table 6.1: Summary of Properties at River Sampling Sites

Station	water discharge ($m^3x10^3 s^{-1}$)	suspended sediment (mg/L)	Fe concentration in suspended sediment (ppm)	pH	T (°C)	TOC (μM)	dissolved Fe concentration in river (μM)
Macapá [a]	174[b]	50-235[c]	60000[d]	6.8[e]	27[e]	529[e]	2.5[f]
Solimões	85-115[g]	53-226[b&d]	55000[d]	6.7-7.2[e]	27-28[e]	530[e]	0.6-2.1[f]
Negro	20-40[h]	5-12	41400[d]	4.8-5.4[e]	29[e]	763[e]	4.6[f]

a) Estimates of water flow, suspended sediment, and pH estimated for this site based on data from an upriver site at Óbidos.

b) Meade et al. (1985); c) Meade et al. (1979); d) Gaillardet et al. (1997); e) Stallard (1980)

f) This study. Concentration data from the filtered samples (<0.4 μm) measured for Fe isotopic composition. Concentrations agree with previously reported values for the Solimões and Negro rivers from Stallard (1980).

g) HIBAM; h) Brinkmann (1987)

the Andean Cordillera and accounts for roughly half of the Amazon River water budget (HIBAM, 1999). The trace element budget (including Fe) of the Amazon River is not as well constrained, and many trace elements are decoupled from major dissolved ion chemistry. For example, Fe is enriched in rivers that have high levels of organic material and lower pH (e.g., Negro River, 4.5 μM Fe, pH 4.8) compared with higher pH rivers like the Solimões (1 μM Fe, pH > 6.8) (STALLARD, 1980; SEYLER and BOAVENTURA, 2001). Stallard (1980) found a strong correlation between dissolved organic matter (and pH) and Fe over much of the Amazon drainage basin suggesting that tributaries rich in organic matter play an important role in the budget of Fe in the Amazon system. The Negro River tributary, which joins the Solimões River at Manaus, is a significant tributary in that it has relatively high concentrations of trace elements (Cr, Mn, Co, Ni, Al, Fe) and accounts for approximately 15% of the Amazon water budget (STALLARD, 1980; MEADE et al., 1985; SEYLER and BOAVENTURA, 2001). The Negro River drains the highly weathered Precambrian Shield and the fluvio-lacustrine sediments of the lowlands in the Amazon Basin (STALLARD, 1980). It has a low suspended load and ≈ 50% of the total Fe in the river is carried in the dissolved load, as opposed to the Solimões River where ≈ 0.5% of the Fe is in the dissolved pool (calculations made using data from: STALLARD, 1980; MEADE et al., 1985; BRINKMANN, 1987; GAILLARDET et al., 1997). A summary of the some of the properties of the Negro River, Solimões River, and Amazon River near Macapá is given in Table 6.1.

Another complication for establishing the riverine dissolved Fe input to the ocean is that the flux is largely modified by mixing with ocean water in estuaries. A large fraction of the dissolved Fe flocculates (>90%) from solution in association with high molecular weight organic matter (0.1 to 0.45 μm) upon mixing with high salinity ocean water (SHOLKOVITZ, 1976; BOYLE et al., 1977; SHOLKOVITZ et al., 1978). "Dissolved" Fe (Fe that passes through a 0.2 or 0.4 μm filter) is largely bound to organic colloids or present as Fe oxide or clay colloids, which are stabilized in solution by a slightly negative surface charge. Upon mixing with seawater (high ionic strength), cations neutralize the colloids and they coagulate into large particles that can settle out of solution

(flocculation). The extent to which flocculation reduces the Fe flux from rivers to the coastal ocean varies and depends on river type and composition, but more than 95% of Fe is removed by flocculation in the Amazon River system (SHOLKOVITZ et al., 1978).

Another potential source of Fe to the Amazon plume water and coastal water is from re-suspension of sediments along the dynamic shelf region of South American north of the Amazon mouth (JOHNSON et al., 1999). The Amazon shelf region is characterized by large mudwaves, which advance at 1-3 km/year, made up of Amazon fine-grained material. The mudwaves are 5 to 10 m thick and 10 to 60 km in length (FROIDEFOND et al., 1988). The large organic input to these shelf deposits would lead to anoxic, sulfidic conditions in less dynamic environments, but frequent reworking and re-suspension of the sediments maintains suboxic conditions in the upper meter where microbial Fe and Mn reduction pathways dominate organic matter decomposition (ALLER et al., 1986; ALLER et al., 1996; ALLER, 1998; ALLER et al., in press). Oxygen and nitrate are consumed at shallow depths in the sediments (within 2-6 mm for O_2 and 3 cm for NO_3^-), and dissolved Fe(II) and Mn(II) build up to high concentrations within centimeters of the surface (>0.5 mM for Fe, and 0.1-0.3 mM for Mn). Sediments reach anoxic, sulfate reducing conditions at depths greater than one meter. From the porewater profiles and ^{234}Th data, it is estimated that the upper meter of the shelf deposits are reworked on a monthly timescale (ALLER et al., in press). When the sediments are re-suspended, the mobile Fe(II) is mixed into oxic bottom water and re-oxidized, thereby replenishing the reactive Fe oxide supply to the sediments. Authigenic Fe(II) mineral formation is also common along the shelf. Aller et al. (2004) estimated that 10 to 50% of the reactive Fe in the sediments (Fe mobilized by a 15 min dissolution with 6 N HCl) was in the form of Fe(II) minerals, most likely siderite and authigenic K-Fe-Mg aluminosilicate minerals (MICHALOPOULAS and ALLER, 1995; MICHALOPOULAS et al., 2000). The high levels of dissolved Fe and reactive Fe solids in the porewaters and frequent re-suspension of the Amazon shelf deposits could result in a significant source of Fe to the shelf water column and Amazon plume water.

This study was motivated by one of the first samples measured for Fe isotopic composition by our lab, a plankton tow collected in the western tropical Atlantic at 10.5°N, 56.6°W in the upper 5 m of a low salinity (32 PSU) plume (Figure 6.1a). It was interpreted from the low salinity (32 PSU) and high total Fe of the plume water (≈ 7 nM) that the freshwater source and elevated Fe concentrations for this water were likely from the Amazon River and shelf region. Initial isotopic results indicated that the Fe from this plankton tow had a $\delta^{56}Fe$ of -0.34‰ relative to igneous rocks (BERGQUIST and BOYLE, 2001). The Fe isolated from this plankton tow is dominantly a mixture of intracellular Fe and Fe attached to the surface of the biomass (both adsorbed and particulate). In order to interpret the $\delta^{56}Fe$ of this plankton tow, the isotopic composition of the source of Fe for the Amazon plume plankton tow was needed. Filtered river water (0.4 μm) and suspended material were collected at three sites in the Amazon River system: 1) the Amazon River near the mouth at Macapá, 2) the Solimões River near Manaus, and 3) the Negro River near Manaus. River water-seawater mixing experiments were performed both with Amazon River water at Macapá and the Solimões River water near Manaus. An Amazon shelf porewater sample from the upper 10 cm of sediment (courtesy of Dr. R. Aller) was also analyzed to assess the potential source of Fe from re-suspension of shelf sediments. Sample collection locations are shown in Figure 6.2.

6.2. SITES, SAMPLE COLLECTION, AND METHODS

6.2.1. River Dissolved Fe and Suspended Sediment

Filtered river samples and suspended sediment samples were collected at three sites in the Amazon region in April, 2002. Two main channel sites were chosen, both at the mouth of the Amazon River at Macapá and upstream of Manaus in what is considered the main tributary of the Amazon River, the Solimões River. A third site, the Negro River, was also sampled in order to characterize an organic rich tributary. The Macapá site was chosen in order to sample a site of the Amazon River near the mouth that is relatively free from industrial development. The Manaus site was chosen because it is near the confluence of the two very different tributaries, the Solimões River and the

Negro River. These two rivers represent two extreme river types in the Amazon system. As stated before, the Solimões River carries half of the major-ion dissolved load and the water budget of the Amazon River. This river is draining the Peruvian Andes, it is relatively cool, has a high suspended sediment load, and a high pH (>6.8). In contrast, the Negro River drains the lowlands that includes the most weathered terrain in the Amazon (STALLARD, 1980). It is warmer than the Solimões River by 1-2°C, has a high concentration of organic matter, a low suspended sediment load, and a significantly lower pH of 4.8. A summary of the different properties of the river sites and their references are given in Table 6.1. Because of the different densities of these two rivers, they do not mix for tens of kilometers after they merge near Manaus (Figure 6.2b).

At each of the three sites, filtered river water samples and suspended sediment samples were collected in the river channel at least 1 km from the river bank. Water samples were collected, using a plastic pole sampler with an acid cleaned polyethylene (HDPE) bottle attached to the end, upstream and to the side of a small boat while the boat moved forward. Multiple samples were collected in one liter acid cleaned polyethylene bottles, and each sample was vacuum-filtered twice through 0.4 μm acid cleaned and trace metal clean water rinsed Nuclepore filters within 12 to 24 hours of collection. Rivers with high suspended loads are notorious for particles leaking through the filter during filtration, therefore each sample collected for dissolved Fe was filtered twice. Filtered samples were acidified two weeks after collection at MIT in a class 100 clean laminar flow environment with trace metal clean 6 M HCl, which was purified by triple distillation in a Vycor still, in a ratio of 1 ml acid to 1 L of sample . The suspended sediment samples and filters were placed in acid cleaned plastic filter holders and stored with the sediment side of the filter up.

Approximately 200 ml of an acidified river sample was evaporated inside a class 100 clean laminar flow environment by multiple additions to a 100 ml Teflon beaker with a small amount of HNO_3 (Optima grade) and a drop of diluted H_2O_2 (EM Science, reagent grade) to create an oxidative environment. When the volume was small enough, the sample was transferred to a quartz beaker and taken to dryness prior to combustion.

a)

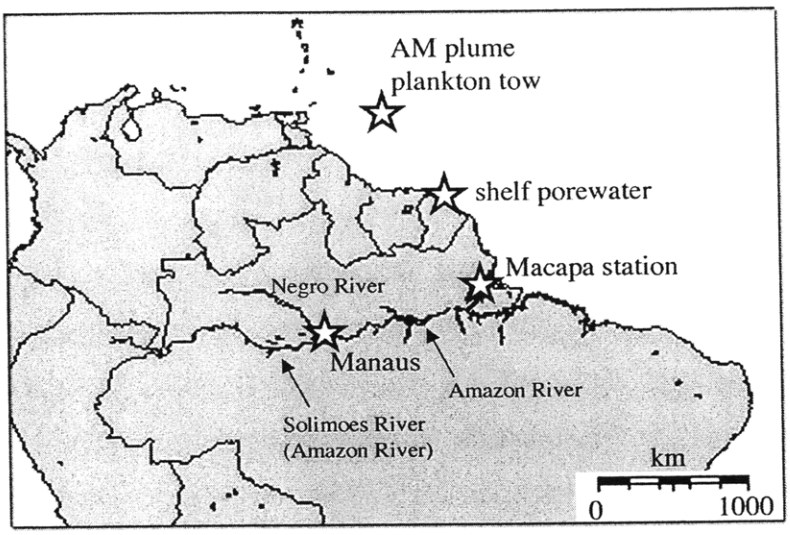

b)

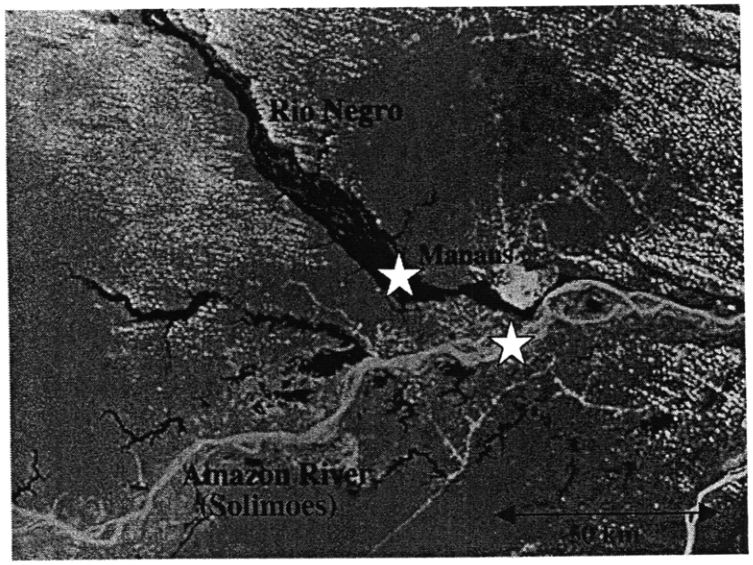

Figure 6.2: Locations (☆) where samples were collected in the Amazon River region including an open ocean site where a plankton tow was collected in Amazon River plume water. 6.2a) Sample locations for the Amazon plume plankton tow, the porewater sample (courtesy of Dr. R. Aller), and Amazon river samples. River water-seawater mixing experiments were performed at both the Macapá and Manaus (Solimões river) station. 6.2b) Satellite image of two of the main tributaries of the Amazon river converging near Manaus (Global Resource Information Data Base, http://www.grid.inpe.br/). The Negro River is an organic rich, low pH (4.8), warm river draining the Amazon lowlands. The Solimões River, which is also considered the Amazon River upstream of the convergence, is a sediment rich, higher pH (>6.8), colder river draining the Andean Cordillera. The water of the two rivers does not mix for tens of kilometers due to the density difference. The stars indicate where river samples were taken up-river of the confluence of the rivers near Manaus.

Suspended sediment samples were dissolved in a 4:1 HF:HNO_3 solution (Seastar or Optima grade) at 80°C for 4-5 days. Samples were then evaporated to dryness several times with HCl and HNO_3 to evaporate excess HF, transferred to quartz beakers, and evaporated to dryness in a class 100 laminar flow clean environment prior to combustion.

6.2.2. River Water-Seawater Mixing Experiments

River water-seawater experiments were performed based on the experimental methods outlined in Sholkovitz (1976). Trace metal clean surface seawater (4 L) was collected one week prior to Amazon field trip during the March 2002 R/V Endeavor 367 cruise (24.5°S, 37°W). Surface seawater was collected with a "towed fish" sampling device (VINK et al., 2000), filtered through acid cleaned 0.4 μm Nuclepore filters rinsed with seawater, and refrigerated. River water-seawater mixing experiments were performed at both the Macapá and the Solimões River sampling sites. River water (1 to 2 L) was collected, filtered twice through acid cleaned and trace metal clean water rinsed 0.4 μm Nuclepore filters, and then homogenized prior to the experiments. In order to have enough iron for iron isotope analysis, ≈ 200 ml of river water was used in each river water-seawater mixing experiment and the amount of seawater varied to achieve different final salinities in the mixtures. The different ratios of the filtered river water and seawater were mixed together in acid cleaned 500 ml polyethylene (HPDE) bottles and allowed to mix for a few hours to allow the organic matter to coagulate and flocculate. Sholkovitz (1976) found no difference between experiments performed for one half hour and for 24 hours. After letting the mixture stand, the mixtures were filtered and the flocculent collected on 0.4 μm Nuclepore filters. Filtrates were acidified with triply distilled Vycor 6 M HCl (1 ml acid to 1 L solution). The filters were folded with Teflon tweezers to trap the flocculent, placed in acid cleaned polyethylene bottles, and frozen.

Filtrates were analyzed for their Fe concentration (not for Fe isotopes), and the flocculents analyzed for their Fe isotopic composition. The flocculants were thawed, and the Fe dissolved with 5 ml of 1 M HCl (triply distilled Vycor) and 0.5 M HNO_3 (Optima grade). Sholkovitz (1976) demonstrated that Fe attached to the flocculated organic

material could be released into solution by decreasing the pH to less than 2. The acidic solution was warmed for one hour (60°C) and allowed to sit overnight for complete leaching. The leachate was transferred to a quartz beaker and taken to dryness in a class 100 clean laminar flow environment prior to combustion.

6.2.3. Amazon Shelf Porewater

The Amazon-Guianas shelf porewater was collected by Dr. R. Aller and colleagues in June 2003, 6-7 km off shore, and 3 km west of the Sinnamary River mouth (5.5°N, 53.0°W) just behind the leading edge of a coastal mudwave. A description of the sample collection and methods for storage can be found in Aller et al. (in press). Sediment was sampled by diving and inserting plastic tubes into the seabed. Cores were capped, and stored in an insulated box (care was taken not to disturb the sediment-water interface) before samples were returned to the lab (within 3-4 hours of collection). The sample measured for Fe isotopic composition was a 0-10 cm sample, in which the bottom water was removed and the mud stored in a polyethylene bottle inside an oxygen impermeable bag until the sample was sent to MIT. For porewater separation, the sample was centrifuged in the oxygen impermeable bag, and then transferred to a N_2 filled glove box for handling and filtration. Acid cleaned and trace metal clean water rinsed 0.2 μm cellulose acetate syringe filters plus plastic syringes (without o-ring) were placed in the N_2 filled glove box and degassed three times. The sample was opened in the glove box and poured into the syringe for filtration. Several milliliters of the porewater were used to rinse the filter and acid cleaned polyethylene collection bottles before two sequential 20 ml splits of the porewater were collected (A and B). Porewater samples were acidified with 100 μl additions of Vycor triply distilled 6 M HCl and stored until analysis. Splits of the acidified porewaters were transferred to a quartz beaker and taken to dryness in a class 100 clean laminar flow environment prior to combustion.

6.2.4. Amazon Plume Plankton Tow

The plankton tow sample was collected on July 20, 2001 (R/V Knorr, Kn162 cruise) in the western tropical Atlantic (10.5 °N, 56.6 °W) at 5 m depth in a 25 m deep low salinity cap (32 PSU) overlying 36 PSU seawater (Figure 6.1a). Light penetration was only a few meters due to a large bloom of larvaceans ("salps") and diatoms with symbiotic nitrogen fixers. The trace metal clean horizontal plankton tow was performed employing techniques similar to those described in Collier and Edmond (1984). A 64 μm nylon mesh plankton tow with a plastic ring and fittings (Sea-Gear Corporation) was deployed from a nylon rope with plastic coated lead weights from the side of the ship. Some organisms smaller than 64 μm are retained by the net due to mesh clogging and turbulent flow in the net, but the abundance of smaller organisms is not known (and organisms smaller than 10 to 20 μm are probably not retained). Care was taken to ensure that the plankton net never touched the side of the ship and was only handled by gloved hands. The lead weights were deployed first and were separated from the plankton tow by 6 m of nylon rope. Plankton tows were performed 3 to 5 m from the side of the ship with the ship steaming at 1-2 knots. Therefore, the plankton tow sampled water moving parallel to the ship and not water that had contact with the ship. This technique is commonly used in trace metal surface water sampling (e.g., "towed fish" device (VINK et al., 2000)). Between deployments, the plankton tow was stored in an EDTA solution and then deployed without a collection bottle (cod end) for at least 5 minutes to flush the plankton net thoroughly with seawater prior to sample collection.

At the sampling site, three 10 minute tows were performed to accumulate enough biomass for Fe isotope analysis. Two of the plankton tows were immediately vacuum filtered sequentially through acid cleaned and seawater rinsed 10 μm and 1 μm Nuclepore polycarbonate filters in class 100 clean laminar flow benches. Complete filtration took several hours, and samples were refrigerated until filtered. Plankton material plus filters were frozen and the final filtrate (< 1 μm) acidified and archived. The third plankton tow was split into two 250 ml acid cleaned polycarbonate bottles, frozen, and archived. For Fe isotope analysis, the frozen plankton tow filters were

thawed and a split transferred to a quartz beaker with an acid-cleaned plastic scoop or pipette tip. Samples were dried on a hot plate overnight (60 to 80°C) prior to combustion. Organic carbon estimates (for Fe:C ratios) were estimated by weighing the sample before and after the muffle furnace combustion and assuming complete combustion of organic carbon to CO_2. This method underestimates the amount of organic carbon by approximately 40% (based on a comparison to estimates made from phosphate measurements made on later plankton tow samples), and Fe:C estimates were adjusted for the Amazon plume plankton tow assuming this value.

At the plankton tow site, trace metal clean surface seawater was collected over a period of 4 days by a drifting buoy array with the automated MITESS water sampler (BELL et al., 2002) attached at approximately 10 m depth. Six samples were collected over 4 days and acidified upon retrieval of the drifting array with Vycor triply distilled 6 M HCl (ratio 1 ml acid to 500 ml seawater). Iron concentrations measured from these samples represent total Fe measurements.

6.2.5. Fe Concentration Measurements

For samples with higher Fe concentrations and for determining sample post-column recoveries, Fe concentrations were measured by UV-VIS spectroscopy using the Ferrozine method (STOOKEY, 1970) separating the Ferrozine and hydroxylamine hydrochloride reagents (to avoid precipitation of the Ferrozine with HCl). This method has a detection limit of 0.2 μM using a 1 cm pathlength cell and lab-grade reagents. Process blanks were always below the detection limit by the Ferrozine UV-VIS method, therefore blanks were measured on the IsoProbe using a simple two-point linear calibration curve. Seawater Fe concentrations were analyzed by isotope dilution MC-ICPMS ($Mg(OH)_2$ co-precipitation) by a modified version of a method developed by Wu et al. (2001) (BERGQUIST AND BOYLE, in prep). See Chapter 2 for more details.

6.2.6. Fe Purification and Isotopic Analysis

Methods for Fe purification, separation, and Fe isotopic analysis are described in Chapter 4. Briefly, all samples are combusted at 550°C for 8 hours, re-dissolved in 7 M HCl (Optima grade), and purified by anion exchange chromatography. Approximately 300 ng of Fe was used for measurement of Fe isotopic composition on the MIT GV Instruments IsoProbe MC-ICPMS. Instrumental mass bias was corrected for using standard-sample bracketing (SSB), and matrix effects on the instrument mass bias were evaluated using "standard isotope dilution" (also discussed in detail in Chapter 4). All sample Fe isotope data is reported in delta notation:

$$\delta^{56}Fe\ (‰) = \left(\frac{^{56}Fe/^{54}Fe_{sample}}{^{56}Fe/^{54}Fe_{standard}} - 1 \right) \times 1000$$

Samples are referenced to the mean of all the individual analysis of seven splits of Rhode Island Granite (USGS, G-2) and Hawaiian Basalt (USGS, BVHO-1), which had a an average $\delta^{56}Fe_{wrk\ std}$ of -0.23 ± 0.04‰ (2σ, n=30) (see Table 4.6) or a $\delta^{56}Fe$ of 0.00 ± 0.04‰ (2σ, n=30) when referenced to themselves. Some laboratories use the IRMM-014 standard as a reference material instead of igneous rocks. The measured difference between igneous rock and the IRMM-014 standard was -0.13 ± 0.07‰ (2σ, n=12), which agrees well with estimates of -0.09 ± 0.01‰ (2σ, n=52) by Beard et al. (2003a).

The uncertainties in the average $\delta^{56}Fe$ measurements quoted in this chapter are the 2σ standard error (2 standard deviation (SD) divided by the square root of the number of analysis). If multiple measurements were not performed for a sample, an uncertainty of ± 0.22‰ (2σ) is applied to samples referenced to the working standard and ± 0.24‰ (2σ) to samples referenced to mean of the igneous rock. There is a slight increase in the uncertainty due to error propagation when the sample $\delta^{56}Fe_{wrk\ std}$ (sample referenced to the working standard) is converted to $\delta^{56}Fe$ referenced to igneous rocks. The estimates of uncertainty are based on the long-term external precision of a single granite sample split

(± 0.22‰, 2 SD, n=22, Table 4.6, granite D). The standard deviation (1 SD), standard error (2σ), and number of measurements within an analytical session are reported for all samples in the data tables. Individual samples listed and plotted in the tables and figures represent samples or sub-samples that were processed through the entire Fe separation and purification chemistry separately.

6.3. Results and Discussion

The Fe isotopic composition of samples in the Amazon region and plume show a range in $\delta^{56}Fe$ of ≈ 1.5‰ (Figure 6.3, Tables 6.2 and 6.3). The isotopically lightest sample is the Amazon shelf porewater sample (-1.4‰) and the heaviest sample is the Negro River dissolved Fe (+0.14‰). The following sections will discuss each sample type along with the river water-seawater mixing experiments in more detail.

6.3.1. River Dissolved Fe and Suspended Sediment

Dissolved Fe and the suspended sediment from the Amazon River samples are isotopically light relative to igneous rocks, with the exception of the dissolved Fe from the Negro River. Multiple river samples were collected and filtered at each station. Filtration took several hours per sample, and there was concern that flocculation or adsorption of dissolved Fe onto particles or the bottle walls might affect the Fe isotopic composition of samples. In order to evaluate this possibility, the order in which samples were filtered (1,2,3...) was noted. No systematic trends in measured Fe concentration or isotopic composition is observed in the riverine dissolved Fe data. The measured Fe concentrations are similar to concentrations measured at stations near the sites in this study by Stallard (1980). The Solimões River samples have a range of measured Fe concentrations (0.6 to 2.1 μM), which is likely due to particle leak through during filtration, filter clogging, or the variability in Fe that passes through a 0.4 μm filter in a river with high suspended load (226 mg/L). Despite the differences in concentration, the

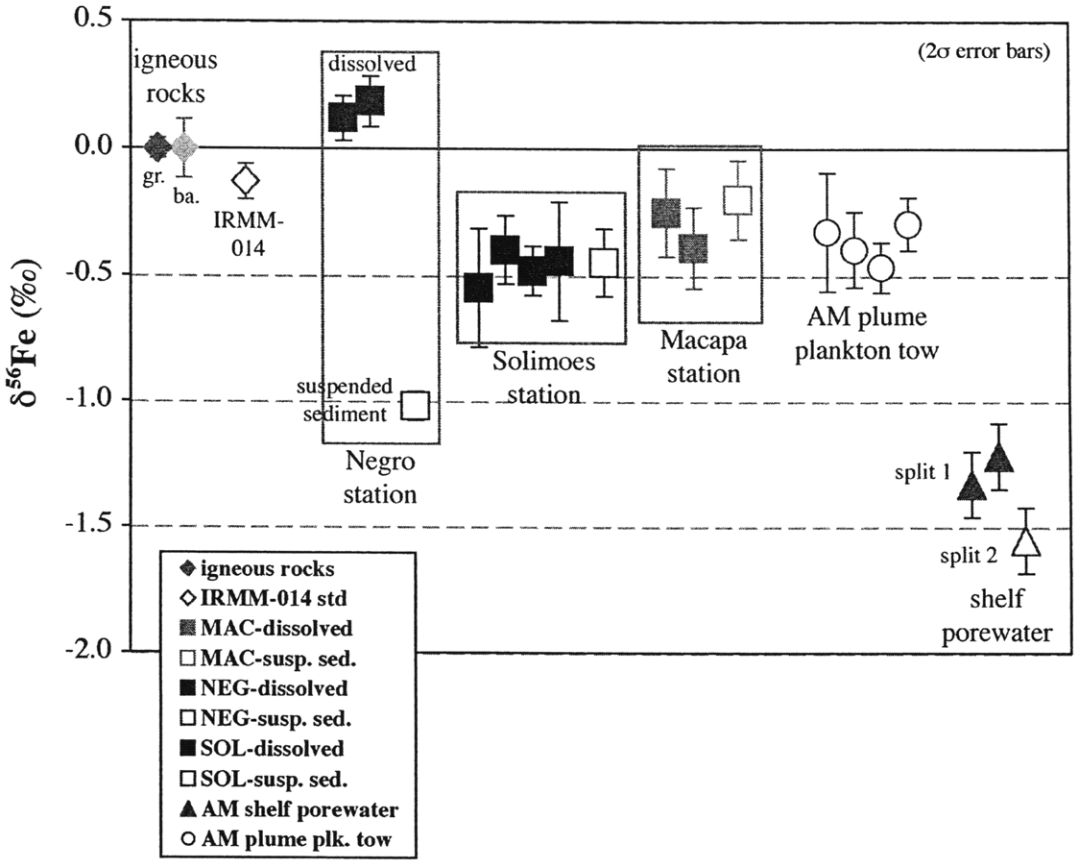

Figure 6.3: Summary of Fe isotopic data for samples from the Amazon region. The granite (USGS, G-2) and basalt (BVHO-1) splits along with the IRMM-014 standard are shown for reference. The dissolved Fe (■, <0.4 μm filtered) and suspended sediment (□) are plotted for the three river sample sites. Also shown are the Amazon plume plankton tow and shelf porewater sample. The replicate points for samples represent the $\delta^{56}Fe$ for a sample or a sub-sample that was processed through the entire Fe separation and purification chemistry. Error bars are 2σ standard errors of replicate measurements. If multiple measurements were not made within an analytical session, then a 2σ uncertainty of ± 0.24‰ is used based on the long term external precision of a granite sample (± 0.22‰, 2 SD, n=22, Table 4.6, granite D). There is a slight increase in the uncertainty due to error propagation when the sample $\delta^{56}Fe_{wrk\ std}$ (sample referenced to the bracketing sample) is converted to $\delta^{56}Fe$ referenced to igneous rocks. Data can be found in Tables 6.2 and 6.3.

Table 6.2: Fe Isotope Composition of Amazon River Samples

Sample ID	proc. Fe[a] (μg)	river water Fe (μM)	analysis date	$\delta^{56}Fe$[b] (‰)	1 SD[c]	2σ unc[d] (2 std error)	n	Inlet[e]
Amazon River - Macapá Station (0.0°, 51°W), Mar. 25, 2002								
dissolved Fe (<0.4 μm)								
AM-Macapá station sample 1[f]	13	2.6	8/7/03	-0.20	0.22	0.25	3	spray
			8/1/03	-0.46	0.12[g]	0.24[g]	1	spray
			5/28/03	-0.21	0.12[g]	0.24[g]	1	Aridus
AM-Macapá river sample 2	29	2.4	8/7/03	-0.32	0.12[g]	0.24[g]	1	spray
			11/5/03	-0.47	0.12[g]	0.24[g]	1	APEX (no des), Cu spike[h]
average AM-Macapá river sample 1:				-0.25	0.20	0.18	5	
average AM-Macapá river sample 2:				-0.39	0.11	0.16	2	
average Macapá station dissolved Fe measurements:				-0.29	0.13	0.10	7	
suspended sediment Fe								
AM-Macapa suspended sed	230		4/24/04	-0.20	0.17	0.16	5	APEX des.
Negro River Station (35 km up river from Manaus (3.1°S, 60°W)), Mar. 28, 2002								
dissolved Fe (<0.4 μm)								
AM-Negro River sample 1	45	4.6	5/28/03	0.08	0.12[g]	0.24[g]	1	Aridus
			8/7/03	0.15	0.12[g]	0.24[g]	1	spray
AM-Negro River sample 2	59	4.6	8/7/03	0.32	0.12[g]	0.24[g]	1	spray
			4/24/04	0.14	0.05	0.05	3	APEX des.
average AM-Negro River sample 1:				0.12	0.06	0.09	2	
average AM-Negro River sample 2:				0.19	0.10	0.10	4	
average Negro River dissolved Fe measurements:				0.16	0.09	0.07	6	
suspended sediment Fe								
AM-Negro suspended sed			4/24/04	-1.02	0.05	0.06	3	APEX des.
Solimões River Station (5-10 km up river from Manaus (3.1°S, 60°W)), Mar. 27, 2002								
dissolved Fe (<0.4 μm)								
AM-Solimões River sample 1	6	0.6	8/1/03	-0.55	0.12[g]	0.24[g]	1	spray
AM-Solimões River sample 2	20	2.1	4/24/04	-0.37	0.12[g]	0.24[g]	1	APEX des.
			8/7/03	-0.33	0.08	0.12	2	spray
			8/1/03	-0.58	0.12[g]	0.24[g]	1	spray
AM-Solimões River sample 3	9	0.8	5/28/03	-0.50	0.12[g]	0.24[g]	1	Aridus
			7/10/03	-0.53	0.12[g]	0.24[g]	1	Aridus
AM-Solimões River sample 4	9	1.0	4/24/04	-0.44	0.12[g]	0.24[g]	1	APEX des.
average all AM-Solimões river sample 2:				-0.40	0.13	0.13	4	
average all AM-Solimões river sample 3:				-0.48	0.07	0.10	2	
average Solimões River dissolved Fe measurements:				-0.45	0.11	0.08	8	
suspended sediment Fe								
AM-Solimões suspended sed[i]	150		4/24/04	-0.40	0.17	0.20	3	APEX des.
AM-Solimões suspended sed[j]	150		4/24/04	-0.52	0.11	0.15	2	APEX des.
average Solimões suspended sed. Fe measurements:				-0.45	0.15	0.13	5	

a) Amount of Fe processed through the Fe separation and purification chemistry.

b) Sample $\delta^{56}Fe$ values are referenced to the mean of igneous rocks (0.00 ± 0.04‰, 2σ, n=30).

c) SD is the standard deviation of the individual measurements.

d) 2σ uncertainty is the uncertainty in the mean of replicate sample measurements (2 standard error).

e) Several inlet systems were used including a cyclonic spray chamber (spray chamber), the Aridus desolvating system (Aridus), and the APEX system with (APEX with des.) and without a desolvator (APEX (no des)). See Chapter 4 for more details.

f) Every sample or sub-sample was processed through the Fe separation and purification chemistry separately. Sample number denotes sequence of filtration in the field.

g) If only one measurement was made for a sample, a 2σ uncertainty of ± 0.24‰ (2 SD) was applied to the sample. The 2σ uncertainty was estimated is based on the long term external precision of a granite sample.

h) Cu internal standardization along with SSB was used to correct for instrument mass bias for one session.

i) Sample was combusted prior to column separation chemistry only.

j) Sample was combusted both before and after column separation chemistry.

Table 6.3: Fe Isotopic Composition of Misc. Samples from Amazon System								
Sample ID	**proc. Fe[a] (μg)**	**Sample Fe (μM)**	**analysis date**	**$\delta^{56}Fe$[b] (‰)**	**1 SD[c]**	**2σ unc[d] (2 std error)**	**n**	**inlet[e]**
MP3-S23 Plankton Tow (10.5°N, 56.6°W), July 20, 2001								
tow 1[e] (<10 μm), split A[f]	?		10/24/03	-0.33	0.12[g]	0.24[g]	1	spray
tow 1 (<10 μm), split B	?		10/24/03	-0.40	0.11	0.15	2	spray
tow 2 (<10 μm)	26		10/24/03	-0.47	0.07	0.10	2	spray
tow 1 (>10 μm)	68		5/15/03	-0.18	0.12[g]	0.24[g]	1	Aridus
			5/28/03	-0.32	0.12[g]	0.24[g]	1	Aridus
			7/10/03	-0.44	0.13	0.18	2	Aridus
			8/7/03	-0.17	0.05	0.07	2	spray
			1/22/04	-0.36	0.12[g]	0.24[g]	1	APEX (no des)
average all tow 1 (>10 μm):				-0.30	0.14	0.10	7	
average all individual measurements:				-0.34	0.13	0.07	12	
Amazon-Guianas shelf porewater (5.5°N, 53°W), June 2003								
AM shelf porewater split 1-A	54	242	4/24/04	-1.33	0.12	0.14	3	APEX des.
AM shelf porewater split 1-B	7	242	4/24/04	-1.22	0.12[g]	0.24[g]	1	APEX des.
AM shelf porewater split 2	54	244	4/24/04	-1.55	0.04	0.06	2	APEX des.
average of split 1:				-1.30	0.12	0.12	4	
average of all measurements:				-1.39	0.16	0.13	6	
Amazon River-Seawater Mixing Experiments								
Macapa St. (Mar. 25, 2002)		**salinity (PSU)**						
AM-Macapá mixing expt 1	160	9	4/24/04	-0.19	0.06	0.08	2	APEX des.
AM-Macapá mixing expt 2	152	15	4/24/04	-0.01	0.09	0.12	2	APEX des.
Solimoes St. (Mar. 27, 2002)								
AM-Solimões mixing expt 4	24	14	4/24/04	-0.26	0.04	0.06	2	APEX des.
AM-Solimões mixing expt 5	25	6	4/24/04	-0.25	0.04	0.06	2	APEX des.

a) Amount of Fe processed through the Fe separation and purification chemistry.
b) Sample $\delta^{56}Fe$ values are referenced to the mean of igneous rocks (0.00 ± 0.04‰, 2σ, n=30).
c) SD is the standard deviation of the individual measurements.
d) 2σ uncertainty is the uncertainty in the mean of replicate sample measurements (2 standard error).
e) Several inlet systems were used including a cyclonic spray chamber (spray chamber), the Aridus desolvating system (Aridus), and the APEX system with (APEX with des.) and without a desolvator (APEX (no des)). See Chapter 4 for more details.
f) Every sample or sub-sample was processed through the Fe separation and purification chemistry separately. Sample number denotes sequence of filtration in the field.
g) If only one measurement was made for a sample, a 2σ uncertainty of ± 0.24‰ (2 SD) was applied to the sample. The 2σ uncertainty was estimated is based on the long term external precision of a granite sample.

isotopic composition of the replicate Solimões River samples were very similar with an average δ^{56}Fe -0.45 ± 0.08‰ (2σ,n=8) (Table 2).

The δ^{56}Fe of all the samples (both dissolved and suspended load) from the main channel sites, the Macapá and Solimões stations, are very similar. The Solimões Riverdissolved Fe and suspended sediment Fe are isotopically identical (-0.45‰), and slightly isotopically lighter than samples from the Macapá station (dissolved: -0.29‰; suspended sed: -0.20‰). The samples from the Macapá station were quite variable in their δ^{56}Fe composition from session to session (Table 6.2), and this is reflected in the reported precision for these samples. The variability in the measured isotopic composition of the Macapá samples may be due to some interference or matrix induced instrument mass bias variability (see Chapter 4 for discussion). The similarity of the dissolved and suspended sediment Fe isotopic compositions at these two stations and overwhelming majority of the Fe in the suspended fraction suggests that perhaps the dissolved δ^{56}Fe is somehow controlled by the suspended fraction. A majority of the "dissolved" Fe at these stations is colloidal including Fe-oxides, clays, and high molecular weight organic compounds. It may be that the colloidal Fe in these rives is dominated by the Fe-oxide and clay particles that are derived from the same source material as the suspended sediment and are just a different size fraction of the same material (soils and weathering of products from the Andes). Also, it might be that Fe bound to high molecular weight organic matter in these rivers is not isotopically different from the inorganic particles and colloids.

The source of the isotopically light Fe (-0.2 to -0.45‰) in the river samples from the Macapá and Solimões river stations is not known. However, exchangeable Fe from a soil was found to have a δ^{56}Fe of -0.6‰ (BRANTLEY et al., 2001). The δ^{56}Fe of our river samples is in the same range as the soil leachate. It is possible that these weathering products may be enriched in Fe that has been mobilized from rock sources. As stated in the introduction, organic leaching and microbial enhanced dissolution preferentially releases Fe that is isotopically light, -0.6 to -0.8‰ (BRANTLEY et al., 2001). Also, Fe reducing bacteria produce Fe(II) from solid Fe(III) sources that is isotopically light by -

1.3‰. The isotopically light Fe can then be re-oxidized and precipitated as Fe-oxide coatings and other reactive Fe minerals. These are all processes that are likely to occur to material as it is weathered and transported in the environment. Paleosol samples (ancient soil samples) measured by Arnold et al. (2004) are enriched +0.8‰ suggesting that perhaps isotopically light Fe is removed during weathering processes. It also may be that the observed isotopically light Fe in the suspended sediment and dissolved Fe reflects the isotopic composition of the source rocks in the Andes (e.g., isotopically variable shales or Banded Iron Formations (BEARD et al., 2003a; YAMAGUCHI et al., 2003)).

In contrast to the Macapá and Solimões river stations, the dissolved and suspended sediment Fe of the Negro river have distinct isotopic compositions. The dissolved fraction of the Fe is slightly isotopically heavy relative to igneous rocks (+0.14‰); whereas the suspended sediment Fe is light (-1‰). The observations are opposite of what might be predicted based on the laboratory leaching experiments and soil leachate measured by Brantley et al. (2001). Unlike the main channel river samples, approximately half of the Fe carried in the dissolved load in the Negro River. This leads to an overall δ^{56}Fe of the river (suspended plus dissolved) of -0.4‰. The combined dissolved and suspended sediment Fe being carried by the river is isotopically light, which is consistent with weathering processes removing light Fe preferentially. The organic rich waters of the Negro also probably lead to most of the dissolved, colloidal, and particulate Fe being bound to organic matter with Fe oxide and clay colloids being a minor component. The Negro River drains the intensely weathered Precambrian Shield of the Central Amazon lowlands. The suspended load is dominated by quartz, kaolinite (cation depleted clay), and particulate organic matter. The total dissolved load (which is an order of magnitude lower than the main channel) reflects the dissolution of the shield with elevated levels of dissolved Fe and Al (STALLARD, 1980; STALLARD, 1988; MARQUES et al., 2003). It can be estimated that as much as 50-60% of the Fe has been leached from the soils (compared with average continental rock) in the Negro drainage basin (KONHAUSER et al., 1994). The mechanism responsible for the large difference

(1.1‰) in the Fe isotopic composition of the dissolved and suspended sediment Fe in the Negro River is not known, but might be indicative of intense humid chemical weathering.

The isotopic contrast between the Fe in the dissolved and suspended loads in the Negro may be due to differences in the species of Fe present in the dissolved and particulate phases or perhaps equilibrium fractionation between the different phases (organic ligands?). It is likely that much of the suspended load Fe is bound with particulate organic matter, and some pseudo-equilibrium could be occurring between the organic phases of the dissolved and suspended load. Also, the low pH and high organic concentrations in the Negro river suggest that photochemical reduction of Fe(III) species might also be happening in the river. Many organic bound Fe complexes are photolabile and the reaction rates are enhanced under lower pH conditions (review: MOFFET, 2001). Photochemical reduction might lead to large Fe isotopic fractionations based on the observed difference between Fe(II) and Fe(III) aquo-complexes (JOHNSON et al., 2002; WELCH et al., 2003). One might predict that the Fe(II) species would be isotopically light based on the observations for Fe aquo-complexes or based on kinetic reaction arguments. In either case the more solube Fe(II) species (and predicited isotopically lighter Fe) would be in the dissolved phase. The Negro River observations are opposite from this prediction, but the Fe species involved in the chemical reactions in the Negro are not known. Similar processes could be occurring in the sediment-rich rivers like the Solimões River, but the signal is overwhelmed by the large amount of freshly weathered suspended sediment and inorganic colloids associated with that material.

The isotopic similarity of dissolved and suspended Fe at the Amazon main channel sites suggest that the organic rich tributaries with high dissolved Fe concentrations and low suspended sediment loads do not control the δ^{56}Fe of the dissolved load of the Amazon River. This conclusion is based on only three sites sampled in the Amazon. Numerous other tributaries join the Amazon River between the Solimões site and Macapá. Also, Fe likely undergoes chemical processes in the river itself (e.g., exchange with particles, biological uptake, coagulation). The unique isotopic composition associated with the intense weathering regime of the Negro River may be

overwhelmed by large amounts of freshly weathered suspended sediment and the high discharge of in the Solimões River. The combined flow of the Solimões and Negro River account for approximately 65% of the Amazon River water budget. If the suspended load and dissolved load were mixed conservatively (without exchange between the dissolved and particulate Fe), then the resulting δ^{56}Fe would be -0.11‰ for the dissolved load and -0.47‰ in the suspended sediment. Although the Macapá station dissolved Fe is isotopically heavier than the Solimões River station, the suspended sediment Fe is as well (opposite of what would be predicted from conservative mixing of the two tributaries). Other Fe sources and Fe chemistry must play an important role in determining the isotopic composition of the Amazon River at Macapá. One possibility is that organic matter from the organic rich tributaries may coagulate (along with Fe) with larger particles upon mixing with the main channel, which has higher concentrations of total dissolved solids.

6.3.2. River Water-Seawater Mixing Experiments

Riverine input to ocean is modified in estuaries during the mixing of high ionic strength seawater with river water. This process was simulated in field experiments by mixing filtered seawater and filtered river water together in different ratios, and then collecting the flocculent by filtration (SHOLKOVITZ, 1976). The results of this experiment are plotted in Figure 6.4 (isotope data in Table 6.3). The filtrate of the mixing experiments was measured for Fe concentration and the flocculent was measured for Fe isotopic composition.

In the mixing experiments performed at the Solimões River station, 88% of the Fe from the river water had flocculated at 18 PSU salinity. This agrees well with other mixing experiments and field data of Fe behavior in estuaries (SHOLKOVITZ, 1976; SHOLKOVITZ et al., 1978; BOYLE, 1997). The measured δ^{56}Fe for the river water endmember was -0.45 ± 0.10‰ (2σ,n=8), and both flocculent samples measured in the 6 PSU and 14 PSU experiment were isotopically heavier (6 PSU experiment: -0.26 ± 0.06‰ (2σ,n=2); 14 PSU experiment: -0.27 ± 0.06‰ (2σ,n=2)). The differences

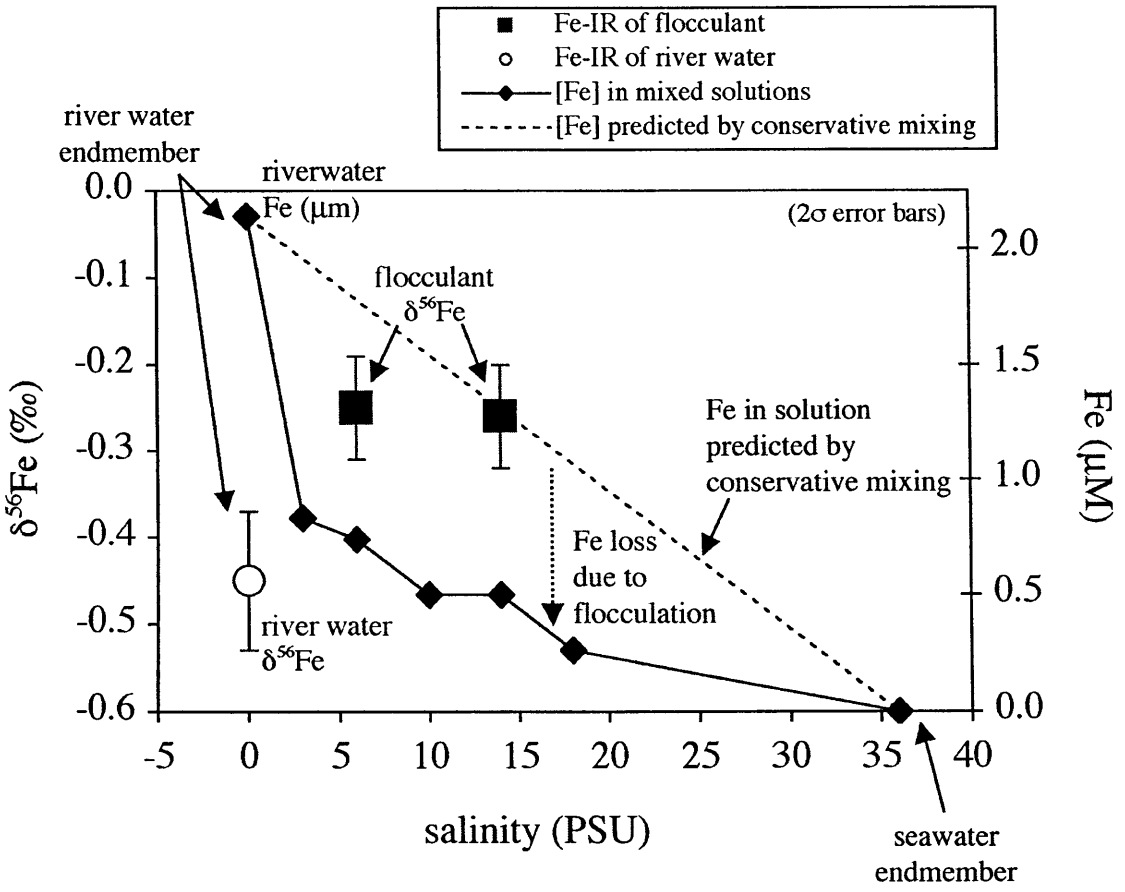

Figure 6.4: River water-seawater mixing experiment. The Fe (◆) concentration of the river water-seawater solutions after the flocculant was removed by filtration are shown with the solid line. The dashed line is the Fe concentration predicted if the river water and seawater were to mix conservatively. The Fe loss due to colloidal coagulation and flocculation is represented by the difference between the two lines. The river water $\delta^{56}Fe$ (O) is shown for reference, -0.45 ± 0.08‰ (2σ, n=8). Specifically the sample of river water used for this experiment was Solimoes River sample 3, which had slightly higher dissolved Fe (2.1 μM) compared with the other samples (<1 μM). This could be due to particle leak through during filtration or the variability of Fe that passes through a 0.4 μm filter in a river with high suspended load (226 mg/L). Despite the difference in concentration, the isotopic composition of the different Solimoes River samples were the similar. The flocculant (■) in this experiment was isotopically heavier than the river water Fe from which it was derived (6 PSU expt: -0.26 ± 0.06‰ (2σ, n=2); 14 PSU expt: -0.27 ± 0.06‰ (2σ, n=2)). This implies that the remaining dissolved Fe must be isotopically light (-0.9 to –1.1‰) compared to the river water endmember. The Fe contribution from seawater is likely negligible in this experiment. The dissolved Fe in seawater endmember was 0.37 nM (< 0.03% contribution to the total Fe in the experiment), and would have to be > +70 ‰ to be responsible for the observed isotopic shift. Error bars are 2σ standard errors of replicate measurements.

between dissolved river $\delta^{56}Fe$ and the flocculent $\delta^{56}Fe$ are significant at the 95% confidence level using the t-test and a distribution-free test, the Kolmogorov-Smirnov test (HOLLANDER and WOLFE, 1973). In a second mixing experiment performed at the Macapá River station, the filtered river water was not homogenized prior to the mixing experiments and a few of the experiments were contaminated by particle leak through during filtration. However in the 15 PSU experiment, where a majority of the dissolved Fe had flocculated, the collected flocculent was also isotopically heavier (-0.01‰) than the starting dissolved Fe in the river water endmember (-0.29‰). The Fe contribution from seawater is likely negligible in these experiments. The dissolved Fe in the seawater endmember was 0.37 nM (<0.03% contribution to the total Fe in the experiments), and would have to have a $\delta^{56}Fe$ of +70‰ to be responsible for the observed isotopic shift.

Although the isotopic shifts in the flocculent (+0.2 to 0.3‰) are small, the isotopically heavy flocculent implies that the remaining Fe in solution will be isotopically lighter than the Fe in the river water endmember. Based on the Solimões River station data and isotopic mass balance calculations, the remaining Fe in solution would be -0.9 to –1.1‰ (≈ -0.5‰ lighter than the river water endmember). The mechanism for this observed fractionation is not known, and it might be suspected that Fe should not fractionate due to flocculation. The species of Fe that are flocculating in estuaries are colloids (Fe-oxides, clays, and high molecular weight organic matter). The mass differential caused by the different isotopes of Fe in these high mass colloids would not affect the overall mass of the colloid, and therefore one might not expect Fe fractionation during flocculation. However if the Fe in the colloids is in some sort of chemical equilibrium with a truly soluble phase and there were an isotopic fractionation between the colloidal Fe and the soluble phase, then it might appear that "dissolved" Fe was fractionated when the colloidal fraction was removed from solution. Equilibrium fractionation between dissolved species of Fe is predicted (SCHAUBLE et al., 2001; ANBAR et al., submitted) and there could be significantly different bonding environments for Fe in the colloidal and soluble species. The dissolved load of the Negro suggests that isotopically heavy species of Fe exist. Kinetic fractionation mechanism may also be

responsible for the observed fractionation. For example, there could be fractionation between different Fe complexes if Fe is actively being exchanged between different species (MATTHEWS et al., 2001) or there could be competition between adsorption and complexation reactions.

6.3.3. Amazon Shelf Porewater

The porewater sample from the Amazon shelf region is the isotopically lightest sample measured in this study (-1.39 ± 0.16‰, 2σ,n=6). The source of the porewater Fe(II) in the Amazon shelf muds is from microbial reduction of solid phase Fe(III) minerals (ALLER et al., 1986). The fine-grained mud in the shelf region is dominantly of Amazon origin (MEADE et al., 1985; FROIDEFOND et al., 1988), and therefore should have an isotopic value similar to the observed isotopic value of suspended sediment at Macapá River station (-0.21‰). Therefore the fractionation observed in the porewater relative to igneous rock sources could be slightly smaller when compared to its source material (-1.1 to -1.2‰). Our observation of isotopically light porewaters are in good agreement with the observed δ^{56}Fe in porewaters from non-sulfidic sediments on the California margin (SEVERMAN et al., 2003). The Fe(II) in the Amazon shelf sediments is frequently re-suspended and re-oxidized to reactive Fe(III) minerals that can be used again for Fe-reduction. Aller et al. (in press) also estimated that 10 to 50% of the microbially produced Fe(II) is lost to authigenic mineral formation (e.g., siderite, K-Fe-Mg aluminosilicate minerals). In such a dynamic system, determining the mechanisms of Fe fractionation based solely on the porewater sample is impossible.

We suggest two ways to account for the observed fractionation: 1) fractionation during microbial Fe reduction and 2) progressive removal of isotopically heavy Fe by authigenic Fe mineral formation. The depleted δ^{56}Fe value of the soluble Fe(II) is in good agreement with observations of Fe fractionation (-1.3‰) by Fe reducing bacteria in laboratory experiments (BEARD et al., 1999; BEARD et al., 2003a; BRANTLEY et al., submitted). Although it is likely that the depleted δ^{56}Fe is related to microbial reduction of Fe, there are other potential pathways for Fe fractionation especially if microbial

reduction of the reactive Fe(III) phases is nearly quantitative. The loss of the Fe(II) through authigenic mineral formation could change the bulk isotopic composition of the reactive Fe pool (reactive Fe(III) phases and the dissolve Fe(II) pool). Formation of siderite from aqueous Fe(II) has been observed to produce siderite that is 0.5‰ heavier than the aqueous Fe(II) (WIESLI et al., 2003). In our system, heavy isotopes of Fe may preferentially be removed from the reactive pool of Fe by formation of authigenic minerals. If the authigenic Fe(II) minerals do not get recycled back into the reactive pool, an overall negative shift in the Fe isotopic composition of the reactive Fe pool would occur. It is also possible that the reactive pool of Fe(III) in the sediments will have zoned isotopic compositions. Rapid oxidation of Fe(II) in laboratory experiments produces Fe oxides that are isotopically heavy (+0.8‰) (BULLEN et al., 2001). The Amazon-Guianas shelf sediments are frequently re-suspended and the Fe(II) precipitated as Fe oxides. It is likely that re-oxidation is nearly quantitative and therefore the bulk composition of the combined reactive oxide pool plus dissolved Fe(II) might not change (but might be isotopically zoned).

In order to evaluate these possible mechanisms, the different fractions of Fe need to be separated and measured in the Amazon shelf system. The δ^{56}Fe in the marine sediments and porewaters may be useful in quantifying authigenic mineral formation or the extent of microbial Fe reduction. If Fe from re-suspension of shelf sediments is a significant source of Fe to the water column in the shelf region, it is likely that it will have a depleted δ^{56}Fe signal (based on the dissolved porewater).

6.3.4. Amazon Plume Plankton Tow

The plankton tow collected in Amazon plume water in the open ocean had a δ^{56}Fe value of -0.34 ± 0.07‰ (2σ,n=12). Different size fractions of the plankton tow (>10 μm and 1 to 10 μm) and different tows were measured to ensure that the filtering at sea did not affect the Fe isotopic composition of the sample. It took several hours to completely filter one plankton tow at sea through the 10 μm filter, and then through the 1 μm filter before filtering the second tow. If bacterial degradation or cell lysis in the plankton tow

were affecting the isotopic composition, then potentially the >10 μm and 1 to 10 μm splits would be different. The Fe isotopic data for the Amazon plume plankton tow is given in Table 6.3. The different size fractions and splits of the plankton tow show little isotopic variability suggesting that the filtering technique and time did not affect the isotopic composition of the Fe.

Fe isolated from the plankton tow includes both intracellular Fe and Fe attached to the surface of organisms (both particulate and adsorbed). The measured Fe:C ratio was ≈ 600 μmol/mol, which is 10 times higher than the required Fe:C ratio for maximum growth. The Fe:C ratio needed for optimal growth determined in laboratory cultures for a variety of marine organisms is less 70 μmol/mol (SUNDA and HUNTSMAN, 1995; HO et al., 2003), which agrees well with field observations for coastal organisms (MARTIN and KNAUER, 1973; BRULAND et al., 1991; SCHMIT and HUTCHINS, 1999). However, organisms will often take up Fe in excess of what they need if more Fe is available (luxury uptake). In laboratory cultures of a coastal diatom, Fe:C ratios greater than 100 μmol/mol were observed when available Fe exceeded 1 nM (SUNDA and HUNTSMAN, 1995; HO et al., 2003). The Fe:C continued to rise with increasing Fe, but the intracellular Fe:C plateaued at 120 μmol/mol with the increase in Fe above that due to extracellular Fe adsorption (HO et al., 2003). The ratio of intracellular Fe to external Fe is difficult to quantify in natural samples because of the variable Fe:C ratios and because plankton wash methods for removing extracellular Fe at sea were not available until recently (TOVAR-SANCHEZ et al., 2003). Tovar-Sanchez et al. (2003) found that 16 to 86% of the Fe measured in plankton tows from the Southern Ocean was extracellular. The plankton tow samples in this study were not washed and were collected in water with high total Fe (≈ 7 nM). It is likely that a large fraction of the Fe (>80%) in the Amazon plankton tow collected in this study is extracellular Fe, and therefore the δ^{56}Fe of the plankton tow will be more reflective of Fe attached to the surface of the plankton rather than intracellular Fe.

The isotopically heavier Fe from the Amazon plume plankton tow compared with the isotopically lighter open ocean plankton with low Fe:C ratios of less than 100

μmol/mol (-2 to -4‰, Chapter 5) suggests that the $\delta^{56}Fe$ in the plankton tow is dominated by extracellular Fe. However, this is the only plankton tow collected with a coastal-type organism assemblage (diatoms and larvaceans). Therefore, the comparison should not be overstated. The $\delta^{56}Fe$ (-0.34‰) of the Amazon plume plankton tow is also similar to the $\delta^{56}Fe$ of the Amazon River dissolved Fe collected near the mouth (-0.29‰). Based on the river water-seawater mixing experiments though, this riverine $\delta^{56}Fe$ may have been modified in the estuary as isotopically heavy Fe was removed during flocculation. Between the estuary and plankton tow site, Fe in the upper water column is cycled through the biological loop several times and a fraction lost through biological export and scavenging. Also, injection of new Fe from deeper water through mixing events potentially could add Fe to the system with different isotopic compositions (e.g., porewater and reactive Fe from sediment re-suspension events). If the main source of the Fe to the plankton tow were from the Amazon River and the $\delta^{56}Fe$ was modified to lighter values in the estuary (-1‰), it would suggest that isotopically light Fe is removed from the Amazon plume water through biological export and scavenging.

6.4. CONCLUSIONS

Iron isotopes in the dissolved, biological, and mobile particulate phases in the Amazon region and outflow have a 1.5‰ range in $\delta^{56}Fe$. The most depleted sample is the porewater (-1.4‰) collected in the upper 10 cm of the Amazon shelf region where microbial reduction of Fe dominates organic matter decomposition. The heaviest sample collected was dissolved Fe from an organic rich tributary, the Negro River, in the Amazon River system. Although the Negro River dissolved phase was isotopically heavy relative to igneous rock, its suspended sediment Fe was isotopically light (-1‰). The reason for the difference between the two pools of Fe is not known, but may be due to differences in speciation of Fe (e.g., isotopic fractionation between dissolved organic species and surface bound Fe). Because Fe in this river is evenly distributed between the dissolved and suspended loads, the overall $\delta^{56}Fe$ of the Negro tributary is $\approx$ -0.4‰. The main channel Amazon River samples (Solimões River and Macapá stations) have similar

δ^{56}Fe compositions with the Solimões River having slightly isotopically lighter Fe (-0.45‰) than the Macapá station (-0.2 to –0.3‰). The similarity of the dissolved and suspended sediment Fe at both main channel stations suggests that the dissolved fraction is dominated by colloids with similar composition as the suspended load (e.g., Fe oxides, clays).

Based on river water-seawater mixing experiments, the δ^{56}Fe of the dissolved Fe of the Amazon River may be modified in the estuary when >90% of the Fe flocculates upon mixing with ocean water. This flocculent is isotopically heavy compared with the riverine dissolved Fe, which would lead to the dissolved Fe that is transported to the ocean being isotopically lighter than the river endmember (≈ -1‰ or lighter). However, neither the proposed isotopically light Fe from the modified riverine input nor from shelf porewater matches the Amazon plume plankton tow δ^{56}Fe (-0.34‰). From the high Fe:C ratios measured in the Amazon plume plankton tow (≈ 600 μmol/mol), it is likely that most of the Fe collected in the plankton tow is extracellular Fe and the δ^{56}Fe reflects the composition of particles and Fe attached to the surface of the plankton. If the plankton tow δ^{56}Fe is similar to the plume water δ^{56}Fe, then processes in the euphotic zone (biological cycling/export, scavenging) may modify the proposed light δ^{56}Fe (-1‰) of the Amazon River input by preferentially removing isotopically light Fe. A more detailed study of the Amazon system is needed to elucidate the mechanisms of δ^{56}Fe fractionation and follow Fe cycling.

This study demonstrates that aqueous and biological samples in the environment have a measurable range in δ^{56}Fe values, and that these signal might be useful in tracking Fe pathways. Riverine δ^{56}Fe may reflect the degree or type chemical weathering in a basin and overall balance of the Fe in a drainage basin. More detailed studies of marine sediments and porewater δ^{56}Fe could possibly be used to quantify authigenic Fe mineral formation or other processes such as the extent of microbial Fe reduction. Following Fe and δ^{56}Fe from its source (e.g., riverine in this case) into the open ocean may be useful in estimating Fe loss in the estuary and also the degree recycling versus Fe export in the euphotic zone. Separation of intracellular Fe from extracellular Fe and measurement of

the $\delta^{56}Fe$ in seawater are necessary to evaluate the potential applications of Fe isotopes to tracing Fe in the marine environment.

References for Chapter 6

Aller R. C. (1998) Mobile deltaic and continental shelf muds as suboxic, fluidized bed reactors. *Marine Chemistry* **61**, 143-155.

Aller R. C., Blair N. E., Xia Q., and Rude P. D. (1996) Remineralization rates, recycling and storage of carbon in Amazon shelf sediments. *Continental Shelf Research.* **6**, 263-289.

Aller R. C., Heilbrun C., Panzeca C., Zhu Z., and Baltzer F. (in press) Coupling between sedimentary dynamics, early diagenetic processes, and biogeochemical cycling in the Amazon-Guianas mobile mud belt: coastal French Guiana. *Marine Geology.*

Aller R. C., Mackin J. E., and Cox R. T. J. (1986) Diagenesis of Fe and S in the Amazon inner shelf muds: apparent dominance of Fe reduction and implications for the genesis of ironstones. *Continental Shelf Research.* **6**, 263-290.

Anbar A. D., Jarzecki A., and Spiro T. (submitted) Theoretical investigation of equilibrium iron isotope fractionation between $Fe(H2O)_6^{+2}$ and $Fe(H2O)_6^{+3}$. *Geochimica et Cosmochimica Acta.*

Anbar A. D., Roe J. E., Barling J., and Nealson K. H. (2000) Nonbiological fractionation of iron isotopes. *Science* **288**(5463), 126-128.

Arnold G. L., Weyer S., and Anbar A. D. (2004) Fe isotope variations in natural materials measured using high mass resolution multiple collector ICPMS. *Analytical Chemistry* **76**(2), 322-327.

Beard B. L. and Johnson C. L. (1999) High precision iron isotope measurements of terrestrial and lunar materials. *Geochimica et Cosmochimica Acta* **63**, 1653-1660.

Beard B. L., Johnson C. L., Cox L., Sun H., Nealson K. H., and Aguilar C. (1999) Iron isotope biosignatures. *Science* **285**, 1889-1892.

Beard B. L. and Johnson C. M. (2004) Fe isotope variations in the modern and ancient earth and other planetary bodies. In *Geochemistry of Non-Traditional Stable Isotopes.*, Vol. 55 (ed. C. M. Johnson, B. L. Beard, and F. Albarede), pp. 319-357. The Mineralogical Society of America.

Beard B. L., Johnson C. M., Skulen K. H., Nealson K. H., Cox L., and Sun H. (2003a) Application of Fe isotopes to tracing the geochemical and biological cycling of Fe. *Chemical Geology* **195**, 87-117.

Beard B. L., Johnson C. M., Von Damm K. L., and Poulson R. (2003b) Iron isotope constraints on Fe cycling and mass balanced oxygenated Earth. *Geology* **31**, 629-632.

Bell J., Betts. J., and Boyle E. A. (2002) MITESS: A Moored In-situ Trace Element Serial Sampler for Deep-Sea Moorings. *Deep-Sea Research I* **49**, 2103-2118.

Bergquist B. A. and Boyle E. A. (2001) Isotopic composition of marine samples: preliminary results. *Eos Trans. AGU, Ocean Science Meeting Supplement*, Abstract OS21B-17.

Borstad G. A. (1982) The influence of the meandering Guiana Current and Amazon River discharge of surface salinity near Barbados. *Journal of Marine Research* **40**, 421-434.

Boyle E. A. (1997) What controls dissolved iron concentrations in the world ocean - a comment. *Marine Chemistry* **57**, 163-167.

Boyle E. A., Edmond J. M., and Sholkovitz E. R. (1977) The mechanism for iron removal in estuaries. *Geochimica et Cosmochimica Acta* **41**, 1313-1324.

Brantley S. L., Liermann L., and Bullen T. D. (2001) Fractionation of Fe isotopes by soil microbes and organic acids. *Geology* **29**(6), 535-538.

Brantley S. L., Liermann L., Wu S., and Bullen T. D. (1999) Concentration and isotopic signature of trace metal release during abiotic and biotic dissolution of hornblende. *AGU Abstracts with Programs, 1999 AGU Fall Meeting*, H521-03.

Brantley S. L., Liermann L. J., Anbar A. D., Icopini G. A., Guynn R. L., and Barling J. (submitted) Fe isotopic fractionation during mineral dissolution with and without bacteria. *Geochimica et Cosmochimica Acta.*

Brinkmann W. L. F. (1987) Particulate and dissolved materials in the Rio Negro, Amazon Basin. In *Sediments and Water Interactions* (ed. P. G. G. Sly), pp. 3-12. Springer-Verlag.

Bruland K. W., Donat J. R., and Hutchins D. A. (1991) Interactive influences of bioactive trace metals on biological production in oceanic waters. *Limnology and Oceanography* **36**, 1555-1577.

Bullen T. D. and McMahon P. M. (1998) Using stable isotopes to assess microbially-mediated Fe^{+3} reduction in a jet-fuel contaminated aquifer. *Mineralogical Magazine* **62A**, 255-256.

Bullen T. D., White A. F., Childs C. W., Vivit D. V., and Schulz M. S. (2001) Demonstration of significant abiotic iron isotope fractionation in nature. *Geology* **29**(8), 699-702.

Callede J., Guyot J. L., Molinier M., Guimaraes V., Oliveira E., and Filizola N. P. (1997) La variabilite des delbits de l'Amazone a Obidos (Amazone, Bresil). In *Sustainability of Water Resources under Increasing Uncertainty* (ed. D. Rosbjerg, N. E. Boutayeb, Z. W. Kundzewicz, A. Gustard, and P. F. Rasmussen), pp. 163-172. IAHS.

Croal L. R., Johnson C. M., Beard B. L., and Newman D. K. (in press) Iron isotope fractionation by Fe(II)-oxidizing photoautotrophic bacteria. *Geochimica et Cosmochimica Acta.*

Dessier A. and Donguy J. R. (1993) The sea-surface salinity in the tropical Atlantic between 10S and 30N - seasonal and interannual variations. *Deep-Sea Research Part I* **41**, 81-100.

Froidefond J.-M., Gardel L., Guiral D., Parra M., and Ternon J.-F. (2002) Spectral remote sensing reflectances of coastal waters in French Guiana under the Amazon influence. *Remote Sensing of Environment* **80**, 225-232.

Froidefond J.-M., Pujos M. M., and Andre X. (1988) Migration of mud banks and changing coastline in French Guiana. *Marine Geology* **84**, 19-30.

Gaillardet J., Dupre B., Allegre C. J., and Negrel P. (1997) Chemical and physical denudation in the Amazon River Basin. *Chemical Geology* **142**, 141-173.

Hellweger F. L. and Gordon A. L. (2002) Tracing Amazon River water into the Caribbean Sea. *Journal of Marine Research* **60**, 537-549.

HIBAM. (1999) Hydrology and Geochemistry of the Amazon Basin (Project). pp. http://www.unb.br/ig/hibam. University of Brasilia.

Ho T., Quigg A., Finkel Z. V., Milligan A. J., Wyman K., Falkowski P. G., and Morel F. M. (2003) The elemental composition of some marine phytoplankton. *Journal of Phycology* **39**, 1145-1159.

Hollander M. and Wolfe D. A. (1973) *Nonparametric Statistical Methods*. John Wiley & Sons, Inc.

Johnson C. M., Beard B. L., Beukes C., Klein C., and O'Leary J. M. (2003) Ancient geochemical cycling in the Earth as inferred from Fe isotope studies of banded iron formations from Transvaal Craton. *Contributions to Mineral Petrology* **144**, 523-547.

Johnson C. M., Skulan J. L., Beard B. L., Sun H., Nealson K. H., and Braterman P. S. (2002) Isotopic fractionation between Fe(III) and Fe(II) in aqueous solutions. *Earth and Planetary Science Letters* **195**(1-2), 141-153.

Johnson K. S., Chavez F. P., and Friederich G. E. (1999) Continental-shelf sediment as a primary source of iron for coastal phytoplankton. *Nature* **398**, 697-700.

Kelly P. S., Lwiza K. M. M., Cowen R. K., and Goni G. J. (2000) Low salinity pools at Barbados, West Indies: Their origin, frequency and variability. *Journal of Geophysical Research* **100**, 2355-2375.

Konhauser K. O., Fyfe W. S., and Kronberg B. I. (1994) Multi-element chemistry of some Amazonian waters and soils. *Chemical Geology* **111**, 155-175.

Levasseur S., Warthmann R. J., and Halliday A. N. (2002) Fractionation of Fe isotopes by anaerobic phototrophic bacteria. *Geochimica et Cosmochimica Acta* **66**, A450.

Marques A. N., Al-Gharib I., Bernat M., and Fernex F. (2003) Uranium and thorium isotopes in the rivers of the Amazonian basin: hydrology and weathering processes. *Hydrological Processes* **17**, 17-31.

Martin J. H. and Knauer G. A. (1973) The elemental composition of plankton. *Geochimica et Cosmochimica Acta* **37**(1639-1653).

Matthews A., Zhu X. K., and O'Nions K. (2001) Kinetic iron stable isotope fractionation between iron (II) and iron (III) complexes in solution. *Earth and Planetary Science Letters* **192**, 81-92.

Meade R. H., Dunne T., Richey J. E., Santos U. D. M., and Salati E. (1985) Storage and remobilization of suspended sediment in the lower Amazon River of Brazil. *Science* **228**, 488-490.

Meade R. H., Nordin C. F., Curtis W. F., Rodriques F. M. C., Vale C. M., and Edmond J. M. (1979) Sediment loads in the Amazon. *Nature* **278**, 161-163.

Michalopoulas P. and Aller R. C. (1995) Rapid clay mineral formation in the Amazon delta sediments: reverse weathering and oceanic elemental cycles. *Science* **270**, 614-617.

Michalopoulas P., Aller R. C., and Reeder R. (2000) Conversion of diatoms to clay minerals during early diagenesis in tropical, continental shelf muds. *Geology* **28**, 1095-1098.

Moffett J. W. (2001) Transformations Among Different Froms of Iron in the Ocean. In *The Biogeochemistry of Iron in Seawater*, Vol. 7 (ed. K. A. Hunter and D. Turner), pp. 343-372. John Wiley & Sons, Ltd.

Muller-Karger F. E., McClain C. R., and Richardson P. L. (1988) The dispersal of the Amazon's water. *Nature* **333**, 56-59.

Ohno T., Kouge I., and Hirata T. (2004) Iron isotopes in human blood. *Geochimica et Cosmochimica Acta* **66**(15A), A569-A569.

Roe J. E., Anbar A. D., and Barling J. (2003) Nonbiological fractionation of Fe isotopes: evidence of an equilibrium isotope effect. *Chemical Geology* **195**(1-4), 69-85.

Rouxel O., Dobbek N., Ludden J., and Fouquet Y. (2003) Iron isotope fractionation during oceanic crust alteration. *Chemical Geology* **202**(1-2), 155-182.

Rouxel O., Fouquet Y., and Ludden J. N. (2004) Subsurface processes at the Lucky Strike hydrothermal field, Mid-Atlantic Ridge: evidence from sulfur, selenium, and iron isotopes. *Geochimica et Cosmochimica Acta* **68**, 2295-2311.

Schauble E. A., Rossman G. R., and Taylor H. P. (2001) Theoretical estimates of equilibrium Fe-isotope fractionations from vibrational spectroscopy. *Geochimica et Cosmochimica Acta* **65**(15), 2487-2497.

Schmit M. A. and Hutchins D. A. (1999) Size fractionated biological iron and carbon uptake along a coastal to offshore transect in the NE Pacific. *Deep-Sea Research Part II* **46**, 2487-2503.

Severman S., McManus J., Johnson C. M., and Beard B. L. (2003) Iron isotope geochemistry in California Margin sediments and porewaters. *Eos Trans. AGU, Ocean Science Meeting Supplement* **84**, Abstract#OS31L-019.

Severmann S., Johnson C. M., Beard B. L., German C. R., Edmonds H. N., Chiba H., and Green D. H. (in press) Origin of the Fe isotope composition of the oceans as inferred by Rainbow vent site, Mid-Atlantic Ridge, 36deg14'N. *Earth and Planetary Science Letters.*

Severmann S., McManus J., Johnson C. M., and Beard B. L. (2003) Iron isotope geochemistry in California Margin sediments and porewaters. *Eos Trans. AGU, Ocean Science Meeting Supplement* **84**, Abstract#OS31L-019.

Seyler P. T. and Boaventura G. R. (2001) Trace Elements in the Mainstem Amazon River. In *The Biogeochemistry of the Amazon Basin.* (ed. M. E. McClain, R. L. Victoria, and J. E. Richey), pp. 307-327. Oxford University Press, Inc.

Sharma. (2001) Iron isotopes in hot springs along the Juan de Fuca Ridge. *Earth and Planetary Science Letters* **194**, 39-51.

Sholkovitz E. R. (1976) Fluctuation of dissolved organic and inorganic matter during the mixing of river water and seawater. *Geochimica et Cosmochimica Acta* **40**, 831-845.

Sholkovitz E. R., Boyle E. A., and Price N. B. (1978) The removal of dissolved humic substances and iron during estuarine mixing. *Earth and Planetary Science Letters* **40**, 130-136.

Signorini S. R., Murtugudde R. G., McClain C. R., Christian J. R., Picaut J., and Busalacchi A. J. (1999) Biological and physical signatures in the tropical and subtropical Atlantic. *Journal of Geophysical Research* **104**, 18367-18382.

Stallard R. F. (1980) Major Element Chemistry of the Amazon River System. Ph.D. Dissertation, MIT/WHOI Joint Program.

Stallard R. F. (1988) Weathering and erosion in the humid tropics. In *Physical and Chemical Weathering in Geochemical Cycles*. (ed. A. Lerman and M. Meybeck), pp. 225-246. Kluwer.

Stallard R. F. and Edmond J. M. (1983) Geochemistry of the Amazon. 2. The Influence of the geology and weathering environment on the dissolved load. *Journal of Geophysical Research* **88**, 9671-9688.

Steven D. M. and Brooks A. L. (1972) Identification of Amazon River water at Barbados, W. Indies, by salinity and silicate measurements. *Marine Biology* **14**, 345-348.

Stookey L. C. (1970) Ferrozine – a new spectrophotometric reagent for iron. *Analytical Chemistry* **42**, 779-781.

Sunda W. G. and Huntsman S. A. (1995) Iron uptake and growth limitation in oceanic and coastal phytoplankton. *Marine Chemistry* **50**(189-206).

Tovar-Sanchez A., Sanudo-Wilhelmy S. A., Garcia-Vargas M., Weaver R. S., Popels L. C., and Hutchins D. A. (2003) A trace metal clean reagent to remove surface-bound iron from marine phytoplankton. *Marine Chemistry* **82**, 91-99.

Vink S., Boyle E. A., Measures C. I., and Yuan J. (2000) Automated high resolution determination of the trace elements iron and aluminum in the surface ocean using towed Fish coupled to a flow injection analysis. *Deep-Sea Research I* **47**, 1141-1156.

Walyczyk T. and von Blanckenburg F. (2002) Natural iron isotope variations in human blood. *Science* **295**, 2065-2066.

Welch S. A., Beard B. L., Johnson C. M., and Braterman P. S. (2003) Kinetic and equilibrium Fe isotope fractionation between aqueous Fe(II) and Fe(III). *Geochimica et Cosmochimica Acta* **67**(22), 4231-4250.

Wiesli R. A., Beard B. L., and Johnson C. M. (2003) Experimental determination of Fe isotope fractionation between aq. Fe(II), "green rust", and siderite. *Geochimica et Cosmochimica Acta* **67**, A533.

Yamaguchi K. E., Beard B. L., Johnson C. M., Ohkouchi N., and Ohmoto H. (2003) Iron isotope evidence for redox stratification of the Archean oceans. *Geochimica et Cosmochimica Acta* **67**, A550.

Zhu X. K., Guo Y., Williams R. J. P., O'Nions R. K., Matthews A., Belshaw N. S., Canters G. W., de Waal E. C., Weser U., Burgess B. K., and Salvato B. (2002) Mass fractionation processes of transition metal isotopes. *Earth and Planetary Science Letters* **200**(1-2), 47-62.

Zhu X. K., O'Nions R. K., Guo Y. L., and Reynolds B. C. (2000) Secular variation of iron isotopes in North Atlantic Deep Water. *Science* **287**(5460), 2000-2002.